Factors Affecting Human Achilles Sub-tendon Mechanical Behaviour and the Clinical Application Potential

Nai-Hao Yin

October 2021

A thesis submitted to University College London for the degree of

Doctor of Philosophy

Research Department of Orthopaedics and Musculoskeletal Science

Division of Surgery and Interventional Science

University College London

I, Nai-Hao Yin confirm that the work presented in this thesis is my own. Where information has been derived from other sources, I confirm that this has been indicated in the thesis.

Acknowledgement

Foremost, I would like to thank the generosity of the Taiwanese Government in providing the scholarship to support my study.

I would like to express my sincere gratitude to my supervisor Professor Helen Birch, for her support, guidance, and valuable feedback at every stage of this study. I would not achieve this without her help. Thank you to Dr Ian McCarthy, my secondary supervisor, for providing feedback and support on the biomechanical part of the study.

I would like to thank Professor Anthony Parker and Professor Pavel Matousek for teaching me essential spectroscopy skills. Thank you, Professor Paul Fromme, for assisting and refining the modelling study. Special thanks to the members of the tendon meeting at QMUL for the fruitful discussion, the members of the MLL at RNOH for helping with motion analysis. A big thank you to all the participants who joined my study.

Thank you to my beloved family, friends, and other PhD students at Stanmore. Your unconditional love and support made the lone journey (aggravated by lockdown due to the global pandemic) much more bearable.

Abstract

The human Achilles tendon is composed of three twisted sub-tendons, arising from soleus and gastrocnemii muscles, but the interaction between these sub-tendons during body movements is largely unknown. The most widely reported phenomenon is the non-uniform intra-tendinous displacements during movements; however, how this non-uniformity contributes to the overall tendon mechanical behaviour has not been thoroughly studied. This thesis aims to investigate the potential factors affecting this intra-tendinous displacement non-uniformity, by conducting mechanical and material characterisation and *in silico* modelling on Achilles sub-tendons, and to discover possibilities to translate these findings into clinical applications.

The study conducted on the equine bifurcated tendon-ligament model demonstrated that differences in the material and mechanical properties at the fascicle and sub-tendon levels may be associated with displacement non-uniformity. Human Achilles sub-tendon material properties were not statistically different but a greater cross-sectional area, failure force and displacement were found in the soleus than gastrocnemii sub-tendons. These results suggest that the material and mechanical properties of sub-tendons may affect the overall tendon level mechanical behaviour.

Finite element analysis on three reconstructed Achilles sub-tendon models identified that reduced inter-sub-tendon sliding, as reported previously in aged tendons, reduced displacement non-uniformity. Comparing the results

from different models further suggested that the inherent tendon morphology, with different length, twist, and sub-tendon arrangements, could result in different tendon level displacements and stress distributions.

The results from Raman spectroscopy on both equine and human tendon tissues demonstrated the ability to differentiate tendon samples with known compositional differences based on spectral features alone, suggesting that Raman spectroscopy has the potential for rapid analysis of tendon compositions in the future.

In conclusion, this thesis has identified three factors that could affect the overall Achilles tendon mechanical behaviour and proposed potential approaches for future clinical applications to improve tendon healthcare.

Impact Statement

This thesis aims to explore the complex interactions between sub-structures of the Achilles tendon, which is a topic considering the forefront of the tendon and tendinopathy research (Maas et al., 2021). Fully characterisation of the mechanical behaviour of the Achilles sub-tendons could potentially improve our future tendon healthcare.

A range of measurement techniques was applied in this thesis on isolated *ex vivo* tendon tissues to characterise the material and mechanical properties and the biochemical compositions of the tendon sub-structures. In addition, an equine tendon model and finite element analysis, conducted on reconstructed human tendon computer models, were both applied to study the potential influencing factors of the tendon level mechanical behaviour, such as the sub-tendon mechanical properties and compositions, the sliding ability between sub-tendons, and the inherent tendon morphological differences.

The research reported in this thesis has resulted in several important discoveries that advance tendon knowledge and have the potential to improve the current healthcare of tendon diseases. Firstly, the overall tendon level mechanical behaviour is the aggregated result of sub-tendon level interactions. Studies from the equine tendon model (Ch. 2) and human tendon simulations (Ch. 6 & 7) both identified that the tendon level displacement can differ between loads imposed on different sub-tendons. Reduced sub-tendon sliding ability in the simulation studies also demonstrated a decreasing trend in the tendon level displacements. These findings suggest the traditional thinking of the Achilles tendon as a homogeneous tissue should be discarded

and future studies should focus on the interaction between Achilles sub-tendons under different muscle loading conditions or between people with different sub-tendon sliding abilities.

Secondly, the thesis identifies two different approaches that may have clinical application potentials. Raman spectroscopy (Ch. 4 & 5) can probe tendon compositions rapidly and non-destructively and can differentiate tendons with known compositional differences by spectral features alone. The results were in excellent agreement with conventional biochemical approaches. These encouraging *in vitro* findings should be further investigated under *ex vivo* and *in vivo* conditions and ideally compare between healthy and injured tendons in the future. In Chapters 6 and 7, combining computer simulation with *in vivo* data appears to be a potential surrogate to circumvent the current inability to differentiate internal Achilles sub-tendon arrangements non-invasively, while at the same time, quantifying and visualising tendon stress during activities (Pizzolato et al., 2020).

Lastly, direct findings from conventional biochemistry (Ch. 2 & 3) and indirect findings from Raman spectroscopy (Ch. 4 & 5) both suggest the compositional differences could exist at or below the sub-tendon level. Detailed investigation of the tendon extracellular matrix compositions, especially the proteins facilitating sliding (Godinho et al., 2017) or the glycation crosslinks affecting the mechanical stiffness of the matrix (Collier et al., 2018), could give further insights on the fundamental biological differences, induced by ageing or localised mechanical environment, within different internal regions of the Achilles tendon.

Table of Contents

Table of Tables

Table of Figures

List of Abbreviations

AGEs – Advanced glycation end-products

AL – Accessory ligament (of the deep digital flexor tendon)

CDET – Common digital extensor tendon (of equine forelimbs)

CCD – Charged coupled device

CSA – Cross-sectional area

DDFT – Deep digital flexor tendon (of equine forelimbs)

ECM – Extracellular matrix

FEA – Finite element analysis

GAG – Glycosaminoglycans

IFM – Inter-fascicular matrix

MRI – Magnetic resonance imaging

PCA – Principal component analysis

SDFT – Superficial digital flexor tendon (of equine forelimbs)

Chapter 1 Introduction and Literature Review

1.1 Introduction

The human Achilles tendon is composed of three smaller sub-tendons, arising from gastrocnemii and soleus muscles, and the structure-function relationship of the sub-tendons has been actively studied in the recent decade (see editorial (Maas et al., 2021)). Fascicles within each sub-tendon do not intertwine and, with the aid of dissection microscopy, three sub-tendons can be isolated from the seemingly homogeneous Achilles tendon (Szaro et al., 2009, Edama et al., 2015a, Edama et al., 2016). *In vitro* studies utilised selective loading on individual muscle demonstrated that some degree of independent sub-tendon displacement exists within the whole Achilles tendon (Arndt et al., 1999a, Arndt et al., 1999b, Finni et al., 2018, Maas et al., 2020). This phenomenon can be observed *in vivo* under 2-D sagittal plane ultrasound imaging as the different displacements between superficial (posterior, assuming medial gastrocnemius sub-tendon) and deep (anterior, assuming soleus sub-tendon) layers (Arndt et al., 2012, Slane and Thelen, 2014, Slane and Thelen, 2015).

For individual sub-tendon movement to happen, the interface between sub-tendons, termed inter-sub-tendon matrix (Gains et al., 2020), must allow a certain degree of sliding. Studies on animal tendons have demonstrated that sliding of sub-structures (fascicles and fibres), which is facilitated by several specialised proteins at the interface, greatly affects the mechanical behaviour of the tendon as a whole (Sun et al., 2013, Thorpe et al., 2013c, Thorpe et al., 2015b, Thorpe et al., 2016c, Godinho et al., 2017, Godinho et al., 2021). The inter-sub-tendon matrix of the human Achilles tendon may have a similar specialised composition and exhibit similar sliding properties. In addition, several observational studies proposed a potential relationship between reduced intra-tendinous displacement non-uniformity and inferior tendon functions (Franz and Thelen, 2015, Slane and Thelen, 2015, Froberg et al., 2017, Couppe et al., 2020), but the underlying mechanisms and causes have not been systematically studied.

This thesis aims to characterise the complex mechanical behaviour of human Achilles sub-tendons, investigate the factors that could affect the displacement non-uniformity, and explore possibilities to translate this knowledge into future clinical exploitation.

1.2 Tendon Composition and Structure

Young and healthy human tendon tissues are usually scarce for conducting *in vitro* mechanical testing or biochemical assays. Therefore, animal models are frequently used in tendon-related studies. Comparison between different methodologies and between different species however is not always applicable. Generally, rodent and rabbit tendons are good models for studying tendon injury and repair, due to their faster metabolism and shorter lifespan; while equine tendons, for their longevity and exposure to high-intensity exercise, are more often used in function-related and age-related tendon research (Thorpe et al., 2010a, Patterson-Kane et al., 2012, Moura Junior Mde et al., 2015, Huisman et al., 2016). The equine superficial digital flexor tendon (SDFT) is a widely accepted model for studying the energy-storing function and overuse tendinopathies in the human Achilles tendon. These tendon types are similar in terms of their energy-storing role, high strains (~ 17% for the SDFT during galloping (Stephens et al., 1989)), and high incidence of injury (Thorpe et al., 2010a).

In this thesis, the term ‘fibre’ (Section 1.2.4) is reserved (Handsfield et al., 2016) for specifically indicating the hierarchical level between fibril (Section

1.2.3) and fascicle (Section 1.2.5). ‘Fibrous’ and ‘fibre-like’ are used for general description. Similarly, ‘tendon function’ together is reserved for describing athletic and movement-related mechanical force transmission function of the tendon, as in ‘Regular physical training improves tendon function.’ While the generic, non-specific, and even sometimes ambiguous (e.g., biological function or anatomical function) adjective use of the term ‘function’ remains unrestricted but scarce to prevent confusion.

1.2.1 Tendon Hierarchy

Tendons are dense connective tissues linking muscles and bones providing mainly a force transmitting role. Tendons have a hierarchical structure (Figure 1-1), but the variation and inconsistent use of different nomenclature in the literature from different research groups are sometimes confusing, especially at the fibre and fascicle levels. For the human Achilles tendon, the fascicles from three ‘fascicle bundles’ originating from different muscles do not intertwine or overlap (Szaro et al., 2009). The term ‘sub-tendon’ is used to describe this hierarchy (Handsfield et al., 2016, Finni et al., 2018, Gains et al., 2020).

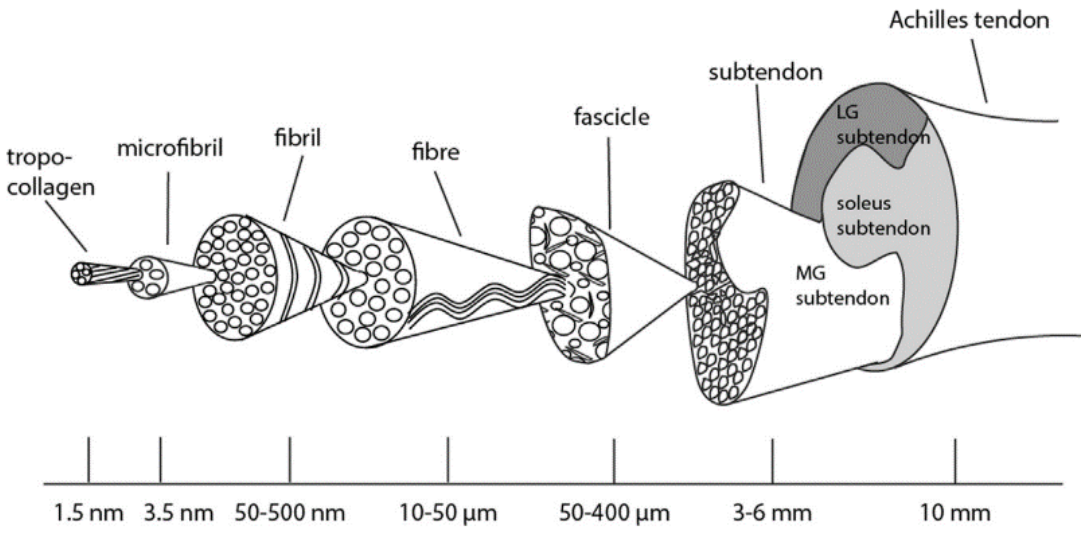

Figure 1-1. Achilles tendon hierarchy (adapted from (Handsfield et al., 2016)).

Snedeker and Foolen (Snedeker and Foolen, 2017) defined two distinct compartments within tendons based on their primary physiological function. The intrinsic compartment comprises mainly the collagenous matrix and tenocytes forming the hierarchical structures (Figure 1-1) and is the primary load-bearing structural component of the tendon providing its mechanical strength. The extrinsic component comprises synovial tissues surrounding fascicles, sub-tendons, and the whole tendon with primarily a supportive metabolic function. The extrinsic component is metabolically more active than the intrinsic collagenous matrix (Thorpe et al., 2010c, Birch et al., 2013, Thorpe et al., 2016c) and is likely associated with the initiation of injuries in energy-storing tendons (Cook and Screen, 2018). Recent *in vitro* and *in silico*

studies have demonstrated the importance of the inter-fascicular matrix (IFM, surrounding fascicles) and inter-sub-tendon matrix (surrounding sub-tendons) on facilitating the relative sliding between sub-components to achieve an optimal tendon function (Section 1.3.3 and 1.3.4). However, to isolate the contribution of sub-components during *in vivo* activities or between healthy and injured tendons remains technologically challenging.

Tendons can be categorised into energy-storing or positional tendons based on their primary mechanical function (Birch, 2007). Most of the tendons in the human body fulfil their mechanical role of precisely positioning the joint in space by transmitting the force produced by the muscle without much tendon strain (e.g., anterior tibialis tendon). However, for energy-storing tendons (such as human Achilles tendon and equine SDFT) their ECM is specialised to withstand a large strain and have high fatigue resistance (Birch, 2007, Thorpe et al., 2016d). Therefore, these tendons can utilise the elastic energy by storing it during lengthening (e.g., from heel-strike to before heel-off, passive ankle dorsiflexion and eccentric contraction of calf muscles during the stance phase) and timely release this energy (e.g., from heel-off to toe-off) to propel the body forward. This spring-like function of energy-storing tendons can greatly reduce the energy cost of locomotion.

Water accounts for approximately 70% of the tendon weight. The major component (~ 70%) of dried tendons is collagen, followed by proteoglycans, glycoproteins, and elastic fibres (Thorpe and Screen, 2016). Cells are sparse in tendons. The tendon compositional features will be introduced and reviewed at the most relevant (or most abundant) hierarchical level; however, the actual distribution of certain compositions is often across multiple levels.

1.2.2 Collagen (molecular) Level

Collagen is a family of proteins containing 28 different types and serving a wide range of biological functions (Kadler et al., 2007). This section reviews the fibrillar collagen types (especially types I, II, and III, which form fibrils) that are the major components of tendons and significantly affect tendon mechanical properties. Type I collagen is the most abundant collagen (~ 95%) in tendons and provides the overall mechanical strength. Type III collagen is prominent in tendons or certain internal tendon regions that are more compliant, and, instead of type I, is primarily synthesised and upregulated after injury (Birch et al., 1998, Rees et al., 2014). Increased type III collagen concentration can reduce tendon material stiffness and results in an inferior mechanical function of injured tendons. Type II collagen can be found in

certain tendon regions frequently subjected to compressive forces, such as periarticular regions or around bony prominences (Benjamin and Ralphs, 1998, Waggett et al., 1998). Compressive forces can also induce upregulation of large aggregating proteoglycans (Section 1.2.3.3.2) which help to attract water to the tendon tissue, reducing and dissipating the detrimental compressive stress (Cook and Purdam, 2012). Interestingly, being the foundation of the tendon hierarchical structure, collagen content and types are largely similar between different species and among tendons of different functions (Elliott, 1965, Rumian et al., 2007).

The collagen molecule is composed of three polypeptide chains (α chains), with each chain containing primarily the repeating amino acid motif (Gly – X – Y). While X and Y can be any amino acid, proline and hydroxyproline are the most frequent. The three peptide chains form a right-handed triple helix with the small R group of all the glycine residues in the core while the larger R groups of amino acids in the X and Y position are on the surface of the collagen molecule. Collagen type I has two identical α1 chains and one α2 chain. Collagen type II and III are both homotrimeric, composed of three identical α chains (Kadler et al., 2007).

Within fibroblasts, polypeptide chains are synthesised and undergo a series of post-translational modifications (e.g., hydroxylation of proline and lysine) which are essential for maintaining the structural stability of the triple helix since these modifications directly affect the intra- and inter-molecular crosslinks formation (Section 1.2.3.2.1). Polypeptide chains are then associated and start to form the helical structure. This newly formed procollagen molecule is transported out of the cell to the ECM, where the cleavage of N- and C-terminal and the formation of covalent crosslinks starts (Hulmes, 2008).

Collagen in tendons is exceptionally long-lived and has little turnover after skeletal maturation compared to other non-collagenous proteins (Thorpe et al., 2010c, Heinemeier et al., 2013). However, traditional sampling methods only reflect the overall tendon composition while overlooking potential regional differences. One recent study that investigated different tendon compartments reported the turnover rate of collagen in the IFM is significantly faster than collagen in the fascicles (Choi et al., 2020). Interestingly, some studies suggested that although the majority (98%) of the collagen in the tendon does not turnover, a fraction of the collagen (likely from small diameter fibrils) is synthesised and removed based on the circadian rhythm (Yeung and Kadler,

2019). These recent discoveries suggest that the heterogeneity of the tendon may be related to the underlying protein dynamics, which is important for our understanding of tendon injury and healing.

1.2.3 Fibril Level

In the ECM, procollagen molecules self-assemble into collagen fibrils, in both linear and lateral directions (Silver et al., 2003). This is a spontaneous phenomenon but carefully regulated by enzymes, proteoglycans and other matrix components.

1.2.3.1 Collagen fibril assembly

The enzymatic removal of the N- and C-terminal of procollagen molecules triggers the self-assembly process that forms collagen fibrils resulting in a staggering structure that gives rise to the D-period (65 – 67 nm), a characteristic feature of collagen fibrils (Hulmes, 2008). With the help of lysyl oxidase, the lysine and hydroxyproline residues in the N- and C-terminal telopeptide regions are converted to aldehydes, and these aldehydes form intra- and inter-molecular crosslinks with other aldehydes, lysine, or hydroxylysine residues that stabilise the fibril structure.

Five collagen molecules bond together and form pentafibrils (or microfibrils), a subunit of the fibril. Pentafibrils are then packed, oriented toward the long axis of the tendon to form fibrils. Fibrils are often regarded as the smallest structural unit of the tendon. Type I collagen fibrils are up to 1 cm long and 500 nm in diameter (Shoulders and Raines, 2009), but some recent studies suggested that fibrils may be continuous and undisrupted along the length of the whole tendon, with considerable variation in fibril diameters (Svensson et al., 2017, Hijazi et al., 2019). Insufficient proteoglycan interaction at this stage can negatively affect fibril formation and structural integrity, consequently altering the mechanical properties of the tendon.

Collagen type V, usually co-assembles with type I collagen and helps to regulate fibril assembly and control fibril diameter (Fichard et al., 1995, Hulmes, 2008). The final step of fibril formation is the attachment of other ECM molecules, such as proteoglycans or fibronectin, to form a stabilised fibril structure.

1.2.3.2 Collagen crosslinks

1.2.3.2.1 Enzymatic mediated crosslinks

Many collagen crosslinks are induced by the oxidation of specific lysine or hydroxylysine residues that form lysine- or hydroxylysine-aldehydes. These aldehydes later react with hydroxylysine from an adjacent molecule and form a Schiff base, or aldimine, inter-molecular crosslink. The divalent aldimine crosslink can form two immature crosslinks: deH-HLNL and deH-LNL. The Schiff base can also form a keto-amine, HLKNL, by the Amadori rearrangement. The deH-HLNL reacts with histidine to form the mature crosslink HHL, while keto-amine later forms Hyl-Pyr and pyrroles crosslinks (Avery and Bailey, 2008). The increased concentration of these mature crosslinks correlates with the mechanical strength of adult animal tendons. However, the altered mechanical properties in aged tendons are associated with an increase in non-enzymatic mediated crosslinks instead of changes to the mature enzymatic mediated crosslinks levels (Snedeker and Gautieri, 2014, Svensson et al., 2018).

1.2.3.2.2 Non-enzymatic mediated crosslinks

As tendon ages, the adventitious, non-enzymatic mediated reaction between collagen and glucose forms different crosslinks to the enzyme-

mediated crosslinks, which plateau in concentration after skeletal maturation. The process ultimately leads to the formation of advanced glycation end-products (AGEs). Glycation is considered the main contributor to age-related and diabetic-related mechanical changes in almost all the tendon hierarchical levels (Fessel et al., 2014, Gautieri et al., 2017). Two prominent AGEs identified in tendons are pentosidine and glucosepane, with the latter having a greater quantity and thus more likely to contribute a significant mechanical or physiological impact than other AGE crosslinks. A recent study combining molecular modelling and sequential enzymatic digestion of human tendon tissues quantified and isolated the effect of glucosepane on the structural and material properties of type I collagen (Nash et al., 2019). The results demonstrated that glucosepane can disrupt the local collagen triple helix structure and increase water content within and between fibrils. These nanoscale changes were also associated with an altered thermo-kinetic property of aged tendons.

Collagen in human tendons shows minimal renewal after skeletal maturation (Heinemeier et al., 2013), making tendons especially prone to the accumulation of AGEs. Besides age advancement, a high-sugar diet (Lingelbach et al., 2000) and the lack of physical activity (Couppe et al., 2014)

can both increase the rate of AGEs accumulation in tendons and other collagenous tissues. The level of AGEs in tissue can be conveniently measured by its fluorescence since most of the AGEs are fluorescent. This fluorescence level can be easily measured by conventional biochemistry or using spectroscopic methods.

1.2.3.3 Proteoglycan

Proteoglycans are a sub-category of glycoproteins having one or several long polysaccharide chains (glycosaminoglycans, GAG). Proteoglycans are the most abundant non-collagenous component in tendons and play a crucial role in both the mechanical and biological functions of the tendon, mainly by maintaining structure integrity, providing structural support, and modulating collagen fibrillogenesis and fibril diameter (Yoon and Halper, 2005, Parkinson et al., 2011). Common proteoglycans found in tendons can be categorised into small-leucine rich proteoglycans (SLRP) or large aggregating proteoglycans by their molecular size. The distribution of proteoglycans shows regional variation within tendons, with SLRPs (such as decorin and biglycan) predominantly in the tensional region and the larger proteoglycans usually in the compressive region (Rees et al., 2000, Yoon and Halper, 2005).

Traditionally, GAGs are believed to alter the mechanical properties of the attached protein (proteoglycan) and affect the tendon level mechanics. However, many recent studies have suggested that the removal of GAG does not significantly affect the tensile, shear, or viscoelastic properties of the tendon (see review (Ryan et al., 2015)). Negatively charged GAG molecules can help to attract water and provide resistance to compressive force in tissues, as in cartilages (Henninger et al., 2010). GAG content within tendons can change with age, physical activity levels, and pathologies (Ryan et al., 2015). Although measuring total GAG content is an easy way to quantify the whole proteoglycan content in tendons, investigation of spatial distribution and quantification of individual proteoglycan are often required for a detailed analysis of tendon composition.

1.2.3.3.1 Small-leucine rich proteoglycans (SLRP)

SLRP is the dominant type of proteoglycan in tendons. The SLRP decorin accounts for approximately 80% of the total proteoglycan in the tensional region of tendons (Samiric et al., 2004). It has a U-shape core protein structure with both ends attach to collagen molecules in the gap region of the fibril (Samiric et al., 2004). The single GAG side chain of decorin can interact with the GAG chain from another decorin, forming a bridge between adjacent

fibrils and enabling fibril-to-fibril interactions (Vesentini et al., 2005). Decorin regulates fibrillogenesis and fibril bundling in both longitudinal and lateral directions (Zhang et al., 2005). With insufficient decorin concentration, collagen assembles into fibrils with variable (usually larger) diameters, and these fibrils form a mechanically loose and weak network structure *in vitro*, decreasing the overall mechanical strength (Iwasaki et al., 2008). Decorin knock-out mice showed decreased tendon viscoelastic but not tensile properties compared to wild type mice (Elliott et al., 2003, Dourte et al., 2012).

Biglycan, another SLRP with two GAG side chains, shares the same binding site with decorin on type I collagen. It has some overlapping function with decorin in regulating fibril structure, and an acute absence of both SLRPs causes a shift in fibril diameter distributions and alters tendon level mechanical properties in mature tendons, suggesting their role in maintaining tendon homeostasis (Robinson et al., 2017). Decorin and biglycan can be found between fibrils (Samiric et al., 2004) and fascicles (Kim et al., 2010). In knock-out mice models, biglycan was reported to have less effect on the tendon mechanical properties than decorin (Dourte et al., 2013). Biglycan is highly expressed during post-natal periods (Zhang et al., 2005) and after tendon injury (Dunkman et al., 2014).

1.2.3.3.2 Large aggregating proteoglycans

Both aggrecan and versican are highly glycosylated and have numerous GAG chains attached to the core protein, resulting in their large molecular weight. These GAG chains help to attract water (can reach 50 times of their molecular weight) and significantly increase the resistance of the tissue to compressive forces (Benjamin and Ralphs, 1998). Aggrecan and versican are usually localised in the fibrocartilage region of the tendon. This localised distribution of large aggregating proteoglycans at the compressive region of the tendon is an adaptative response initiated by tendon cells, which also demonstrate some characteristic features of chondrocytes (see review (Vogel, 2004)). In fibrocartilage, inter-fibril aggrecan aggregates provide compressive stiffness for the tissue and dissipate the force imposed on collagen fibres by providing a viscous environment. Aggrecan is also detected in human supraspinatus tendon fascicles, suggesting its potential role in the fascicle level mechanics (Vogel, 2004).

Versican can be found around tenocytes, in the IFM, and around micro-vessels in tendinopathic tendons (Bode-Lesniewska et al., 1996, Scott et al., 2008). Increased synthesis of large proteoglycans in pathological tendons

could potentially result from the increased cellularity or an altered local mechanical environment (Koob et al., 1992).

1.2.4 Fibre Level

1.2.4.1 Fibre

Fibrils aggregate into fibres. The diameter of collagen fibres ranges from 10 to 50 μm. This hierarchy level is less well-defined than the fibril or the fascicle and is sometimes confusing in the literature due to the ambiguity of the general meaning of ‘fibre’. At this level, structural tendon characteristics can be visualised using light imaging techniques, and functionally different tendons demonstrate distinct fibre alignment and structural features (Thorpe et al., 2013b) (Figure 1-2). Moreover, tendon cells align to the fibre in the longitudinal direction. Tenocytes can sense the mechanical load imposed on fibres and consequently affect their gene expression and the following biological cascades; however, details of the mechano-transduction mechanism remain unknown.

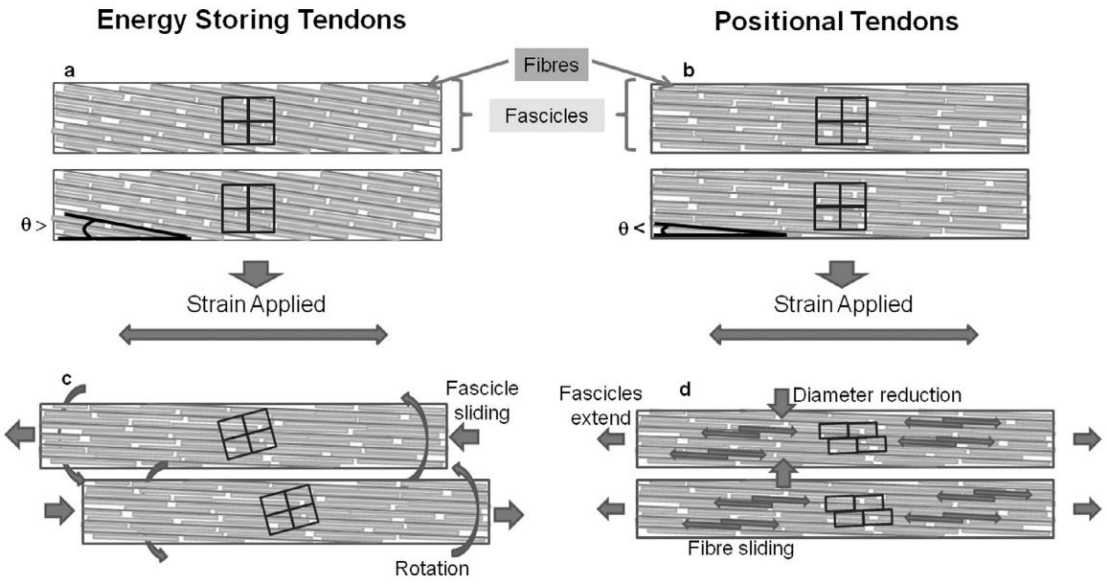

Figure 1-2. Schematic illustration of fibre orientation and strain behaviour in functional different tendons (adapted from (Thorpe et al., 2013b)). (a) un-strained energy-storing tendons, (b) un-strained positional tendons, (c) strained energy-storing tendons, (d) strained positional tendons.

Different fibre structure exists between energy-storing and positioning tendons and between healthy and injured tendons. In the energy-storing equine SDFTs, the fibres are twisted into a helical structure, which seems not to be present in the positional CDETs (Thorpe et al., 2013b). Ruptured and injured tendons have a smaller fibre diameter and fibril crimp angle than healthy tendons (Jarvinen et al., 2004, Spiesz et al., 2018). Having a larger crimp angle extends the toe region of the stress-strain curve of tendons but does not affect the linear region (Shearer et al., 2017). These structural differences at the fibre level contribute to the overall tendon mechanical

behaviour (Section 1.3.2) and are likely the result of functional specialisation moderated by the interaction between tenocytes and the surrounding ECM.

1.2.4.2 Tendon cells

The main component of the tendon cell population is the tenocyte, a specialised type of fibroblast, which produces ECM proteins and maintains tendon homeostasis. Tenocytes are long-shaped cells attached to tendon fibres and sensitive to strain intensities. Both under- (3% *in vitro* strain) and over-strain (9%) can induce catabolic responses such as disordered fibre structure and organisation, increased cell roundness and apoptosis rate, and upregulated collagen type III synthesis and matrix metalloproteinase (MMP) expression (Wang et al., 2013b).

Cells are abundant in tendons during early life and gradually decline as age advances. Foetal bovine tendons are high in cellular density and have similar cell shapes across different tendon regions. In adult tendons, cellular density decreases to only about 10% of the foetal tissue, and cell shapes demonstrate spatial differences between tensional and compressive regions (Perez-Castro and Vogel, 1999). Aged tendons are generally lower in cellular content than younger tendons. Interestingly, a study conducted on a total of

32 equine SDFTs showed no significant cell number decline and the synthetic ability of tendon cells remained throughout life (Thorpe et al., 2016b). The authors suggested that the age-related decline in tendon function and reduced repair ability cannot be attributed to cellular changes alone. Besides low cell count in adult tendons, these tenocytes are relatively dormant unless triggered by injury. Following injury, tendon cells can migrate to the injury site and proliferate, resulting in the consequent ECM protein synthesis (Lundborg et al., 1985, Maffulli et al., 2002).

Both excessive and insufficient load imposed on tendons are detrimental to tendon cell metabolism. High tendon strains can induce apoptosis in a relatively short timeframe (6 hours), as measured by single-strained DNA breaks and caspase-3 cleavage (Scott et al., 2005). Tendon overload causes tenocytes to become more rounded and increase the secretion of inflammatory and matrix degradation markers (Thorpe et al., 2015a). On the other hand, stress deprivation causes a catabolic response initiated by tendon cells, including increased MMP levels and cell apoptosis (Arnoczky et al., 2007, Egerbacher et al., 2008). Unloading tendons also causes an increased level of pro-inflammatory cytokines and matrix turnover markers. However, these changes do not seem to result in an immediate

change in either gross collagen, GAG, or DNA levels within a week (Connizzo and Grodzinsky, 2018). Fatigue loading can also induce cell apoptosis, but interestingly, tendons subjected to higher loading cycles (7200 cycles) did not exhibit higher apoptotic activity than tendons subjected to much fewer (100) cycles (Andarawis-Puri et al., 2014).

MMPs are a family of cell-secreted endopeptidases that degrade ECM proteins and are an important regulator in many biological and pathological processes. The tissue inhibitors of metalloproteinases (TIMPs) are the primary endogenous inhibitor of MMPs (Murphy, 2016). The balance between MMPs and TIMPs activity is crucial for regulating tendon remodelling. MMP-1, MMP-8, and MMP-13 are called collagenases and can cleave the fibrillar collagens (type I, II, and III) at a specific glycine-isoleucine or glycine-leucine bond ((Williams and Olsen, 2009) and review (Del Buono et al., 2012)). The synthesis rate of MMPs is generally low but can be upregulated by stimuli from cytokines, growth factors, or cell-cell and cell-matrix interactions (Del Buono et al., 2012). The relationship between tendinopathy and MMPs is reviewed in Section 1.5.1.

Chronic tendinopathy has been considered a degenerative process with minimal inflammation. However, several studies have identified inflammatory cells residing in tendons and the inflammatory-mediated process that governs ECM protein synthesis and degradation (Section 1.5.1 and review (Rees et al., 2014, Jomaa et al., 2020)). Recently, tendon progenitor cells have been identified within tendons. With the ability to self-renew and differentiate into tenocytes, tendon progenitor cells are believed to play a role in normal tendon homeostasis and repair (Costa-Almeida et al., 2015).

1.2.5 Fascicle Level

1.2.5.1 Fascicle

Fascicles (50 – 400 μm) are visible to naked eyes (Handsfield et al., 2016) and can be dissected out with care and the aid of a dissection microscope. This is the smallest hierarchical level that allows 'macroscopic' mechanical testing and is a generally continuous structure connecting musculotendinous and osteotendinous junctions. Fascicles from energy-storing tendons demonstrate a more helical arrangement of fibres than positional tendons (Thorpe et al., 2013b), suggesting a close relationship exists between fascicle structure and tendon function. Between fascicles lies

the inter-fascicular matrix (IFM, or endotenon), an extrinsic component according to the definition proposed by Snedeker and Foolen (2017) that has more synovial-related characteristics. Cells within the IFM are distinct from those intra-fascicular cells (i.e., tenocytes lying adjacent to fibres) and are more metabolically active compared to the dormant tenocytes in matured tendons (Section 1.2.5.2).

1.2.5.2 Inter-fascicular matrix (IFM, endotenon)

The IFM is rich in proteoglycans, glycoproteins, and elastic fibres, contrary to the fascicles which are predominantly composed of collagen (Thorpe et al., 2013a, Thorpe et al., 2016a, Thorpe et al., 2016c). Lubricin and elastin are localised to the IFM and both are important in facilitating fascicle sliding and rotation during tendon loading. It has been suggested that the age-related decline of both proteins disrupts this optimal sliding behaviour and may predispose aged tendons to injury (Section 1.3.3).

Studies have identified different compositions between fascicles and IFM, and these differences exist between functionally different tendon types and between young and aged tendons (Thorpe et al., 2016a, Thorpe et al., 2016c). The fascicle consists of more extracellular matrix proteins but the IFM

has more cell-related proteins (Thorpe et al., 2016c). More fragmented proteins with faster tissue turnover rates are found in the IFM compared to the fascicle, suggesting a greater matrix degradation and synthesis in this compartment (Thorpe et al., 2016c, Choi et al., 2020). The IFM is rich in collagen type III, which is more compliant than collagen type I, while the fascicle is predominantly composed of type I collagen (Thorpe et al., 2016c). Generally, total protein abundance in the IFM does not reduce with age but lubricin and elastin show age-related reduction in both mRNA (Kostrominova and Brooks, 2013, Thornton et al., 2015) and protein levels (Godinho et al., 2017). Cell number in the IFM is significantly higher than the fascicle, and cell morphology differs with rounder cells in the IFM and elongated cells in the fascicle (Thorpe et al., 2016c). Neurovascular tracts and fat droplets can also be found in the IFM (Haraldsson et al., 2008). Together, these findings suggest that the IFM is actively involved in maintaining tendon homeostasis and may play an important role in tendon injury and repair (Haraldsson et al., 2008, Snedeker and Foolen, 2017, Cook and Screen, 2018).

1.2.5.3 Glycoprotein – lubricin

Lubricin (also known as superficial zone protein or proteoglycan 4) is a type of glycoprotein secreted by synovial cells and chondrocytes to improve

joint lubrication and to prevent cell and protein adhesion (Funakoshi et al., 2008). It was initially identified in articular cartilages and fibrocartilage regions of certain tendons, but later discoveries revealed a wider distribution within animal tendons (Sun et al., 2006, Funakoshi et al., 2008, Sun et al., 2013, Thorpe et al., 2016a) and human Achilles tendons (Sun et al., 2015). Lubricin is localised predominantly to the IFM of both SDFT and CDET, suggesting its role in facilitating sliding between fascicles (Thorpe et al., 2016a). It is reported that imposing mechanical stimuli on chondrocytes upregulates lubricin synthesis and secretion *in vitro* (Grad et al., 2005). Short-term unloading of canine tendons showed a 40% decline in both lubricin expression and content, but interestingly, this lower lubricin content in unloaded tendons did not significantly increase the tendon gliding resistance (Sun et al., 2013). However, decreased lubricin content in more chronic conditions seems to correlate with the deterioration of overall joint functions. For example, a significant reduction of intra-articular synovial fluid lubricin content has been observed in osteoarthritis and anterior cruciate ligament (ACL) injury patients (see review (Jay and Waller, 2014)), but whether lubricin content changes in tendon pathologies remains unknown.

1.2.5.4 Elastic fibre

Elastic fibres account for approximately 2% of the tendon dry weight and provide the elasticity and resilience of tendons since they can be stretched up to 1.5 times the initial length without failure (Kristensen and Karsdal, 2016). Elastic fibres are primarily found in arteries, lungs, and skin tissues. The main component of an elastic fibre is elastin (~ 90%), with a small percentage of fibrillin and fibulin (Kristensen and Karsdal, 2016). Tropoelastin, the precursor of elastin, is secreted by fibroblasts or chondrocytes and cleaved before processing to elastin. These elastin monomers can crosslink to form desmosine and isodesmosine. Due to its highly crosslinked and hydrophobic properties, elastin is remarkedly stable and can resist proteolytic degradation (Kristensen and Karsdal, 2016). Like collagen, the elastin turnover rate diminishes quickly after adulthood. In mature tissues, the accumulation of elastin fragments, as the result of repetitive stretch and recoil (Godinho et al., 2017), can be used as an indicator of tissue pathology or reflecting the 'tissue age'. Interestingly, the elastin fragments could also serve as physiological mediators in lung or skin diseases (Kristensen and Karsdal, 2016); however, its physiological role in tendon homeostasis is currently unknown.

In tendons, elastin can be found localised around tendon cells (Grant et al., 2013, Pang et al., 2017) and in the IFM (Godinho et al., 2017). Elastin content in the equine SDFT is significantly higher than the CDET, suggesting that higher elastin may account for the high stretch-recoil ability of energy-storing tendons (Godinho et al., 2017). Age-related decline of elastin content and the increased disorganisation of elastic fibres are also reported in the SDFT (Thorpe et al., 2015b, Godinho et al., 2017). In human supraspinatus tendons, elastase treated tendons showed significantly lower shear stress at the lower experimental strains (Fang and Lake, 2016). Similarly, another study on porcine ligaments demonstrated peak stress and elastic modulus reduction after elastase treatment (Henninger et al., 2015). Together, these studies suggest that the elastin content can affect tendon axial and shear mechanical behaviour.

Elastin distribution can be semi-quantified by histological stains or immunohistochemistry techniques (Thorpe et al., 2016a). For quantification, native elastin is heated and hydrolysed multiple times to convert it into α-elastin, which can be compared with standards using spectrophotometric methods (Godinho et al., 2017). Elastin fragmentation can be indirectly measured by quantifying desmosine content from soluble proteins using

GuHCl extraction and ELISA (Gunja-Smith, 1985). Besides biochemical assays, vibrational spectroscopic methods are also used in studying elastin structures (Debelle et al., 1995, Debelle et al., 1998). However, most of the studies used purified or concentrated elastin to obtain the isolated spectrum. The spectroscopic method for the quantitation of elastin within tendons remains challenging due to the low content and highly localised distribution.

1.2.6 Sub-tendon and Tendon Levels

Tendon transmits force produced by muscular contraction through the musculotendinous junction, tendon proper, and osteotendinous junction to the bony insertional site. Certain tendons, such as the Achilles tendon of humans, rats (Finni et al., 2018) and rabbits (Pang et al., 2017), have multiple sub-tendon structures that originated from different muscle bellies. Fascicles from these sub-tendons do not intertwine and can be regarded as different functional units within the tendon. Human Achilles sub-tendon structural features are introduced in Section 1.4.2.1.

It has been suggested that having individual control of different sub-tendons allows better mechanical output from muscles due to the distinct anatomy and different functional requirements between the gastrocnemii and

soleus muscles (Finni et al., 2017, Maas and Finni, 2018). However, since the sub-tendon geometry and morphology differ greatly among individuals (Section 1.4.2.1), sub-tendon mechanics can have high individual differences. For the individual control of sub-tendons to happen, the interface, termed inter-sub-tendon matrix (Gains et al., 2020), must enable a certain level of sliding. This sliding ability is reported to decline with age and after injury (Section 1.4.4).

Tendon is surrounded by epitenon, a continuous structure from the IFM with no clearly separable characteristics. It has been shown that in the rat Achilles tendon, the inter-sub-tendon matrix has a similar composition to the IFM, such as high collagen III, elastin, lubricin content and cellularity (Gains et al., 2020). There is no clear difference between the IFM and the inter-sub-tendon matrix under visual inspection. Therefore, it may be possible that the IFM, inter-sub-tendon matrix and epitenon are one continuous viscous structure with regional adaptation facilitated by the local mechanical demand. Intuitively, the inter-sub-tendon matrix is subjected to higher shear stress than the IFM, which is presumably more homogeneously loaded within each sub-tendon. The epitenon is more likely subjected to frictional or compressive forces from other peritendinous tissues.

For some tendons, the paratenon (tendon sheath or tendon envelope) wraps around the tendon to reduce the friction between the tendon and other peritendinous tissues (Thorpe and Screen, 2016). The paratenon is composed of different types of tissues including synovial and adipose tissues and is rich in blood supply and innervation, with certain sensory neuro-mediators found in the paratenon (Ackermann, 2013). The paratenon is highly metabolically active and sensitive to physical exercise (Langberg et al., 1999) and can initiate immune responses once injured, suggesting its role in traumatic tendon injuries and repair (Ackermann et al., 2016). However, these periphery responses seem to have minimal influence on the tendon core.

1.3 Tendon Multiscale Mechanics

The tendon is an anisotropic fibrous composite biological tissue with viscoelastic properties. Mechanical characterisation of tendons primarily focuses on tensile loading through its longitudinal axis since the major function of the tendon is to transmit tensile loads. Viscoelastic properties of tendons significantly affect the overall mechanical behaviour, especially during fatigue loading or under different loading rates. The viscoelastic

properties of tendons are independent of muscular strength and the CSA of the tendon (Suydam et al., 2015), suggesting potentially different mechanisms exist between modulating viscoelasticity and tensile properties. However, axial loaded, conditioned tendons are sometimes considered to be pure hyperelastic, neo-Hookean solids for simplification in modelling studies (Section1.6.2), as tendons almost completely recover to their initial length even when subjected to relatively large strains.

The Young's modulus (or elastic modulus) decreases as the hierarchy level moves up spatially. This supports the idea that the whole tendon level mechanics is heavily influenced by both sub-structure sliding at the interface between fibrous components and the straightening, rotation, or re-arrangement of the stiffer lower hierarchies (Sherman et al., 2015). Although it is possible to isolate sub-components for mechanical testing, this artificial removal of one structure from its native environment may affect the testing results and should be interpreted with caution (Thorpe et al., 2012).

1.3.1 Molecular and Fibril Levels

Using atomistic modelling, it is calculated that the collagen molecule shows a linear strain response between 2.5 to 4.0% strain and has an

average Young's modulus of 4.8 ± 1.0 GPa (Lorenzo and Caffarena, 2005). Tissue hydration level significantly affects its mechanical properties. Drying tendons causes conformational changes to the collagen molecules and complete drying (~ 5% hydration) of tendons creates large stress on collagen molecules of approximately 100 MPa, many orders above the estimated peak stress during muscle contractions, 0.4 MPa (Masic et al., 2015).

The mechanical strength of collagen molecules and fibrils is primarily attributed to the intra-molecular and inter-molecular crosslinks. Immature tissues, characterised by having high immature collagen crosslink concentrations, are mechanically weaker than mature tissues. In rat and chicken tendons, inhibition of lysyl oxidase causes reduced Young's modulus and ultimate tensile strength (see review (Eekhoff et al., 2018)). In aged or diabetic tendons, the accumulation of AGEs has a widespread effect on the tendon mechanical properties, such as increased modulus and ultimate tensile strength in small animal tendons (Svensson et al., 2018). However, the correlation between crosslinking and tendon mechanical properties is sometimes inconclusive and likely depends on the species studied and the experiment methodology (Thorpe et al., 2010b, Eekhoff et al., 2018). At the molecular level, the presence of glucosepane significantly increases the

tensile Young's modulus of collagen molecules by 3.0 to 8.5% in low (< 15%) strains (Collier et al., 2018).

The Young's modulus of type I collagen fibrils ranges from approximately 0.2 to 1.0 GPa, depending on the measurement protocol and method (Sherman et al., 2015). Normally, the load transmitted through fibrils is dissipated by inter-fibrillar shear stress, creating inter-fibrillar sliding (Szczesny and Elliott, 2014a, Szczesny and Elliott, 2014b). It has been suggested that overuse damage is initiated in the inter-fibrillar structure, demonstrated by the non-recovery of fibril slippage in fatigue loaded rat tail tendons (Lee et al., 2017). The authors suggested that fibril kinking or rupture are likely to be secondary events occurring after this impaired sliding ability. Interestingly, one study suggested that the inter-fibrillar load sharing is not achieved by the ECM proteins but is likely from smaller diameter fibrils or lateral fusion of fibrils (Szczesny et al., 2017). The exact inter-fibrillar sliding mechanism warrants further research. Fibril sliding is decreased in methylglyoxal (MGO) treated rat tail tendons and results in an increased ultimate tensile strength, but the study showed no difference in Young's modulus between treated and control fibrils, suggesting the change in the tendon level material stiffness in aged tendons may originate from other

hierarchies (Fessel et al., 2014). In human dermal collagen fibrils, the transverse elastic modulus is lower in old compared to young tissue donors and is related to the interaction between hydrophilic AGE crosslinks and collagen fibril density modulated by water retention (Ahmed et al., 2017). Fibrils in aged tendons also demonstrate lower viscoelasticity compared to those in younger tendons (Gautieri et al., 2017).

1.3.2 Fibre

The Young's modulus of fibres ranges from approximately 100 to 500 MPa (Sherman et al., 2015). In rat tail tendons, shear at the fibre level can contribute to approximately half of the tensile strength of the single fascicle (Kondratko-Mittnacht et al., 2015). In equine SDFT, fibres are orientated helically relative to the tendon longitudinal axis and show greater rotation but less sliding when loaded compared to the CDET, providing greater strain recovery and less hysteresis (Thorpe et al., 2013b). In the transverse (perpendicular to the long axis) direction, fibres from the CDET show greater strain than the SDFT. CDET fibres also have a higher Poisson's ratio than the SDFT. The recovery of fibre longitudinal and transverse strains and sliding are higher in the SDFT than in the CDET (Thorpe et al., 2013b).

A study using bovine DDFT in shear and compressive fibre level mechanical tests demonstrated that fibre sliding, rotation, and realignment all contribute towards normal tendon elongation under load (Fang and Lake, 2015). Regional differences in fibre mechanics were also reported despite having similar gross tensional properties. The authors suggested that changes in fibre orientation are likely the result of regional ECM adaptation to meet the mechanical demands.

Age-related mechanical changes at the fibre level are more prominent in the SDFT than in the CDET. Aged SDFT fibres show lower transverse strain, less rotation, and less recovery from stretch compared to younger SDFT fibres (Thorpe et al., 2013b). Similarly, decreased fibre sliding is confirmed in ribose-treated rat tail tendons (Gautieri et al., 2017). Therefore, the age-related increase of injury risk at the fibre level could result from a failed compensatory response. Fibre helical angle decreases in aged tendons, reducing the fibre rotation during load. As a result, the sliding between fibres increases to match the ultimate fascicle level strain but may fail to recover after a finite number of cycles (Thorpe et al., 2014), imposing a greater load on fibres and leading to injury.

1.3.3 Fascicle

A substantial amount of research has been conducted to compare equine SDFT (energy-storing) with CDET (positioning) to understand the fascicle level and whole tendon level mechanics. The Young's modulus of fascicles ranges from 200 to 700 MPa, depending on the species or tendons studied (Screen et al., 2004, Komolafe and Doehring, 2010, Thorpe et al., 2012). At the tendon level, the SDFT has a greater ultimate strain and lower modulus than the CDET. However, at the fascicle level, both tendons showed similar moduli and the CDET fascicles showed a greater ultimate strain, closer to the value of the whole tendon (Thorpe et al., 2012). This discrepancy between fascicle and tendon strain in the SDFT suggested that the IFM strain contributes significantly to the whole tendon level mechanics.

The difference in failure strains between the SDFT fascicles and the whole tendon was approximately 10% and can be achieved by IFM displacement alone with only about 30% of its failure force (Thorpe et al., 2012). Studies conducted on human patellar and Achilles tendon fascicles and bovine hindlimb flexor tendons however showed minimal force transmission between fascicles, suggesting a minimal influence of the IFM on

fascicle mechanics (Haraldsson et al., 2008, Purslow, 2009, Komolafe and Doehring, 2010). It is not known whether the difference arises from different species or different tendons tested. The IFM sliding capacity is reduced in aged equine tendons (Thorpe et al., 2013c). Although the ultimate tensile properties of the IFM were similar between young and old tendons, a greater toe-region and a larger area under the force-elongation curve were evident in aged tendons, suggesting a higher force is required for a given displacement (Thorpe et al., 2013c). This could be detrimental since fascicles have less repair capacity than the IFM (reviewed in Section 1.2.5.2).

In aged equine SDFT, the IFM showed a decreased displacement when loaded and lower fatigue resistance compared to young tendons (Thorpe et al., 2017). This decrease in fatigue resistance coincides with the reduction in elastin content of aged tendons (Godinho et al., 2017). Interestingly, the failure force and displacement were similar between the two age groups (Thorpe et al., 2017). The authors concluded that the IFM sliding capacity is reduced under physiological loads and could prematurely impose strain on fascicles. Fascicles, mainly collagenous matrix, have a lower repair capacity due to having a longer turnover rate compared to the IFM (Thorpe et al., 2013a). This sliding capacity could be a specialised adaption for energy-

storing tendons since minimal age-related mechanical and compositional changes are found in the positioning CDET.

Both SDFT fascicles and IFM can withstand a great number of loading cycles and have lower hysteresis and creep compared to the positioning CDET (Thorpe et al., 2016d). Interestingly, both SDFT fascicles and IFM showed a similar degree of age-related reduction in fatigue resistance but not viscoelastic properties (Thorpe et al., 2017). The difference in fatigue resistance between young and old tendon fascicles could result from the altered helical fibre structure and fibre-level loading responses (Section 1.3.2). The reduced mechanical properties after fatigue loading can also be explained by a shear lag model, suggesting plastic, not elastic, deformation of the inter-fibrillar structure after loading (Lee et al., 2017).

Induced glycation can drastically reduce post-yield fascicle mechanical properties in rat tail tendons. Ribose treated fascicles have increased failure stress and a decreased failure strain compared to control fascicles, but both treated and control fascicles have similar Young's modulus. Treated fascicles demonstrated decreased stress relaxation, suggesting glycation can affect viscoelastic properties at the fascicle level (Gautieri et al., 2017).

1.3.4 Sub-tendon

Despite not being thoroughly studied, the complex mechanical behaviour of sub-tendons is likely influenced by a combination of different factors including the tensile force from different muscles, shear stress from neighbouring sub-tendons, the inherent mechanical properties of sub-tendons and inter-sub-tendon matrix, and the different shape and geometry of each sub-tendon. How these factors interact is explored using modelling techniques in Chapters 6 and 7. Having individual control of each sub-tendon may better fulfil the functional requirements of the human Achilles tendon, compared to having one homogeneous, uniform tendon. The gastrocnemii muscles are smaller than the soleus and spanning across both knee and ankle joints and serve with a more explosive role that facilitates forward propulsion (McGowan et al., 2008, Angin and Demirbüken, 2020). Soleus and gastrocnemii muscles also show different neuromechanical properties (Crouzier et al., 2018), different morphological changes after stretching exercises (Simpson et al., 2017) and after prolonged unloading (Seynnes et al., 2008). With a uniform Achilles tendon, these structural and functional differences between muscles are unlikely to exist. Besides, the human ankle (sub-talar) joint and foot are highly mobile to allow firm ground contact in uneven terrains. Having

individual control of certain muscle-(sub-)tendon units may help to dissipate the multidirectional ground force, resulting in a balanced and stable stance.

In rat Achilles tendons, one study demonstrated that the sub-tendon displacements are highly variable between different loading conditions (Finni et al., 2018). When the soleus and lateral gastrocnemius muscle were loaded, the connected sub-tendons showed greater strains (e.g., soleus sub-tendon strain when soleus muscle was stimulated) compared to the other unloaded sub-tendons. Interestingly, when the medial gastrocnemius muscle was stimulated, both soleus and lateral gastrocnemius sub-tendon showed minimal to even negative strains, suggesting a potentially loose mechanical coupling between medial gastrocnemius and the other two sub-tendons. The inter-sub-tendon matrix between rat soleus and gastrocnemius has been mechanically tested through shear loading (Gains et al., 2020). Their result demonstrated an extended toe region that could enable free sliding between sub-tendons under low loads while ensuring force transmission between sub-tendons in higher loads.

For human Achilles sub-tendons, many *in vivo* studies have used sagittal plane ultrasound with speckle tracking technique and arbitrarily assigned the

superficial (posterior) tendon region to gastrocnemii and the deep (anterior) region to the soleus sub-tendon. However, considering the highly variable individual tendon shape and geometry (Section 1.4.2.1), arbitrary assigning sub-tendon territories is likely to produce an experimental error, especially when comparing between different individuals. Despite this limitation, these ultrasonography studies provide indirect but valuable knowledge for our understanding of sub-tendon mechanics, and this relatively easy application of ultrasound methodology has been widely used in physiotherapy and sports medicine fields. These *in vivo* results are reviewed in Section 1.4.4.

Recently, finite element analysis (FEA) has been used for studying human Achilles sub-tendon mechanics by manipulating simulated muscular force on subject-specific tendon morphologies. One study reconstructed an Achilles tendon model from MRI scanning and arbitrarily assigned the sub-tendon territories and imposed different proximal muscular forces to replicate the reported *in vivo* displacement non-uniformity by ultrasound speckle tracking (Handsfield et al., 2017). Their results demonstrated that having a compliant interface for sub-tendon sliding is important for reproducing the observed displacement non-uniformity. Another study reconstructed the gross (tendon level) shape of the Achilles tendon then incorporated fascicles with

different degrees of twist and conducted simulated failure tests (Shim et al., 2018). The results suggested that both high and low twist angles reduced rupture force, and the optimal twist angle for improving tissue strength is between 15° and 30°, corroborating a previous report suggesting that stress responses in tendons are more sensitive to the tendon geometry than the mechanical properties of the tissue (Hansen et al., 2017).

1.3.5 Tendon

Wren and colleagues (2001) studied the *in vitro* mechanical properties of Achilles tendons by conventional mechanical testing protocols. In total 11 pairs of Achilles tendon specimens (35 to 80 years) were subjected to tensile testing to failure and their results showed that the Young's modulus was on average 819 ± 208 MPa, with high failure force (5098 ± 1199 N) and high failure strain (14.5% ± 3.2%). The study also reported a negative correlation between the specimen age and the measured mechanical properties.

The earliest attempt to directly measure *in vivo* Achilles tendon stress and strain was performed by inserting buckle transducers under surgery (Komi et al., 1987, Ravary et al., 2004). Strain gauges are attached to the transducers and their deformation, caused by tendon movements, alters the

output electrical resistance. The output signal is then calibrated, usually in-directly by inverse dynamics in human studies, to convert the signal into tendon stress and strain (Ravary et al., 2004). Earlier studies reported that *in vivo* Achilles tendon force during hopping (3786 N) was higher than static jump (2233 N) and counter-movement jump (1895 N) in one healthy young male participant (Fukashiro et al., 1995); Achilles tendon force during walking, measured by invasive optic fibre, was approximately two times the body weight (~ 1500 N) (Finni et al., 1998); and a single bout of dorsiflexion stretch (1.2 rad/s) exerted just over 300 N on the Achilles tendon (Nicol and Komi, 1998). The limitation of this approach includes the requirement of surgical procedure and post-surgical pain affecting movements, potential impingement or compression from peripheral tissues, and the inevitably induced tendon curve that could alter the load distribution (Ravary et al., 2004).

In vivo, non-invasive measurements of human tendon level mechanical properties are predominately performed using ultrasonography combined with a dynamometer to circumvent the need for surgical insertion of force transducers. This indirect approach includes fixation of the ankle joint before participants perform a ramped isometric contraction during which the produced ankle torque is measured continuously. Torque is then converted to

force by dividing the ankle joint moment arm. Using an ultrasound probe placed at the musculotendinous junction, tendon displacement is calculated from the ultrasound image by measuring the movement of an anatomical marker, usually the tendon junction or muscle fascicles, during ramped contractions. Then, the force-displacement relationship (such as the material stiffness) of the tendon can be calculated. Additional quality control methods include correcting for the antagonist muscle contribution by using electromyography (EMG) and the inevitable ankle joint rotation by motion sensors. Participants are usually required to perform ramped maximal isometric contractions lasting a few seconds to fully obtain the load-displacement relationship of the tendon (as in (Magnusson et al., 2001)). This method allows the non-invasive measurement of tendon mechanical properties and has been widely applied. However, the contraction time significantly affects the measured mechanical properties, making studies using different protocols difficult to compare directly (McCrum et al., 2018b).

In general, studies utilising this traditional approach demonstrated that tendon mechanical properties differ among different populations. However, this approach disregards individual tendon shape and geometry, which could produce measurement errors. Moreover, changing the inter-sub-tendon matrix

properties can substantially alter the tendon displacement under the same load (Handsfield et al., 2017). It is technically challenging at this stage to measure the inter-sub-tendon matrix properties using available clinical imaging modalities, but extra caution should be placed when comparing two different groups that potentially have different sub-tendon sliding abilities, such as between young and old, or between healthy and post-rupture repaired tendons.

1.3.6 Summary of Ageing Effects on Tendon Mechanics

Ageing is one of the most important factors affecting tendon mechanical properties at multiple hierarchical levels. At the molecular level, high AGEs levels form intra-molecular and inter-molecular crosslinks and increase the modulus and tensile strength of collagen. The increased tensile strength is maintained at the fibril level, without significant change in Young's modulus. In fibres and fascicles, the aged tendons predominately show alteration in the interface mechanics, especially in energy-storing tendons. The reduced helical angle, diminished sliding and rotation are thought to be the most important age-related changes of fibre and fascicle level mechanics. Fatigue resistance also decreases in aged energy-storing tendons. The interface

properties between sub-tendons may also show age-related changes but this has not been investigated to date. At the tendon level, it is generally agreed, but inconclusive (see review (Birch et al., 2016, McCrum et al., 2018a)), that aged tendons are mechanically inferior to younger tendons. However, other factors influencing the measured mechanical properties are numerous and usually difficult or impossible to study in isolation in living people.

1.4 Achilles Tendon Anatomy and Mechanics

1.4.1 Nomenclature

The human Achilles tendon is the common tendon of soleus and gastrocnemii muscles that insert on the posterior side of the calcaneus bone. The complex anatomy of the Achilles tendon has resulted in various terms being used to describe it, sometimes confusing. Table 1-1 summarises several terms used to describe different tendon regions in the literature and the terms that will be used in this thesis.

Table 1-1. Commonly used nomenclatures of the Achilles tendon

The term used in this thesis	Terms in the literature	Description
Achilles tendon	Free (Achilles) tendon, distal Achilles tendon, calcaneal tendon	The joined tendon distal to the soleus musculotendinous junction.
Sub-tendons	Intra-tendinous fascicles, fascicle bundles	Grouped fascicles within the Achilles tendon that can be traced back to the origin from either soleus or gastrocnemii muscles. Three sub-tendons can be separated without fascicles intertwining (Figure 1-3).
Gastrocnemii tendons	Proximal Achilles tendon	The tendinous structure connected distally to gastrocnemii musculo-tendinous junctions between the gastrocnemii and the soleus musculotendinous junction.
Inter-sub-tendon matrix		The matrix between Achilles sub-tendons.

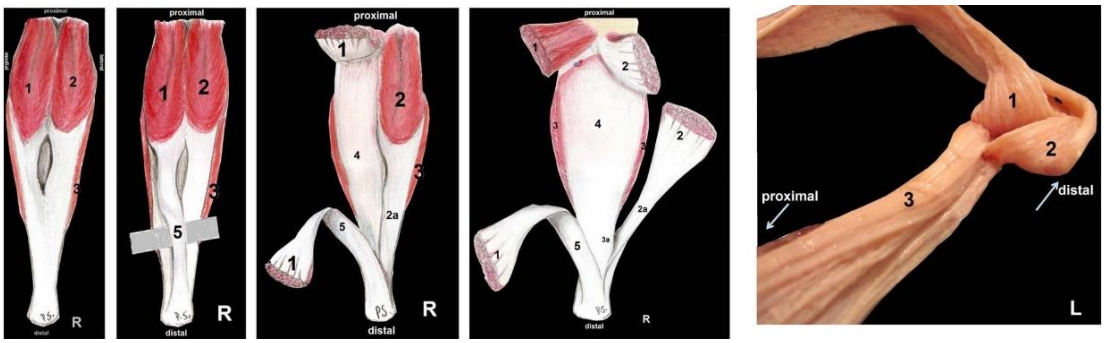

Figure 1-3. Human Achilles sub-tendons and the separation process (adapted from (Szaro et al., 2009)). From left to right: the procedure of isolation of sub-tendons. 1 & 5: medial gastrocnemius muscle and sub-tendon. 2 and 2a, lateral gastrocnemius and sub-tendon. 3, 3a, and 4: soleus muscle, sub-tendon, and aponeurosis.

1.4.2 Anatomical Features and Composition

1.4.2.1 Anatomical features

Although it is long known that the Achilles tendon arises from three muscle bellies, it is until very recently that researchers have started to realise the relative independence of sub-tendons and their mechanical roles. The soleus muscle directly links to the Achilles tendon, so the mechanical behaviour of the tendon is closely related to the activation of the soleus. On the other hand, the gastrocnemii have long tendinous portions, which are flat, thin and overlie the soleus muscle. The connection between gastrocnemii tendon and soleus aponeurosis is loose at the proximal region and gradually tightens distally (Blitz and Eliot, 2007). Having the greatest CSA and force-

generating capacity of all the calf muscles, a contracting soleus muscle can create a large deformation of its aponeurosis (Finni et al., 2003b) and could influence the covering gastrocnemii tendons. Despite not being directly studied, the behaviour of gastrocnemii tendons is likely influenced by this transverse force produced from the bulging soleus and longitudinal tensile force from the contracting gastrocnemii muscles. Therefore, despite demonstrating a similar trend, the displacement of medial gastrocnemius junction is not identical to the soleus junction during calf contractions (Ishikawa et al., 2005), and a direct comparison of properties reported in different studies between ‘free’ and ‘proximal tendon’ should be avoided.

The medial gastrocnemius tendon is usually more tightly connected to the soleus aponeurosis than the lateral gastrocnemius. The average length of the medial gastrocnemius musculotendinous junction to soleus musculotendinous junction is 1.8 to 5 times shorter than the lateral gastrocnemius (Blitz and Eliot, 2007). Medial gastrocnemius muscle was found longer than the lateral gastrocnemius by approximately 2 cm in 90% of the studied specimens (n = 45), but this length difference was not correlated with leg length, body height, or left/right side (Antonios and Adds, 2008). The length of the Achilles tendon varies among individuals. In a study with 80 specimens, 70% of the

measured Achilles tendon length was between 1 and 3 inches (mean: 5.3 cm) but longer and shorter tendons were also reported, ranging from 1.27 to 11.75 cm. Similarly, the authors did not find a significant correlation between leg length and tendon length (Pichler et al., 2007).

The whole Achilles tendon and each sub-tendon demonstrate a variable degree of internal rotation when descending. It has originally been proposed and measured only in the medial gastrocnemius tendon, which lies posteriorly and is the easiest accessible muscle-tendon unit (van Gils et al., 1996). In one early report, the rotation angle of the medial gastrocnemius tendon was used to represent the whole Achilles tendon torsion. Large individual variation was reported in the torsion angle (11° to 65°) and the percentage of medial gastrocnemius occupying (49% to 71%) the calcaneal insertion (van Gils et al., 1996). More recently, a study separated and specifically quantified the individual twist angle of each sub-tendon. Their results demonstrated that the medial gastrocnemius is the least twisted and the lateral gastrocnemius and the soleus sub-tendon exhibit approximately 3 to 5 times larger twist angle than the medial gastrocnemius (Pękala et al., 2017). The Achilles tendon torsion was categorised into three types (Figure 1-4) according to the distal sub-tendon arrangements (Edama et al., 2015a). The most extreme twist type

accounted for only 7% (8 out of 110) of the tendons studied but exhibited a most surprising 68° of medial gastrocnemius and over 200° of lateral gastrocnemius and soleus sub-tendons rotation on average (Figure 1-5) in the aformentioned quantitative study (Pękala et al., 2017).

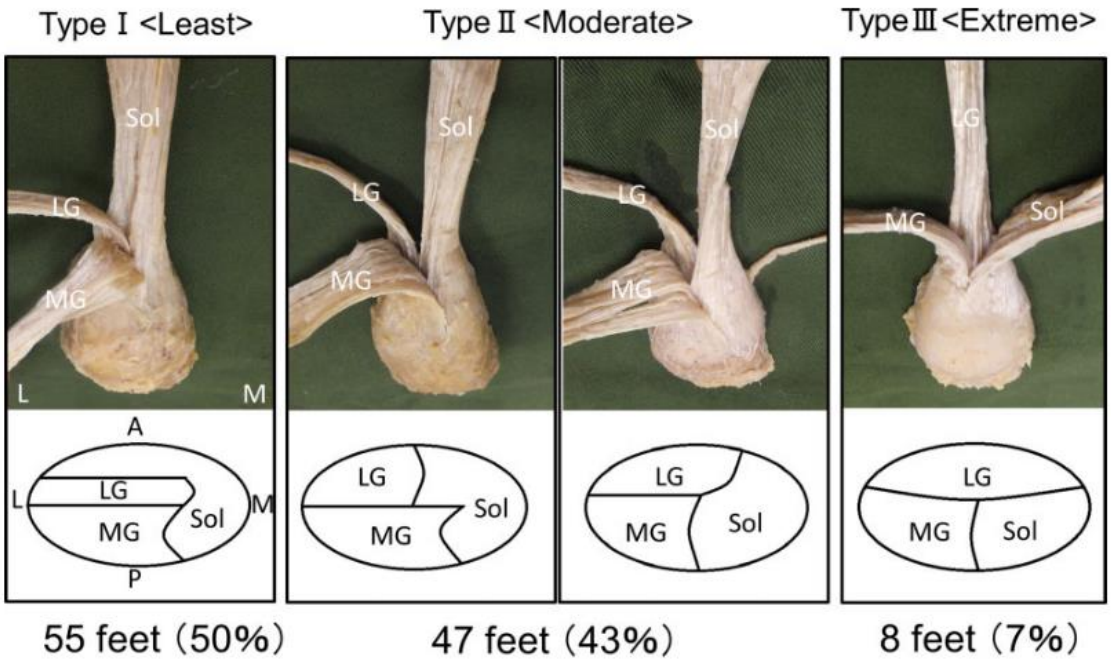

Figure 1-4. Categorising sub-tendon twist based on the occupying territories (adapted from (Edama et al., 2015a)).

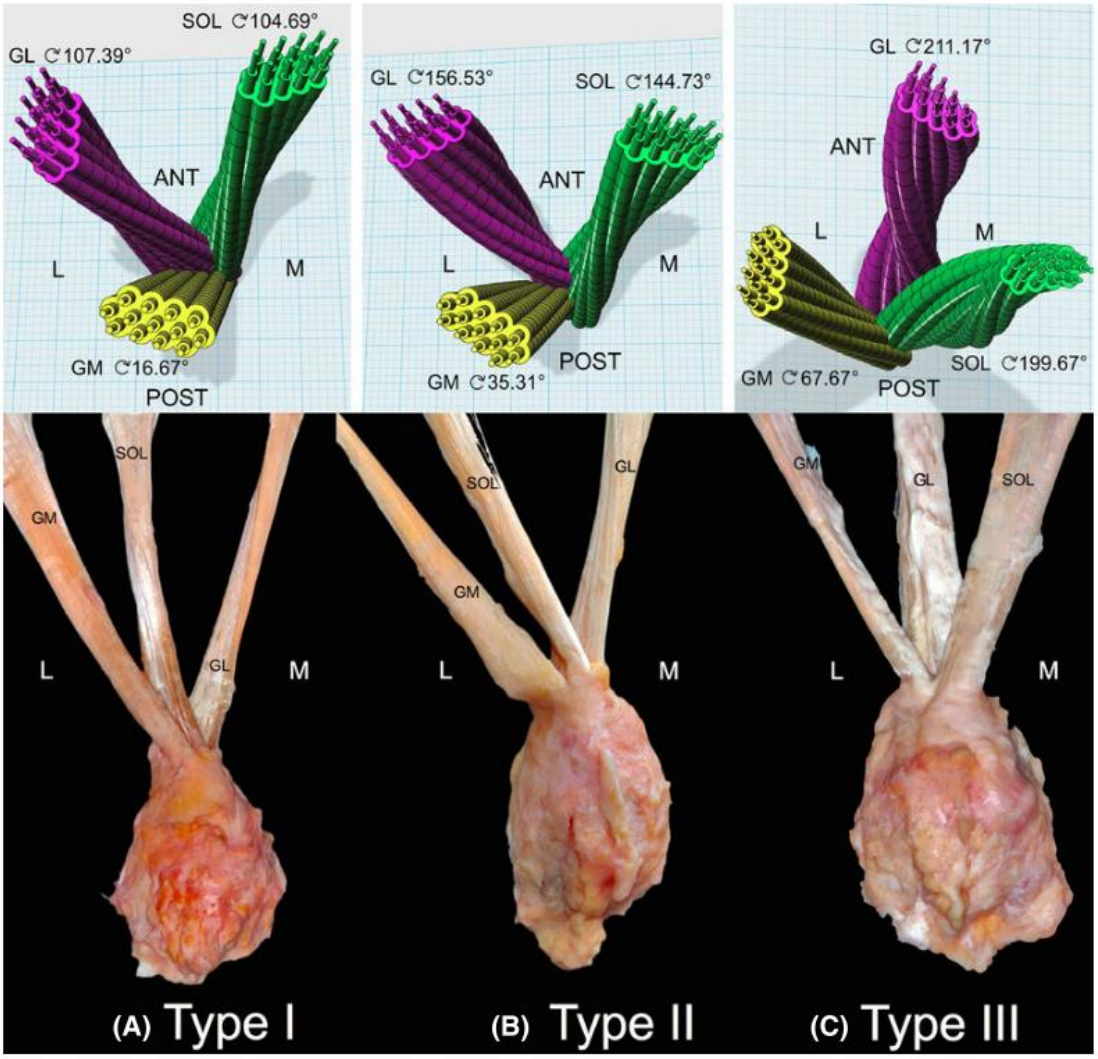

Figure 1-5. Quantitative measurement of sub-tendon torsion angle of different twist types (adapted from (Pękala et al., 2017)).

1.4.2.2 Composition

The composition of the Achilles tendon is largely similar to other tendons. Waggett and colleagues (1998) investigated the Achilles tendon composition using comprehensive biochemical methods. The mRNA expressions of collagen types I, III, and VI were present in the tendon, but type II (except for

one patient) was only expressed at the insertion. Interestingly, type II collagen at the protein level was not detected in the tendon, even for the tendons in which mRNA expression was seen. Decorin, biglycan, fibromodulin, lumican were all detected with aggrecan predominantly present at the insertion and versican at the mid-tendon region. The authors did not report any regional differences in the ECM proteins in the sub-tendons. The human supraspinatus tendon, a tendon also subjected to complex tensile and compressive forces, demonstrates large regional differences in the proteoglycan composition (Matuszewski et al., 2012). Given the similar complex force interaction of the Achilles tendon and the twisted sub-tendon structure, compositional differences may exist between sub-tendons to adapt to the different local mechanical demands.

Lubricin is localised to the IFM of the Achilles tendon with regional differences between proximal, mid-tendon, and insertional sites. The lubricin content is generally higher in the distal than proximal region, but high individual variation (both location and concentration) were reported (Sun et al., 2015). Elastin has been identified in the IFM using proteomic and immunohistochemistry methods and found to be localised to the IFM and co-locates with collagen type III (Sato et al., 2016). However, these studies did

not investigate whether regional distribution differences exist between Achilles sub-tendons. Studies have yet to investigate whether these ECM proteins differ between sub-tendons or between inter-sub-tendon matrix and IFM.

Injured or ruptured Achilles tendons show significantly different histological and compositional features which are introduced in Section 1.5.

1.4.3 Achilles Tendon Functions

In the last two decades, non-invasive *in vivo* methods have been widely applied for measuring tendon mechanical properties (reviewed in Section 1.3.4). One systematic review, summarised 21 studies on the immediate effect of exercise on *in vivo* mechanical properties, found that maximal isometric contraction and long-duration stretching exercise reduce Achilles tendon stiffness but running and hopping show minimal effect (Sancho et al., 2019). Tendon diameter also reduces after dynamic exercises, with the most pronounced reduction after eccentric exercise (Obst et al., 2013). These acute effects (in minutes) are more likely related to the changes in the fluid distribution rather than actual structural changes (Yin et al., 2014).

The Achilles tendon is specialised to facilitate forward propulsion during the push-off phase of gait (Angin and Demirbüken, 2020). This is achieved by

having a specialised matrix composition and structural adaptation for optimising energy storage, in addition to the timely coordination from triceps surae muscles. During the stance phase of gait, the eccentric contraction of muscles (active lengthening) and the passive ankle dorsiflexion due to weight-bearing accumulate elastic potential energy stored in the tendon. At the later phase of the stance (heel-off), the elastic energy stored in the tendon is released to the foot, producing a rapid and strong plantar flexion torque to push the body forward (Akalan and Angin, 2020). The pure elastic recoil of the Achilles tendon alone can account for 16% of the total energy cost during one-leg hopping (Lichtwark and Wilson, 2005).

1.4.4 Sub-tendon Level Mechanical Behaviour

1.4.4.1 In vitro and in vivo investigations

Non-uniform displacements within human and rodent Achilles tendon has been tested *in vitro* using induced muscular forces (Arndt et al., 1998, Arndt et al., 1999a, Arndt et al., 1999b, Finni et al., 2018), corroborating the idea that a certain degree of mechanical independence exists between sub-tendons. Arndt and colleagues were among the first to study this non-uniformity in the human Achilles tendon, both *in vitro* and *in vivo*. Their results demonstrated

that the force transmitted through the Achilles tendon *in vivo* changed at different knee angles, consequently affecting the gastrocnemii contraction force (Arndt et al., 1998). The later *in vitro* study reproduced these medial-lateral force differences from manipulating the applied gastrocnemii force levels (Arndt et al., 1999a). Tension from lateral gastrocnemius was associated with an increase in lateral tendon force and ankle eversion moment, while a loaded medial gastrocnemius induced the opposite. Although the study represented the first evidence of the sub-tendon involvement in Achilles tendon mechanics, the authors did not consider the individual differences of the twisted sub-tendon structure. Thus, the same location for their measurement (3 cm proximal to the insertion) may not represent the same sub-tendon across different specimens tested.

A later paper by Arndt and colleagues (2012) utilised ultrasound speckle tracking technique (*in vivo*) and confirmed that the deep (anterior) tendon region exhibits greater deformation than the superficial (posterior) region during passive ankle movements, with a mean difference of 2.1 mm (range 1.0 to 4.4 mm, Figure 1-6). Studies from Slane and Thelen (2015) compared the non-uniform displacement in young and middle-aged adults during passive stretches and eccentric contractions. Their findings demonstrated that

the deep region consistently showed a larger deformation than the superficial region. Passive stretch produced greater deformation than the eccentric contraction, and the tendons in the middle-aged group elongated more but with a less between-layer difference (i.e., more homogeneous) than the younger group. The same research group later demonstrated that the measured non-uniformity increased with faster walking speed (Franz et al., 2015) and decreased in the aged population (Franz and Thelen, 2015). The authors concluded that non-uniformity is important for achieving optimal triceps surae function since decreased non-uniformity was associated with lower ankle torque output in aged people (Franz and Thelen, 2015).

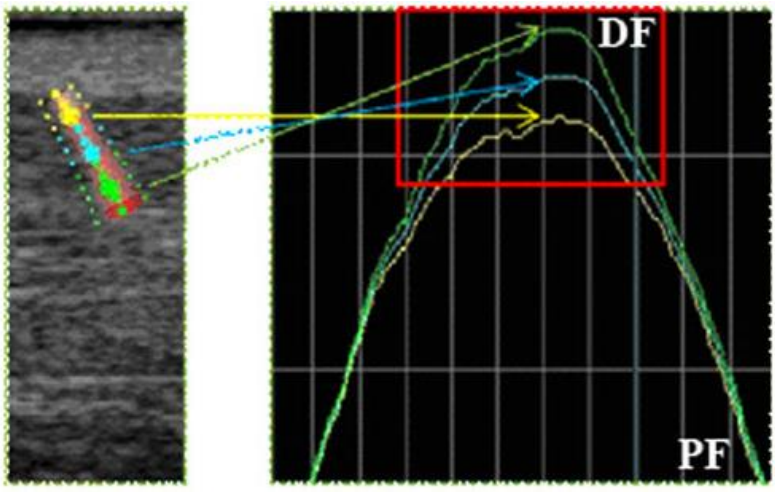

Figure 1-6. Displacement non-uniformity between superficial and deep regions during passive ankle dorsiflexion (adapted from (Arndt et al., 2012)). DF: dorsiflextion, PF: plantar flexion.

One potential explanation of the deep layer moving more during ankle movements is the compressive force exerted from the prominent calcaneal tuberosity (Chimenti et al., 2016). When dorsiflexed, the compressed anterior (deep) portion of the Achilles tendon may induce compressive strain compared to the unaffected posterior, superficial portion. However, since this study was performed in weight-bearing conditions, this compression-induced displacement non-uniformity is likely small in the non-weight bearing and passive ankle motions, which exhibited even higher non-uniformity than active, muscle-action involved movements (Slane and Thelen, 2015).

Another research group using 3D free-hand ultrasound demonstrated that the Achilles tendon externally rotates during isometric contractions, especially at the mid-tendon. Meanwhile, a decrease in the CSA when loaded resulted from a reduction of Achilles tendon medial-lateral diameter but an increase of the anterior-posterior diameter (Poisson's ratio: 0.55 ± 0.30), suggesting certain heterogeneity exists within the 'whole' Achilles tendon (Obst et al., 2013, Obst et al., 2014). This decrease in the CSA can be detected after just 3 sub-maximal isometric contractions (Nuri et al., 2017), and is then fully recovered in two hours.

Besides tendons, the soleus aponeurosis can also exhibit non-uniform deformation: the middle region elongates while the distal region shortens during muscle contractions (Finni et al., 2003a, Finni et al., 2003b). Similar non-uniformity also presents in the medial gastrocnemius aponeurosis (Kinugasa et al., 2008). Since the gastrocnemii tendons lie superficial to the soleus muscle and aponeurosis, the mechanical behaviours of gastrocnemii tendons are likely affected by both longitudinal (from contracting gastrocnemii) and transverse (from the bulging of contracting soleus) directions (Farris et al., 2013). It is not known how this multi-directional force from the proximal gastrocnemii tendons affects the mechanical behaviour of the distal gastrocnemii sub-tendons.

It is worth noting that although most of the studies simplified the ankle joint as only performing sagittal plane movements (plantar flexion and dorsiflexion), both the talocrural and sub-talar joint can produce a significant amount of frontal plane movement. The Achilles tendon attaches to the calcaneal tuberosity, which is distal to both joints, and may produce non-negligible torque other than pure plantar flexion depending on the individual ankle morphology and the exact joint position. Cadaveric studies have suggested that certain sub-tendons are strained more at different ankle

inversion or eversion degrees (Arndt et al., 1999b, Lersch et al., 2012). However, due to the large individual variation of both Achilles tendon and ankle/foot joint morphologies, the actual sub-tendon strain patterns likely varies between individuals.

1.4.4.2 Conditions reducing non-uniformity

Aged tendons demonstrate a more uniformed *in vivo* internal displacement than younger Achilles tendons, under both passive and active movements (Franz and Thelen, 2015, Slane et al., 2015, Slane and Thelen, 2015, Clark and Franz, 2020). This reduced non-uniformity has been suggested as a result of decreased sliding between sub-tendons, an effect similar to the age-related stiffening of the IFM reported in the equine SDFT (Thorpe et al., 2013c). However, the observed uniformity may also originate from altered tendon and aponeurosis mechanical properties, since *in vivo* studies usually report increased strain and displacement in aged tendons at given force levels, suggesting reduced material stiffness in aged tendons. Unfortunately, it is technically challenging to isolate the effect of reduced sub-tendon sliding from altered tendon mechanical properties by *in vivo* methods.

The non-uniform displacement also diminishes in surgically repaired Achilles tendons and does not recover with functional improvement (Froberg et al., 2017, Beyer et al., 2018). One study showed a trend towards a lower non-uniformity in tendinopathic tendons compared to healthy tendons (Couppe et al., 2020). However, it is currently unknown whether this diminished sliding is the cause or the result of tendinopathy. Combining the results from aged tendons, current *in vivo* evidence suggests sufficient non-uniformity and inter-sub-tendon sliding are required for optimal Achilles tendon function.

1.4.4.3 Methodological limitations

Despite the recent advances in the resolution of ultrasonography, some fundamental limitations still exist when studying *in vivo* sub-tendon mechanics. First, the ultrasound probe usually only produces a single plane (mostly sagittal plane) 2-D image, meaning a limited field of view at any given time. The measured displacement is only representable for a small portion of the tendon. Second, the Achilles tendon shows great individual variability (Section 1.4.2), suggesting data pooling or direct comparison between individuals can induce errors. For example, the deeper region could be the lateral gastrocnemius sub-tendon, instead of the soleus sub-tendon, for the

most twisted type of sub-tendon arrangements (Figures 1-4 and 1-5). Current technology has yet to develop enough imaging fidelity or resolution to detect the internal sub-tendon boundaries. One study that retrospectively analysed 200 MRI scans of the ankle joint found only a few of the scans demonstrated separable features (most likely the isolation of lateral gastrocnemii) between Achilles sub-tendons, suggesting a limited ability to differentiate sub-tendons using MRI (Szaro et al., 2020).

Last, most *in vivo* studies have utilised electromyography (EMG) to estimate or used a dynamometer to measure force imposed on the Achilles tendon. The EMG is best correlated with muscular force in static, isometric contractions, and can produce artefacts when used to estimate muscle force in concentric or eccentric contractions, especially during high-speed movements. The dynamometer (or force plates) can only measure the sum of force or torque exerted, so the estimated force from individual muscle often relies on normalising using the physiological cross-sectional area of each muscle (Crouzier et al., 2018). The measured ankle plantar flexion torque also requires precise measurement of the ankle joint moment arm to correctly calculate tendon force. Individual morphology differences can therefore result in high variance of measured mechanical properties. Although these

limitations are well-known in the research field, few other non-invasive methods exist for studying tendon mechanical properties *in vivo*.

1.4.4.4 Factors affecting sub-tendon sliding

A few potential factors could affect sub-tendon sliding. Structurally, the more twisted the sub-tendon, the more transverse plane movement when strained. This ‘untwisting’ could exert shear or compressive forces on the adjacent sub-tendon and affect the observed axial displacement, compared to a straight sub-tendon alignment. The inherent mechanical or material properties of different sub-tendons could also result in different strains between sub-tendons. Differences in the muscle properties or ankle range of motion may facilitate or inhibit certain sub-tendon movements (Edama et al., 2015b), and the difference is likely aggravated by increased physical demands, such as sports.

At the fascicle level, lubricin and elastin have been confirmed in the Achilles tendon IFM, corroborating their role in facilitating fascicle sliding as demonstrated in the equine SDFT. In rodent Achilles tendons, both elastin and lubricin are found in the inter-sub-tendon matrix, suggesting a similar mechanical role in facilitating sub-tendon sliding (Gains et al., 2020). It is not

known whether these proteins are localised to the human inter-sub-tendon matrix. Non-enzymatic glycation of proteins in the equine IFM has been linked with decreased fascicle sliding capacity (Thorpe et al., 2013c). Age-related decrease in Achilles tendon non-uniformity could, therefore, be a result of stiffening the inter-sub-tendon matrix as aged tendons have a significantly higher level of glycation crosslinks than younger tendons (Nash et al., 2019).

No study has systematically investigated the degree of sub-tendon sliding or the mechanical consequences after changing the sliding ability between human Achilles sub-tendons.

1.5 Tendon Diseases

Here the discussion is limited to chronic, poor load management induced tendon diseases while excluding acute traumatic injuries. It has been suggested that the inflammatory response differs between these two conditions. Indeed, when considering the most extreme conditions, it is not uncommon to find patients with spontaneous and insidious supraspinatus tendon rupture having minimal pain or swelling but very few patients suffering

from laceration wounds or direct blows to tendons without debilitating painful sensations.

1.5.1 Tendinopathy

The term ‘tendinitis’ used pre-1990 suggested tendon injuries are at the phase of acute inflammation. Afterwards, histological studies confirmed that minimal inflammation presents in most overuse tendon injuries, and the term ‘tendinopathy’ has been introduced to emphasise the lack of inflammation in chronic tendon injuries. The paradigm beginning since the end of the 20th century is that the degenerative process of tendon pathology is non-inflammatory, and the term ‘tendinosis’ has appeared in the literature, emphasising the degenerative nature of the disease. However, with the current advancement of biochemical techniques, many recent studies suggest that inflammation does play a role in tendinopathy development. For example, inflammatory cells reside in tendons and secrete inflammatory cytokines that facilitate ECM synthesis and degradation (see review (Rees et al., 2014, Dean et al., 2017)). These results suggest that the degeneration of the tendon is associated with inflammatory responses, despite not always presenting the traditional signs and symptoms of inflammation.

Clinical symptoms such as swelling or pain during movement are often reported in tendinopathic patients. However, these clinical symptoms usually mismatch with histological or imaging findings. The exact reason behind this mismatch between symptoms and tissue degeneration is still unknown but neurological mechanisms have been proposed (Dean et al., 2013). Under ultrasound imaging, tendinopathic tendons appear hypoechogenic and may show signs of hypervascularity. These imaging features however can be found on asymptomatic tendons as well. Similarly, patients with symptomatic tendinopathy can present normal imaging evaluation, and imaging profile may resolve, remain unchanged, or progress with time despite no change in symptoms (Bley and Abid, 2015).

Tendon tears or acute ruptures are extreme but not uncommon conditions, with increasing prevalence (Hopkins et al., 2016), that involve partial or complete loss of tendon structural integrity. Despite its ‘acute’ nature, almost all ruptured tendons were not healthy and already presented with degenerative changes (Kannus and Jozsa, 1991). This brings up an important but baffling idea that the link between degenerative changes and symptoms, mainly pain, is weak, and many Achilles ruptured patients are asymptomatic before rupture. Since pain is usually the limiting factor during

athletic activities, there is an urgent need for developing clinical screening tools to objectively monitor the tissue changes alongside testing tendon functions, without the influence of symptom presentations.

Achilles tendinopathy is a multifactorial and complex pathology with prominent risk factors including age, repetitive use, or change in the loading conditions. Certain links between metabolic profiles (such as high cholesterol or diabetes) and the development of tendinopathy have also been proposed (Dean et al., 2017). The histological presentation of tendinopathy is, overall, pathological chondroplasia, replacing normal tensional tenocyte morphology with the fibrocartilage-like phenotype (see review (Dean et al., 2017)). The presence of aggrecan and versican increase in pathological human patellar tendons (Parkinson et al., 2010), and increased aggrecan and biglycan levels have been found in Achilles tendinopathic specimen samples (Corps et al., 2006). Fibronectin, a glycoprotein, has been observed in regions of degeneration (Jozsa et al., 1989). Both Achilles and patellar tendinopathic tendons showed increased apoptotic cells compared to healthy, asymptomatic tendons (Lian et al., 2007, Pearce et al., 2009). In patients with a torn supraspinatus, pro-inflammatory cytokine expression, which is crucial in oxidative-stress-mediated apoptosis, increased compared to controlled

tendons (Millar et al., 2009). In ruptured tendons, a high number of fibroblasts, myofibroblasts, and inflammatory cells are usually found (Khan et al., 1999). Compared to healthy tendons, tendon cells demonstrate a rounder shape in tendinopathic tendons and produce more type III collagen (Maffulli et al., 2000, Pingel et al., 2014). The fibrils are more disorganised and buckled and show an increased ratio of small to large diameter fibrils compared to the adjacent healthy regions (Pingel et al., 2014).

Several studies have shown altered MMPs and TIMPs levels in pathological tendons. The MMP levels were found to be increased in human torn rotator cuff tendons (Dalton et al., 1995). The MMP-1 and MMP-13 levels were reported higher and had a more widespread distribution in aged articular cartilage compared to younger cartilage (Wu et al., 2002). A study combining human hamstrings tendon culture and an *in vivo* rabbit tendon overuse model demonstrated that increased MMP-2 level is correlated with greater (either higher frequency or higher strain) mechanical stimulation (Huisman et al., 2016). In rodent Achilles tendons, moderate exercise for 8 weeks demonstrated a significant upregulation of MMP-13 and TIMP-1 compared to the control condition. However, the high-intensity exercise group showed a higher MMP-13 level than both the control and moderate exercise group, but

TIMP-1 levels dropped below that of the control groups. Moderate exercise also showed the highest collagen type I and decorin mRNA expressions, suggesting an overall beneficial anabolic effect of moderate physical activities (Xu et al., 2018). *In vitro* cyclic loading of SDFT fascicles, mimicking a bout of high-intensity exercise, showed altered cell shape, disorganised fibrils, and increased levels of inflammatory markers (interleukin-6), MMP-13, and collagen degradation markers. The greater staining of MMP-1, MMP-13, and collagen markers in the IFM compared to fascicles suggests that the damage may initiate from the IFM and also suggests a potential role for early inflammation in the tendon healing response (Thorpe et al., 2015a). High-intensity exercise training for 18 months in horses induced tendon tissue changes similar to age-associated features in the energy-storing SDFT but not the positioning CDET (Birch et al., 2008a).

Tendinopathic tendons show changes to their mechanical properties and is more compliant and have a lower elastic modulus than healthy tendons. However, the change is not universal and is different from tendon to tendon and even the same tendon but different lesion sites (Obst et al., 2018). The inferior mechanical properties demonstrated in midportion Achilles tendinopathic patients are widely agreed, but conflicting results from the

patellar tendinopathy cohort suggest the association between pathology and mechanical properties may not always be present.

Currently, tendon loading exercise is the most effective treatment for tendinopathies (Martin et al., 2018). In the past, eccentric exercise has been proposed as the preferred type of exercise to reduce pain and improve function. However, recent studies have suggested that sufficient loading is more important than the type of muscle contraction, and heavy-slow concentric contractions can achieve a similar beneficial outcome (Beyer et al., 2015). Other passive intervention methods, such as night splints, orthoses, taping, low-level laser therapy, soft tissue mobilisations, and acupuncture, are generally not recommended due to the low effectiveness or contradicting evidence. Stretching exercises and neuromuscular re-training of abnormal kinetics/kinematics may show some benefits but the general evidence levels for both are weak (see review (Martin et al., 2018)).

1.5.2 Tendon Tear and Rupture

Tendon tear and rupture occur with macroscopic loss and disruption of tendon tissue integrity and are usually diagnosed by medical imaging such as ultrasound or MRI. Achilles tendon ruptures are most prevalent in the middle-

aged population during athletic activities that require a sudden change of movement direction combined with fast acceleration and deceleration, such as badminton, volleyball, and football (Lantto et al., 2015). Although Achilles tendon rupture almost always incapacitates one immediately, a rupture in the supraspinatus tendon is sometimes insidious and, since older people rarely require raising arms overhead, can be diagnosed long after rupture.

Ruptured Achilles tendons usually undergo surgical repair and require post-operational physiotherapy for 6 to 12 months. These repaired tendons, unfortunately, are unlikely to achieve pre-injury functional levels. It is worth noting that surgical repairment ‘binds’ sub-tendons together (Winter et al., 1998), diminishing their relative displacements even after 2 years (Froberg et al., 2017, Beyer et al., 2018). Ruptured Achilles tendons can also be treated non-operatively by wearing a cast for a prolonged duration. One meta-analysis of randomised controlled trials reported a reduced risk of Achilles re-rupture in surgically repaired groups, while the complications (development of deep venous thrombosis and limited range of motion) and functional performance showed no differences between repair and conservative treatment groups (Deng et al., 2017). No study has reported the effect of conservative treatments on sub-tendon sliding.

1.5.3 Ageing

While ageing per se is natural and should not be regarded as pathological, several age-related changes in tendons can alter, and usually deteriorate, the mechanical properties associated with optimal tendon function. One important aspect when studying age-related tendon changes is to separate the maturation process from ageing. Tendon studies often utilised short-lived animal models, such as rodents or rabbits, to investigate the relationship between chronological age and tendon structural or compositional changes. However, the ageing process of human tendons takes decades and is difficult to replicate by using animal tendon models where life expectancy is a few months or years. Horses, on the other hand, are a better model for studying the tendon ageing process due to their longer lifespan (~ 30 years).

Despite having fewer physical activities and generally lower exercise intensity, aged people are more likely to suffer from tendon injuries than young adults, affecting their daily activities and requiring them to seek medical help. However, studies on tendon level mechanical properties in aged human Achilles and patellar tendons do not provide a conclusive answer as to whether aged tendons are mechanically weaker than younger tendons, both

in vitro and *in vivo* (see review (Birch et al., 2016)). Similarly, no correlation was observed between old and young equine SDFTs in the ultimate (failure) mechanical properties (Thorpe et al., 2013c). Age-related changes in tendon mechanical properties are prominent at the lower hierarchies (reviewed in Section 1.3.6), but these changes do not seem to be detectable in the overall properties at the whole tendon level. At the sub-tendon level, aged human Achilles tendons show less non-uniformity during movements compared to younger tendons (reviewed in Section 1.4.4). This reduced sub-tendon sliding can alter the mechanical behaviour of the whole Achilles tendon.

The inferior motor performance of aged adults is a combined result of inevitable age-related tissue and cell changes and reduced physical activities, resulting in decreased muscle mass, sub-optimal neuromuscular control, and potentially inferior tendon mechanical properties. For Achilles tendons, weak triceps surae muscle strength usually accompanies low *in vivo* tendon material stiffness (Mademli and Arampatzis, 2008, Holzer et al., 2018); however, the relationship between knee extensor (quadriceps femoris) strength and patellar tendon stiffness is less obvious (Carroll et al., 2008, Burgess et al., 2009). The maximal strength of lower limb muscles declines sharply after 50 years old (Kemmler et al., 2018). Compared to younger

adults, people in this age group demonstrate lower mechanical power in jumping and this difference cannot be explained by the decline in muscle strength or tendon mechanical properties alone, suggesting the influence from neuromuscular control and motor planning affects the functional performance in the aged population (Konig et al., 2018). It remains technically challenging to isolate these neurological and muscular effects when studying *in vivo* tendon properties.

Total collagen content and cellularity in tendons does not change significantly with age advancement (Thorpe et al., 2010c, Thorpe et al., 2016b). The matrix turnover rate decreases in both aged SDFT and CDET when measured by the D/L ratio of aspartic acid (Thorpe et al., 2010c). The decrease in turnover rate in aged SDFT is limited to the collagenous matrix as the turnover rate of the non-collagenous matrix remains similar to younger tendons. In humans, the matrix turnover rate appears to drop significantly after adulthood (Heinemeier et al., 2013). The reduced turnover rate does not correlate with reduced gene expression or increased MMP activities and could be the combined effect of cellular senescence and ageing tendon stem cells (see review (Birch et al., 2016)). The most prominent age-related matrix change is the accumulation of AGEs and the formation of non-enzymatic

crosslinks between or within collagen molecules (reviewed in Section 1.2.3.2.2). These crosslinks have a widespread effect on mechanical properties at multiple hierarchical levels. Elastin content declines in aged equine SDFT and its orientation is more distorted compared to younger SDFT (Godinho et al., 2017). This decline is mainly localised to the IFM and correlates with the observed age-related stiffening and reduced IFM sliding.

In conclusion, age-related decline in tendon function is multifactorial and could result from a combination of increased AGE crosslinks, decreased matrix turnover rate, inferior mechanical properties, and impaired neuromuscular control, from the molecular level to the organism level.

1.6 Approaches for *in Vivo* Tendon Characterisation

Here, two approaches used in this thesis for potential *in vivo* characterisation of Achilles tendons are reviewed: Raman spectroscopy, which enables non-invasive and label-free characterisation of tendon composition with high potential in the future for clinical application; and finite element analysis, which allows manipulation of force level, sub-tendon sliding ability and individual tendon geometry to understand the complex tendon

mechanical behaviour. The following sections succinctly summarise the principles of these techniques, their strengths, and their current application in tendon-related research.

1.6.1 Raman Spectroscopy for Probing Tendon Composition

1.6.1.1 Principles

Raman spectroscopy, a type of vibrational spectroscopy, measures the molecular vibrations induced by the incident light, enabling both qualitative and quantitative analysis of the sample composition at the molecular level. Elastic scattering (or Rayleigh scattering) happens when photons are scattered by a material. These scattered photons have the same frequency and wavelength as the incident photons. Raman scattering (or Raman effect) on the other hand, describes the inelastic scattering effect that changes the energy level of the scattering photon. When light shines on a piece of material, on some occasions, energy exchange occurs between molecules and the incident photons, causing a frequency shift between the incident and scattered photons (Larkin, 2011a). Stokes Raman scattering describes the effect that energy is transferred from incident photons to the material, resulting in scattered photons having lower energy than the incident photons.

Anti-Stokes Raman scattering describes the contrary but is less likely to happen under room temperature since this requires the material being tested to be already in a higher vibrational state, i.e., hot.

Raman scattering is closely related to the chemical molecular bonds, molecular structure, and polarisation of the material. The frequency shift (x-axis), expressed in wavenumbers (cm^{-1}), between the incident and scattering photons is independent of incident light but highly linked to the molecule structures. The band intensity (y-axis) is proportional to the molecules interrogated. Hence, by analysing the frequency shift and the different band intensities, the molecular structure and the relative quantity can be probed, providing a 'fingerprint' of the studied sample (Larkin, 2011d, Larkin, 2011e).

To successfully analyse the composition of complex compounds requires prior knowledge of the basic chemistry and a systematic way of spectral interpretation, which often requires referencing from both spectral libraries and empirical frequencies from different chemical functional groups (Larkin, 2011b). The collected spectrum from a compound is often complex and can represent either molecule with many attached functional groups or

compounds with many different components. Analysing biological tissues is challenging due to their complexity in composition and tissue heterogeneity.

Besides, many molecules found in biological tissues show auto-fluorescence, which can mask the underlying Raman spectrum due to their overlapping signal wavelength dimensions. The fluorescence background is several orders higher than the Raman intensity and requires either modification to the sample (e.g., surface-enhanced Raman spectroscopy) or the instrument (e.g., resonance and stimulated Raman spectroscopy) before spectral acquisition or applying correction methods afterwards. Common fluorescence correction or suppression methods can be categorised into time-domain, frequency-domain, wavelength-domain, and algorithm-based methods (see review (Wei et al., 2015)). Using a low-level polynomial to fit the fluorescence baseline then subtracting it from the original spectrum is one commonly used computational method for correcting the fluorescence background (Wei et al., 2015).

Near-infrared spectroscopy, another type of vibrational spectroscopy, is often used in combination with Raman spectroscopy to fully interrogate the underlying composition of a sample. However, it is less commonly used in

testing biological tissues since water content highly affects the collected infrared spectrum and can mask certain important spectral features.

1.6.1.2 Application to tendon tissues

1.6.1.2.1 Spectral features of collagen

Collagen produces several characteristic bands related to its composition and structure. Various strong bands at wavenumbers 800 cm^{-1} to 1000 cm^{-1} are assigned to collagen C—C backbone, proline, and hydroxyproline, the two most abundant amino acids in collagen besides glycine. The narrow band at 1002 cm^{-1} is assigned to the amino acid phenylalanine, the intensity of which can sometimes be used as a normalisation reference due to its ring structure providing stable Raman intensity (Fields et al., 2017). Prominent amide III (centre at ~ 1240 cm^{-1}) and amide I (centre at ~ 1660 cm^{-1}) are two large compound bands closely related to the collagen secondary structure (Rygula et al., 2013) or the fibrous orientation of collagen molecules and fibrils (Van Gulick et al., 2019). Deconvoluting the amide bands by curve fitting is often required to interrogate the changes in the collagen secondary structure. The CH_2/CH_3 bending band (~ 1450 cm^{-1}) is frequently used to indicate the total protein content or the lipid content within samples (Talari et al., 2014).

The spectral features of collagen can be influenced by various conditions (see review (Martinez et al., 2019)), both physiological (tissue hydration, temperature) and pathological (wound, ageing, diseases). Raman spectroscopy, therefore, has a high clinical potential to differentiate normal and abnormal tendon conditions in a rapid, label-free manner. However, due to the complexity of biological tissue composition and the aggregated, combined spectral features, identifying a specific compositional change from the Raman spectrum alone can be challenging, especially when the underlying components and concentrations are not known.

As introduced previously, the high fluorescence background in collagenous tissue hinders interpretation of the Raman spectrum and is often corrected (removed) at the beginning of the spectral analysis. However, it is possible that preserving the fluorescence signal may provide important information and improve age-differentiation in tendons since aged tendons have a much higher fluorescence level than younger tendons, as shown using conventional biochemical approaches (Birch et al., 1999, Thorpe et al., 2010c, Nash et al., 2019).

1.6.1.2.2 Spectral features of elastin and proteoglycans

Raman spectral features of elastin are characterised by prominent amide I and III bands, centred at 1668 cm^{-1} and 1254 cm^{-1} respectively (Frushour and Koenig, 1975). The band at 1326 cm^{-1} is assigned to elastin and correlates with tissue integrity in one study investigating wound healing of guinea pig skin (Alimova et al., 2009). Using Fourier transform infrared spectroscopy, a study reported the human elastin consists of largely unordered structures (56%) and beta-sheets (36%) (Debelle et al., 1998).

In cartilages, the 1063 cm^{-1} and 1375 – 1410 cm^{-1} bands are commonly assigned to the sulphated glycosaminoglycans. However, these bands are usually weak and masked in the collected tendon spectra, in which type I collagen signal dominates (Esmonde-White, 2014, Bergholt et al., 2019).

1.6.1.2.3 In vivo applications

Raman spectroscopy has been used in many dermatological studies, for the tissue's easy accessibility, to differentiate age-related (Gniadecka et al., 1998) and diabetic-related (Pereira et al., 2015) compositional and structural changes in human dermis, and in induced skin incision in rats (Jain et al., 2014) and guinea pigs (Alimova et al., 2009). By correlating spectral features

with histological staining, the *in vivo* use of Raman spectroscopy on skin tissue can categorise skin wounds into haemostasis, inflammation, and proliferation stages, allowing label-free identification of skin conditions (Alimova et al., 2009).

For tendons, studies have investigated the Raman spectral differences between tendon regions (tendon versus enthesis (Wopenka et al., 2008, Genin et al., 2009), mineralised versus non-mineralised regions (Kerns et al., 2016)) and between healthy and injured tendons (Moura Junior Mde et al., 2014, Moura Junior Mde et al., 2015). However, most of the studies were conducted on animal tendons and no research has investigated the human Achilles tendon using Raman spectroscopy. The development of Spatially-Offset Raman spectroscopy (SORS) allows *in vivo* collection of the signal underneath the skin (Matousek et al., 2006) and has been applied in some small-scale studies to non-invasively differentiate *in vivo* tissue composition. The human Achilles tendon, being a superficial, thick, and injury-prone tendon is an ideally suited target for SORS to detect the underlying molecular changes to the tendon.

1.6.2 Finite Element Analysis for Force Interactions

1.6.2.1 Principles

Finite element analysis is a computational method capable of answering complex real-world engineering questions by dividing the continuity of field variables (i.e., temperature, displacement, force) within a structure into a finite number of elements and computing the response of each element. Approximated functions (termed interpolated functions) are calculated at each node, which lies along the element boundaries. Different element shapes and node selection will affect the approximated functions and consequently the outcome (Madenci and Guven, 2015).

Having many elements, in general, provides a better approximation result closer to reality (i.e., the assumed continuity of variables). However, the computational cost increases sharply, and a fine mesh (high element numbers) could increase round-off error. At a sharp angle, a fine mesh could also result in stress singularity, which results from having a high force imposing on a very small area, induced by the small element size. By calculation, the stress at this point (the sharp angle) increases with the element number. This phenomenon contradicts the physical law and should

be regarded as an error that needs correction. It is important to balance the computational cost and the accuracy of the result obtained from the analysis. The criterion indicating a sufficient mesh number can be having less than 1 to 5% of outcome differences when doubling the element size (Madenci and Guven, 2015).

A boundary condition is required in the FEA as it provides the calculation of the whole system with a unique solution. Boundary conditions in the static structural analysis are usually load and displacements. Setting the displacement boundary condition governs the overall displacement of the geometry, and each element is then calculated to match the internal gradients of this gross displacement. Hence, the original gross-level physical question is broken down into numerous solvable equations for each element. The current commercially available software allows the creation of 3-D structural geometry, generation of mesh (creating elements), assignment of material properties and boundary conditions, and post-processing into graphical presentations after solution.

Tendons are considered to be transverse isotropic, viscoelastic, incompressible materials. Viscoelasticity should be considered when the

tendon is subjected to slow deformation or fatigue settings but is less important during low number cyclic testing at relatively high speeds (Weiss et al., 1996).

1.6.2.2 Applications

FEA is widely used in the engineering field and has been increasingly applied in biomechanical studies to help understand difficult and complex problems, for its ability to simulate the mechanical behaviour from the molecular to the organ level. The human Achilles tendons is a good candidate for applying FEA on the complex mechanics, since it is composed of three twisted sub-tendons and subjected to high asymmetrical forces.

The Achilles tendon has been modelled as a neo-Hookean hyper-elastic solid with a strain energy density function (Weiss et al., 1996), which is then solved by the approximation of the available experimental data to obtain the tendon material properties. Using this approach, studies have demonstrated several important findings of the tendon and sub-tendon level mechanical responses under load. The stress, failure force, and rupture location are more sensitive to the subject-specific Achilles tendon geometry than the material properties (Shim et al., 2014, Hansen et al., 2017). The sliding between sub-

tendons is an important factor for reproducing the observed *in vivo* non-uniform Achilles tendon displacement during movements (Handsfield et al., 2017). The (whole tendon) twist angle affects stress distribution, and a moderate twist (15° to 30°) achieved the highest simulated rupture load (Shim et al., 2018). Together, these FEA findings suggest the mechanical behaviour of the Achilles tendon varies greatly between individuals and is largely dictated by the inherent tendon shape, which has been neglected in current clinical examinations and treatments. With the advancement of clinical imaging modalities and the improvement of computational speed and power, it is possible to incorporate the movement-specific kinetics and kinematics into the constructed subject-specific tendon geometry for simulation and to provide real-time feedback of tendon responses during exercise training (Pizzolato et al., 2020).

1.7 Rationale for Research Study and Overall Design

Tendon structure and composition are specialised and finely tuned to meet the imposed mechanical demands during activities. Recently, researchers have highlighted the importance of fascicle and sub-tendon

sliding on maintaining normal tendon homeostasis and achieving the optimal mechanical strength to fulfil the functional demands of the tendon. Using different animal models and testing modalities, most studies come to an agreement that ageing causes a reduction in the natural sliding at various hierarchical levels and likely results in a decline in tendon function and an increased injury risk. However, little is known about the sub-tendon composition, mechanical properties, and the interaction between inherent sub-tendon shapes and age-related decline in the sliding ability. How these factors affect the Achilles tendon level mechanical behaviour remains unknown but may be important for improving our current clinical treatment and developing prevention strategies for Achilles tendon injuries. Current medical imaging devices have yet to develop a successful method to visualise or analyse sub-tendon structure or composition *in vivo*, making the current basic science knowledge difficult to translate to clinical settings.

The work described in this thesis aims to address some of the unanswered questions concerning the Achilles tendon mechanical behaviour and to discover potential approaches for clinical applications. In Chapter 2, experiments were conducted to develop a novel equine tendon model – the deep digital flexor tendon (DDFT) and its accessory ligament (AL) – for

studying the mechanical behaviour of different materials (similar to sub-tendons) joining into one seemingly homogeneous tendon. The sub-tendon level and fascicle level mechanics and the ECM composition were measured and analysed across different tendon regions.

In Chapter 3, similar experiments (biomechanics and compositional analysis) were conducted for characterising human Achilles sub-tendons.

Chapter 4 and 5 utilised Raman spectroscopy to investigate the possibility of non-destructively detecting different tendon compositions in different tendon types with differences in specimen age, and between different Achilles sub-tendons.

In Chapters 6 and 7, the properties of the inter-sub-tendon matrix were manipulated using finite element analysis to study the age-related effect of sliding decline on the Achilles tendon mechanical behaviour during passive and dynamic loading conditions.

Chapter 2 An Equine Tendon Model for Studying Intra-tendinous Shear Mechanics

2.1 Introduction

Achilles tendon injury is prevalent in both athletes and the general population, but our limited understanding of the pathogenesis has hampered the development of successful prevention and interventional strategies. From the material point of view, the susceptibility of injury relates to the intrinsic Achilles anatomy (shape and geometry) and the internal complex force interactions (Magnan et al., 2014) between two longer and thinner gastrocnemii tendons and a shorter and thicker soleus tendon. Although the different contributing tendons on visual inspection appear to merge into one homogeneous tendon, the tendon fascicles originating from different muscle bellies do not merge or intertwine within the Achilles tendon until reaching the distal calcaneal tuberosity (Szaro et al., 2009, Edama et al., 2015a, Edama et al., 2016). Achilles sub-tendons are believed to facilitate movement efficiency by allowing a certain degree of individual response from contracting muscles to meet the demands from locomotive activities.

Individual control of sub-tendons creates non-uniform displacements within the Achilles tendon, and this non-uniformity has been observed in both passive (Arndt et al., 2012, Bogaerts et al., 2017, Stenroth et al., 2019) and dynamic (Slane and Thelen, 2014, Slane and Thelen, 2015) movements. Furthermore, the displacement between the sub-tendons shows an age-related and disease-related decline (Franz et al., 2015, Froberg et al., 2017, Beyer et al., 2018). At the fascicle level, studies on the equine SDFT, an extreme example of an energy-storing tendon, have demonstrated that the high failure strain of this tendon is achieved by having a compliant IFM, which allows sliding of fascicles (Thorpe et al., 2012, Thorpe et al., 2015b). This sliding capacity decreases with age due to the stiffening of the IFM (Thorpe et al., 2013c), presumably imposing premature strains on fascicles and increasing the risk of injury. The human Achilles tendon, the most important energy-storing tendon in human locomotion, exhibits a similar fascicle sliding mechanism and compliant IFM (Patel et al., 2016, Patel et al., 2021). The matrix between sub-tendons, termed the inter-sub-tendon matrix (Gains et al., 2020), has more complex requirements than the IFM as it is subjected to high asymmetric loads due to the aforementioned individual control from different muscles. The inter-sub-tendon matrix is therefore likely to demonstrate a

more extreme specialisation than the more homogeneously loaded IFMs within each sub-tendon (Gains et al., 2020). The detailed sliding behaviour between human Achilles sub-tendons is difficult to study both *in vivo* and *in vitro* due to the highly complex, individually variable rotatory morphology of the tendon and sub-tendon (Edama et al., 2016, Pękala et al., 2017) in addition to the difficulties of obtaining sufficient healthy specimens to study.

In this chapter, a novel equine tendon model is proposed for studying the sliding mechanism between sub-tendon structures – the deep digital flexor tendon (DDFT) and its accessory ligament (AL). The SDFT is a commonly accepted animal model for the human Achilles tendon and has a comparable energy-storing function. However, the SDFT does not possess sub-tendon level structures and cannot provide an understanding of shear mechanics between human Achilles sub-tendons. The DDFT and AL have a separate origin and proximal portion but combine to form one, seemingly homogeneous, structure. The DDFT lies just beneath the extensively studied SDFT and provides a more supporting and positioning role during locomotion compared to the SDFT (Denoix, 1994). The loading pattern differs between the two branches of this structure. The DDFT originates from the deep digital flexor muscle and its loading is directly associated with muscular actions; the

AL originates from the common palmar ligament of the carpus, so its mechanical behaviour is largely dictated by the metacarpophalangeal joint angle (Denoix, 1994). Along the descent, the AL gradually flattens and wraps around the DDFT at the mid-metacarpus level. A considerable degree of sliding is required at the junction due to the different mechanical demands and different strain patterns during gait cycles between structures. Distally, the AL completely blends with the DDFT, forming one elliptical adjoined tendon before passing through the metacarpophalangeal joint (Figure 2-1). Given this bifurcated geometry and the different functional roles, the regional mechanical properties are likely different between the two proximal ends and joined regions. It has been demonstrated that the proximal DDFT is a stiffer structure than the proximal AL (Denoix, 1994, Swanstrom et al., 2004), but no previous study has investigated the mechanical properties at the junction, where the two structures join. The junction is subjected to intermittent high asymmetrical loads transmitted from either the AL or DDFT, resulting in complex force interactions. The shear-related displacement of the less-strained contralateral side will be influenced by the properties of the inter-sub-tendon matrix governing the force transmission and the relative sliding behaviour between the two structures. The complex force interaction at the junction can also

induce compositional adaptations, allowing this tendon complex to withstand its mechanical demands and potentially preventing injury development, which is seldom reported in this tendon.

This chapter aims to explore the mechanical response at the junction between the AL and DDFT and along the length of the tendon when subjected to asymmetrical loads at both whole tendon and fascicle levels. In addition, we tested whether the AL and DDFT demonstrate regionally different matrix compositions between structures and between different tendon regions.

2.1.1 Hypothesis

Hypothesis 1 – The ECM composition and mechanical properties differ between the AL and the DDFT, and between different tendon regions within the same structure (AL or DDFT).

Hypothesis 2 – The junction exhibits different shear-related displacements when loaded through different structures.

2.1.2 Objectives

- Compare basic ECM composition (water, collagen, glycosaminoglycan, DNA, collagen-linked fluorescence) between

the AL and the DDFT, and between different tendon regions (proximal, mid-tendon, distal).

- Conduct non-destructive tendon level mechanical testing on the intact AL-DDFT complex through sequential loading of the proximal AL and the proximal DDFT.

- Conduct destructive fascicle level mechanical testing on isolated fascicles and fascicle pairs to characterise fascicle level mechanical properties.

- Measure displacement discrepancy at the junction between the AL loaded and the DDFT loaded condition.

2.2 Methods

2.2.1 ECM Composition

2.2.1.1 *Sample preparation*

In total eleven equine forelimb DDFT and AL of various ages were harvested, and 11 sites from each were selected for biochemical assays based on the anatomical features (Figure 2-1). Right limbs were chosen for

matrix composition analysis and left limbs for biomechanical tests (Section 2.2.2), assuming no significant limb differences between left and right sides.

Proximally, free-end regions were defined by the length, measured by a ruler with 1 mm accuracy, between the most proximal part of AL and the junction. The length was then divided and proximal (1st quarter), midpoint, and distal AL (3rd quarter) regions were defined accordingly. Proximal DDFT, midpoint DDFT, and distal DDFT were defined as the identical level of their AL counterparts (Figure 2-1).

Joined regions were arbitrarily defined by the inter-sub-tendon properties. The loosely joined region, where AL and DDFT are connected by a thin transparent mesh-like structure, can be easily separated with a scalpel without damaging fascicles. Distally, the tightly joined region is defined as the region where fascicles start to intertwine and separating the AL and DDFT will inevitably damage the fascicles (Figure 2-1). As many intact fascicles as possible were preserved during the dissection at the tightly joined region. At the distal end, the merged region was defined as the most distal tensional region (proximal to the fibrocartilage region), where the cross-sectional view shows visually homogeneity between the two structures.

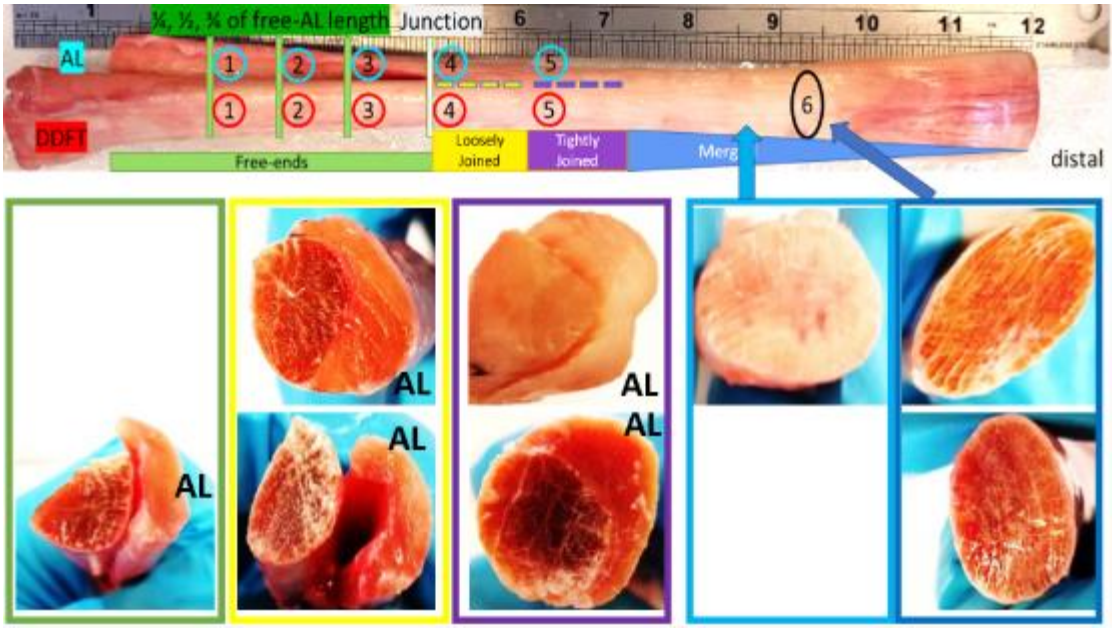

Figure 2-1. Different regions of the accessory ligament (AL) and the deep digital flexor tendon (DDFT). 1. Free-ends, proximal; 2. Free-ends, midpoint; 3. Free-ends, distal; 4. Loosely joined; 5. Tightly joined; 6. Merged region. The lower column represents cross-sections referring to individual regions with colour coded (green: free-ends, yellow: loosely joined, purple: tightly joined, and blue: merged). The white bar represents the AL and DDFT junction.

Approximately 1 cm^3 of tissue was sampled out from the tendon/ligament core of each region. Samples were then weighed, freeze-dried, and re-weighed to calculate the water content. After crushing under room temperature using scissors and a scalpel, approximately 20 mg of dried tissue sample was then weighed out and suspended in 2 ml of buffer solution (phosphate-buffered saline with 5 mmol/L cysteine.HCl and 5 mmol/L EDTA, pH 6.0) with papain (31 units/mg, P3125, Sigma-Aldrich). Digestion was carried out at 60°C for over 16 hours, and samples were mixed several times

during the digestion (Birch et al., 1998). Each sample was completely solubilised at the end of the process.

2.2.1.2 *Collagen assay*

Total collagen content was quantified by a spectrophotometric method which measures the imino acid hydroxyproline concentration within the tissue. (Bannister and Burns, 1970, Birch et al., 1998). An aliquot of papain digests (100 µl) was first hydrolysed using 6M HCl at 110°C for 24 hours. Hydrolysed samples were then dried under a vacuum, and then re-dissolved in deionised water. A standard curve obtained from 1 to 10 µg/ml L-hydroxyproline (104506, Merck) was prepared for calculation, assuming hydroxyproline content to be present at 14%. Collagen content was expressed as mg/mg sample dry weight.

2.2.1.3 *DNA assay*

DNA content was quantified in an aliquot of the papain digest by the fluorometric method with bisbenzimidazole dye (Hoechst 33258) (Birch et al., 1998, Kim et al., 1988). Fluorescence was measured again without bisbenzimidazole dye to obtain the reading from background collagen-linked fluorescence. Previous studies have reported an age-related increase in the

fluorescence level; therefore, a sub-group analysis was performed to compare the tendons of different ages (young: < 10 years, n = 4; middle: 10 – 20 years, n = 3; old: > 20 years, n = 4). DNA concentration within each sample was calculated from a standard curve obtained from 1 to 10 µg/ml calf thymus DNA (D3664, Sigma-Aldrich). DNA content was expressed as µg/mg sample dry weight.

2.2.1.4 *Glycosaminoglycan assay*

Total sulphated GAG content was quantified in an aliquot of the papain digest by the spectrophotometric method with dimethylmethylene blue dye (Birch et al., 1998, Farndale et al., 1986). GAG concentration within each sample was calculated from a standard curve obtained from 10 to 100 µg/ml bovine trachea chondroitin sulphate (C9819, Sigma-Aldrich). GAG content was expressed as µg/mg sample dry weight.

2.2.1.5 Statistical analysis

Repeated measure one-way ANOVA was used to compare ECM composition (water, DNA, GAG, collagen, collagen-linked fluorescence) at different regions within the same structure (AL or DDFT). Bonferroni adjustment was used for *post hoc* analysis. Paired t-tests were used to

compare the composition between structures (AL and DDFT) in each region. Pearson's correlation coefficient was calculated for relationships between horse age and collagen-linked fluorescence for both structures at different regions. Statistical tests were conducted by SPSS (v25, IBM, US) with the two-tailed significant level set at 0.05.

2.2.2 Tendon Level and Fascicle Level Mechanical Testing

2.2.2.1 Sample preparation

In total 17 pairs of equine forelimbs (aged from 3 to 24 years) were collected at a commercial abattoir where horses are euthanised for reasons other than research. The Animal (Scientific Procedures) Act 1986, Schedule 2, does not define collection from these sources as scientific procedures. The DDFT and AL between the carpus and metacarpophalangeal joint of each forelimb were harvested within 24 hours and kept frozen at -80°C until further analysis. No sign of tendon pathology was noticed during the harvest.

2.2.2.2 Tendon level mechanical testing

On the test day, specimens (n = 10) were thawed at room temperature before measuring the CSA of different regions by moulding in dental alginate paste as previously described (Goodship and Birch, 2005). The CSA of free-

AL and free-DDFT were measured at a point 30 mm proximal to the junction. The CSA of the joined region was measured at a point 30 mm distal to the junction (Figure 2-2, *blue lines*).

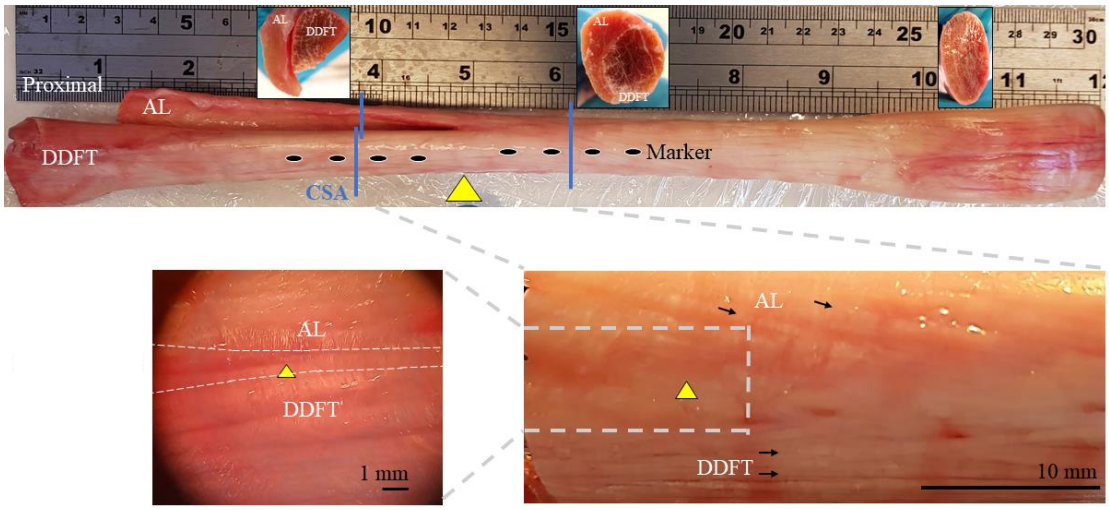

Figure 2-2. The deep digital flexor tendon (DDFT), its accessory ligament (AL), and the inter-sub-tendon matrix *(lower left)*. Yellow triangles: the junction between two structures. Blue lines: levels measuring cross-sectional area. Upper row insets: cross-sections at corresponding longitudinal regions. Black arrows: tendon/ligament fascicles.

Non-destructive quasi-static tests were conducted with sequential loading (AL then DDFT) of two proximal free ends. Specimens were vertically mounted, distal part at the bottom and proximal parts at the top, secured by cryoclamps in a screw-driven mechanical testing device (Instron 5967, Instron, US) with a 30 kN load cell. The free-AL was mounted first while

keeping the free-DDFT relaxed. After securing the specimen in the device, four markers with approximately 25 mm apart were placed directly on the surface along the midline at the regions where the CSAs were measured on the free-AL and free-DDFT and both sides of the joined AL and DDFT (Figure 2-1, *black dots, schematic representation*). A preload of 100 N was applied for 1 min, and the effective gauge length was measured between the two freeze lines. The specimen was then preconditioned by applying a 5% strain for 20 cycles using a triangular wave at 1 Hz frequency. After the last cycle, the specimen was returned to the slack position before being pulled to 10% strain at a speed of 12 mm/sec. A high-speed loading scenario was chosen to closely represent the *in vivo* physiological loading condition. The free-AL of the specimen was dismounted, and the free-DDFT of the same specimen was then mounted and tested under an identical protocol. The AL was chosen to load first as the pilot data showed that the AL is a more compliant structure and therefore the target strain of 10% is reached at a lower load with less chance of damage. Tested specimens were visually inspected after loading through the AL and showed no sign of structural disruption. Subsequently, the force-displacement relationship was checked to ensure no reduction in gradient providing further evidence that the structure had not been damaged.

2.2.2.3 Mechanical properties calculation

Global force and displacement data were recorded by the mechanical testing machine at 100 Hz. During the test, marker movements were captured at 30 Hz by two video cameras, one facing each side of the specimen (Figure 2-3). The pixel movements of the four markers were captured in each video frame and the inter-marker distances were calculated. The regional displacement was then calculated by subtracting the initial inter-marker distance and averaged across the three inter-marker displacements. This regional displacement (from video) was then synchronised, using external auditory cues generated by the mechanical testing machine, with force data to plot the regional force-displacement relationship and the linear region was used for calculating stiffness. Regional stress (force / regional CSA) and regional strain (difference in the regional displacement / initial length) were then further calculated and the linear region of the stress-strain relationship was used for calculating Young's modulus of the free-AL and free-DDFT. An in-house MATLAB (R2020, MathWorks, US) code was used for video processing, regional displacement measurement, offline synchronisation, and mechanical property calculations.

2.2.2.4 Fascicle level mechanical testing

A further seven tendons were used for IFM and inter-sub-tendon matrix testing. The peritendinous tissues were carefully removed and the junction of the AL and DDFT was visually identified (Figure 2-2, *yellow triangles*). For the inter-sub-tendon matrix isolation, a fascicle pair (one fascicle from the AL and one from the DDFT) was visually tracked and separated from proximal (~ 5 mm above the junction) to distal, retaining the inter-sub-tendon matrix that binds the AL and DDFT together (Figure 2-2, *bottom left*). For the IFM of AL and DDFT, the fascicle pairs were selected at the same junction region of the inter-sub-tendon separation, but with sufficient distance from the inter-sub-tendon matrix (e.g., Figure 2-2, *black arrows*). Fascicle pairs were approximately 30 mm in length and each fascicle was cut leaving a 10 mm IFM (Thorpe et al., 2012) or inter-sub-tendon matrix for testing (Figure 2-3). It was only possible to separate the inter-sub-tendon matrix in the periphery due to the difficultly of tracking fascicle origins at the core. However, previous studies on other equine tendons found no significant difference in mechanical properties between fascicles isolated from the core or the periphery (Thorpe et al., 2012).

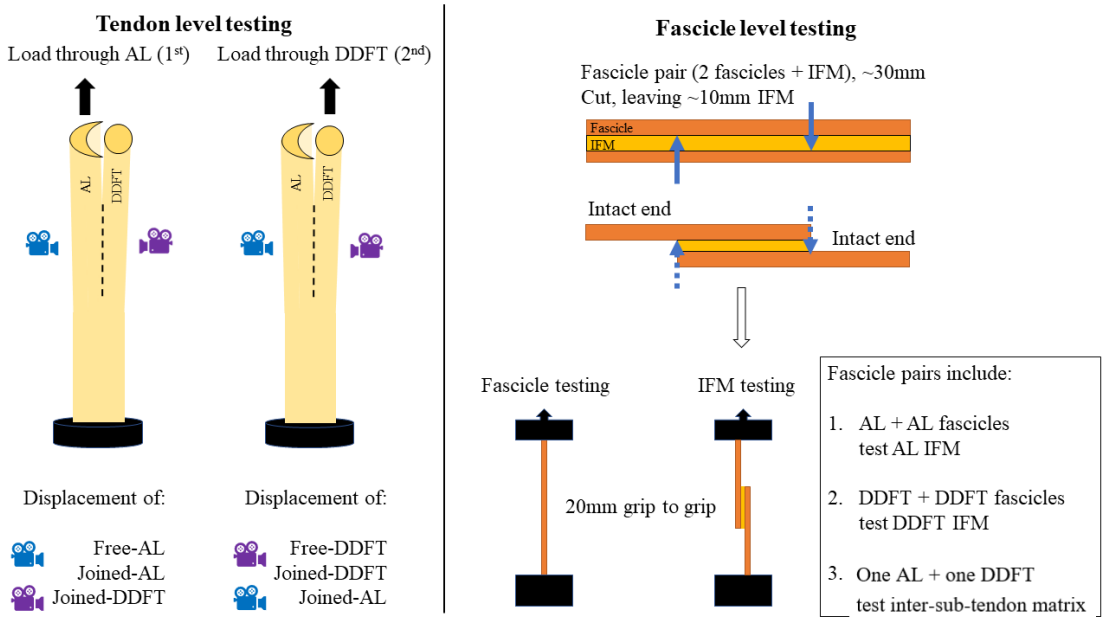

Figure 2-3. Diagram of tendon level *(left)* and fascicle level *(right)* mechanical testing. The IFM was subjected to shear loading during testing and the fascicles to tensional loading (Thorpe et al., 2012, Thorpe et al., 2015b).

The intact ends of the fascicles were mounted in a mechanical testing machine (Instron E1000) with a 250 N dynamic load cell (2527-131 Dynacell, Instron) and custom-made jagged grips. Grip to grip distance was 20 mm (Figure 2-3, *right*). A preload of 0.02 N was applied and the specimen was preconditioned with 10 cycles of sine waves between 0 to 0.5 mm. The structure was then allowed to slacken before being pulled to failure at 1 mm/s (Thorpe et al., 2015b). Force and displacement were recorded at 100 Hz during the test. To normalise data for comparison, the force-displacement relationship was displayed by plotting each 10% of maximal displacement

against force. The stiffness was calculated as the slope of the linear region of the force-displacement relationship of each specimen. Additionally, single fascicles (~ 30 mm in length) from AL and DDFT (n = 7) were dissected and mechanically tested using an identical testing protocol as the IFM, but with load applied in tension instead of shear (Figure 2-3).

2.2.2.5 Statistical analysis

Statistical analysis was performed using SPSS (v. 26, IBM, US) with two-tailed significant level set at 0.05. A one-way ANOVA with Bonferroni *post hoc* adjustment was performed to compare the CSA of three regions. Paired t-tests were performed to compare the means of mechanical testing results between free-AL and free-DDFT, between joined-AL and joined-DDFT, and between AL and DDFT fascicles. Strain and stiffness were also compared between the free and joined region within the AL or the DDFT. One-way ANOVAs with Bonferroni *post hoc* adjustment were conducted for comparing tendon level displacements when loaded in isolation (e.g., free-DDFT, joined-DDFT, and joined-AL when DDFT was loaded) and also inter-fascicular mechanical properties (AL IFM, DDFT IFM, and inter-sub-tendon matrix).

2.3 Results

2.3.1 ECM Composition at Different Tendon Regions

The ECM composition differed between the AL and the DDFT and demonstrated a high variation within the same structure. The AL consistently showed higher water, GAG, DNA content, and lower collagen-linked fluorescence than the DDFT (Figures 2-4 to 2-9). Besides the total collagen content, the merged region demonstrated intermediate water, DNA, and GAG content compared to the AL and the DDFT.

The joined-AL had significantly lower water content than the free-AL, but no statistical difference was found between the free-DDFT and the joined-DDFT (Figure 2-4). No statistical differences were found in total collagen content between different regions (Figure 2-5). Higher cellularity was found at the joined regions of both structures compared to the free-ends (Figure 2-6). However, only the DDFT demonstrated a higher GAG content at the joined region than the free ends (Figure 2-7). No regional differences in the measured collagen-linked fluorescence were found (Figure 2-8), but positive correlations existed between horse age and the fluorescence level (AL:

averaged r = 0.82, from 0.79 to 0.84; DDFT: averaged r = 0.78, from 0.72 to 0.81; Figure 2-9).

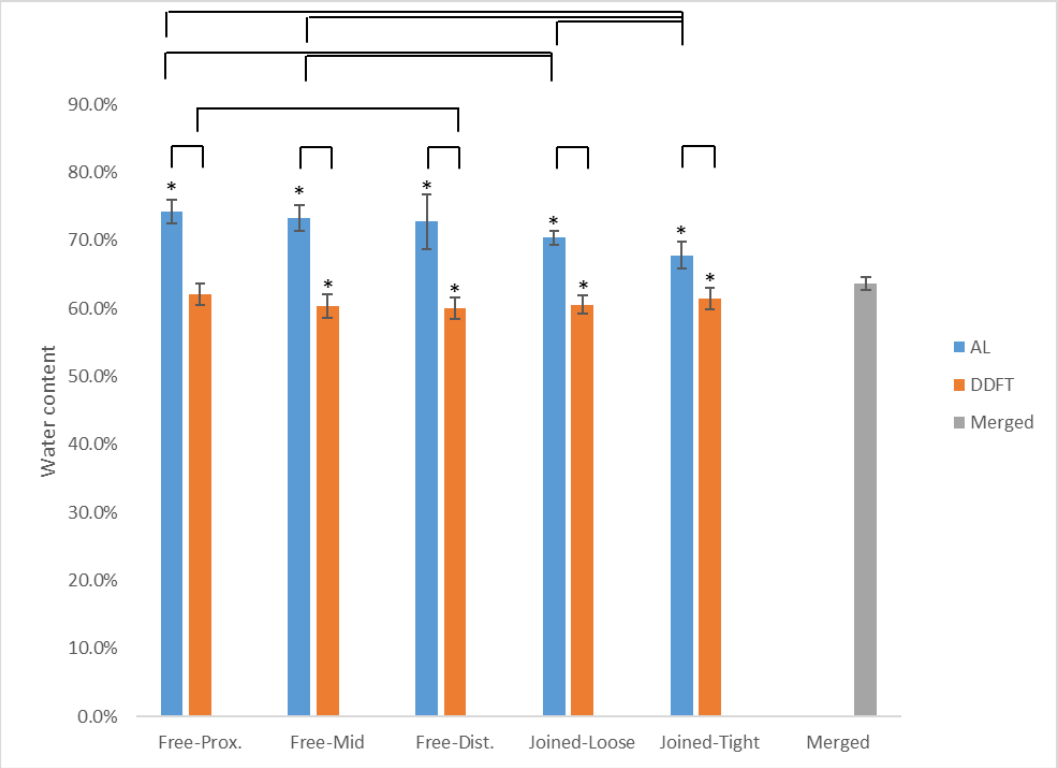

Figure 2-4. Water content of AL and DDFT at different regions. *: significantly different than the merged region.

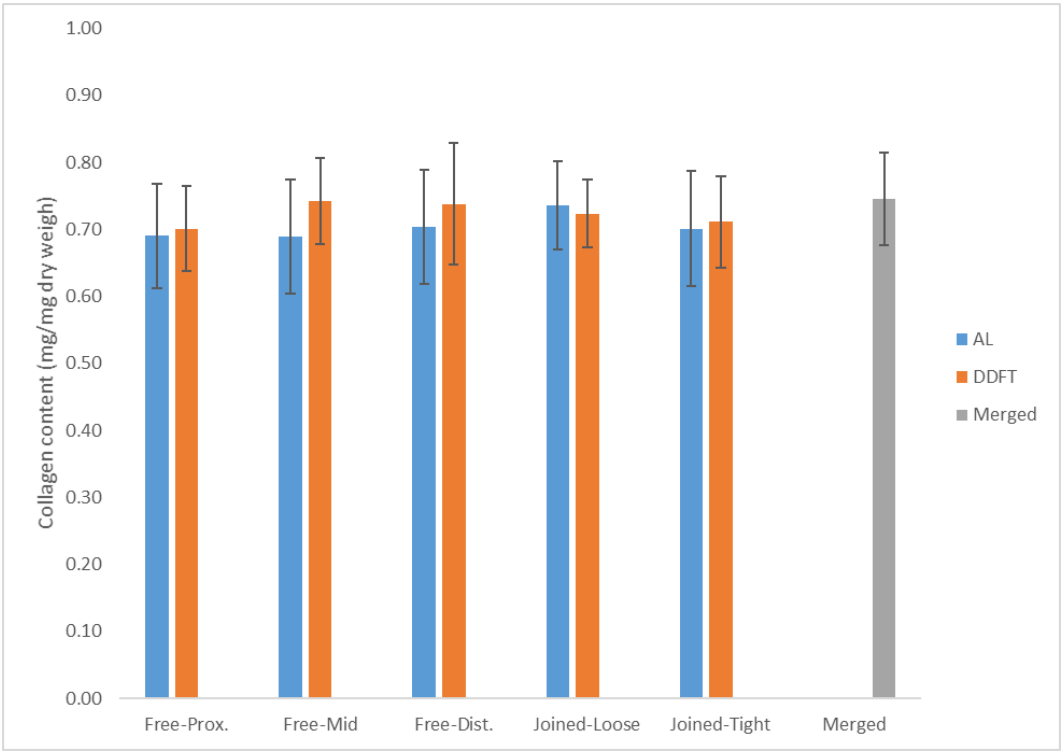

Figure 2-5. Total collagen content of AL and DDFT at different regions.

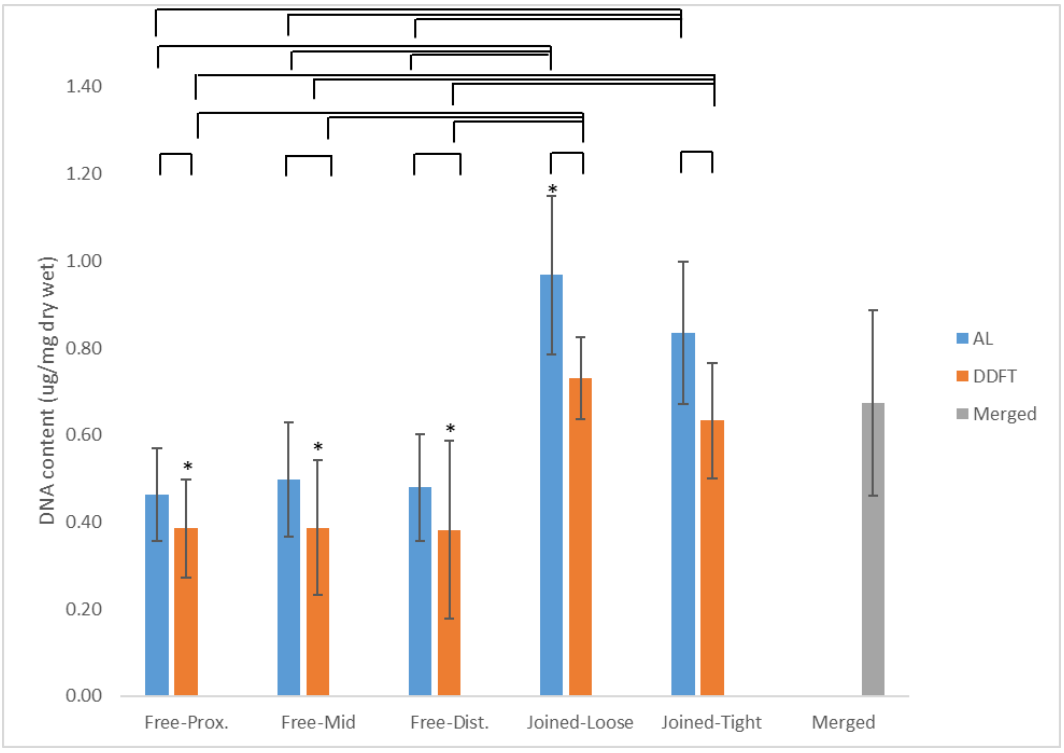

Figure 2-6. DNA content of AL and DDFT at different regions. *: significantly different than the merged region.

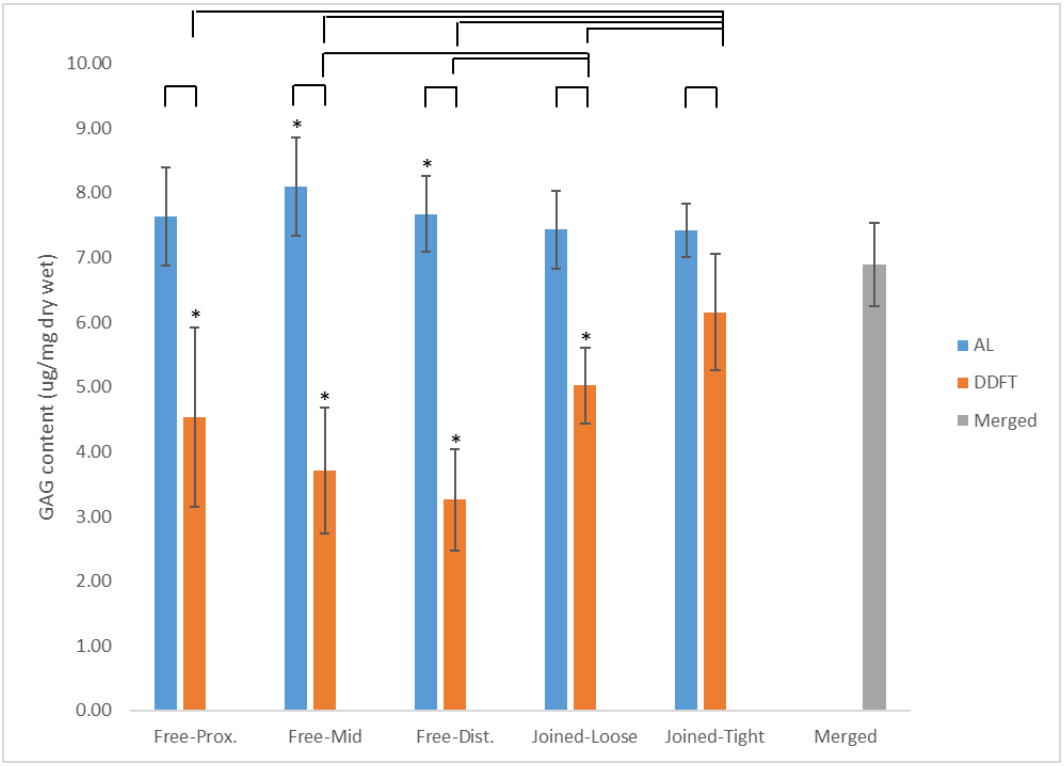

Figure 2-7. GAG content of AL and DDFT at different regions. *: significantly different than the merged region.

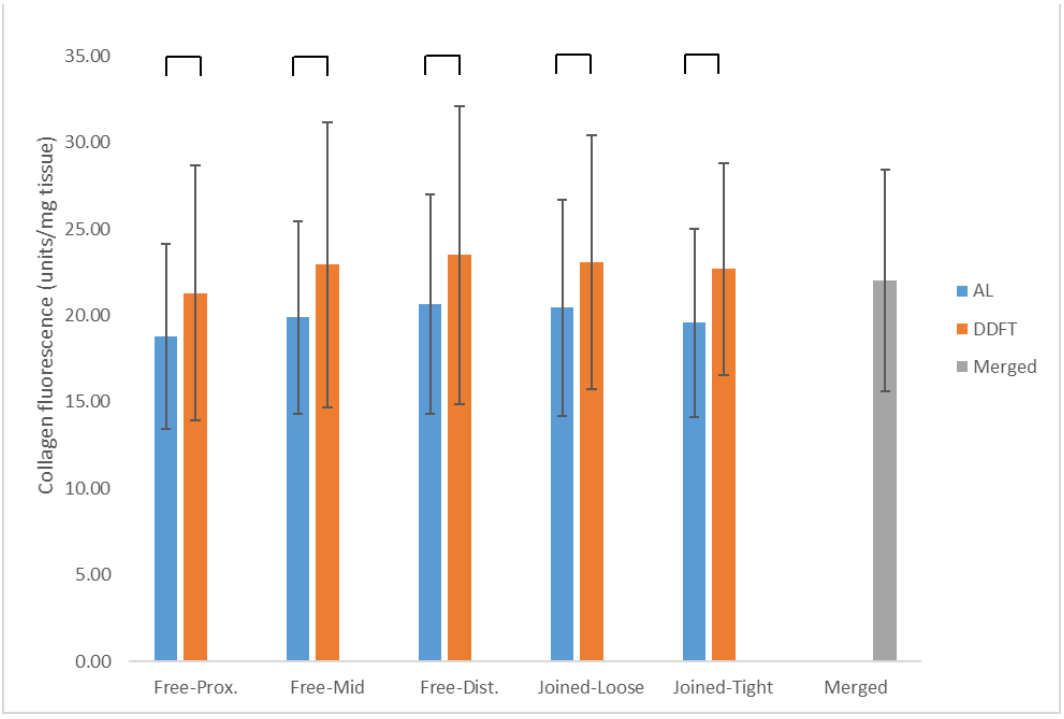

Figure 2-8. Collagen-linked fluorescence level of AL and DDFT at different regions.

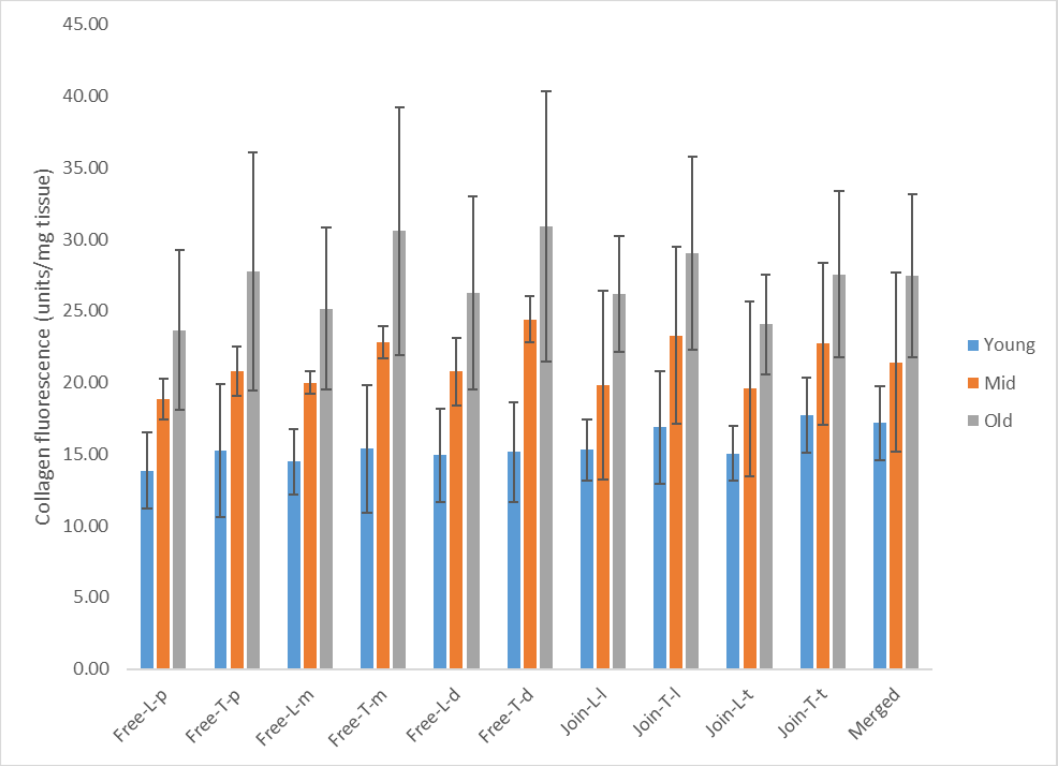

Figure 2-9. Fluorescence level of different age groups at different regions. L: accessory ligament, T: deep digital flexor tendon. p: proximal, m: midpoint, d: distal, l: loosely joined, t: tightly joined region.

2.3.2 Tendon Level Mechanical Properties

The CSA (n = 10) of the joined region (159.4 ± 30.3 mm^2) was significantly larger than the free ends of both AL (96.4 ± 31.6 mm^2) and DDFT (89.2 ± 28.4 mm^2) but smaller than the combined CSA of the free ends. The mechanical testing results of the tendon level (n = 7) and fascicle level (n = 7) are summarised in Tables 2-1 to 2-3. The tendon level mechanical testing

data from 3 limbs were discarded due to poor image quality or clamp slippage during testing.

When the AL was loaded, the machine recorded lower maximal force (global) compared to the DDFT loading condition. The regional displacement and strain (measured by cameras) showed significant regional differences between free-AL, joined-AL, and joined DDFT, which receives load only through shear. The stiffness of the free-AL was significantly lower than the joined-AL when the AL was directly loaded (Table 2-1).

When the DDFT was loaded in isolation, the displacement, strain, and stiffness were similar between the free- and joined-DDFT, contrary to the AL loading condition (Table 2-2). Comparing the two loading conditions revealed that the free-DDFT was a stiffer structure than the free-AL and had a higher material stiffness (Figure 2-10).

Table 2-1. Mechanical testing results when load was applied through the AL

	Global	Regional		
		Free-AL	Joined-AL	Joined-DDFT
Maximal force (N)	4320±1684			
Displacement (mm)	13.2±1.8	5.0±1.4[a, b]	3.6±1.5[b]	1.9±0.8
Stress (MPa)		44.8±15.4[c]		
Strain (%)	10.0±0.0	6.8±2.0[a, b, c]	4.0±1.3[b]	1.9±0.8
Young's modulus (MPa)		639±24[c]		
Stiffness (N/mm)		841±328[c]	1247±836	

Data are shown as mean ± SD (n = 7). a: Significant difference from joined-AL. b: Significant difference from joined-DDFT. c: Significant difference from the same location as DDFT (Table 2-2).

Table 2-2. Mechanical testing results when load was applied through the DDFT

	Global	Regional		
		Free-DDFT	Joined-DDFT	Joined-AL
Maximal force (N)	5370±2108			
Displacement (mm)	14.4±2.4	4.1±1.4[b]	4.2±1.1[b]	1.2±1.5
Stress (MPa)		60.7±26.9[c]		
Strain (%)	10.0±0.0	5.3±1.5[b, c]	4.9±1.8[b]	1.4±1.8
Young's modulus (MPa)		1158±459[c]		
Stiffness (N/mm)		1387±640[c]	1224±486	

Data are shown as mean ± SD (n = 7). a: Significant difference from joined-DDFT. b: Significant difference from joined-AL. c: Significant difference from the same location as AL (Table 2-1).

Interestingly, when comparing the displacement of the contralateral joined regions, the force transmittance pattern was different between AL and

DDFT loading conditions. When the DDFT was directly loaded, the joined-AL remained stationary and started to elongate only after a substantial force (~ 4000 N) was imposed on the DDFT (Figure 2-11, *right*). When the AL was loaded, the joined-DDFT displaced proportionally to the joined-AL strain (Figure 2-11, *left*). Maximal displacement discrepancy at the junction was about 3 mm (DDFT loaded, 3920 N) and 1.7 mm (AL loaded, 4192 N).

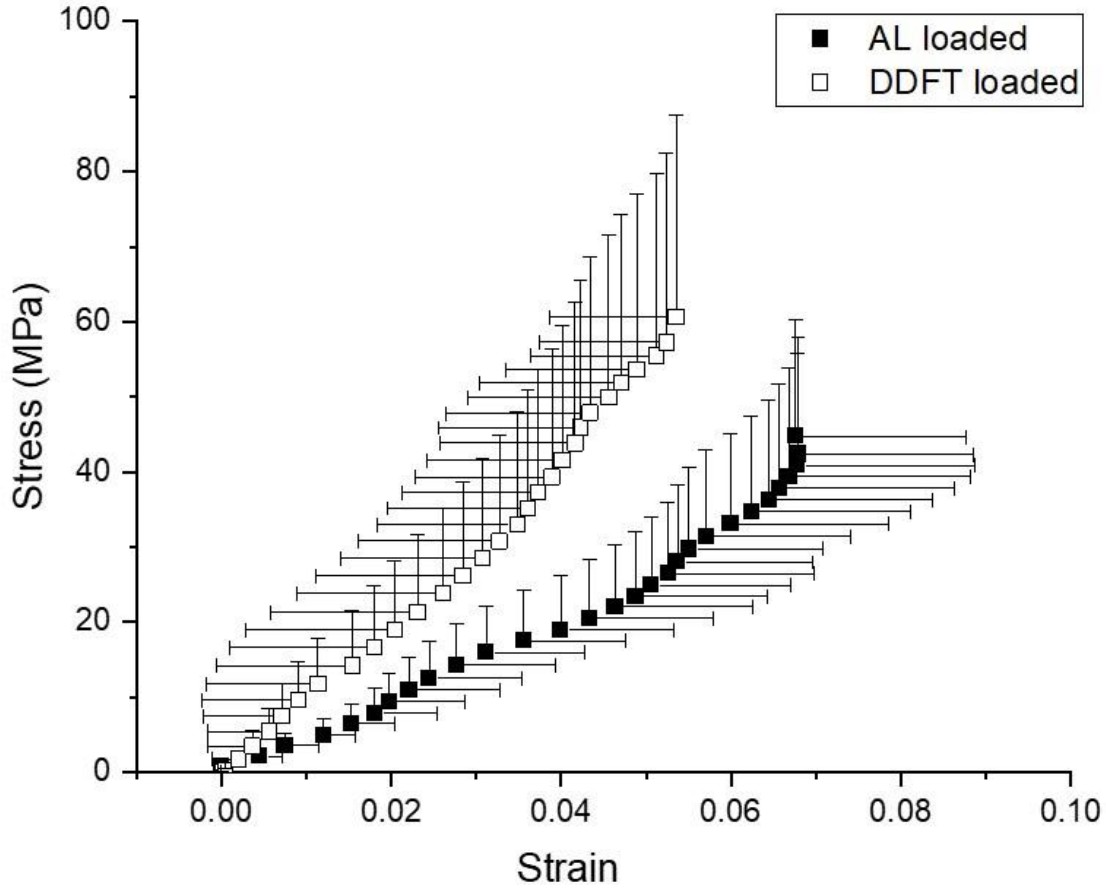

Figure 2-10. Averaged (n = 7) stress-strain relationship of free-AL and free-DDFT

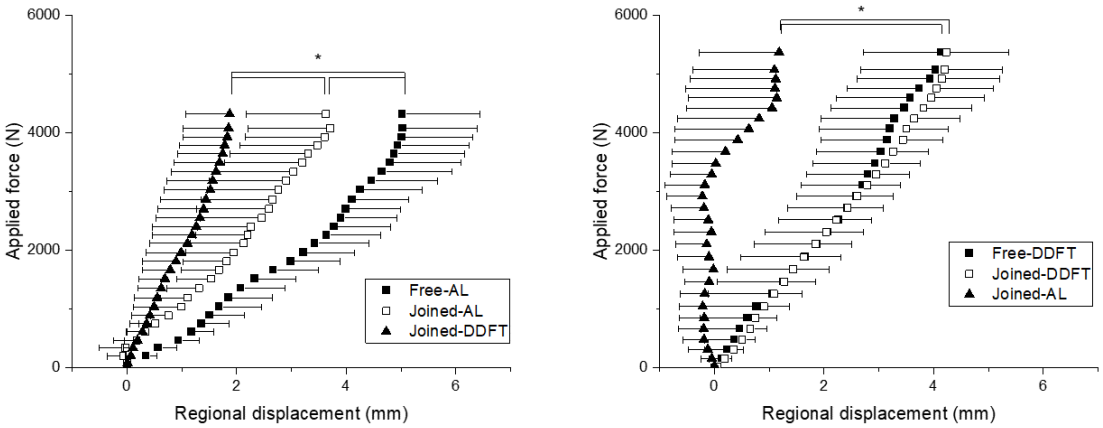

Figure 2-11. Averaged (n = 7) force-displacement relationship when AL *(left)* and DDFT *(right)* were loaded in isolation. The contralateral side (joined-DDFT when AL loaded, joined-AL when DDFT loaded; *closed triangles*) was shear loaded alone. Asterisks: significant difference in maximal displacement.

2.3.3 Fascicle Level Mechanical Properties

AL and DDFT fascicles exhibited similar failure force and maximal displacement (Table 2-3) and their mechanical properties were not significantly different. The averaged AL IFM appeared to have a slightly higher failure force and stiffness than the DDFT IFM and the inter-sub-tendon matrix, but the differences were not statistically significant (Table 2-3). The relationship between load and displacement however differs significantly; at 20% and 30% of normalised displacement levels, AL IFM exhibited significantly higher force than the inter-sub-tendon matrix (Figure 2-12). At higher normalised displacement levels differences were not significant.

Table 2-3. Mechanical properties of fascicles and inter-fascicular matrices

	Inter-fascicular matrices			Fascicles	
	AL	DDFT	Inter-sub-tendon	AL	DDFT
Failure force (N)	2.2±1.1	1.4±0.8	1.1±0.8	5.3±0.9	4.9±2.5
Failure strain (%)				7.5±5.5	7.5±4.5
Maximal displacement (mm)	1.9±0.7	1.7±0.5	1.8±0.7	1.5±1.1	1.5±0.9
Stiffness (N/strain%)				0.7±0.2	0.7±0.6
Stiffness (N/mm)	1.6±0.7	1.3±0.7	0.9±0.6	4.3±2.3	3.2±2.2

Data are shown as mean ± SD (n = 7). N.B displacement for the inter-fascicular matrix is given in mm due to un-defined effective gauge length.

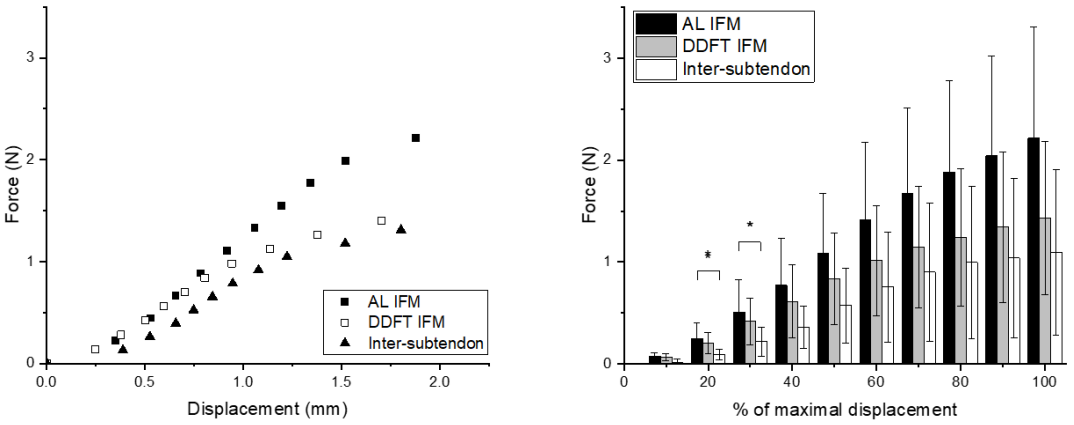

Figure 2-12. Relationship between force and displacement in AL IFM, DDFT IFM, and inter-sub-tendon matrix (n = 7). *: significant difference after *post hoc* analysis ($p < 0.017$).

2.4 Discussion

The biochemical assay results are in line with previous studies comparing ligaments with tendons (Batson et al., 2003, Rumian et al., 2007).

Interestingly, after seemingly joining together as one homogeneous tissue, the AL and the DDFT preserve their distinct composition traits as a tendon or a ligament within the conjoined structure while, at the same time, demonstrating significant regional variations that are likely as a result of the complex mechanical force interaction at the junction.

Ligaments are generally higher in water, proteoglycan, and cellular contents but not necessarily higher in collagen content than tendons (Batson et al., 2003, Rumian et al., 2007). One previous study, which analysed four equine forelimb tendon and ligament tissues of different functions, reported that the CDET had the highest collagen level (~ 80%) and the suspensory ligament had the lowest (~ 65%), with both flexor tendons (SDFT and DDFT) demonstrating a similar intermediate level of collagen content (~ 76%) (Thorpe, 2010). In sheep, one study demonstrated that higher collagen content was found in tendons compared to peri- and intra-articular ligaments from different anatomical locations, but these differences were more likely related to the local mechanical stimuli than the simple classification of bone-to-bone or muscle-to-bone (Rumian et al., 2007). Therefore, it is possible that the different mechanical demands of the AL and DDFT were not drastic enough to induce fundamental changes to the total collagen content, or the

adaptation of the matrix may be more subtle than simply the total collagen content, such as different collagen types, variable fibril diameters, the difference in collagen crosslinking or an altered IFM to fascicle ratio (Amiel et al., 1984, Rumian et al., 2007).

Having a higher number of cells within ligaments or tendons may be beneficial since it preserves the reparative potential of the tissue (Riley, 2011). The prognosis after ligament injuries is usually better and more likely to fully recover than tendon injuries. Compared to the proximal free ends, the twofold increment of the cellularity at the joined regions of both AL and DDFT could be an adaptative strategy by preserving more cells during skeletal maturation in this high-shear, potentially injury-prone region. However, it is worth noting that a higher cell count does not always result in a higher tissue turnover rate. The more injury-prone equine SDFT has a lower matrix turnover rate compared to the seldom injured CDET, despite having higher cellularity (Birch et al., 2008b, Thorpe et al., 2010c). Our DNA and collagen-linked fluorescence results both suggest that the AL is more frequently renewing its ECM and is likely to have a higher reparative potential than the DDFT. Future studies focusing on the matrix turnover rate, collagen and non-collagenous matrix protein synthesis would improve understanding of the mechanism

behind this increase in cell count at the joined regions. Similar to previous reports, we found a good correlation between collagen-linked fluorescence and horse age in both AL and DDFT, suggesting the accumulation of glycation crosslinks (Section 1.2.3.2.2), which are frequently reported among aged equine tendons (Birch et al., 1999, Thorpe et al., 2010c).

The AL demonstrated a high regional variation in water content and the changes were paralleled with the GAG content. Interestingly, the DDFT, despite having a small variation in water content between regions, demonstrated a twofold increase in the GAG content at the joined regions compared to the free ends. Measuring total GAG content is a convenient way to study the proteoglycan content in tendons, and these findings can be interpreted as an increased total proteoglycan quantity or having different proteoglycan types at the joined region. Compared to the tensional regions, both the total GAG content and the level of large aggregating proteoglycans (aggrecan and versican) increase at the compressive tendon regions (Vogel et al., 1993, Yoon and Halper, 2005, Matuszewski et al., 2012). The anatomical feature of the AL, which partially surrounds the DDFT at the junction (Figures 2-1 and 2-2), could exert compressive forces on the DDFT when loaded (see below). It can be hypothesised that the high GAG content

at the joined-DDFT region results from the increase of large aggregating proteoglycan levels. Future histological studies are warranted to characterise the proteoglycan distribution and the detailed composition at the junction.

The tendon level mechanical testing results demonstrate that this equine tendon exhibits a large displacement discrepancy at the junction when subjected to asymmetry loads as expected. The mechanical properties obtained for the free-AL and free-DDFT are comparable with previous studies on isolated AL (Becker et al., 1994) and DDFT (Denoix, 1994). The higher material stiffness of the DDFT fulfils its mechanical role of positioning distal joints in flexion during galloping, a function similar to the equine digital extensor tendons and the human tibialis anterior tendon. Interestingly, in our study, the palmar and dorsal aspects of the joined AL and DDFT structure behaved differently compared to the proximal free regions. The regional strain of the joined-AL was significantly lower than the free-AL, suggesting a large proportion of force transmitted through shear-loaded alone to the contralateral joined-DDFT, the regional strain of which was lower but closely related to the joined-AL. On the contrary, the regional strain of free- and joined-DDFT were almost identical when loaded in isolation, suggesting a more homogeneous structure throughout the DDFT and a lower force transmitting capacity at the

junction compared to force transmission from the AL to the DDFT. The adjacent joined-AL displaced surprisingly little even when the DDFT was subjected to a substantial level of force (~ 4000 N).

This force transmission discrepancy at the junction between different loading conditions is difficult to explain by the mechanical properties alone. One possible explanation of this unique behaviour at the junction is the different geometry between the AL and DDFT. The AL gradually flattens and wraps around the DDFT when descending, forming a C-shape structure surrounding the O-shape DDFT at the junction. Due to Poisson's effect, the C-shape AL when loaded could exert a compressive force on the DDFT, transmitting force through the inter-sub-tendon matrix resulting in a displacement of the joined-DDFT. When the load is applied through the DDFT however, the decreasing CSA of the O-shape DDFT when loaded may make it less likely to exert force on the joined-AL. Although this theory alone does not explain why the joined-AL eventually displaced when high loads were imposed on the DDFT, understanding how the geometry of sub-components within one tendon structure affects mechanical behaviour will be a breakthrough in understanding Achilles tendon mechanics since a similar geometry feature also exists in Achilles sub-tendons where the C-shape

gastrocnemii surround the soleus sub-tendon (Szaro et al., 2009, Edama et al., 2015a, Edama et al., 2016).

The mechanical properties of the inter-fascicular and inter-sub-tendon matrix could also contribute to this unique behaviour seen at the junction. Given the large differences in the force-displacement relationship between the AL IFM and inter-sub-tendon matrix, a near-failure force for the inter-sub-tendon matrix could only result in approximately half of the displacement in the AL IFM. On the contrary, since the force-displacement relationships between DDFT IFM and inter-sub-tendon matrix were similar and both were more compliant and weaker than the AL IFM, a fully loaded AL could result in a substantial displacement of the DDFT, showing a more synchronised displacement between the shear-loaded joined-DDFT and the directly loaded joined-AL. However, these inter-fascicular differences in mechanical properties were only statistically significant at initial displacements (< 30%). This may be due to the small sample size, mixed ages, and the inherent variation between individual animals. We were not able to measure the thickness or CSA of the inter-fascicular matrices or to maintain identical IFM quantity (volume) during our test. Age is likely to have a significant influence on IFM mechanical properties since previous studies have successfully

demonstrated age-related IFM stiffening in the SDFT (Thorpe et al., 2012, Thorpe et al., 2015b). A greater adhesion of the inter-sub-tendon matrix would drastically affect force transmission at the AL-DDFT junction. Future studies may benefit from obtaining a larger sample size with a wide age range to detect potential fascicle IFM and inter-sub-tendon matrix level differences. Our measured fascicle level mechanical properties were similar to those reported for the SDFT (Thorpe et al., 2012, Thorpe et al., 2015b), and these results also imply that inter-fascicular differences have a greater influence on whole structure mechanical properties than the fascicle differences. Additional research is warranted to explore whether fascicle sliding also plays an important role in the DDFT during loading as there are important differences in function and composition between the SDFT and DDFT (Denoix, 1994, Birch et al., 1999). We could only confidently isolate fascicles at the periphery due to the difficulty in tracing the fascicular origin at the core. Previous studies however suggest that the fascicle and IFM mechanical properties are similar at the core and the periphery in other equine tendons (Thorpe et al., 2012). Only the force-displacement relationship was reported due to the difficulties in accurately measuring the CSA of the tested fascicles. The actual material strength of fascicles is supposedly greater than the IFM (Komolafe and

Doehring, 2010). Future studies could also investigate the influence of the lower hierarchies (fibril or fibre level) on the fascicle and sub-tendon level mechanical behaviours (Reese et al., 2010, Thorpe et al., 2013b, Shearer et al., 2017, Karathanasopoulos et al., 2019).

In some specimens, an initial negative displacement of the joined-AL was observed when the DDFT was loaded. This apparent negative displacement could result from an error from our image-based measurement. However, the highest negative displacement measured under 4000 N was -0.017 mm (maximal positive displacement: 0.022 mm). This potential measurement error is therefore unlikely to affect the overall reported outcome. Alternatively, the negative displacement may result from a bending of the structure when the load is initially applied to the contralateral side. It is also worth noting that macroscale strain does not fully represent the microscale strain (Reese et al., 2013). Therefore, the measured external regional strain may not fully represent the internal strain of the highly heterogenous tendon structure.

These mechanical testing results can give an insight into why injury to the AL is more prevalent than injury to the DDFT (Dyson, 1991, Thorpe et al., 2010a). During galloping, the AL is taut rapidly when the carpal joint moves

from flexion to extension while the DDFT remains taut continuously. Taken together that the AL is less stiff than the DDFT and the free-AL is more compliant than the joined-AL, the rapid and high-intensity loading imposed on the whole heterogeneous AL structure may produce localised high strains proximal to the junction and high shear strain at the junction. Indeed, injury to the AL proper (free-AL region) is more frequently reported than injuries to the free-DDFT or below the junction level (Dyson, 1991). It is also worth noting that adhesion between AL and DDFT is sometimes reported with AL desmitis (Dyson, 1991). Adhesion at the junction may be a reaction to injury and may interrupt the unique mechanical response in this tendon complex, but the exact consequence is unknown.

This proposed equine tendon model can help researchers systematically study the shear-related mechanical responses at the interfaces between two structures and understand how tendons adapt their extracellular matrix composition and organisation to withstand the high internal displacement discrepancy.

2.5 Conclusion and Chapter Summary

The AL-DDFT tendon complex shows distinct structural and regional mechanical properties and exhibits large displacement discrepancy at the junction when subjecting to asymmetrical loads. This highly specialised tendon exemplar can be studied macroscopically using conventional mechanical testing devices at both tendon level and fascicle level, providing tendon researchers with an easy-access model to study intra-tendinous shear mechanics, such as the shear between human soleus and gastrocnemii sub-tendons. The biochemical results suggest a potential adaptation strategy of the tendon matrix could exist at the junction to withstand this high shear stress. Studying the shear-related mechanical responses and the ECM adaptation strategies would improve understanding of human Achilles tendons which, in a manner similar to the AL-DDFT, are constantly subjected to asymmetrical loadings, exhibits non-uniform displacements, and have similar features of sub-tendon shape. In addition, the results suggest that besides the differences in mechanical and matrix properties, the morphology and geometry of the contributing structures may also play a key role in the mechanical function.

Chapter 3 Biomechanical Properties and Composition of Achilles Sub-tendons

3.1 Introduction

The Achilles tendon is the combination of three small sub-tendons with individual twist angles. In addition to the complex morphology, the Achilles tendon is frequently subjected to asymmetric forces, either from the proximal muscular pull or from the highly mobile ankle and foot joint during stance. The gastrocnemii and soleus muscle-tendon units exhibit different properties, suggesting that the extracellular matrix may differ to achieve specialisation for function. At the tendon level, the human Achilles tendon demonstrated higher GAG and DNA content than the tibialis anterior tendon (Birch et al., 1999), a positioning tendon subjected to low force and strain during movement, but the matrix composition has yet to be studied at the sub-tendon level. Differences in properties between gastrocnemii and soleus muscle-tendon units also suggest complex mechanical force interaction between different muscle-tendon units and a requirement for specialised matrix between sub-tendons.

The soleus has the greatest muscle volume and can generate more ankle plantar flexion torque than both gastrocnemii combined (Dayton, 2017).

Intuitively, this high force could directly impose on the soleus sub-tendon and result in a higher displacement than the gastrocnemii sub-tendons, creating large shear within the Achilles tendon. An increased load-bearing capacity may be present at the soleus sub-tendon due to this much larger functional demand than the gastrocnemii. Interestingly, using ultrasound speckle tracking technique, the deep region (assumed soleus sub-tendon) displaced more than the superficial region (assumed gastrocnemii sub-tendons) in both active and passive ankle movements (Arndt et al., 2012, Slane and Thelen, 2014, Franz et al., 2015), suggesting a potentially compliant soleus sub-tendon. The exact cause of this larger displacement in the deep region compared to the superficial region is still unknown. However, due to the twisted and individualised sub-tendon morphology, fundamental knowledge of the isolated sub-tendon mechanical properties needs to be characterised first before inferring the origin of this observed non-uniformity.

Tendon composition is closely related to the local mechanical demands (Birch et al., 2013). The results in Chapter 2 demonstrated that regional compositional differences exist in a naturally branched equine ligament-tendon complex between its proximal and distal regions. Through an indirect measure, the proteoglycan (measured by total GAG content) showed regional

differences, which could be in either quantity or types, due to its conjoined structure. Achilles sub-tendons could exhibit similar compositional differences either between different sub-tendons or between different regions within the same sub-tendon. Currently, few studies have investigated the composition of the human Achilles tendon (Section 1.4.2.2), and no study has identified the basic ECM compositions of each sub-tendon.

3.1.1 Hypothesis

Three Achilles sub-tendons exhibit different ECM composition and mechanical properties.

3.1.2 Objectives

- Conduct *in vitro* mechanical testing on separated three Achilles sub-tendons (soleus, medial and lateral gastrocnemii).
- Conduct biochemical assays (total collagen, glycosaminoglycans, DNA, and collage-linked fluorescence) on three sub-tendons.

3.2 Methods

3.2.1 Separation of Achilles Sub-tendons

In total 5 Achilles tendons (from 69 to 87 years, two males and three females, all right limb) were harvested from fresh frozen tendon specimens (Vesalius Clinical Training Centre, University of Bristol, REC 08/H0724/34). Only tendons showing no signs of injury or disease were included. Sub-tendons were separated as described (Szaro et al., 2009). First, the gastrocnemii muscles and their connecting tendons were separated from the underlying soleus. Proximally, gastrocnemii and soleus muscles are loosely connected and can be easily separated with blunt force. The connection between gastrocnemii tendons and soleus aponeurosis is much tighter than the muscular regions. The gastrocnemii tendons can be slowly peeled away (with a scalpel) from the soleus aponeurosis. Within the Achilles tendon (i.e., distal to the soleus musculotendinous junction), the inter-sub-tendon matrix does not exhibit any visual differences from the inter-fascicular matrices of sub-tendons; however, using the proximal-distal dissection approach, the soleus sub-tendon can be slowly separated from the gastrocnemii, due to the continuous fascicle structure. The medial and lateral gastrocnemii tendons

and sub-tendons were separated after the isolation of the soleus muscle-tendon unit. The two gastrocnemii were then separated along the midline, and the same inter-fascicular region (i.e., between the most lateral med. gastrocnemius fascicle and the most medial lat. gastrocnemius fascicle) were tracked and separated throughout the whole tendon length. The three sub-tendons were separated until approximately 1 cm proximal to the calcaneal insertion site, where fascicles from each sub-tendon start to intertwine and overlap, before inserting on the calcaneus.

Dr Diana Corben separated the sub-tendons and collected raw data from mechanical testing (see below) as a part of her MSc student project.

3.2.2 Mechanical Testing

The CSA of each sub-tendon was measured, by moulding in dental alginate paste (Goodship and Birch, 2005), at the same level as the thinnest region (~ 10 mm to 40 mm proximal to the insertion, by visual identification) of the whole Achilles tendon. The reference line (of the thinnest tendon CSA) was drawn before separating the sub-tendons.

Each sub-tendon was then tested using a mechanical testing system (Instron 5967, Instron, US) with a linear electric motor and a 3 kN load cell.

After being secured into cryoclamps with a 60 mm gauge length, a pre-load was applied (10 N for gastrocnemii and 20 N for soleus) and then 20 cycles of pre-conditioning (triangular wave to 5% strain) were applied. The load was removed to allow the specimen to go slack (4 mm) before being pulled to failure (rate: 0.75 mm/s). An in-house MATLAB code (R2020, MathWorks, US) was used to calculate the ultimate stress (failure force / CSA), ultimate strain (displacement / effective gauge length after preload), Young's modulus (slope of the linear region of the stress-strain curve), and stiffness (slope of the linear region of the force-displacement curve).

3.2.3 ECM Composition

Following mechanical testing, a small portion (at mid-tendon level) of the sub-tendon specimens (n = 5 for each sub-tendon) was sampled and weighed. Samples were then freeze-dried overnight and re-weighed to calculate the water content of each sub-tendon. Dried tissue samples were then crushed and approximately 20 mg weighed out and for papain digestion. The digestion process and the biochemical assays (collagen-linked fluorescence, total collagen, DNA and GAG content) were performed using the protocol introduced previously (Section 2.2.1).

3.2.4 Statistical Analysis

Statistical analysis was performed using SPSS (v26, IBM, US) with two-tailed significant level of 0.05. Kruskal-Wallis H tests were used for comparing mechanical properties (CSA, failure force, ultimate stress, ultimate strain, Young's modulus, and stiffness) and ECM composition (collagen-linked fluorescence, collagen, DNA, and GAG content) among sub-tendons. Mann-Whitney U tests with Bonferroni adjustments were used for *post hoc* analysis.

3.3 Results

3.3.1 Sub-tendon Mechanical Properties

The soleus sub-tendon had the greatest CSA, the highest failure force and stiffness compared to both gastrocnemii sub-tendons (Table 3-1). There were no significant differences in the material properties (ultimate stress and strain, and Young's modulus) between the sub-tendons. The soleus sub-tendon appeared to have a higher averaged failure strain than the gastrocnemii, although the difference was not significant. High variation was also observed between individual specimens in the ultimate stress and Young's modulus.

Table 3-1. Mechanical testing results of three Achilles sub-tendons

Specimen	CSA (mm^2)			Failure force (N)			U. stress (MPa)			Ultimate strain (%)			Young's modulus (MPa)			Stiffness (N/mm)		
(age-sex)	LG	MG	S	LG	MG	S	LG	MG	S	LG	MG	S	LG	MG	S	LG	MG	S
69-M	13.6	14.5	39.2	325.0	402.2	1701.2	24.0	27.7	45.3	9.7	10.0	19.1	353.9	375.8	399.4	79.9	97.6	260.6
78-F	12.4	10.8	20.6	154.7	571.1	1155.6	12.5	52.6	56.2	11.6	8.9	17.5	175.0	771.1	421.1	36.7	145.6	167.8
84-F	5.7	10.7	30.9	503.6	621.8	1577.0	89.0	58.3	51.0	8.9	12.2	10.4	1231.5	636.9	734.9	118.2	121.4	385.1
85-F	10.4	14.0	38.2	787.5	688.3	1090.9	75.8	49.0	28.6	11.9	10.6	15.8	853.6	617.2	239.9	151.7	144.7	156.6
87-M	4.6	17.0	35.2	301.6	647.7	1578.5	65.9	38.1	44.9	8.2	10.2	10.8	1033.4	496.2	606.2	80.9	143.0	349.6
Mean	9.3*	13.4*	32.8	414.5*	586.2*	1420.6	53.4	45.1	45.2	10.1	10.4	14.7	729.5	579.4	480.3	93.5*	130.5*	263.9
SD	4.0	2.7	7.6	242.5	111.3	277.1	33.4	12.2	10.4	1.6	1.2	3.9	449.5	149.9	192.7	43.5	20.9	103.4

CSA: cross-sectional area, LG: lateral gastrocnemius, MG: medial gastrocnemius, S: soleus sub-tendon. *: significantly different from soleus sub-tendon after *post hoc* analysis ($p < .017$).

3.3.2 Matrix Composition

The soleus sub-tendon appeared to have a higher water content (66.8% ± 5.1%) than the lateral (63.2% ± 5.0%) and medial (63.0% ± 7.0%) gastrocnemii but the difference was not significant. Matrix compositions between sub-tendons were largely similar except for the DNA content, with significantly higher cellularity in the soleus than the gastrocnemii sub-tendons (Figure 3-1, *lower*). The soleus appeared to have a slightly lower averaged total collagen content (Figure 3-2, *upper*) and the medial gastrocnemius sub-tendon appeared to have a higher averaged GAG content (Figure 3-1, *upper*). However, these differences were not statistically significant.

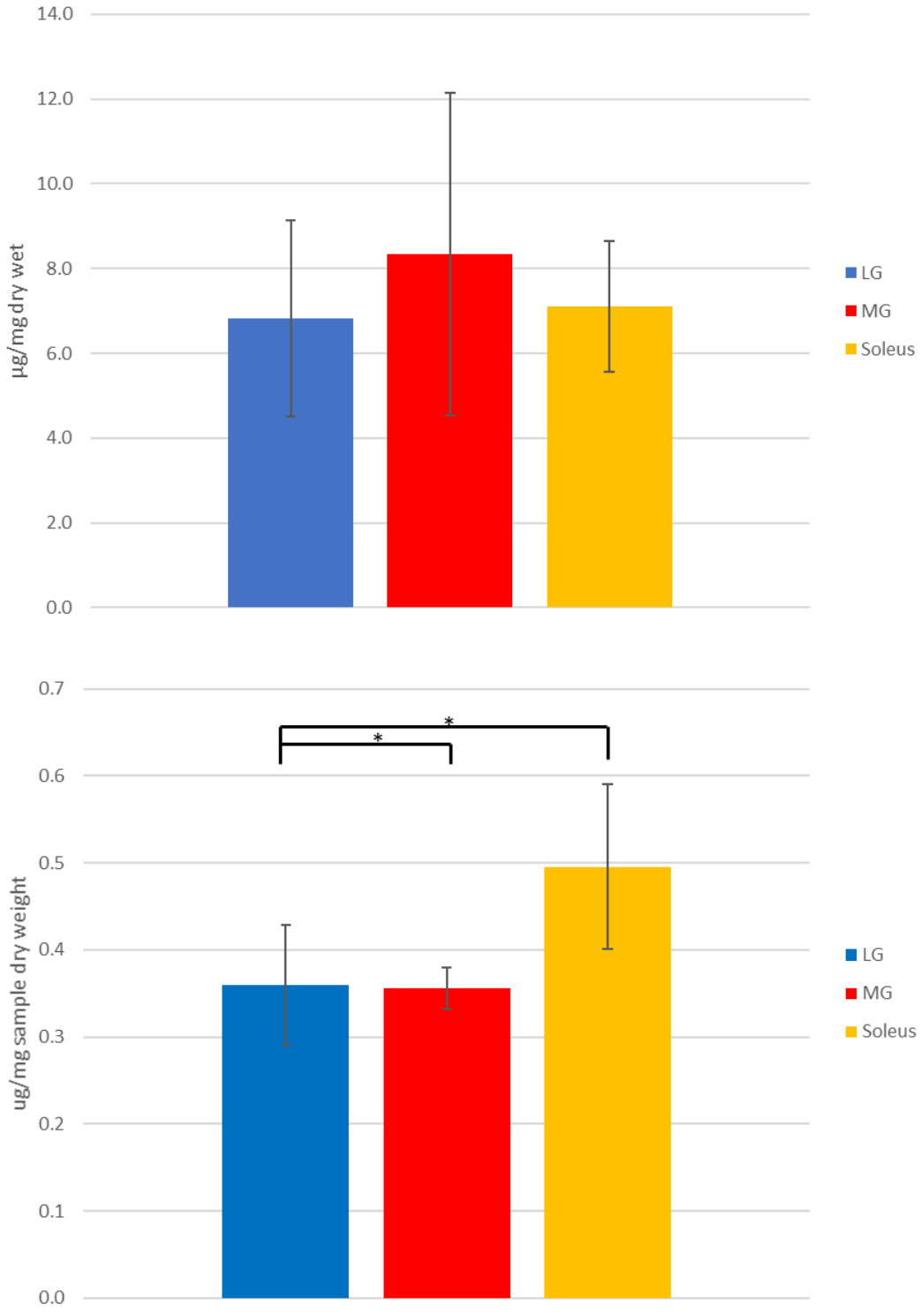

Figure 3-1. GAG *(upper)* and DNA *(lower)* content of Achilles sub-tendons (n = 5). LG and MG: lateral and medial gastrocnemius.

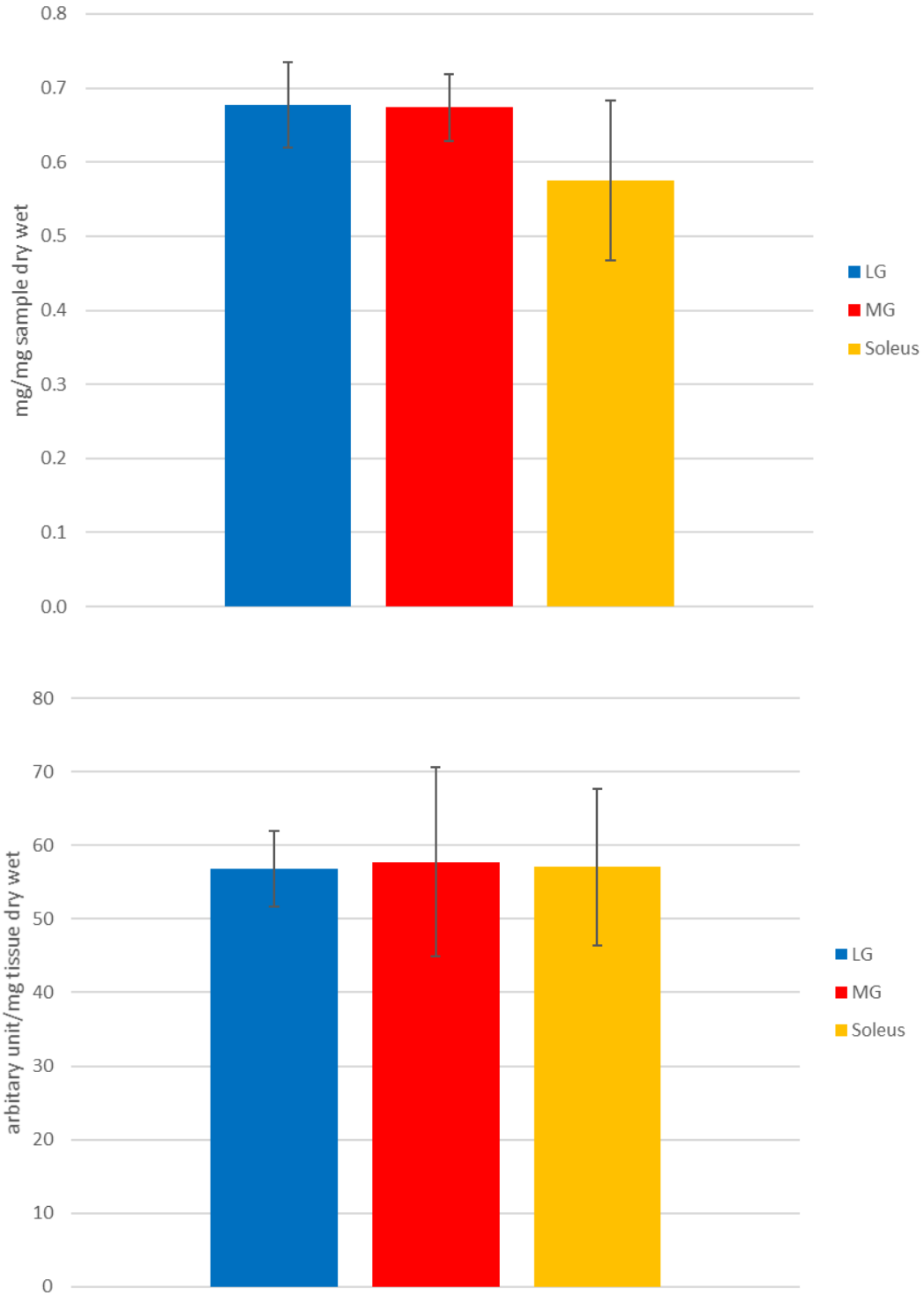

Figure 3-2. Total collagen content *(upper)* and collagen-linked fluorescence level *(lower)* of Achilles sub-tendons (n = 5). LG and MG: lateral and medial gastrocnemius.

3.4 Discussion

The results characterise the fundamental sub-tendon composition and mechanical properties. In general, sub-tendons demonstrated high similarity in the structural matrix compositions (collagen and proteoglycans) and the representative mechanical properties of the material. Interestingly, the mechanical properties of the structure, which reflect the actual force-bearing capacity and displacement under load, demonstrated significant differences between soleus and gastrocnemii sub-tendons.

Different mechanical properties between sub-tendons are due to differences in the CSA and are most likely related to the different properties and functions of their connected muscle bellies. As a result of high muscle mass and relatively short muscle fibre length, the soleus muscle has the greatest force-generating capacity and can produce over half of the total ankle plantar flexion torque (Dayton, 2017). Reflecting this large difference in force-generating capacity between gastrocnemii and soleus, the soleus sub-tendon had the greatest CSA and highest failure force and stiffness among the three sub-tendons. Stiffness could therefore scale with muscular force and CSA among different sub-tendons. It is generally agreed that gender differences exist when comparing tendon mechanical properties, and although not designed to test this, the result showed a similar trend with male specimens having higher averaged combined CSA (M: 62.1 mm^2, F: 51.2 mm^2) and tendon failure force (M: 2478 N, F: 2384 N) than female specimens. Future studies including a larger sample size with detailed exercise history, or normalising the tendon CSA or mechanical properties with the upstream muscle volume, could provide further insight into gender

differences in sub-tendon mechanics. The measured Young's modulus of sub-tendons was approximately two-thirds of that previously reported for the whole Achilles tendon (Wren et al., 2001). This lower value for material stiffness of the sub-units compared to the whole structure may be an artefact of dissection and mechanical testing in isolation, as has been seen previously when testing tendon fascicles isolated from whole tendons (Thorpe et al., 2012), or due to differences in specimen fixation methods and loading protocols. The inconsistency may also be a result of differences in the age groups studied, as the study of whole Achilles tendons (Wren et al., 2001) found a negative correlation between material properties and age and had significantly more younger specimens compared to our relatively old samples. It is generally agreed that the *in vivo* modulus and strength of Achilles tendons decrease with age (Svensson et al., 2016).

This mechanically compliant soleus sub-tendon may result from a low fascicle to IFM ratio, a small fascicle diameter, or a high percentage of collagen type III, all features that were indiscernible with a total collagen content measurement. Besides, the soleus and lateral gastrocnemius sub-tendons demonstrate significantly larger twist angles compared to the medial gastrocnemius (Section 1.4.2.1). The untwisting of the sub-tendons during loading is likely to exert compressive and shear forces to other sub-tendons, inducing potential compositional adaptations that may differ between sub-tendons due to these local mechanical stimuli.

The soleus sub-tendon had the highest water content which may contribute to its higher CSA than the gastrocnemii. Increasing tendon CSA is a commonly reported change after chronic training and can be associated

with fluid retention. Although the GAG content did not demonstrate a significant difference between sub-tendons, the proteoglycan type may be different between sub-tendon such as higher levels of larger aggregating proteoglycans to help attract water. Future studies using proteomics or immunohistochemistry could further detect whether the types of proteoglycan differ between sub-tendons. Also, the accumulation of hydrophilic glucosepane (Nash et al., 2017) may change the water content within sub-tendons, although no significant differences were detected in our measured collagen-linked fluorescence suggested that non-fluorescent AGE crosslinks may also not differ between sub-tendons.

It has been shown previously that energy-storing tendons have a higher cell count than positional tendons in both humans (Birch et al., 2001) and equine tendons (Birch et al., 2008b). Besides matrix compositions, soleus sub-tendons also appeared to have a higher failure strain, another feature of energy-storing tendons, than the gastrocnemii sub-tendons. Since the soleus has the highest CSA among sub-tendons, most of the energy-storing function of the Achilles tendon is likely achieved by the soleus muscle-tendon unit, for its constant activation during upright posture (Angin and Demirbüken, 2020). No macroscopic degenerative changes were found in the tested sub-tendon samples; however, an increase in cell numbers is often reported in tendinopathic Achilles tendons (Section 1.5.1). Given these relatively old tendon samples and the small sample size tested, it is not possible to completely exclude the possibility that the measured higher DNA content in the soleus sub-tendon may be a sign of early tendinopathy. Future studies with a larger sample size and a wider age range are warranted.

3.5 Conclusion and Chapter Summary

In summary, the results demonstrated that sub-tendons within human Achilles tendons exhibit different compositions, CSAs, failure forces, and material stiffness. The larger CSA and higher failure force of the soleus sub-tendon fulfil its mechanical demand from the upstream soleus muscle. Moreover, its composition demonstrates some features similar to other energy-storing tendons, further suggesting that the soleus sub-tendon may act as the main contributor to the whole Achilles tendon energy storage and release.

The generalisability of the data is however limited by the small sample size. In addition, both the mechanical testing and matrix composition results demonstrated high individual variance. Data collected from human tendon specimens are known to be considerably more variable than from experimental animals. Future studies with a larger sample size of the specimen that allows group comparison and has higher statistical power could potentially reduce this variability and reveal differences not apparent in this study.

Chapter 4 Probing Equine Tendon Composition Using Raman Spectroscopy

4.1 Introduction

Tendon pathologies are closely related to the altered state of the extracellular matrix composition. Both aged and injured tendons demonstrate significant compositional differences compared to the young and normal tendon tissue, but these molecular level changes are usually asymptomatic and difficult to assess *in vivo* using traditional imaging modalities in the early stages. For example, acutely ruptured tendons demonstrate altered ECM composition similar to those tendinopathic tendons but were often asymptomatic before rupture (Kannus and Jozsa, 1991). Although pathological changes can be easily detected by conventional biochemical analyses, these techniques are time-consuming and require vigorous *in vitro* sample treatments, thereby hindering our ability to detect and successfully prevent tendon pathologies outside the laboratory.

Alternatively, Raman spectroscopy can provide a comprehensive profile of the molecular composition of tissue in a rapid, label-free, and non-destructive manner (Kumamoto et al., 2018) since the collected Raman spectrum reflects the underlying molecular structures (Larkin, 2011c). The complex and overall chemical composition within the aggregated spectrum acquired by Raman spectroscopy can be analysed by using multivariate analysis methods enabling sample differences to be established (Bonnier and Byrne, 2012, Kumamoto et al., 2018) as, for example, healthy versus

non-healthy tissue (Kerns et al., 2014, Bergholt et al., 2019) or young versus old (Kerns et al., 2016).

Collagen constitutes approximately 80% of the dry weight of the tendon, and therefore, Raman features of tendons are dominated by collagen signals (Esmonde-White, 2014). These signals include the amide bands and the collagen backbone structure region. The amide bands relate to the amide vibrational patterns that indicate the secondary structure of proteins, and the collagen backbone region relates to the C–C stretching and the quantity of proline and hydroxyproline (reviewed in Section 1.6.1.2.1). Previous studies applying Raman spectroscopy to tendons have identified different collagen types, secondary structures, tendon fibril orientation, and have successfully detected degenerative lesions and distinguished stages of the healing process (see review (Esmonde-White, 2014) and (Penteado et al., 2008, Moura Junior Mde et al., 2015, de Carvalho et al., 2016)). The widely studied human Achilles tendon and equine SDFT are two important energy-storing tendons for locomotion and both are susceptible to age-related and sports-related injuries but have not been previously studied using Raman spectroscopy. The ability to detect molecular-level changes in intact tendon tissue would be a considerable advantage in diagnosing tendon pathology.

4.1.1 Hypothesis

Equine tendons of different types and from different age groups can be differentiated by Raman spectroscopy and multivariate analysis.

4.1.2 Objectives

- Conduct and propose a systematic Raman spectroscopy data collection and analytical procedure for tendon tissues.
- Collect and analyse spectral features of young and old equine tendons.
- Collect and analyse spectral features of the equine superficial digital flexor tendon and deep digital flexor tendon.
- Assign band frequencies to tentative molecular origins or microscopic structures.

4.2 Methods

4.2.1 Sample Preparation

Raman spectroscopy is well-known for its low requirement of sample preparation before measurement. Freeze-dried tendons were chosen to measure instead of wet tendons due to the difficulty to successfully maintain the tissue hydration during the measurement (~ 10 min) process when using isolated tissue. Since the collected Raman spectrum is greatly affected by the tissue hydration level (Masic et al., 2015), using *in vitro* dried tissue is a reasonable first step before moving to *in vivo* 'wet tissue' measurements.

Equine forelimbs (n = 15) were collected from horses euthanised for reasons other than tendon injury at a commercial equine abattoir, as a by-product of the agricultural industry. Tendons were carefully inspected during

dissection to ensure that no tendons showing visible signs of pre-existing injury or degenerative changes were included in the study. The SDFT and DDFT were analysed due to their known functional and compositional differences despite lying anatomically adjacent to each other (Denoix, 1994, Birch et al., 1999).

All SDFTs (n = 7, young: old = 3:4) and DDFTs (n = 8, young: old = 4:4) were harvested (from 15 horses) within 24 h and kept frozen at -80 °C. Tendons were assigned into the young (3 to 7) or old (20 to 24 years old) group according to the horse age. On the test day, tendons were defrosted at room temperature and a small cubic of tissue was taken (~ 1 cm^3) from the core. In the SDFT, tissue was taken from the mid-metacarpal level approximately 5 to 7 cm proximal to the metacarpal joint level. In the DDFT, the section site was approximately 2 cm proximal to the metacarpal joint level (Figure 2-1) due to the compositional differences between the merging accessory ligament and tendon at mid-metacarpal level (as in Section 2.3.1).

Tendon tissues were freeze-dried and homogenised under room temperature using scissors and a scalpel. A small volume (~ 2 mm^3) of dried and homogenised tissues were measured under the Raman spectrometer.

4.2.2 Raman Spectroscopy Instrumentation

All samples (dried and homogenised) were analysed with random sequences using a Renishaw inVia Raman spectrometer (Renishaw, Gloucestershire, UK; Figure 4-1) equipped with an 830 nm laser (300 mW at source). Ten Raman spectra from each sample were acquired (5 s exposure time, 10 accumulations) from randomly selected locations to reflect the

heterogeneity of tendon composition. The spatial resolution was 2 × 2 µm using a 50× objective.

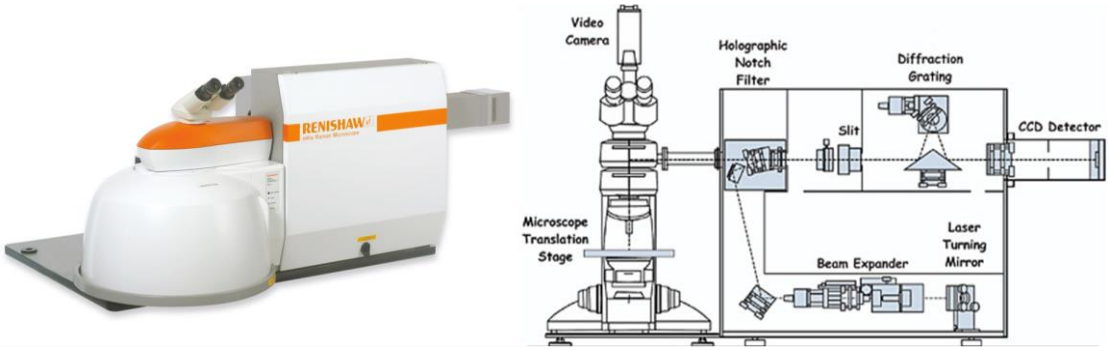

Figure 4-1. The Raman spectroscope used in this study: Renishaw inVia confocal Raman microscope – with circularly polarised 830 nm incident light

4.2.3 Data Treatment and Analysis

A highly fluorescent background in biological tissues is commonly seen as interference in Raman spectroscopy and is usually removed at the first stage in the data analysis (reviewed in Section 1.6.1.1). However, conventional biochemical approaches have demonstrated that the tissue fluorescence level in tendons increases with age (Birch et al., 1999, Thorpe et al., 2010c). With this in mind, a step-by-step analysis including both fluorescence-Raman combined spectra and pure Raman spectra (fluorescence removed) was conducted to establish a method for better understanding the age-related tendon molecular differences.

All collected raw spectra were truncated to wavenumber 800 cm^{-1} to 1800 cm^{-1} since this fingerprint region provides important information regarding tendon matrix composition (Kerns et al., 2014, Kerns et al., 2016).

The truncated spectra were first compared between groups (young vs. old) to understand the discrepancy of the fluorescence-Raman combined signal. Then, spectra were min-max normalised and underwent principal component analysis (PCA, by Origin 2019, OriginLab, US) to detect age-related differences containing both fluorescence and Raman signals. Scatter plots of principal components obtained from PCA were used for objective identification. The fluorescence signal was then removed from the unnormalised raw spectrum by an in-house MATLAB (Mathworks, US) code using 6^{th} order polynomial, and the subsequent Raman spectra were normalised to the amide III peak intensity (between 1230 and 1250 cm^{-1}) (Kerns et al., 2016). Raman spectra were then pooled and underwent PCA to identify the segregation of tendon age and tendon types. Vector loadings of interested PC axes were plotted to visualise the variance in wavenumbers.

Two previously reported age-related ratios used in other collagen-rich tissues were also calculated to explore the usefulness of these ratios in tendon analysis. The calculation was based on the intensities of selected wavenumbers: amide III 1^{st} peak to 2^{nd} peak (1240 cm^{-1}/1270 cm^{-1}) (Dehring et al., 2006), and the amide I pyridinoline to dihydroxylysinonorleucine crosslink ratio (1660 cm^{-1} /1690 cm^{-1}) (Paschalis et al., 2001).

4.3 Results

In total 150 spectra (10 spectra from each tendon sample) were acquired under identical conditions. The charge coupled device (CCD) counts were

higher in old than young tendon samples (Figure 4-2). This unprocessed raw data suggested fluorescence level increases as both tendons age.

The spectra were then min-max normalised to study the relative influence of fluorescence and Raman scattering (Figure 4-3). Visual inspection suggested that the young group in both tendons showed stronger Raman intensities at various peaks than the old group after normalisation. PCA was then performed to objectively identify group separation (Figure 4-4). For both tendons, young and old groups were separated along the maximal variance axis (PC1), and cluster vector plots from PC1 of both tendons demonstrated collagen-related Raman features at wavenumbers between 800-1000 cm^{-1} (usually assigned to the collagen backbone, proline and hydroxyproline), amide III (C—N stretch and N—H bending, 1200-1300 cm^{-1}), CH_2 bending (1450 cm^{-1}), and amide I (C=O stretch, 1600-1700 cm^{-1}) bands. The PC1 vector loading confirmed our visual inspection result.

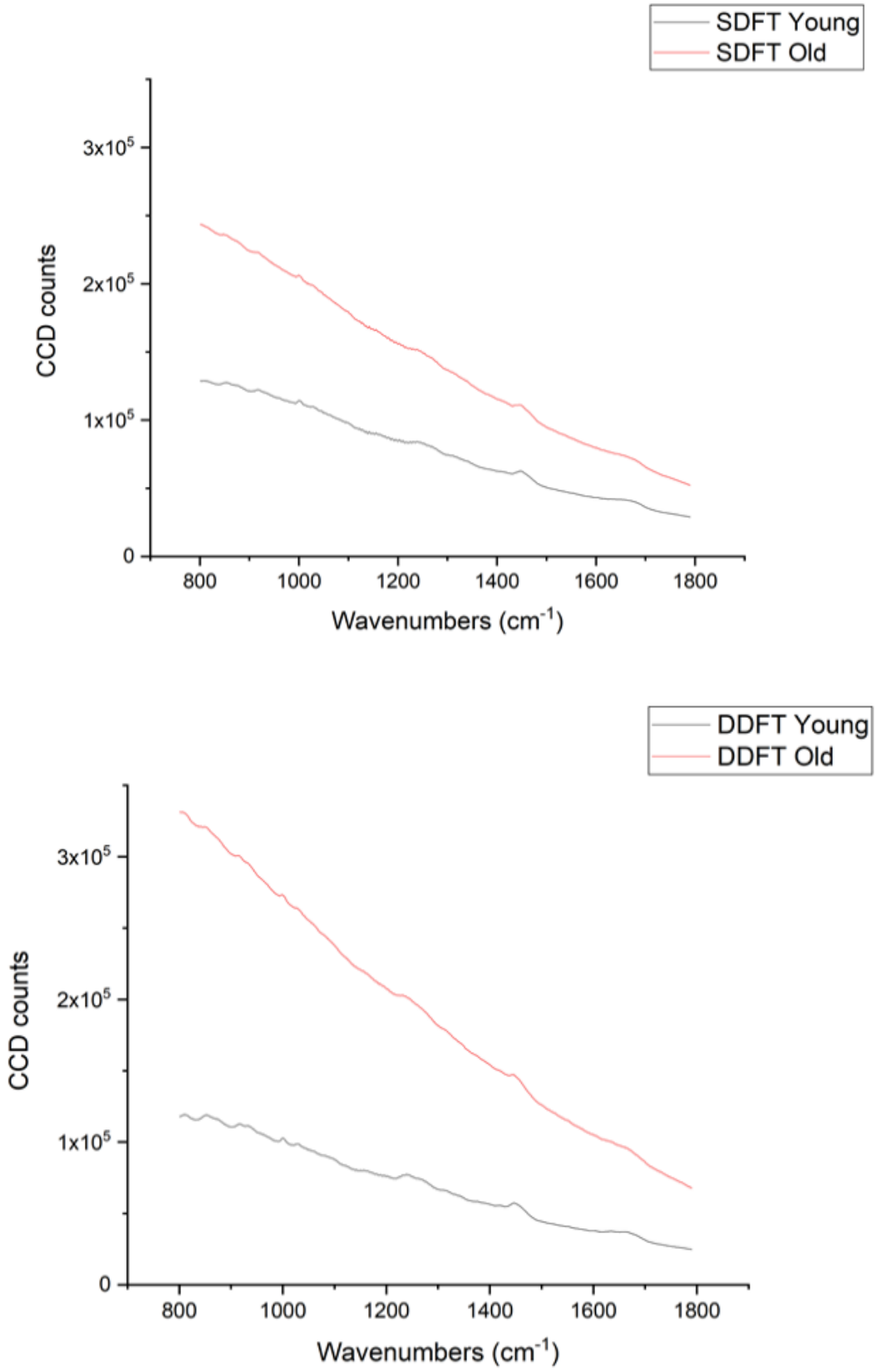

Figure 4-2. Averaged charged coupled device counts of young (40 spectra) and old (30 spectra) SDFTs (*upper*) and DDFTs (*lower*, 40 spectra in both groups).

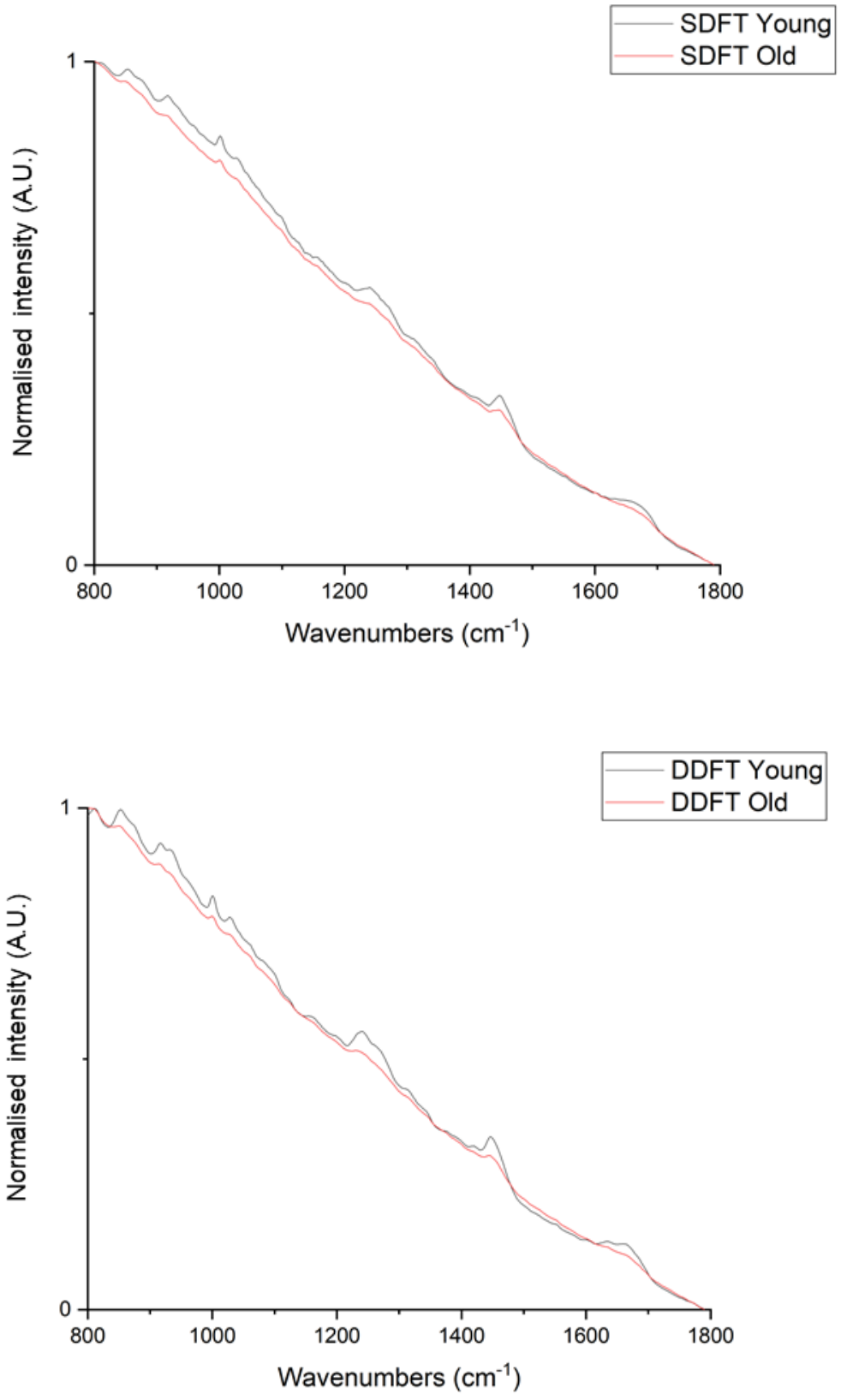

Figure 4-3. Averaged spectra after min-max normalised charge couple device (CCD) counts of the young and old group in SDFTs (*upper*, young:old=40:30 spectra) and DDFTs (*lower*, 40 spectra in both groups).

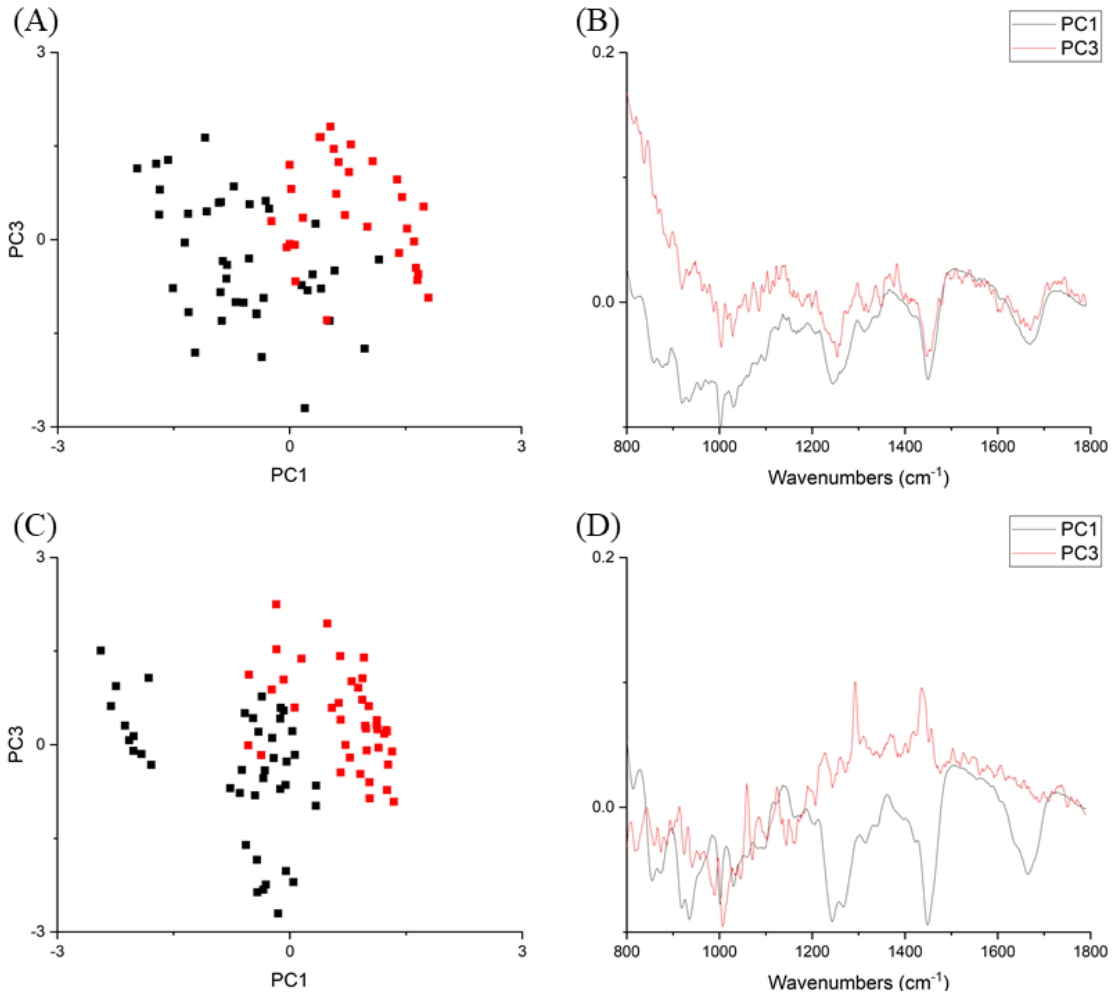

Figure 4-4. Principal component analysis on min-max normalised spectra. (A) SDFT, scatter plot of PC1 and PC3 axis. *Red squares:* young tendons, *black squares:* old tendons. (B) SDFT, PC1 (*black line*) and PC3 (*red line*) vector loading plot. (C) DDFT, scatter plot of PC1 and PC3 axis. *Red squares:* young tendons, *black squares:* old tendons. (D) DDFT, PC1 (*black line*) and PC3 (*red line*) vector loading plot.

The fluorescence signal was then subtracted from each raw spectrum (CCD counts) using a 6th order polynomial fit and normalised to the amide III band (maximal intensity at ~ 1240 cm^{-1}) (Kerns et al., 2016) for comparison between different age groups and different tendons. Both SDFT and DDFT data were pooled for further PCA identification of age-related Raman spectral differences (Figures 4-5 and 4-6).

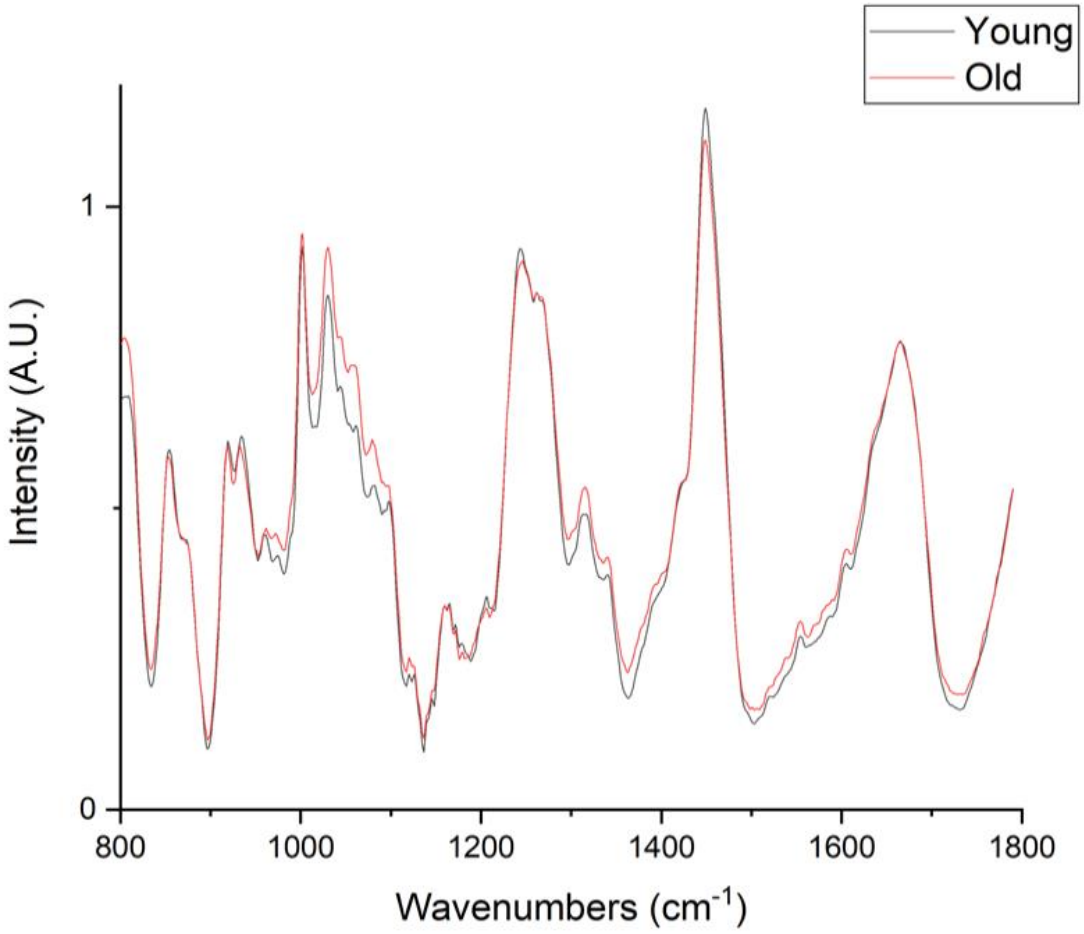

Figure 4-5. Averaged pooled Raman spectra of young (70 spectra) and old (80 spectra) tendons.

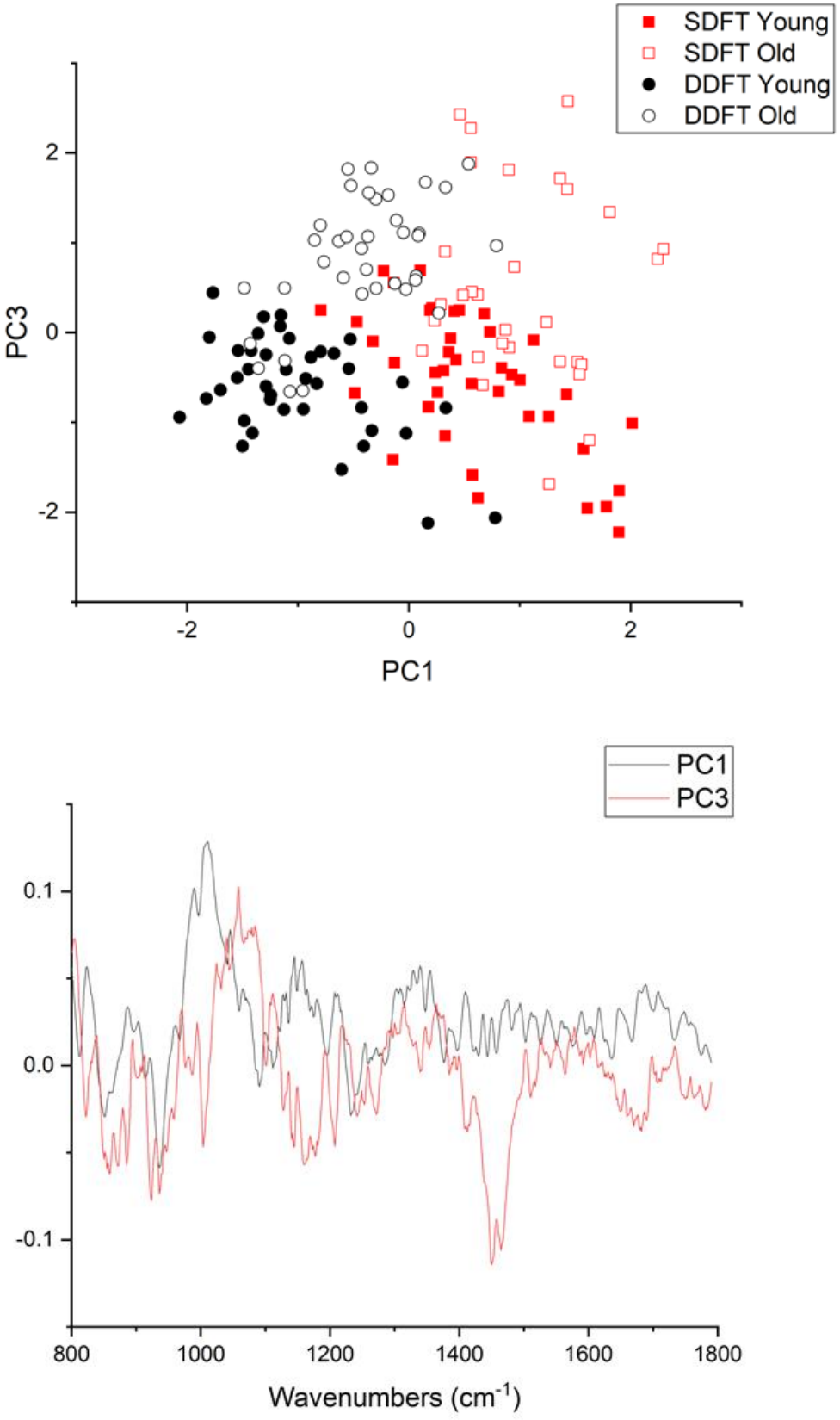

Figure 4-6. Principal component analysis of pooled Raman spectra. *Upper*, scatter plot of PC1 and PC3 axis. PC1 separates tendon types and PC3 separates age groups. *Lower*, PC1 and PC3 vector loadings.

PCA analysis of pooled Raman spectra (Figure 4-6) indicated that young and old groups were separated along the PC3 axis, which explained 4.7% of the total variance. The axis of maximal variance (PC1, 34.5%) separated the two different tendons, indicating compositional differences between the two. Inspecting the vector loadings of PC1 and PC3 revealed that age-related Raman spectral features were different to compositional-related features. PC3 identified two large peaks at wavenumbers between 1000-1100 cm^{-1} (mainly ring-associated and carbohydrate bands) and 1450 cm^{-1} (CH_2 bending), and these two regions showed a clear difference in the pooled spectra (Figure 4-5). On the contrary, PC1 loadings suggested that SDFT and DDFT compositional differences were likely associated with different collagen types since peaks below 1050 cm^{-1} are commonly assigned to proline (853, 934 cm^{-1}), hydroxyproline (872 cm^{-1}), collagen (C–C stretching, 904 cm^{-1}), and phenylalanine (990, 1003 cm^{-1}) (Talari et al., 2014).

Univariate analysis of two reported age-related ratios showed no significant differences between young (amide III: 0.93 ± 0.07, amide I: 0.79 ± 0.08) and old (amide III: 0.95 ± 0.07, amide I: 0.79 ± 0.07) groups.

4.4 Discussion

The results of this study support the hypothesis and demonstrate that Raman spectroscopy can differentiate minimally processed young and old equine tendon tissue. Besides, a clear difference in autofluorescence between young and old tendon tissue was detected. The results also show that it is possible to separate two different tendon types based on the Raman

spectral features alone. PCA, an objective multivariate analysis tool, could separate the young and old tendons both in the fluorescence-Raman combined spectra and the Raman spectra alone and identify relevant molecular information.

Whole tissue fluorescence level was significantly higher in old than young tendons, similar to previous reports on equine tendons (Birch et al., 1999), rat Achilles tendon (Lingelbach et al., 2000) and human patellar tendon (Couppe et al., 2009). However, it is important to note that the excitation wavelength used in this Raman spectroscopy study (830 nm) is different to that used in the literature (295 nm (Couppe et al., 2009), 330 nm (Lingelbach et al., 2000), 348 nm (Birch et al., 1999)), so a direct comparison of the results cannot be made as our longer wavelength (near-infrared) excitation can be expected to excite different chromophores to those in the previous studies. Fluorescence level has been used as a convenient measure of non-enzymatic glycation as many AGEs are fluorescent. As AGEs accumulate with increasing chronological age, fluorescence level has also been used as an indicator of tendon matrix age or rate of turnover (Birch et al., 1999). Due to the difference in excitation wavelength, the measured fluorescence in our study could originate from intra-tendinous fluorophores other than the known collagen related AGEs, such as that associated with elastin, lipids, or cells. Interestingly, after normalising the fluorescence intensity, the spectral shapes were found to remain different between groups, indicating that the range or ratio of fluorophores differs in young and old tendon tissue and that multiple different fluorescence emission spectra overlap each other. The results suggest that including raw spectral analysis,

which contains the fluorescence signal, in the Raman data interpretation may enhance the ability to distinguish between tendons of different ages. Indeed, excluding this signal may be one of the reasons why fewer differences in fluorescence-removed Raman spectra between old and young tendons were detected in the previous report (Kerns et al., 2016), despite using identical instrumentation and a similar protocol.

Our fluorescence-removed Raman spectra showed a lower intensity of the CH_2 bending band (1450 cm^{-1}) in old tendons compared to young tendons. The bending mode of the methylene group has usually been assigned to lipids or regarded as an indication of general protein content (Talari et al., 2014). The lipid content in equine SDFT and DDFT is low. Therefore, lipid-related signals are likely to originate from the cell membrane and may be an indirect indicator of cell numbers. Previous studies using conventional biochemical assays have shown conflicting results about cell numbers and change with age in both SDFT and DDFT (Birch et al., 1999, Thorpe et al., 2016b, Thorpe et al., 2016c). A recent report, specifically investigating the cell count in tendon fascicles and the IFM, identified a trend towards decreasing cell numbers in the IFM but no difference in fascicles (Thorpe et al., 2016c). Raman spectroscopy has a high spatial resolution and can focus on the fascicle or IFM levels, providing an excellent tool for tendon researchers to better elucidate the age-related cell number change in specific anatomical regions or compartments.

Besides the CH_2 bending band, the two groups (young and old) were also different in the various peaks within wavenumbers 1000-1100 cm^{-1}. The peaks in this region are often assigned to phenylalanine (1002, 1030 cm^{-1}) or

carbohydrates (1043, 1064, 1078 cm^{-1}) (Dukor, 2006, Talari et al., 2014). However, phenylalanine only accounts for approximately 1% of amino acid residues in both alpha 1 and alpha 2 polypeptide chains of type I collagen (Bolboacă and Jäntschi, 2007) and is unlikely to change with tendon ageing. Both phenylalanine and carbohydrates have a carbon ring structure; hence, these peaks in tendon tissue were tentatively assigned to other molecular compounds with aromatic rings or having sugar residues. The GAG (carbohydrate) component of proteoglycans has been shown to decrease significantly with increasing age in a positional equine tendon, although the decrease was not significant in the equine SDFT (Thorpe et al., 2010c). Another possibility is that the non-enzymatic-mediated crosslinks pentosidine and glucosepane that both have ring structures and accumulate in tendon with age advancement contribute to this difference (Thorpe et al., 2010c, Nash et al., 2019). In support of this, previous studies on *in vitro* induced collagen glycation showed a similar increase in peaks of this wavenumber region (Jastrzebska et al., 2003, Guilbert et al., 2013), and previous reports from our laboratory confirmed the accumulation of pentosidine and glucosepane in both equine (Thorpe et al., 2010c) and human tendons (Nash et al., 2019).

No between-group difference was found in the peak ratios within the amide III or amide I bands, in contrast to previously reported age-related changes in these ratios in bovine type I (Paschalis et al., 2001) and rat type II (Dehring et al., 2006) collagen. This could be due to different experimental species or different tissues (bones and eyes versus tendons) or the relatively low matrix turnover in the tendon, especially the collagenous matrix, after

maturation compared to other connective tissues. This preliminary study demonstrates that future research is warranted for understanding the usefulness of these ratios in tendons.

Raman spectral features differ between tendon types. The SDFT and DDFT are different in their matrix composition (Birch et al., 1999), which presumably results from their different functional demands. The SDFT, subjected to high stress and strain, stores and releases elastic energy for an energy-saving role during locomotion while the less strained DDFT mainly helps to maintain the stability of distal joints (Denoix, 1994). The SDFT has more type III collagen, more elastin, and a higher proteoglycan content than the DDFT (Birch et al., 1999, Thorpe, 2010). Unsurprisingly, this clear compositional difference was identified by Raman spectroscopy in various bands (800-1000 cm^{-1}) associated with the collagen backbone, proline, and hydroxyproline content.

Ten randomly selected points on homogenised tendon samples were chosen for spectral collection to better reflect the heterogeneity of tendon tissues. Therefore, these results should be interpreted as the averaged spectra of various tendon compartments without potential selection bias. However, this prevents further investigation of the spectral differences among compartments, especially between fascicles and IFM. Since it has been shown that fascicles and IFM have different proteomic profiles and demonstrate different age-related changes (Thorpe et al., 2016c), differences in the Raman spectra can be expected and warrants further investigation.

4.5 Conclusion and Chapter Summary

The study results demonstrate that Raman spectroscopy can detect age-related tendon molecular changes and to differentiate different tendon types. Besides, these findings suggested that incorporating the fluorescence signal helps age differentiation when analysing tendon tissues with significant age differences. Raman spectroscopy could potentially provide an ageing index of the measured tendon that may help the clinician to detect premature or accelerated ageing of the tendon.

Chapter 5 Raman Features in Human tendons

5.1 Introduction

Following the previous chapter, human tendons samples were tested to investigate whether Raman spectroscopy can differentiate human tendons of different types and ages, similar to the results collected from equine tendons. The Achilles tendon, a common site of overuse tendon injury and age-related tendon pathology, and anterior tibialis tendon were chosen for comparison since their distinct roles in human locomotion and the collected Raman spectra can be correlated with conventional biochemical assay results (Birch et al., 2001, Nash et al., 2019). Compared to the energy-storing Achilles tendon, the anterior tibialis tendon is rarely injured and is subjected to much lower stress and strain during locomotion since its main role is to lift (dorsiflex) the foot off the ground during the swing phase (Akalan and Angin, 2020, Angin and Demirbüken, 2020). The anterior tibialis tendon also demonstrates lower water content, GAG content, collagen-linked fluorescence, and cellularity than the Achilles tendon but both tendons have a similar level (~ 77%) of total collagen content (Birch et al., 2001). Both tendons showed a similar age-related increase in glycation crosslinks and the quantity of crosslinks were highly correlated with the chronological age (Nash et al., 2019). From the results of the equine tendon study, it is likely that human tendons could similarly exhibit spectral features that are directly or indirectly associated with the accumulation of the glycation crosslinks.

In addition, whether Raman spectroscopy can differentiate between different Achilles sub-tendons was explored. In Chapter 3, the result from *in*

vitro biochemical assays demonstrated that the soleus sub-tendon had a significantly higher DNA level than the gastrocnemii sub-tendons. However, due to its minor quantity, the small sample size, and high individual variations between samples, the difference may be small and not easily discernible.

5.1.1 Hypothesis

The Raman spectral features exhibit differences between tendons of different ages, between tendons of different functions, and between three Achilles sub-tendons. In addition, several Raman features correlate with the age-related accumulation of glycation crosslinks and specimen age.

5.1.2 Objective

- Collect and analyse spectral features of young and old human Achilles and anterior tibialis tendons.
- Correlate intensities of identified Raman bands with *in vitro* biochemical quantification of pentosidine and glucosepane crosslinks.
- Collect and compare spectral features between Achilles and anterior tibialis tendons.
- Collect and analyse spectral features of Achilles sub-tendons.

5.2 Methods

5.2.1 Sample Preparation

5.2.1.1 Achilles tendon and anterior tibialis tendon

The Achilles tendon (n = 8, young: old = 4:4) and anterior tibialis tendon (n = 8, young: old = 4:4) were collected from amputated limbs from patients (young: 14 – 21 years, old: 65 – 87 years; n = 4 for each group) at the Royal National Orthopaedic Hospital. All patients gave consent for their tissue to be used for musculoskeletal related research (UCL/UCLH Biobank for Studying Health and Disease (HTA license number 12055) with Local R&D approval (Ref: 11/0464)). Only tendons with no visual signs of injury or disease were selected. Tendon was harvested within 24 h of limb amputation, snap-frozen and stored at −80 °C. The samples were then freeze-dried, homogenised and had previously undergone biochemical assays which were performed independently from the Raman measurements (Nash et al., 2019).

5.2.1.2 Achilles sub-tendons

In total 5 Achilles tendons (from 69 to 87 years) were harvested from fresh frozen tendon specimens (Vesalius Clinical Training Centre, University of Bristol, REC 08/H0724/34). Sub-tendons were separated and underwent mechanical testing before being freeze-dried and homogenised as described previously (Section 3.2).

5.2.2 Instrumentation and Data Analysis

The identical Raman spectrometer and spectral collection protocol (Section 4.2.2 and 4.2.3) were used for collecting human tendon data to that

used for equine tissue. The data treatment procedure was identical to the equine tendon studies that sequentially analysed fluorescence-Raman combined spectrum, fluorescence removed Raman spectrum, and then underwent PCA.

5.2.3 Correlation with Collagen Crosslinks Quantities

Biochemical assays were conducted independently (and published previously in (Nash et al., 2019)) to investigate the crosslink profiles of the Achilles and anterior tibialis tendons of different ages. These crosslinks were quantified by an HPLC system following an enzymatic sequential digestion process (Nash et al., 2019).

Raman bands of interest were selected based on the objective PC loadings and by visual inspection of the mean spectrum. Pearson's correlation coefficients were then calculated (by Microsoft Excel, Microsoft Office 365) between Raman band intensities and age, and between band intensities and crosslink quantities.

5.3 Results

5.3.1 Spectral Features of Achilles and Anterior Tibialis Tendons

In total 160 spectra (10 for each specimen) were collected and analysed. The maximum of collected raw CCD counts, which include both fluorescence background and Raman spectra, showed a more than three-fold increase in the aged tendons (Figure 5-1).

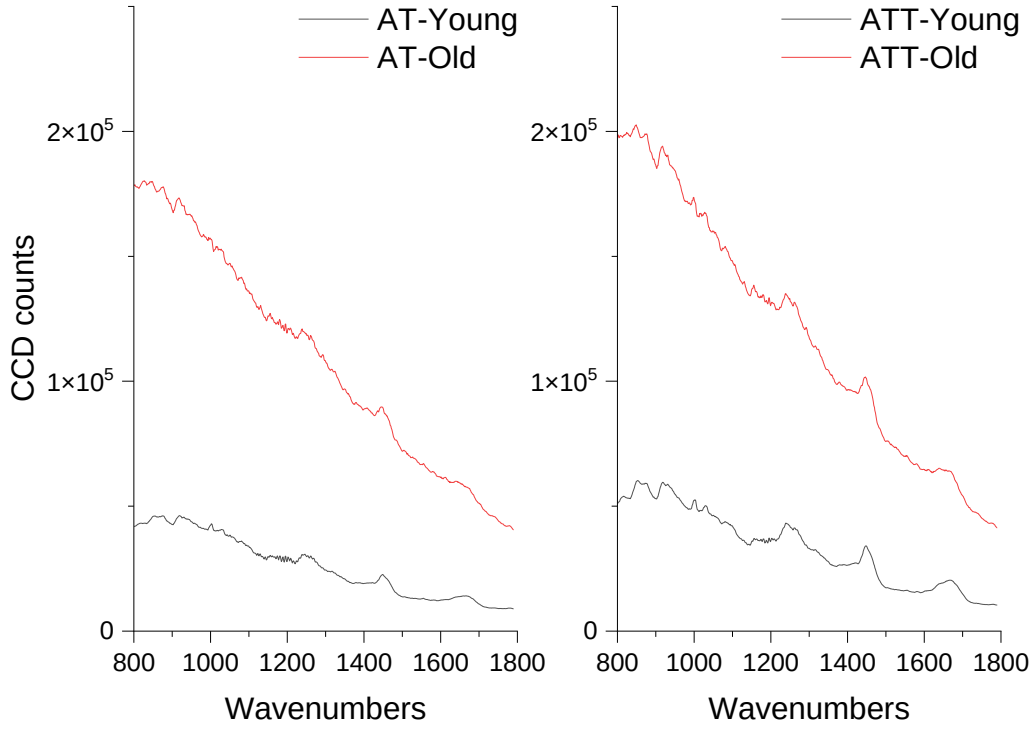

Figure 5-1. Averaged raw CCD counts (n = 160, 40 per group) between young and old Achilles tendons (AT) and anterior tibialis tendon (ATT)

After min-max normalisation of the fluorescence-Raman spectra, visual inspection discovered a large spectral shape difference in the fluorescence background, especially in the wavenumber region between 1100 cm^{-1} and 1800 cm^{-1}, where aged tendons demonstrated a higher intensity and more linear background shape than the lower intensity, reversed S-shape background of the younger tendons (Figure 5-2, *lower left inset*).

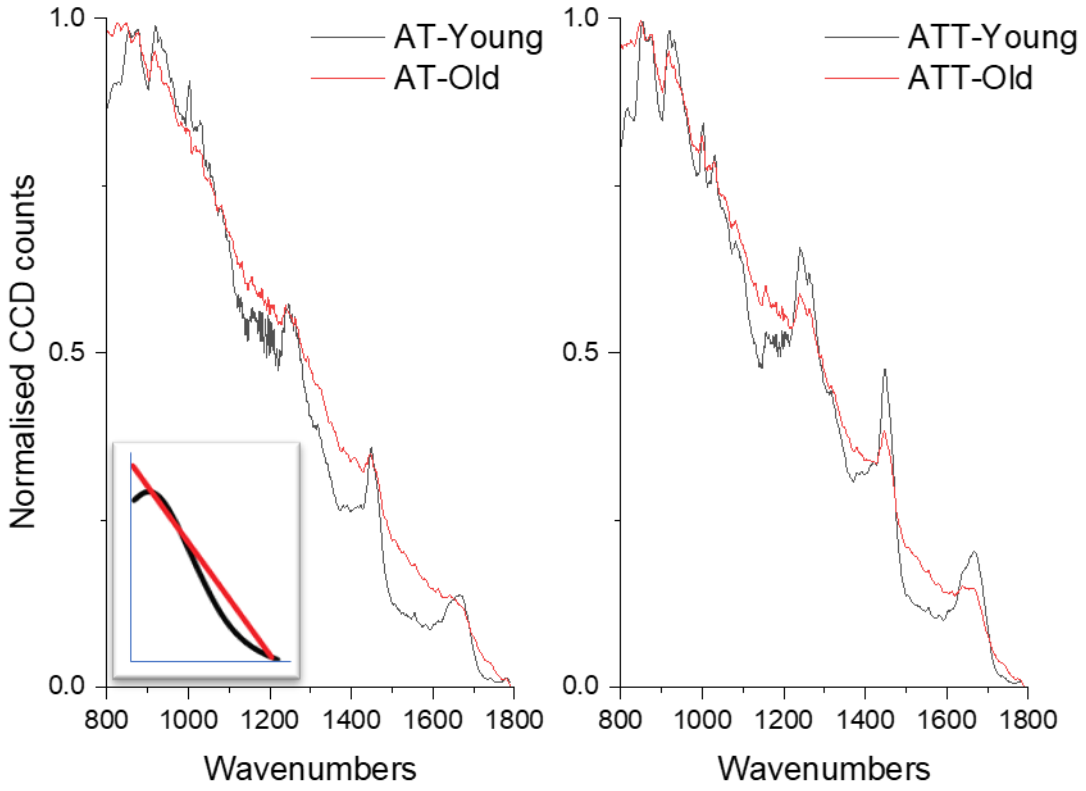

Figure 5-2. Min-max normalised CCD counts (n = 160, 40 per group) between young and old Achilles tendons (AT) and anterior tibialis tendon (ATT). Inset: representative figure of different background shapes between young (black) and old (red) tendons.

After fluorescence background removal, the underlying Raman spectra were pooled and underwent PCA. The Achilles tendon and anterior tibialis tendon were separated primarily along the maximal variance axis (47.8%), PC1, while the different age groups were separated along the PC2 axis (17.6% of variance, Figure 5-3). Visual inspection of the mean Raman spectra suggested the age-related spectral differences were more prominent in the Achilles tendon than the anterior tibialis tendon (Figure 5-4).

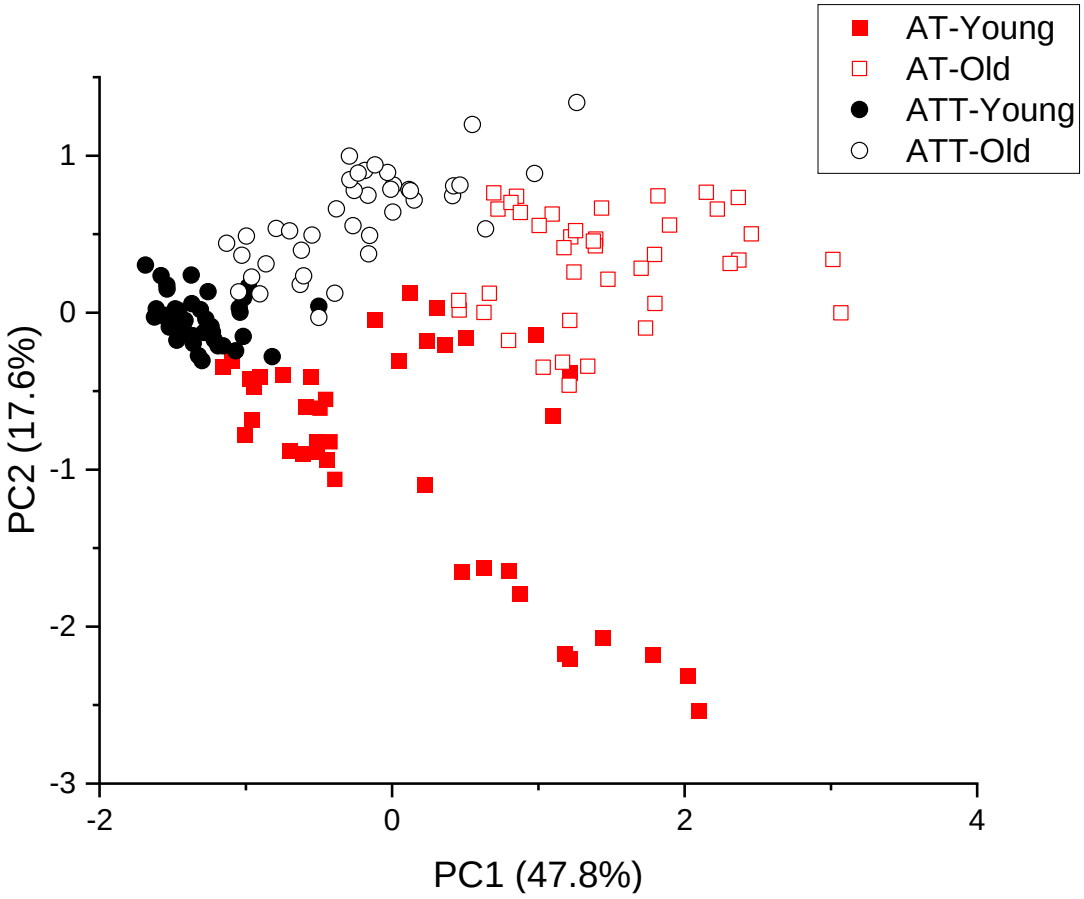

Figure 5-3. Principle component analysis of pooled Raman spectra

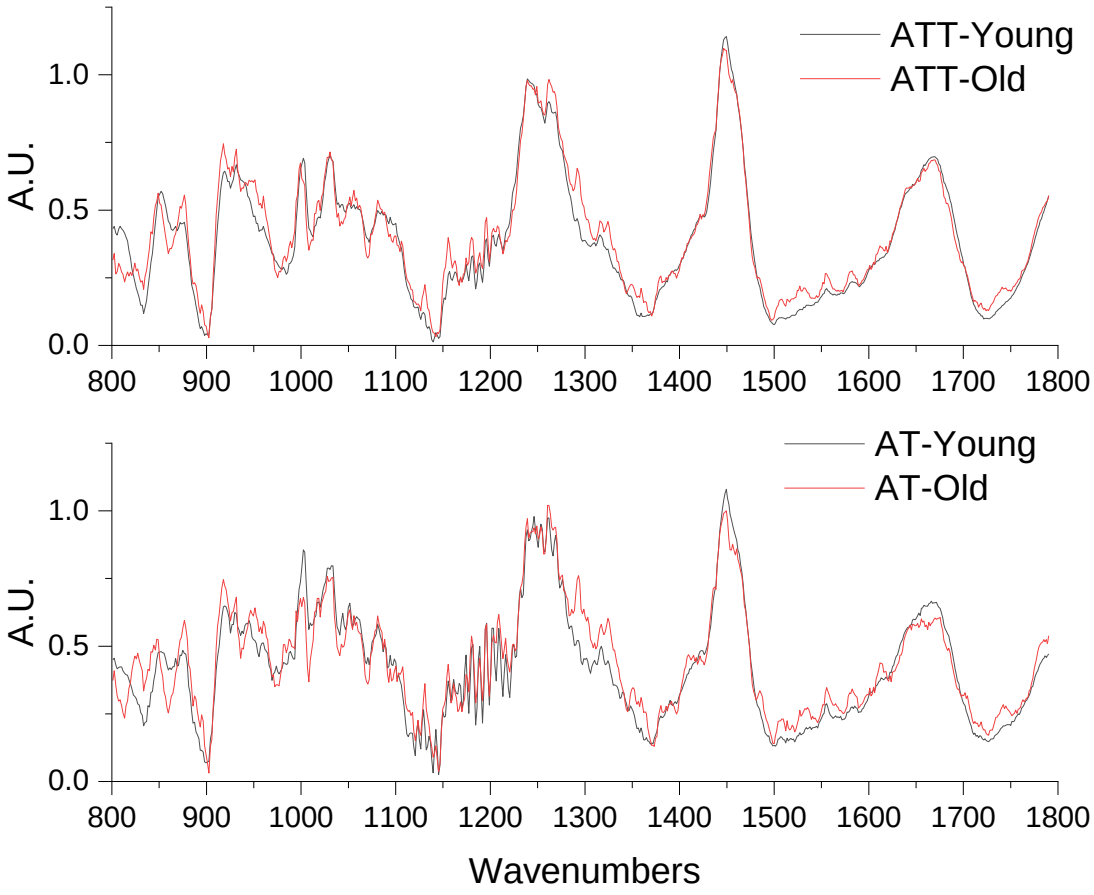

Figure 5-4. Averaged Raman spectra of young (*black lines*) and old (*red lines*) Achilles tendon (*bottom row*) and anterior tibialis tendon (*upper row*)

The two most prominent differences identified by the PC2 were the 1002 cm^{-1} (phenylalanine) and 1293 cm^{-1} (amide III shoulder) bands (Figure 5-5). Comparing the PC2 loading with the mean Raman spectra further revealed differences of several band intensities at the proline and hydroxyproline region (850, 877, 918, 931, and 951 cm^{-1}), the band at 1130 cm^{-1}, amide III and shoulder (1270 and 1324 cm^{-1}), CH_2 bending (1450 cm^{-1}), and amide I band (1660 cm^{-1}).

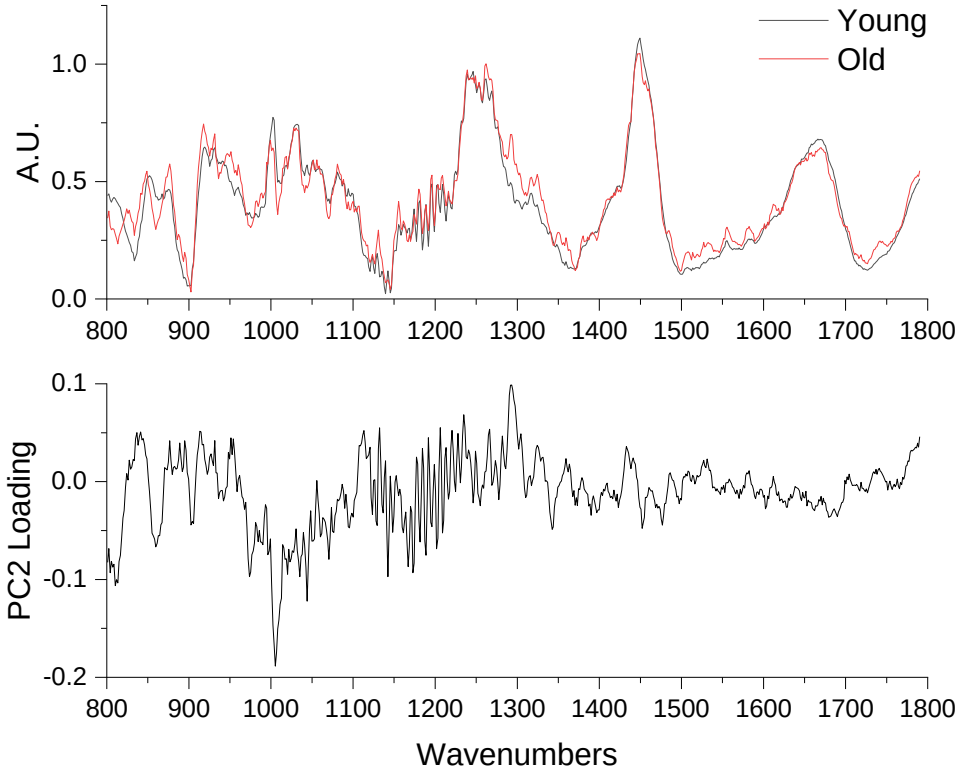

Figure 5-5. Averaged Raman spectra of young (n = 80, *black lines*) and old (n = 80, *red lines*) tendons (*upper row*) and the PC2 loading (*lower row*)

5.3.2 Correlation between Raman Bands and Crosslinks Quantities

Most of the band intensities, identified by PC2 loading and spectra means, were highly correlated with the specimen age and crosslink levels of both tendons (Tables 5-1 and 5-2). In addition, several bands that have been previously assigned to pentosidine and glucosepane (Glenn et al., 2007, Pereira et al., 2015, Alsamad et al., 2021) demonstrated a high correlation with the biochemical results (Table 5-2). The collagen-linked fluorescence, measured by a plate reader with an excitation wavelength of 348 nm, was positively correlated with the raw CCD counts, despite using a different excitation wavelength than the Raman spectroscopy (830 nm).

Table 5-1. Pearson's correlation coefficients between Raman band intensities and age, and between biochemical assays and age of two tendons

Raman Spectroscopy			Biochemical assays*		
Band	Achilles	A. tibialis		Achilles	A. tibialis
CCD count†	0.80	0.73	Fluorescence	0.97	0.98
850 cm^{-1}	-0.10	-0.36	Pyridinoline	-0.66	-0.28
877 cm^{-1}	0.65	0.88	Pentosidine	0.85	0.90
918 cm^{-1}	0.64	0.85	Glucosepane	0.99	0.81
931 cm^{-1}	0.14	0.74			
951 cm^{-1}	0.67	0.94			
1002 cm^{-1}	-0.77	-0.38			
1130 cm^{-1}	0.72	0.89			
1270 cm^{-1}	0.56	0.86			
1293 cm^{-1}	0.85	0.88			
1324 cm^{-1}	0.79	0.88			
1450 cm^{-1}	-0.64	-0.35			
1660 cm^{-1}	-0.79	-0.22			

*Recalculated from (Nash et al., 2019). †integral of the raw spectrum.

Table 5-2. Pearson's correlation coefficients between Raman band intensity and biochemical assays of the Achilles and anterior tibialis tendon

Raman Spec.	Biochemical assays					
	Fluorescence		Pentosidine		Glucosepane	
Band	Achilles	A. tibialis	Achilles	A. tibialis	Achilles	A. tibialis
CCD count*	0.67	0.77				
850 cm^{-1}			0.01	-0.01	-0.09	-0.50
877 cm^{-1} [a,b]			0.75	0.82	0.66	0.79
918 cm^{-1} [b]			0.73	0.73	0.69	0.91
931 cm^{-1} [b]			0.34	0.72	0.17	0.81
951 cm^{-1} [b]			0.75	0.85	0.69	0.88
1002 cm^{-1} [b]			-0.68	-0.09	-0.71	-0.54
1130 cm^{-1} [c]			0.75	0.72	0.74	0.93
1270 cm^{-1}			0.74	0.72	0.53	0.74
1293 cm^{-1}			0.78	0.88	0.81	0.86
1324 cm^{-1} [a]			0.74	0.75	0.77	0.92
1450 cm^{-1} [b]			-0.83	0.04	0.77	-0.66
1660 cm^{-1}			-0.80	0.21	-0.76	-0.55

*integral of the raw spectrum. [a]:(Glenn et al., 2007). [b]:(Alsamad et al., 2021). [c]: (Pereira et al., 2015).

PC1 revealed compositional differences between the Achilles and anterior tibialis tendon (Figure 5-6). These differences were reflected in the proline/hydroxyproline region (800 – 1000 cm^{-1}), carbohydrate-related bands (1000 – 1100 cm^{-1}), the shoulders of amide III (~ 1200 cm^{-1} and ~ 1300 cm^{-1}), CH_2 bending band (1450 cm^{-1}), and the peak intensity and the spectral shape

of amide I band (1600 – 1700 cm^{-1}). These spectral differences (identified by PC1) were not identical to the age-related changes (by PC2, Figure 5-5), demonstrating the ability to differentiate age-related and composition-related tendon molecular differences using a combination of Raman spectroscopy and principal component analysis.

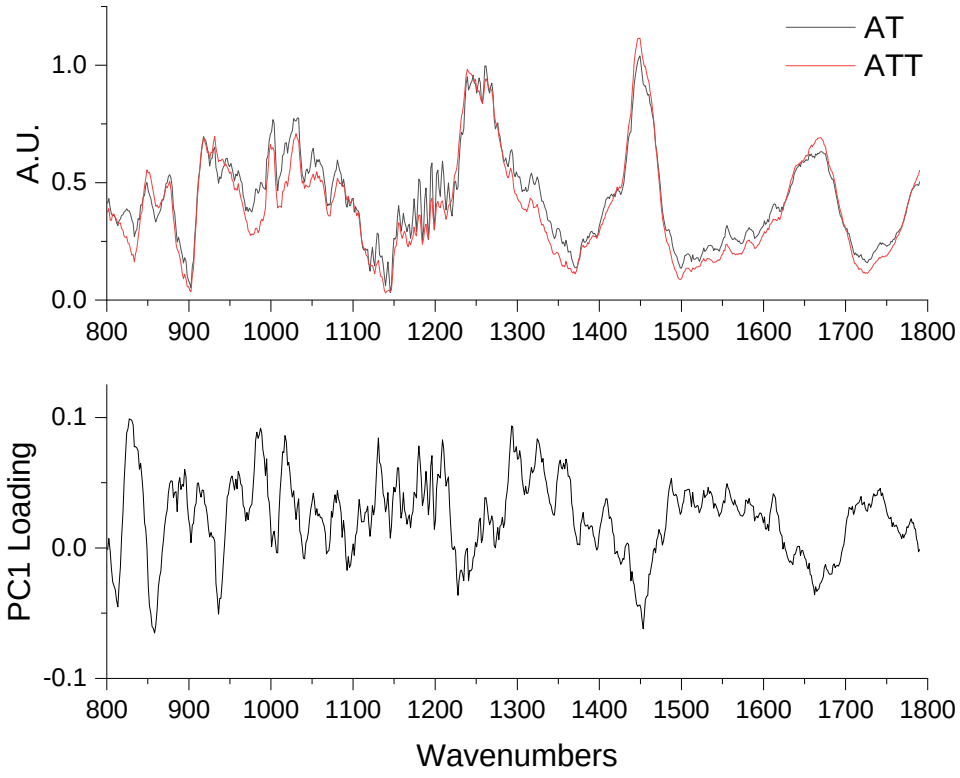

Figure 5-6. Averaged Raman spectra of Achilles (n = 80, *black lines*, *upper row*) and anterior tibialis tendons (n = 80, *red lines*) and the PC1 loading (*lower row*)

5.3.3 Raman Features of Achilles Sub-tendons

The integral of CCD counts was significantly higher in the lateral gastrocnemius than the other two sub-tendons (ANOVA, $p < 0.001$. Post hoc:

lateral versus medial gastrocnemius $p < 0.001$, lateral gastrocnemius versus soleus $p < 0.001$, medial gastrocnemius versus soleus $p = 0.129$; by SPSS v26, two-tailed significance of 0.05). Both the fluorescence level and the shape of the fluorescence background (Figure 5-7) were comparable to the spectra acquired from homogenised old Achilles tendon samples (which disregard sub-tendons, in Figure 5-1).

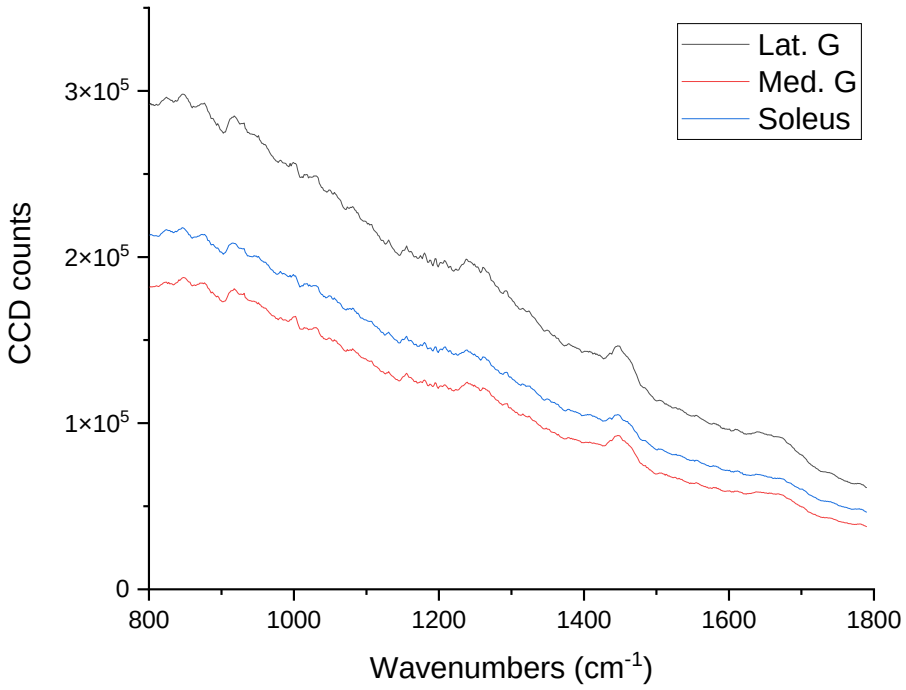

Figure 5-7. Averaged raw CCD counts (n = 150, 50 per group) between lateral and medial gastrocnemii and soleus sub-tendons

The fluorescence removed Raman spectra of sub-tendons were similar under visual inspection. The medial gastrocnemius sub-tendon appeared to have slightly lower CH_2 bending (1450 cm^{-1}) and amide I band (1660 cm^{-1})

intensities compared to the other two sub-tendons (Figure 5-8). PCA of pooled sub-tendon spectra (n = 150) failed to differentiate sub-tendons. Due to the high variation between specimens, PCA was then re-conducted on an individual basis. Good separations for all specimens were found between sub-tendons and the PC loadings revealed differences in the CH_2 bending and amide I bands (Figure 5-9, *red arrows*) in all the studied specimens. The regional spectra (with truncated wavenumbers to include only CH_2 bending and amide I bands) showed subtle differences between each sub-tendon, but no clear pattern was observed among all the studied specimen (Figure 5-10).

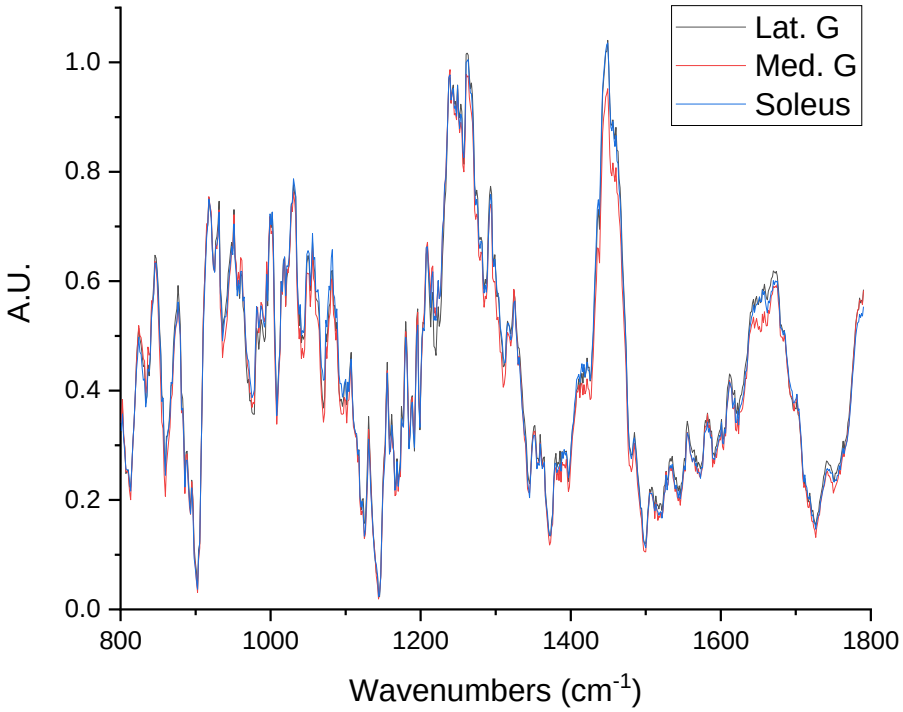

Figure 5-8. Averaged (n = 150) Raman spectra of three sub-tendons

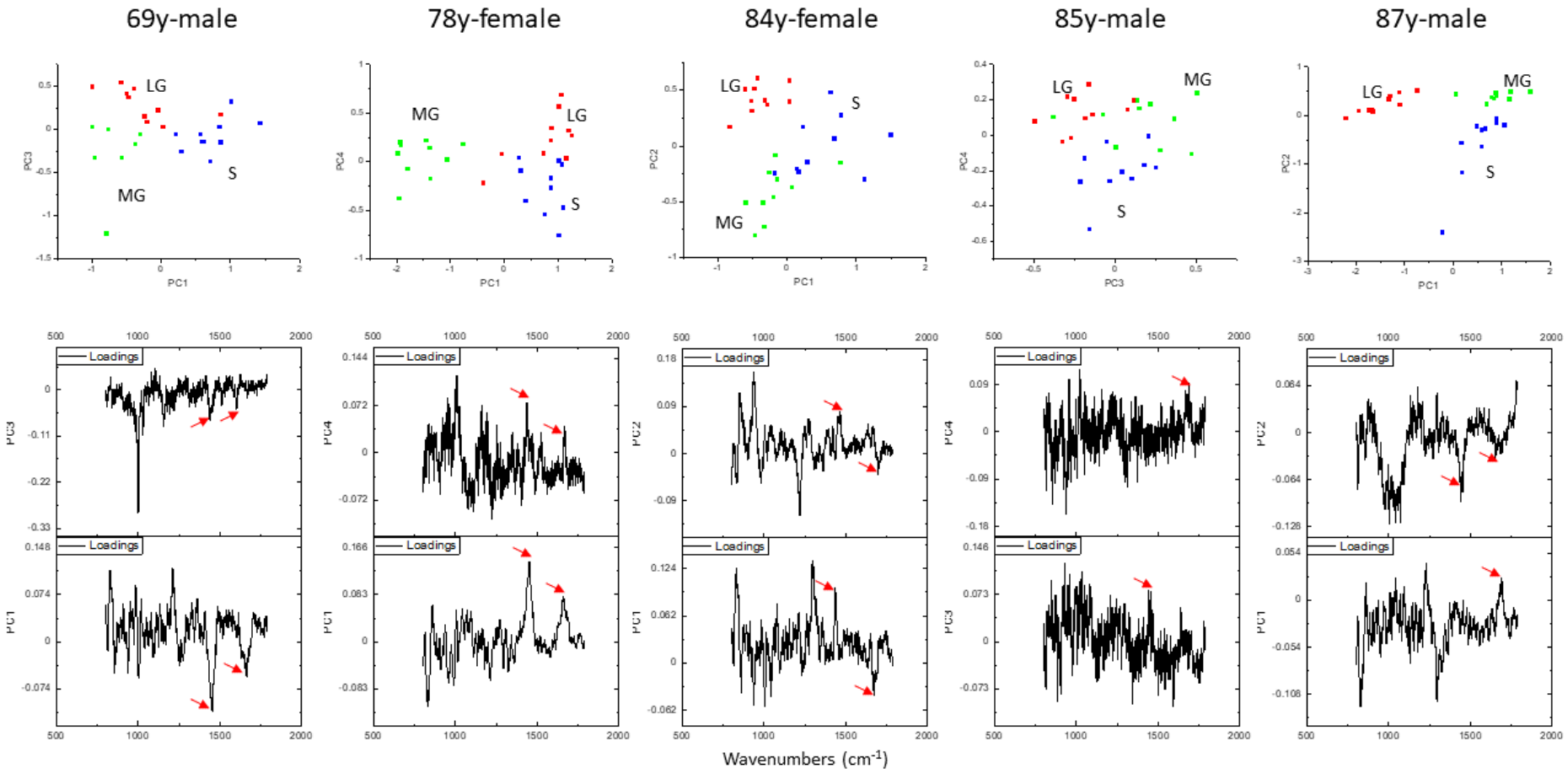

Figure 5-9. PCA (scatter plot, *upper row*; PC loadings, *lower row*) of individual specimen. Red squares: lateral gastrocnemius. Green squares: medial gastrocnemius. Blue squares: soleus. Red arrows: CH_2 bending (1450 cm^{-1}) and amide I bands (1660 cm^{-1}).

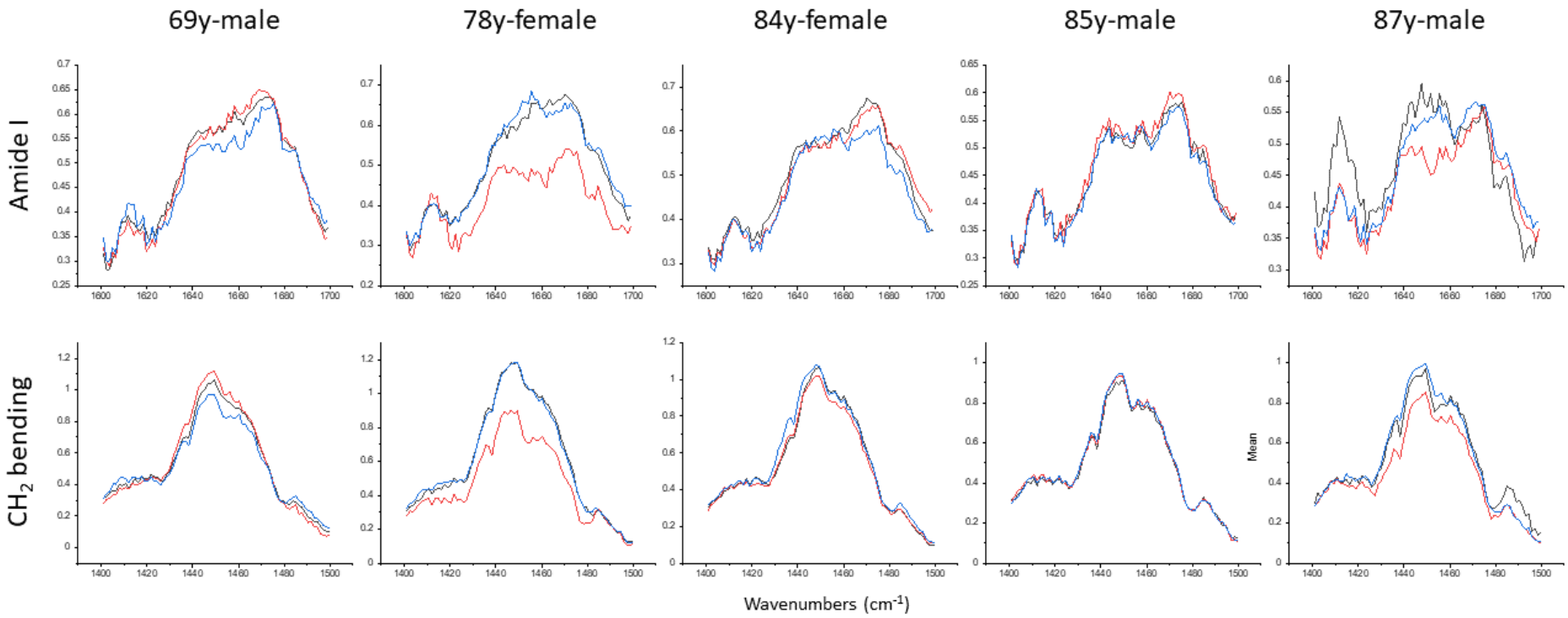

Figure 5-10. Averaged (n = 10, each line) regional (amide I, *upper row*, and CH_2 bending, *lower row*) sub-tendon Raman spectra of individual specimen. Black lines: lateral gastrocnemius. Red lines: medial gastrocnemius. Blue lines: soleus.

5.4 Discussion

To the best of my knowledge, this is the first study to report the Raman spectral features of human Achilles and anterior tibialis tendons. The results demonstrate that combining Raman spectroscopy and PCA can successfully differentiate human tendon samples with different compositions and of different ages. Besides, the age-related spectral changes were highly correlated with the AGE crosslink quantities measured by conventional destructive biochemical methods. This knowledge provides a fundamental step for applying Raman spectroscopy as a potential clinical tool for detecting tendon compositional changes induced by ageing or pathology.

5.4.1 Age-related Differences in Human Tendons

Compared to the younger tendons, aged tendons exhibited greater fluorescence intensities (over threefold). Fluorescence background is often regarded as interference when interpreting the underlying Raman signals; however, as demonstrated here and in Chapter 4, fluorescence intensity alone can easily separate samples of young and old tendons. Interestingly, by normalising the fluorescence-Raman combined spectra, both aged Achilles and anterior tibialis tendon showed similar fluorescence background shape with a near-linear decline in intensities across the studied wavenumber region (800 cm^{-1} to 1800 cm^{-1}, Figure 5-2) while the younger tendons demonstrated an observable drop in the fluorescence spectrum between 1100 cm^{-1} and 1400 cm^{-1}. The different fluorescence background shapes are likely result from the different types or quantities of intra-

tendinous fluorophores. It can be speculated that in younger tendons, one major fluorescence band centred at ~ 900 cm^{-1} dominates the fluorescence spectra along with a few bands (potentially around ~ 1200 cm^{-1}, ~ 1400 cm^{-1}, and ~ 1600 cm^{-1}) with declining fluorescence intensities. In aged tendons, however, the greatly increased overall fluorescence intensity could potentially mask these underlying subtle differences produced by native tendon fluorophores. The increased tissue fluorescence level is likely produced by the non-enzymatic AGE crosslinks formed within and between collagen molecules. These glycation crosslinks can increase many folds in aged tendons while the total pyridinoline crosslinks, the predominant crosslink in adult tendons, remain stable (Birch et al., 1999, Thorpe et al., 2010c) or even slightly decrease with age (Nash et al., 2019).

Glucosepane and pentosidine are two AGE crosslinks commonly found in aged tendons. AGE crosslinks can alter tendon mechanical properties and affect cell-matrix interactions, resulting in a reduced repair ability after injury (Snedeker and Gautieri, 2014, Nash et al., 2017, Nash et al., 2019). The previous report from our lab demonstrated a good correlation between specimen age and the AGE crosslinks, measured by sequential enzyme digestion and an HPLC system (Nash et al., 2019). Similarly, several Raman spectral differences were identified between young and old tendons and most of the band intensities were correlated with age. Among these reported bands, the intensity of several specific AGE crosslink-related bands (Glenn et al., 2007, Pereira et al., 2015, Alsamad et al., 2021) were highly correlated with both the glucosepane and pentosidine levels. Our results showed that using Raman spectroscopy alone could, therefore, rapidly and non-

destructively measure the AGE crosslinks quantities in tendon tissues with minimal sample preparation. Raman spectroscopy has been used in dermatological studies to differentiate skin samples of different ages and between healthy and diabetic tissues (Gniadecka et al., 1998, Pereira et al., 2015). Future research utilising spatially-offset Raman spectroscopy could greatly improve our ability to probe tendon compositions in a clinical setting.

Besides AGE crosslinks, the age-related difference in Raman spectra may be attributed to the altered orientation of tendon fibrous sub-structures. The Raman spectrum of collagen-rich tissue is highly anisotropic and sensitive to the sample orientation (Bonifacio and Sergo, 2010, Masic et al., 2011, Galvis et al., 2013), and when the tissue level orientation is fixed, the spectral differences between young and age tendons could be attributed to the change in the orientation of the sub-structures. Van Gulick and colleagues demonstrated that aged rat tail tendon fibres oriented more parallel to the fascicle long axis than the younger tendons. This altered orientation was correlated with the reduced amide I and CH_2 bending bands, and increased amide III band intensities in the measured Raman spectra (Van Gulick et al., 2019), similar to our findings in aged human tendons. Interestingly, in our previous study on equine SDFT, which has been shown to have an altered fibre orientation in aged tendons (Thorpe et al., 2013b), the Raman spectral differences between the young and old groups were only visible in the CH_2 bending and the amide III bands, suggesting species differences or other influencing factors present. Indeed, these amide bands are large compound bands dominating the spectra of all collagen-rich tissues and can often be assigned to multiple structures or components depending

on the sample studied (Talari et al., 2014), instead of being influenced by tissue orientation alone. Future study is required to understand the relationship between human tendon sub-structural orientation and the Raman spectral changes, especially with large spectral differences between species as we demonstrated between equine and human tissue (Figure 5-11). The human Achilles tendon in general demonstrates lower dominant band intensities but presents with more weaker bands compared to the SDFT.

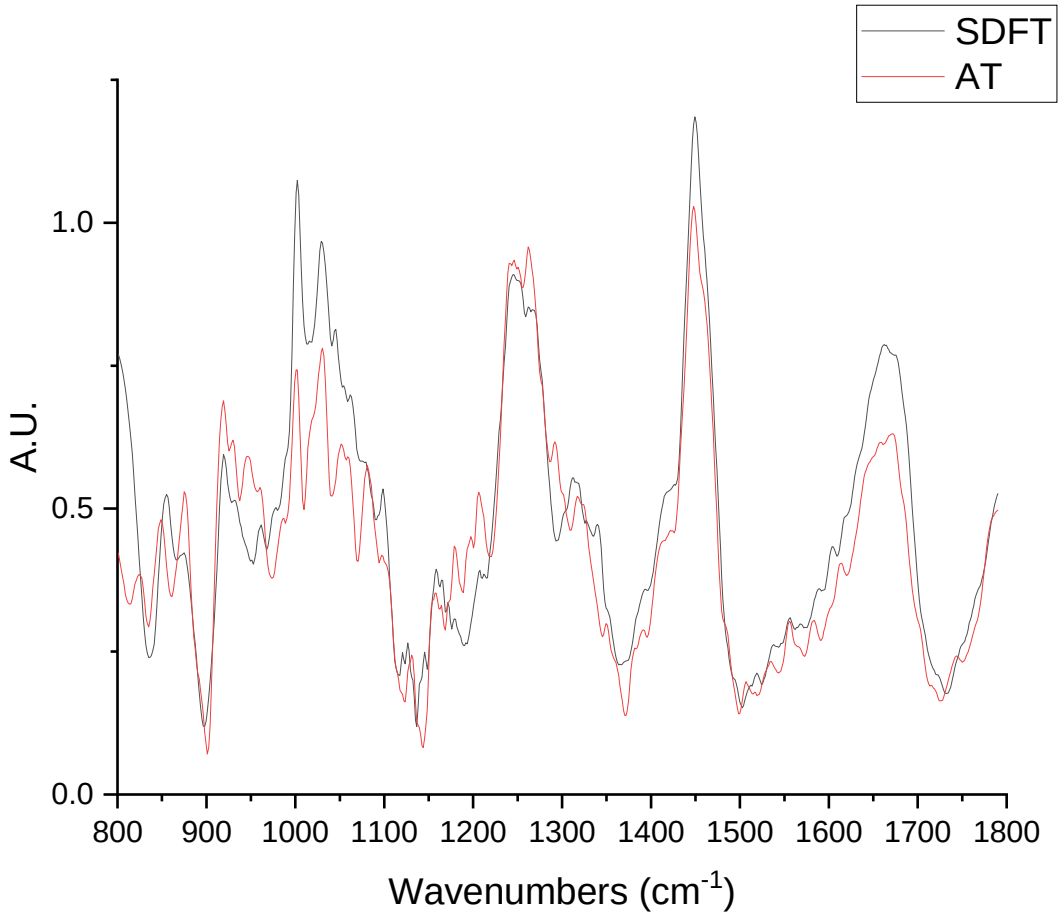

Figure 5-11. Averaged Raman spectra of equine SDFT (n = 70, *black line, from Chapter 4*) and human Achilles tendon (n = 80, *red line*)

5.4.2 Composition Differences between Tendons

The compositional differences between the Achilles tendon and the anterior tibialis tendon can be separated by the PC1 loading. It has been confirmed that the Achilles tendon has higher GAG and DNA content than the tibialis anterior tendon, with a similar total collagen content (Birch et al., 2001, Nash et al., 2019). Compared to the anterior tibialis tendon, the spectra of Achilles tendons showed lower intensities in the amide I, CH_2 bending bands, and higher carbohydrate-related bands (1000 – 1100 cm^{-1}). Interestingly, our previous study demonstrated that the most evident spectral differences between the equine SDFT and DDFT are present in the proline/hydroxyproline region (800 – 1000 cm^{-1}) and the CH_2 bending band, without a significant difference in the amide I band (Section 4.3, Figure 4-6). Tendons from different species are expected to have slightly different compositions. When comparing the human Achilles tendon with the equine SDFT (Figure 5-11), the spectra from both tendons demonstrated similar dominant collagen-related bands while the Achilles tendon had more visible weaker bands. Since the two tendons demonstrated different age-related spectral features, comparison between different studies from different tested species should be made with caution, especially when the vibrational mode of each specific tendon composition has yet to be characterised and is usually difficult to study in isolation. However, the age-related spectral changes appear similar within species, as we reported between the equine SDFT and DDFT (Figures 4-5 and 4-6), and between human Achilles and anterior tibialis tendons (Figure 5-5). Since AGEs crosslinks have been identified in both human and equine tendons, glycation may induce different

conformational changes, depending on the species, to the tendon collagenous matrix, affecting the secondary structure of collagen molecules and reflected in the amide I and amide III compound bands. In the human tendon results, no age-related increase was observed, as our previous findings on equine tendons, among the carbohydrate-related bands (1000 – 1100 cm^{-1}), which was tentatively assigned to the sugar residues resulting from collagen glycation. It is possible that the more complex human tendon compositions, resulting from genetic, diet, or exercise differences, could affect or even mask the changes in this carbohydrate region.

5.4.3 Raman Features of Achilles Sub-tendons

This study, with a small number of samples, demonstrate that Raman spectroscopy has some potential to differentiate sub-tendons on an individual basis, especially at the higher wavenumber regions. However, challenges remain given the high variance in tendon composition between individuals.

In the tested specimens, PCA can differentiate sub-tendons by identifying prominent differences in both CH_2 bending and amide I bands. However, these bands did not show a similar trend across all studied specimens, suggesting high individual differences in sub-tendon level compositions. Similar high variance has been reported in the Achilles tendon for components of the extracellular matrix, such as lubricin content (Sun et al., 2015). Our biochemical findings (Section 3.3.2) demonstrated a significantly higher DNA content in the soleus sub-tendon compared to gastrocnemii sub-tendons, but its minuscule content may be challenging for

this spectroscopic technique to identify directly. In the previous study on equine tendons (Chapter 4), the CH_2 bending band (~ 1450 cm^{-1}), the intensity of which usually correlates with the lipid content within the sample, was tentatively assigned to the total cell content. However, the CH_2 band intensity of the soleus did not appear to be higher than the gastrocnemii sub-tendons, suggesting other factors, either matrix compositions or fibrous orientation (as discussed previously), may influence this CH_2 bending band more than the pure cellular content alone.

The amide I band, usually assigned to the collagen secondary structure, was constantly identified by the PCA and demonstrated sub-tendon level differences but the band shape and intensity varied among studied specimens. Being a large, complex compound band, the amide I band often requires spectral deconvolution, which uses mathematical methods by fitting several smaller peaks to reproduce the original band shape, to fully interrogate the underlying structural or compositional differences. Deconvolution techniques were not performed on the collected spectra, but visual inspection implied that two dominant peaks centred at ~ 1650 cm^{-1} and ~ 1670 cm^{-1} are likely different between sub-tendons and between individuals. As the measured total collagen contents (Section 3.3.2) were similar, these results could imply that conformational differences, instead of total collagen quantity, may exist between different sub-tendons. However, it is not possible to make any further interpretations from the results due to the limited sample tested and the high individual variance.

The results from the homogenised Achilles and anterior tibialis tendon demonstrated that both tendon types and age can affect the intensities of

both CH_2 bending and amide I bands. Therefore, despite the temptation to assign one or a few specific wavenumbers to one compositional component, our current knowledge of microscopic level tendon composition and the effect of these compositional differences on the reflected Raman spectra is still limited and requires further research to fully utilised the benefits of using Raman spectroscopy on probing tendon compositions. Besides, the Raman spectrum of tendons is highly influenced by its fibrous orientation. No study has investigated the microscopic level structure between different Achilles sub-tendons; therefore, it is currently not possible to correlate the measured sub-tendon spectra with the fibrous orientation of the lower hierarchies. Since each sub-tendon demonstrated different twist angles (Edama et al., 2015a, Pękala et al., 2017), different fibrous orientations in the lower hierarchies may exist between sub-tendons to accommodate the complex, multidirectional force. Future studies combining histological or microscopic imaging analysis and Raman spectroscopy may reveal the molecular or structural origin of these spectral differences.

At this stage, the results do not suggest that Raman spectroscopy can consistently differentiate different sub-tendons due to the high individual variance. However, if the composition and microscopic structural features of Achilles sub-tendons are first characterised (by conventional biochemistry, histology, or microscopic imaging techniques), Raman spectroscopy may, given these as a priori knowledge, provide a new method to probe sub-tendon compositions.

5.5 Conclusion and Chapter Summary

Raman spectroscopy can differentiate minimally processed human Achilles and tibialis anterior tendons of different ages and has some potential to discern between Achilles sub-tendons on an individual basis. The age-related spectral changes are highly correlated with the quantity of the glycation crosslinks, suggesting the potential *ex vivo* or *in vivo* use of Raman spectroscopy to rapidly quantify these glycation crosslinks and to provide an overall age index of the measured tendon. Therefore, Raman spectroscopy has the potential to be used in a clinic setting to monitor tendon health, detect premature/accelerated ageing, or track response to treatments for tendinopathies. Future work applying *in vivo*, non-invasive Raman spectroscopy on tendons may greatly enhance our current diagnosis, prevention and treatment regime of tendinopathies.

Chapter 6 Investigation of the Impact of Reduced Sub-tendon Sliding on Tendon Mechanical Behaviour

6.1 Introduction

The human Achilles tendon is composed of three smaller sub-tendons arising from the separate muscle bellies of the soleus, lateral gastrocnemius and medial gastrocnemius muscles. Each sub-tendon has a different CSA and exhibits distinct *in vitro* mechanical properties corresponding to different force-generating capacities of the gastrocnemii and soleus muscles (Chapter 3). Sub-tendons show an internal rotation (counter-clockwise for the right leg in superior view) as they descend towards the insertion site. Each sub-tendon however demonstrates a different degree of rotation, with the medial gastrocnemius sub-tendon the least twisted (Edama et al., 2015a, Pękala et al., 2017). The degrees of rotation of each sub-tendon are highly variable between individuals and can differ by more than 100° between the most twisted and the least twisted Achilles tendon specimen (Pękala et al., 2017). Together, these studies of sub-tendon morphology have improved our understanding of the Achilles tendon and suggest that our traditional thinking of this tendon as a homogeneous structure should be discarded and that the intra-tendinous mechanical behaviour during movements requires further study and characterisation. The less-studied relative movement between sub-tendon interfaces, which likely demonstrate non-linear and complex mechanical behaviour due to the aforementioned mechanical properties and morphology differences between sub-tendons, is likely to dictate *in vivo* Achilles tendon behaviour.

More recently, studies have demonstrated that the Achilles tendon displacement non-uniformity decreases in aged (Franz and Thelen, 2015, Slane and Thelen, 2015) and injured tendons (Froberg et al., 2017, Couppe et al., 2020), providing further evidence that optimal sub-tendon sliding is required for normal tendon function. The impact of reduced sub-tendon sliding on Achilles tendon function is however less clear. It has been suggested that reduced sliding eliminates individual control from gastrocnemii and soleus muscles, resulting in poor mechanical output (Franz et al., 2015, Franz and Thelen, 2015). Indeed, aged and injured tendons often show reduced functional capacity compared to young (Stenroth et al., 2012) or healthy Achilles tendons. On the other hand, reduced sliding resulting from a stiffer interface could also provide a better force sharing capacity between loaded and unloaded sub-tendons, thereby lowering the stress exerted on one single sub-tendon (Maas and Finni, 2018) and potentially reducing overall injury risk. This second suggestion implies that reduced sliding capacity may be beneficial for reducing the risk of Achilles tendon injury, contrary to the common knowledge that older people more frequently suffer from tendon related injuries than their younger counterparts. Currently, we have limited understanding of the consequence of age- and injury-related decline in sub-tendon sliding on Achilles tendon function and whether this change contributes to an increased rate of injury.

In previous work, the non-uniformity of *in vivo* displacement has been detected by ultrasound speckle tracking, as described by Arndt and colleagues (Arndt et al., 2012). This technique tracks sonographic patterns within the Achilles tendon and allows the detection of regional displacements.

However, the primary limitation of using 2-D ultrasound images to measure 3-D tendon displacement is that only a small region of a single plane of view (predominantly sagittal plane) can be measured at any given time. Although it is common and convenient to suggest that the superficial portion of the Achilles tendon belongs to the medial gastrocnemius sub-tendon and the deeper portion belongs to the soleus sub-tendon, this is likely a main source of error when studying Achilles tendon mechanics due to the highly complex and variable rotatory geometry of each sub-tendon (Pękala et al., 2017). This limitation can be overcome by employing finite element analysis (FEA, reviewed in Section 1.6.2) on subject-specific tendon geometries (Hansen et al., 2017) to systematically study the complex interaction between the interface sliding property (Handsfield et al., 2017) and the force output from the associated muscles bellies.

6.1.1 Hypothesis

Changing the properties of the interface between sub-tendons affects sub-tendon displacement and stress distribution in finite element analysis, and the modelling results agree with the measured *in vivo* age-related reduction of sub-tendon sliding.

6.1.2 Objectives

- Reconstruct sub-tendon morphological models from dissection and separation of Achilles sub-tendons.

- Conduct finite element analysis and assign different interface (inter-sub-tendon matrix) properties to simulate the age-related reduction of the sub-tendon sliding ability.
- Plot and analyse tendon displacement and stress distribution under different muscle loading scenarios, interface properties, and between different morphological models.
- Recruit groups (young and old) of participants and conduct *in vivo* tests to identify age-related decline of sub-tendon sliding.
- Compare the trend observed in modelling results with the collected experimental data from participants.

6.2 Methods

6.2.1 Finite Element Analysis

6.2.1.1 Sample Collection and Sub-tendon Separation

Fresh Achilles tendon specimens (n = 3) were collected and used for morphology measurements and computer model construction (UCL/UCLH Biobank for Studying Health and Disease (HTA license number 12055) with Local R&D approval (Ref: 11/0464)). Only tendons showing no signs of injury or disease were included in the study. Sub-tendons were separated as described in the study by Szaro and colleagues (2009). A longitudinal reference line (from the mid-point of calcaneal insertion site to mid-point between the two gastrocnemii bellies) was drawn before separation as a guide to align tendon cross-sections (see below). Exterior moulds were

created to minimise geometry distortion during separation (Goodship and Birch, 2005).

6.2.1.2 CAD models construction

After separation, the three sub-tendons were carefully assembled and fitted into the original exterior mould. Cross-sections (10 mm apart) were cut through the mould and the sub-tendons from proximal to distal, starting from the soleus musculotendinous junction. These cross-sections were then photographed together with a ruler (1 mm accuracy) using a 12-megapixel camera yielding a resolution of 0.014 mm/pixel. Since the fascicles intertwined at the insertion, the reconstructed models end at the level approximately 10 mm proximal to the calcaneus.

Three separate Achilles sub-tendon models were created in a web-based computer-aided design platform (Onshape, PTC, US). First, each sub-tendon cross-section was delineated (perimeter, then internal borders) and aligned according to the longitudinal reference line. The CSA differences between the drawn sub-tendon area and the photographic measurements were less than 1 mm^2. Next, the cross-sections belonging to each sub-tendon were connected from distal to proximal, creating three solid parts. The models constructed were inspected to ensure no penetration or separation between each part before conducting simulations.

6.2.1.3 FEA – materials, geometry, and mesh

A commercially available FEA software (ANSYS v19.0, Ansys Inc., US) was used for mesh generation and static stress analysis. Each sub-tendon was modelled as a hyperelastic, non-linear, neo-Hookean material

(Handsfield et al., 2017, Hansen et al., 2017) with the initial modulus (lat. G: 226.7 MPa, med. G: 143.2 MPa, soleus: 103.1 MPa) obtained by curve-fitting the *in vitro* axial tensile testing results (Section 3.2.2). Sub-tendons were meshed into quadratic 10-node tetrahedral solid elements (TET10). A mesh convergence test was conducted using static stress analysis with criteria of 1% for each model. Maximal element edge length for each model was 0.8, 0.5, and 0.4 mm respectively and yielded 258402, 195286, and 223423 elements, respectively. The contact faces between sub-tendon pairs were manually selected and assigned different contact properties: frictionless, frictional (with coefficient 0.2, 0.4, 0.6, 0.8, and 1.0) and bonded. Surface-to-surface translational joints, with no restriction along the longitudinal axis while limiting transverse plane separation, were assigned at the contact faces to prevent sub-tendon separation. Fixed displacement at distal faces (to mimic the fixed calcaneus insertion) and individual ramped tensile forces at the proximal face of each sub-tendon (to mimic muscular pull) were applied.

6.2.1.4 FEA boundary conditions

Individual 100 N linear tensile force was arbitrarily applied on the proximal face of each sub-tendon model. The averaged axial displacement and the transverse plane displacements of the proximal soleus face were analysed and reported since this is a commonly used anatomical landmark for measuring *in vivo* tendon mechanical properties.

To study the effect of sub-tendon loading on the longitudinal displacement of the proximal soleus face, an FEA of each model with the same axial tension (100 N) in each sub-tendon was run but with different

degrees of sliding between them – namely, frictionless, frictional (with friction coefficient 0.2, 0.4, 0.6, 0.8, and 1.0) and bonded (no sliding).

6.2.2 *In Vivo* Study Participants

The *in vivo* study was approved by the University College London Research Ethics Committee (ref. 1487/1001). All participants were well informed and provided consent in accordance with the Declaration of Helsinki. Participants were assigned into two groups according to their age (Young: 20 to 30 years, Old: over 50 years). The exclusion criteria were having any previous diagnosed Achilles tendon injuries and any systematic disease that may affect muscle-tendon functions.

6.2.3 Experiment Procedures

The participants lay in a prone position on an examination bed with their feet firmly pressed against the wall (ankle ~ 90°). Three pairs of 50 mm diameter electrodes were placed on the motor points of the three muscles bellies (Kim et al., 2005, Botter et al., 2011). The skin was cleaned with alcohol swaps and shaved, if necessary, to ensure minimal intensity for inducing muscular contraction and minimising discomfort. Each muscle was stimulated using a commercially available transcutaneous electrical neuromuscular stimulation device with 30 Hz, 300 μs pulse train and an on-off cycle of 8 seconds (4 s on and 4 s off) for two minutes to induce tetanic contractions. Before the stimulation, an ultrasound probe (2-8 MHz, 9L-D, LOGIQ S8, GE Healthcare) was placed at the musculotendinous junction of the three muscles to ensure proper image quality. During the stimulation, the intensity increased gradually (to ~ 20 mA) until visible displacement of the

stimulated muscle (e.g., medial gastrocnemius) was recorded while at the same time no visible contraction of other muscles (e.g., lateral gastrocnemius and soleus) was observed, before moving the probe to the soleus musculotendinous junction to measure its displacement (Figure 6-1). At least three consecutive contractions were recorded and stored for offline analyses. Randomised sequence and ample rest (> 2 min) between stimulations were used to reduce artefacts.

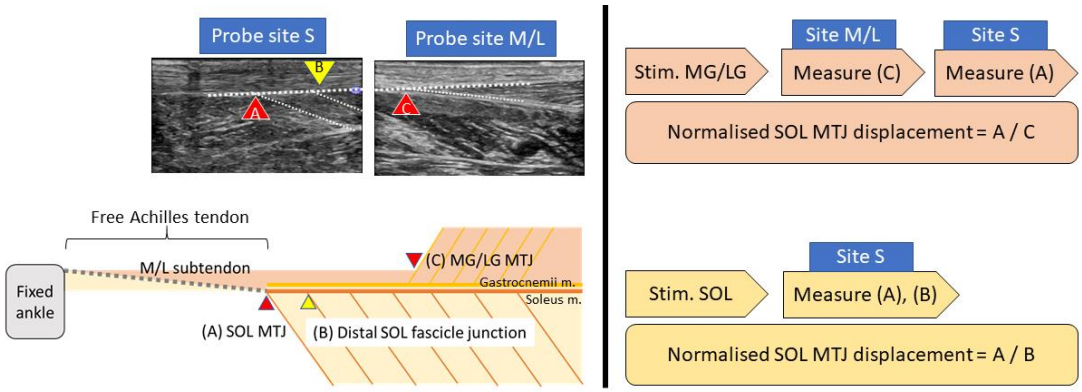

Figure 6-1. Simplified sagittal plane view of triceps surae muscle-tendon units and corresponding ultrasound measurement locations *(left)* and sequences of measurement during each stimulation trial *(right)*. MG/LG: medial or lateral gastrocnemius, SOL: soleus. MTJ: musculotendinous junction. (A) musculotendinous junction of soleus. (B) one distal soleus muscle fascicle junction. (C) musculotendinous junction of gastrocnemii, site M/L.

6.2.4 Ultrasound Image Analysis

The analysis was performed in a semi-automatic way using an in-house MATLAB code (R2019a, MathWorks, US) utilising Computer Vision Toolbox add-on for tracking displacements and correcting movement artefacts. The peak soleus musculotendinous junction displacement of each stimulation trial was tracked and normalised by its contracted muscular displacements (for

gastrocnemii: musculotendinous junction, Figure 6-1, *(C)*; for soleus: one distal muscle fascicle-aponeurosis junction, Figure 6-1, *(B)*), assuming that the muscular displacement is affected only by stimulation intensity while sub-tendon displacement is affected by interface sliding capacity. We arbitrarily chose one distal soleus muscle fascicle-aponeurosis junction as the reference point (Muramatsu et al., 2001) since no clear anatomical landmark lies within the soleus muscle.

6.2.5 Statistical Analysis

Statistical analysis was performed using SPSS (v26, IBM, US). Soleus junction displacement between young and old groups was compared using Mann-Whitney U tests. The level of significance was set at 0.05, two-tailed.

6.3 Results

6.3.1 Sub-tendon Morphologies

The tendons varied in CSA from 42.3 to 90.4 mm^2 and the twist and the internal arrangement of their sub-tendons showed great individual variability (Figure 6-2), as reported previously (Edama et al., 2015a, Pękala et al., 2017). In the proximal part of the tendon, the anterior portion was mostly occupied by the soleus sub-tendon and the posterior portion by medial gastrocnemius on the medial aspect and lateral gastrocnemius on the lateral aspect. Passing distally, the sub-tendons rotate in a lateral direction and the longest tendon (Model 1, 70 mm) rotated the most since its lateral gastrocnemius sub-tendon almost completely occupied the anterior surface.

In the shorter tendons (Models 2 and 3, 40 mm), at the distal end, the anterior portion was occupied by the lateral gastrocnemius and soleus sub-tendons. The tendon used for Model 3 was the thinnest (CSA: 42.3 mm^2) while tendons used in Models 1 and 2 were substantially thicker (89.1 and 90.4 mm^2). The models closely replicated the original sub-tendon geometries, capturing individual variability in sub-tendon arrangements. The tendons (and models) are not intended to represent the geometrical features of a particular group, but to represent diversity among individuals.

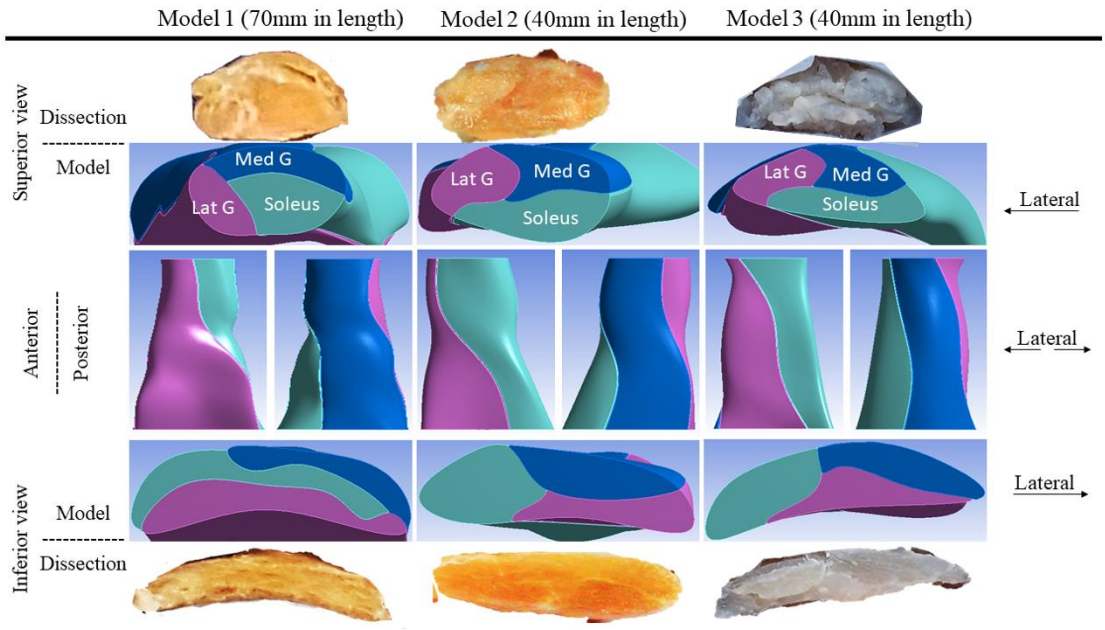

Figure 6-2. Three-dimensional computer models of Achilles sub-tendons

6.3.2 Sub-tendon Displacement Affected by the Degree of Sliding

When the soleus sub-tendon was loaded in isolation, assigning frictional contacts reduced the soleus displacement compared to the frictionless contact across all three models (Figure 6-3, *blue triangles*). When the medial

gastrocnemius sub-tendon was loaded, soleus displacement increased with increasing friction (Figure 6-3, *red circles*). This trend was also observed when the lateral gastrocnemius was loaded, but interestingly only in Models 1 and 2 (Figure 6-3, *black squares*). When loaded, three models showed distinct transverse plane rotation behaviour, which is likely caused by their different geometrical features (Figure 6-4).

Displacement data were normalised to frictionless contact conditions to observe the relative displacement change and therefore the impact of reduced sliding between the sub-tendons, as may occur with ageing (Figure 6-5). When the soleus was loaded, all three models showed a similar decrease in soleus displacement as friction increased. In the gastrocnemii loaded conditions, a substantial increase in soleus displacement was observed in Model 1 and a lesser increase was observed in Model 2, suggesting tendon shapes and geometries affect force transmission across sub-tendons when interface properties change.

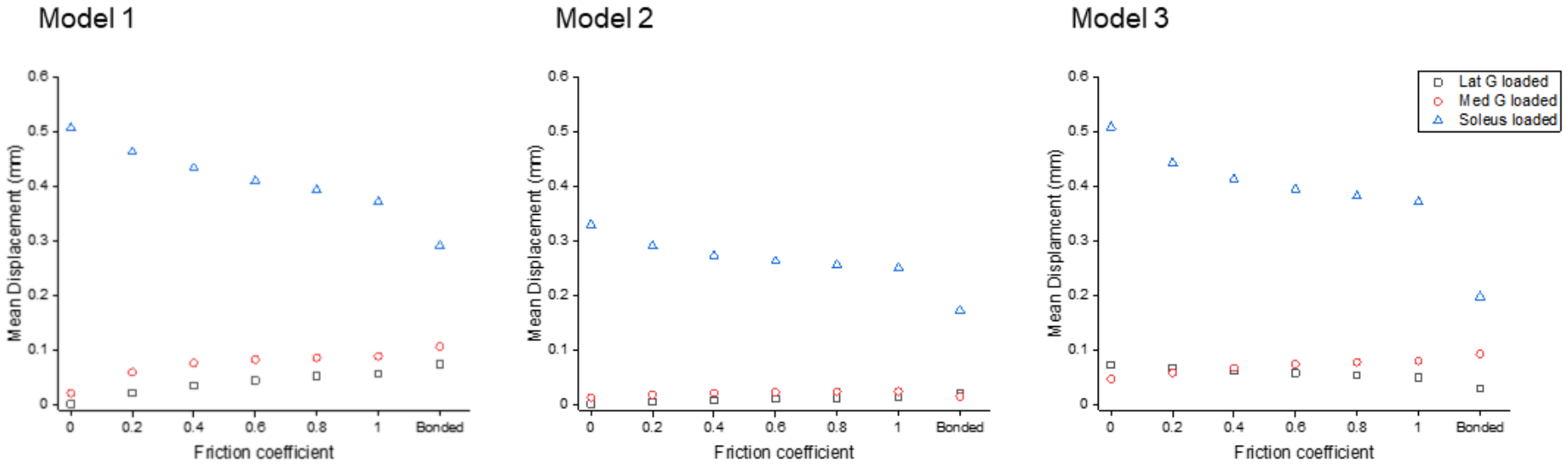

Figure 6-3. Mean displacement of the proximal soleus face of three models with different friction contacts when each sub-tendon was loaded in isolation

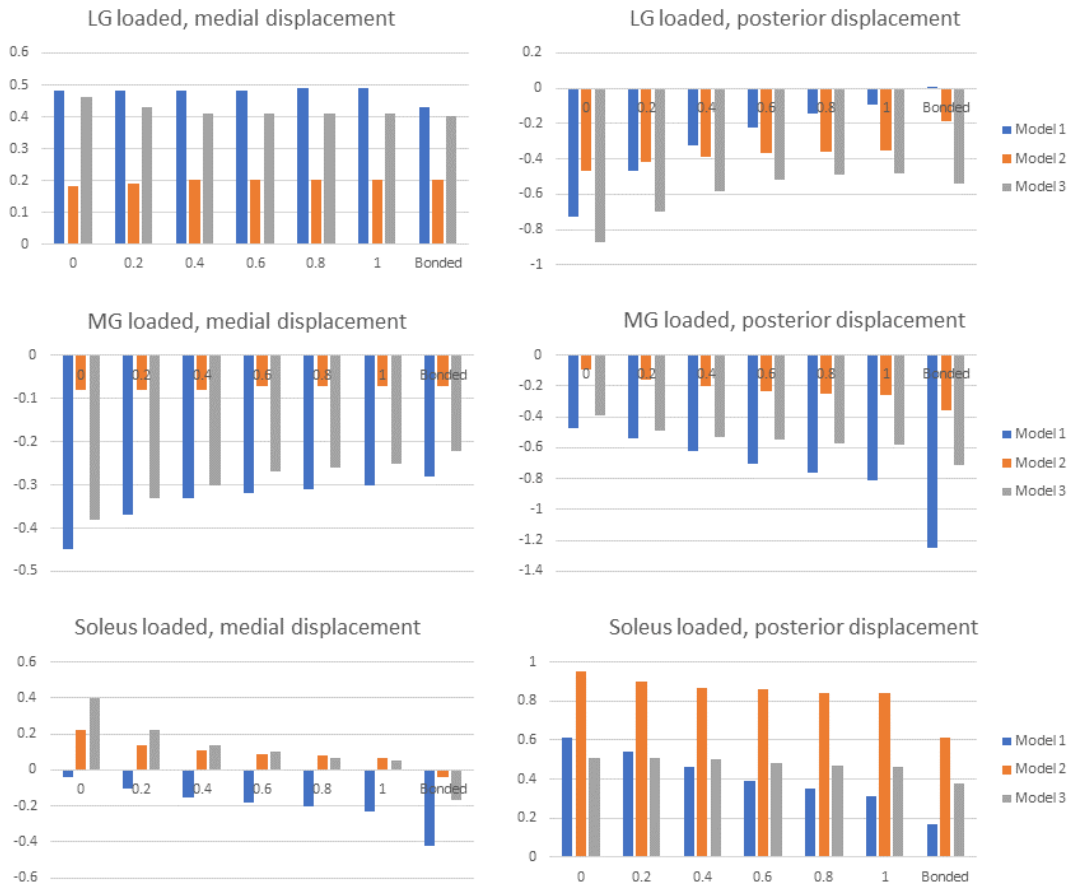

Figure 6-4. Mean transverse plane displacements (in mm) of the proximal soleus face of the three models with different friction contacts (x-axes) when each sub-tendon was loaded in isolation. Note the scale of the y-axes differs to allow better visualisation of differences in the data.

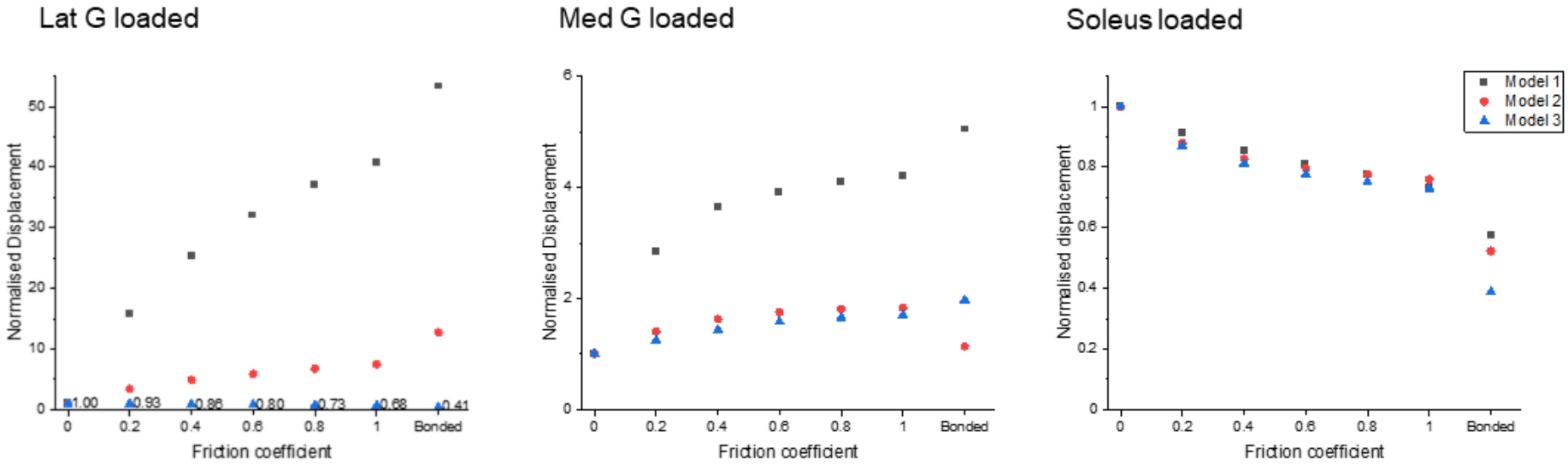

Figure 6-5. Normalised (to frictionless, coefficient = 0) proximal soleus face displacement of different friction contacts when each sub-tendon was loaded in isolation. Note the scale of the y-axes differs to allow better visualisation of differences in the data.

6.3.3 Reduced Sliding Altered Tendon Stress

All models showed decreased mean von Mises stress for frictional and bonded contacts compared to frictionless contact (Figure 6-6, *upper row*); however, the peak von Mises stress, a prediction of material yielding, differed among all three models (Figure 6-6, *lower row*). As friction increased, the peak stress intensity of Model 1 decreased but Models 2 and 3 fluctuated with different sub-tendon loading conditions. For bonded contact conditions all models showed lower peak stress compared to the frictionless and frictional contact conditions, but the size of the decrease varied greatly between models. Furthermore, changing the contact properties, in addition to affecting the intensity of peak stress, also changed the region where the peak stress occurred (Figure 6-7). Due to the large geometry differences (CSA and twist) across the three models, no clear pattern in the change of peak stress location is seen.

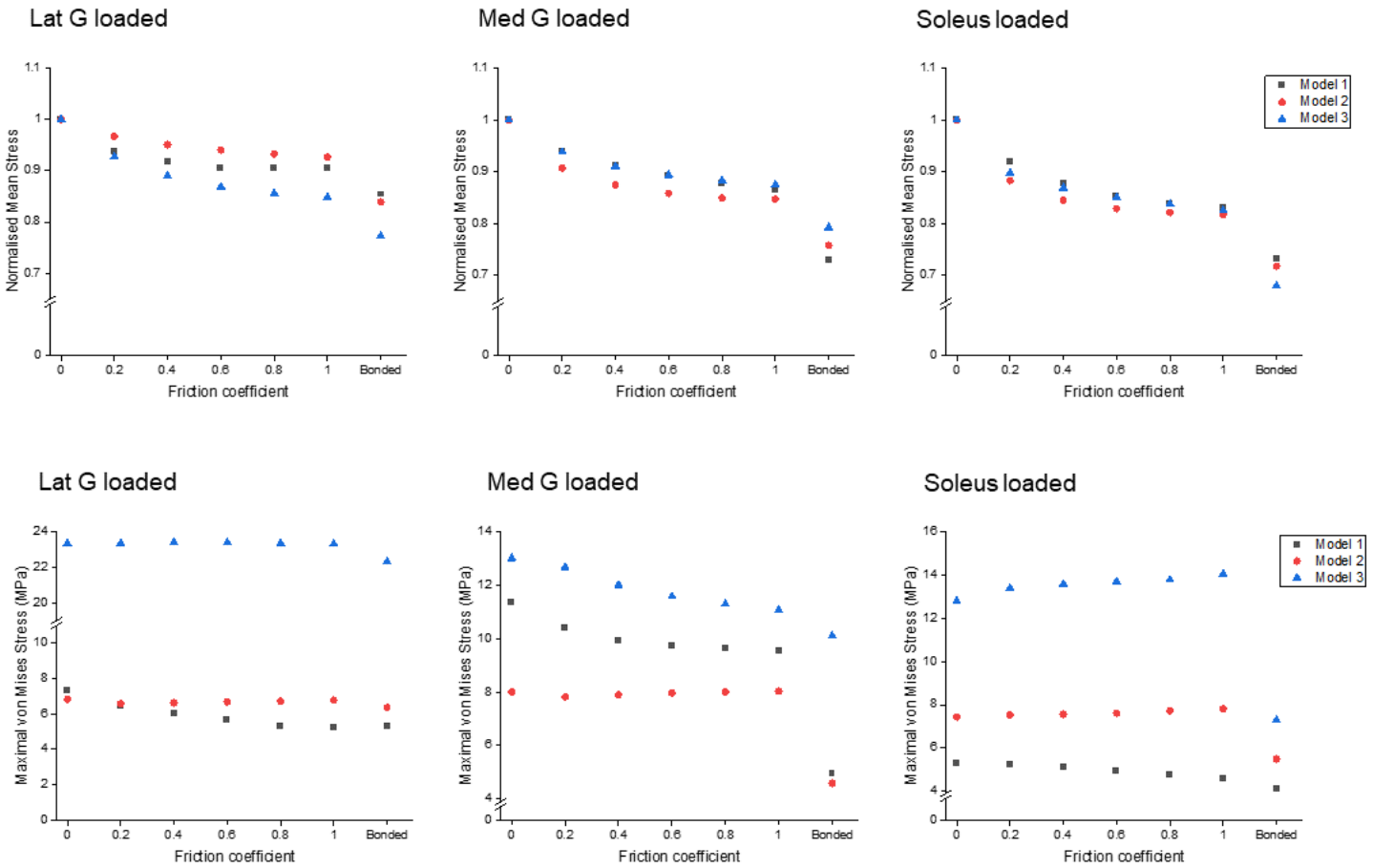

Figure 6-6. Mean normalised *(upper row)* and peak *(lower row)* von Mises stress of the whole Achilles tendon for different friction coefficients when each sub-tendon was loaded in isolation. Note the scale of the y-axes differs.

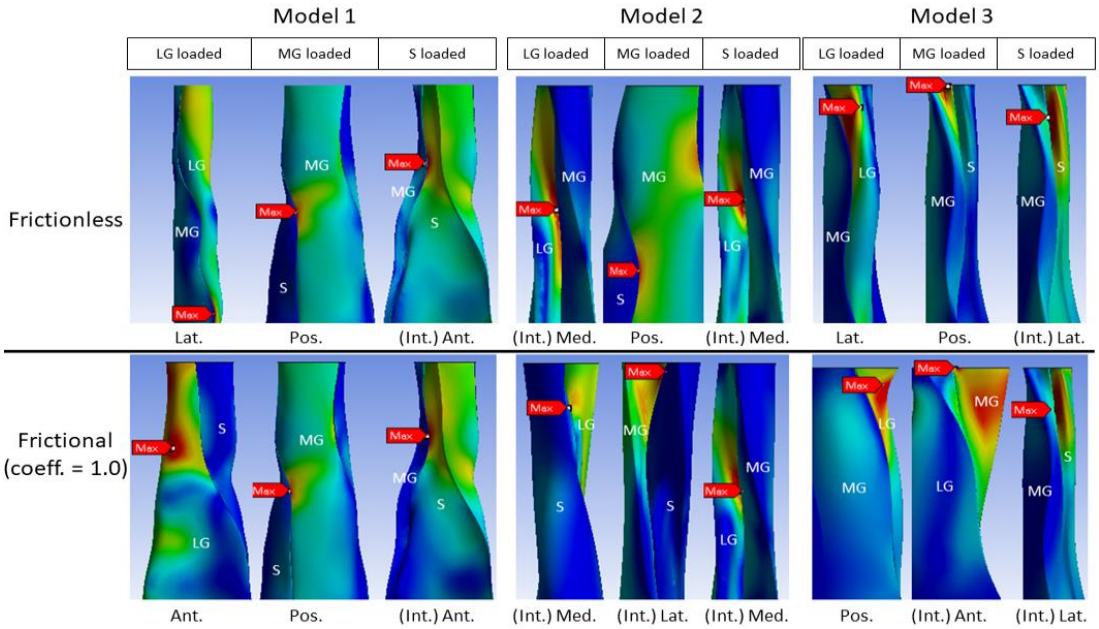

Figure 6-7. Change in peak stress location when shifting from frictionless *(upper row)* to frictional *(lower row)* contact is structural dependent. View planes: Ant.: anterior, Pos.: posterior, Lat.: lateral, Med.: medial, Int.: internal view with the covering sub-tendon removed.

6.3.4 Displacement Non-uniformity Explained by Modelling Results

The older group of participants (n = 7) demonstrated significantly (p = 0.005) lower normalised soleus junction displacement compared to the younger group (n = 9) for soleus stimulation (Figure 6-8). This decrease in displacement with increasing age shows the same trend as the modelling result when the soleus sub-tendon was loaded in isolation (Figure 6-3, *right*). No detectable difference was found in soleus junction displacement between groups for both gastrocnemii stimulation conditions.

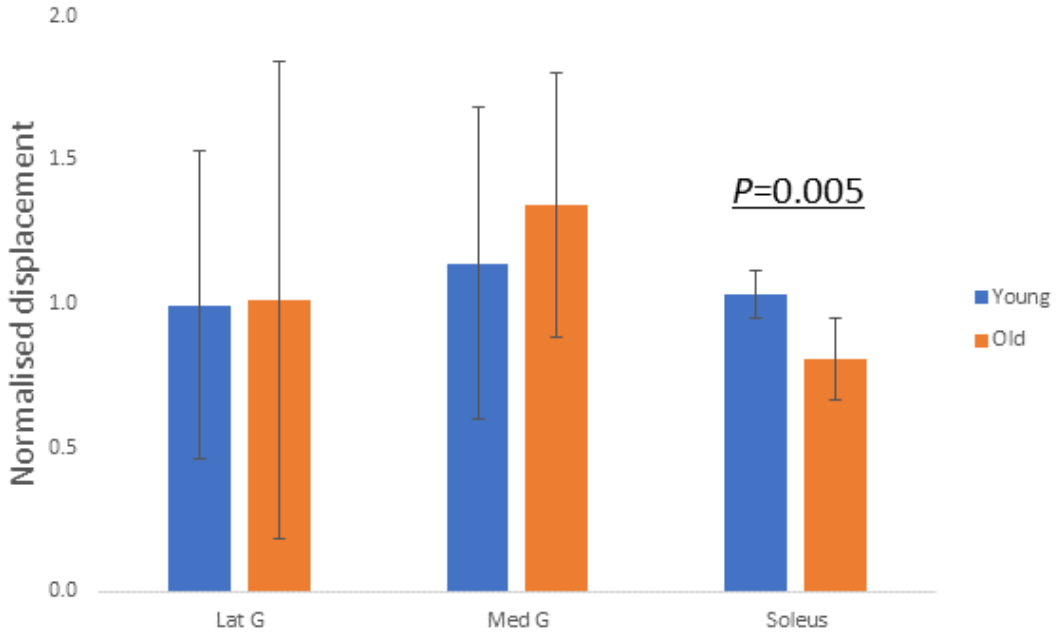

Figure 6-8. Group differences in normalised soleus junction displacement during different stimulation trials.

6.4 Discussion

These results suggested that the mechanical behaviour of the Achilles tendon is complex and can be affected by a combination of factors including individual tendon morphology and changes in sub-tendon sliding.

The modelling results provide insight into the impact of different sub-tendon shapes and orientations on sub-tendon sliding. Furthermore, these results highlight the importance of understanding sub-tendon sliding when considering the non-uniform displacement of the Achilles tendon during movements. Assigning frictional contacts and varying the friction coefficient in the FEA allows a better representation of sub-tendon behaviour, more closely aligned to the physiological conditions, and reflection of changes across the lifespan, instead of the dichotomy between frictionless sliding and completely

bound conditions as has been applied previously (Handsfield et al., 2017). An identical coefficient was arbitrarily assigned across three interfaces, but the true sliding ability between sub-tendons and the rate of age-related decline could be different. An increase in friction in the models, mimicking the age-related reduction in sliding under physiological loads (Thorpe et al., 2013c), greatly affected the sub-tendon displacement and stress distribution. This was highly dependent on geometry and varied between the three models, suggesting the rotation and twist angle of the whole Achilles and sub-tendons affects how they interact.

When increasing the friction between sub-tendons, it is expected to see an increase in the influence of individual muscle belly contractions on adjacent sub-tendons. In keeping with this, the degree of soleus displacement due to gastrocnemius applied load mainly increased but this was much more evident in the longest model with the greatest sub-tendon twist (Model 1) and least in the shorter model with the smallest CSA (Model 3). A greater transfer of load between the gastrocnemius and soleus would be expected to result in reduced soleus displacement when the soleus muscle alone applies force. All three morphologies studied showed reduced soleus displacement with simulated soleus contraction as the coefficient of friction was increased. However, contrary to the above, the result showed the least reduction in Model 1 and the greatest reduction in Model 3 (Figure 6-5, *right*). These results highlight the complexity of the Achilles tendon and suggest that sub-tendon shape, twist, and rotation result in unequal distribution of strain along the length of the tendon.

Similarly, when friction increased, the effect on peak stress intensity differed between the Models. In the most twisted model (Model 1), an increase in friction reduced the peak stress intensity while in the other models peak stress intensity fluctuated under different muscle loading conditions. These results suggest that the impact of age-related changes to the stiffness of the interface can depend on the individual Achilles tendon morphology and balance of muscle strength. Load sharing, such as between adjacent muscle-tendon units (Maas and Finni, 2018) and between fascicles (Thorpe et al., 2013c), has been proposed as a strategy to minimise stress and lower the risk of injury. As it is demonstrated here by static stress analysis however, the reduction of the whole tendon stress does not necessarily translate to a reduction in the peak stress (Figure 6-6), which is more important when considering the strength and integrity of a material under load. The high-stress region during loading could represent a mechanical weak point that may later develop pathological changes. It has been demonstrated that stress distribution within the Achilles tendon is geometry dependent and, interestingly, changing the material properties had minimal effect on tendon stress distribution (Hansen et al., 2017). The study is limited to three different morphologies, but the range of morphologies is likely far greater than that modelled here, and this would result in even more disparate strain and stress distributions between individuals.

The results of the study suggest that using the traditional anatomical landmark (soleus musculotendinous junction, the start of the free Achilles tendon) to measure *in vivo* tendon mechanical properties (Kongsgaard et al., 2011) is problematic, especially when studying aged or repaired Achilles

tendons. The displacement of the soleus musculotendinous junction is used in *in vivo* studies to calculate tendon strain and stiffness; however, the result from our study has shown that displacement is not equivalent nor proportional to whole tendon strain when comparing tendons with different morphologies and sub-tendon arrangements. In low friction conditions, simulating a young person's tendon, the displacement of the soleus junction is predominately from the soleus muscle-(sub-)tendon unit displacement; in high friction conditions, mimicking aged tendons, the displacement of the soleus junction is the combination of both the decreasing trend from soleus and the increasing influence from gastrocnemii muscle-tendon units. Moreover, the exact geometry and mechanical properties of each sub-tendon among individuals are unknown and each associated muscle exhibits different age-related and injury-related compositional (Csapo et al., 2014) and structural (Stenroth et al., 2012) changes. Together, these results suggest that measuring 'whole' tendon properties is insufficient when investigating such tendons. Previous studies have shown that repaired Achilles tendons show higher displacements when loaded compared to healthy tendons, despite being thicker and transmitting lower forces (Wang et al., 2013a, Geremia et al., 2015). Considering that those sub-tendons are surgically bound together and show uniformed displacements (Froberg et al., 2017, Beyer et al., 2018), the actual decline in material properties post-surgery may be even greater than reported since sub-tendons exhibit much lower displacement when bound, given the same force and material properties. However, since repaired tendons demonstrate different properties, it is not suitable to directly infer the role of sub-tendon sliding on

tendon functions from the modelling studies. Future studies incorporating mechanical property testing and displacement uniformity on repaired Achilles tendons could give further insight on the effect of sub-tendon sliding on the tendon level mechanical behaviour after injuries.

A negative relationship was found between participant age and the electrically-induced soleus junction displacements, and this relationship was in line with the FEA results when assigning frictional contacts. No statistically significant difference was detected between young and old groups in both gastrocnemii stimulation trials. The modelling results suggested that gastrocnemii-induced soleus displacement is generally low and, importantly, depends on the shape and twist of the tendon that was not possible to measure in the *in vivo* studies. Furthermore, the gastrocnemii have longer tendinous parts that have complex interactions with the underlying soleus muscle and aponeurosis (Finni et al., 2003b, Magnusson et al., 2003), and the CSA of gastrocnemii sub-tendons are smaller and may have less influence on the larger soleus sub-tendon. The simplification of this *in vivo* study may therefore overlook certain age-related features in muscle-tendon units and surrounding structures that may potentially affect the results. The use of minimal electrical intensity during stimulation prevented co-contraction of other muscles, but the expected contraction force was low and less than most physiological loading scenarios.

Besides the differences in sub-tendon sliding properties, other factors could also contribute to the observed displacement decline in the aged group. Firstly, the muscle architecture and composition change with age. Compared to younger adults, aged people usually show a lower muscle

mass (Mitchell et al., 2012), reduced muscle thickness and muscle fascicle length (Kubo et al., 2003), and an increased adipose tissue infiltration (Kubo et al., 2003, Kragstrup et al., 2011). Secondly, the reduction of type II muscle fibre (mainly gastrocnemii) with age (Tieland et al., 2018) could affect the observed outcome between different stimulation trials since the soleus muscle is predominantly composed of type I fibres, which is generally less affected with age advancement. Lastly, the neural excitability and the excitation-contraction coupling can differ between young and old adults (Scaglioni et al., 2003, Kawashima et al., 2004, Tieland et al., 2018). Despite being a relatively simple and low-cost setup, the validity and usefulness of our selective muscle stimulation methodology to detect the *in vivo* sub-tendon sliding ability require further investigation.

6.5 Conclusion and Chapter Summary

In conclusion, this study provides novel concepts and improves our understanding of Achilles tendon mechanical behaviour. These results suggest that using the musculotendinous junction displacement to measure Achilles tendon strain *in vivo* should be done with caution and should not be used to compare tendons from different individuals without regard for tendon morphological variations, such as CSA, shape, and twist, or the sub-tendon sliding ability. Differences in the transfer of force between sub-tendons with different geometrical arrangements suggest that some tendon morphology types have higher localised stress and that sites within the tendon will vary between individuals.

Chapter 7 Sub-tendon Mechanical Behaviour under Simulated Gait Patterns

7.1 Introduction

In the previous chapter, it was demonstrated that sub-tendon mechanical behaviour is heavily influenced by the sub-tendon morphology, the inter-sub-tendon matrix sliding ability, and the loading from muscle contractions. FEA allows modification to the tendon geometry and simulation of the age-related decline in the sliding ability. In addition to the passive loading conditions (arbitrarily 100 N from each muscle, in FEA; electrical stimulation (~ 20 mA) on different muscle bellies of participants) conducted in the previous chapter, the sub-tendon behaviour during physiological bipedal walking is further explored in this chapter to understand how variable force input from different muscles affects the sub-tendon displacement and stress distribution. By changing the sub-tendon sliding properties, the question of whether the age-related decline of sub-tendon non-uniformity (reviewed in Section 1.4.4) can be reproduced and whether this reduced non-uniformity results in a similar stress response across different tendon models are explored and tested.

7.1.1 Hypothesis

Hypothesis 1 - Non-uniform sub-tendon displacements are observed in simulated gait conditions (collected from *in vivo* gait analysis and ultrasonography) and the non-uniformity is more evident when assigning frictionless contacts than frictional contacts between sub-tendons.

Hypothesis 2 - The stress within the tendon shows a general decreasing trend when changing from frictionless to frictional contacts.

7.1.2 Objectives

- Conduct *in vivo* gait analysis and extract sub-tendon strain values from participants and approximate force for each sub-tendon morphology model to replicate this experimental strain.
- Conduct finite element analysis and assign frictionless and frictional contact properties to evaluate the displacement non-uniformity of different simulated gait patterns.
- Analyse stress intensity and distribution between frictionless and frictional contacts under the influence of different gait (varying loadings from muscles) and different morphology models.

7.2 Methods

7.2.1 Participants

This study was approved by University College London Research Ethics Committee (ref. 1487/1001). Two volunteers were informed and provided consent. Both participants had no previously diagnosed Achilles tendon injuries and no known neurological or musculoskeletal disease that may affect muscle-tendon functions. The experimental protocol and simulation procedure are summarised in Figure 7-1.

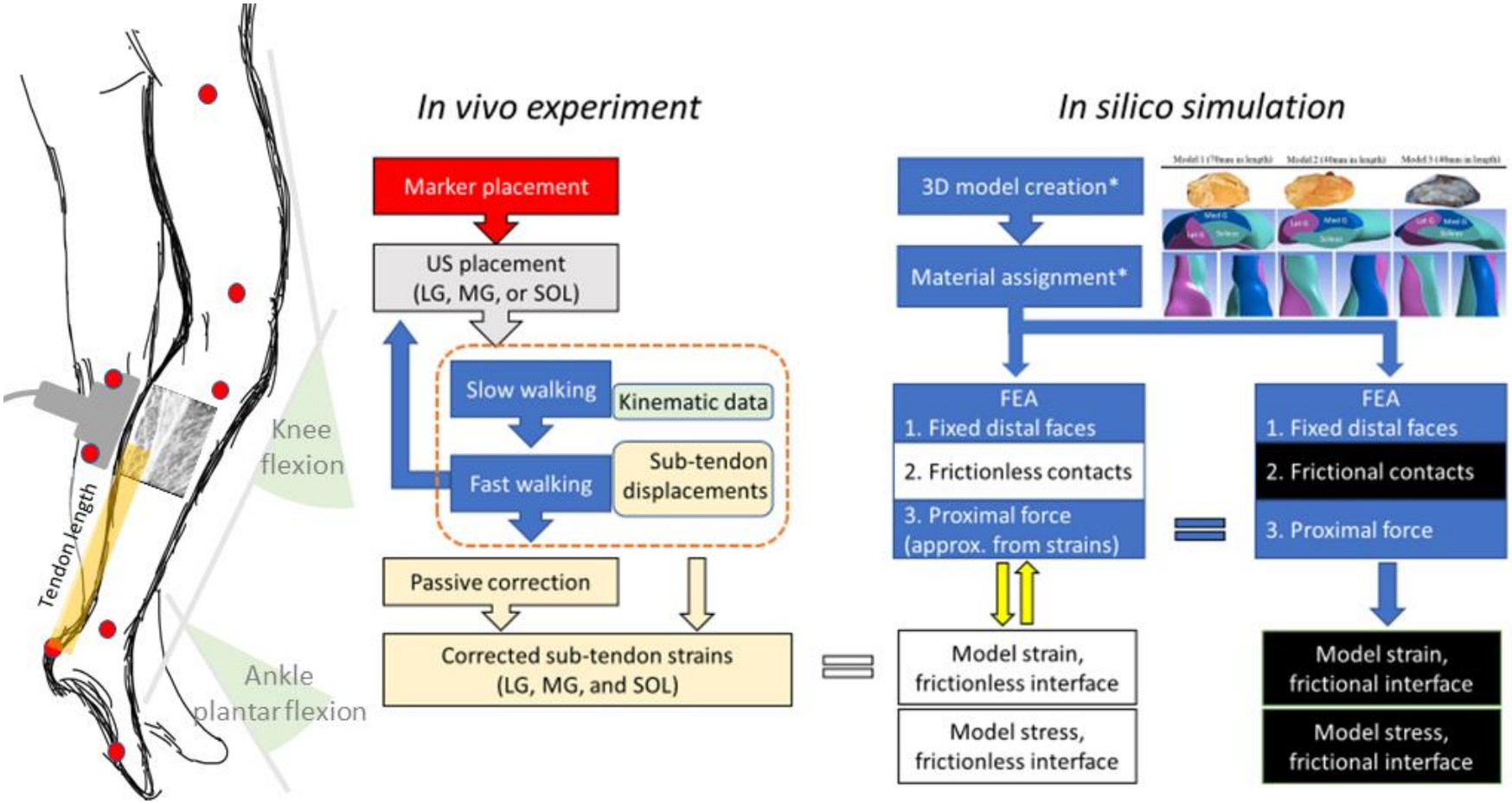

Figure 7-1. Experimental protocol combining *in vivo* experimental data and *in silico* simulations. US: ultrasound (probe), LG: lateral gastrocnemius, MG: medial gastrocnemius, SOL: soleus, FEA: finite element analysis. *: as in Section 6.2.

7.2.2 *In Vivo* Gait Analysis

Kinematic data were collected using a Gait Real-time Analysis Interactive Lab (GRAIL, Motek Medical, UK) featuring an instrumented treadmill and 10 Vicon cameras for motion capture. A set of reflective markers (n = 6) were placed on participants' right lower limb to capture sagittal plane joint kinematics. Knee flexion degree was calculated by the angle between thigh markers (on femur greater trochanter and lateral epicondyle) and lower leg markers (on the fibular head and lateral malleolus). Ankle plantar flexion and dorsiflexion was calculated by the angle between lower leg markers and the foot markers (on the calcaneus and the 5th metatarsal base). This simplified setup measures only sagittal plane movements and assumes joint axes remain stationary during movements. After marker placement, an ultrasound probe (9L-D, LOGIQ S8, GE Healthcare) was attached at the musculotendinous junctions for measuring tendon displacements (Figure 7-1, *left, grey*).

Participants were then asked to walk comfortably on the treadmill for approximately 3 minutes for each speed (slow: 0.8 m/s, fast: 1.0 m/s). During walking, the ground reaction force, collected from the integrated instrumented treadmill, marker movements and ultrasound images were collected and synchronised, by movement cues with the additional two markers on a switch. Only the kinematic data and tendon displacement during the stance phase were analysed. Kinematic data and the ultrasound measured musculotendinous displacements of five consecutive gait cycles were averaged.

From the kinematic data, five different stance phase gait features (foot-flat, contralateral toe-off, midstance, heel-off, toe-off (Akalan and Angin, 2020)) were identified by both knee and ankle joint kinematics and ground reaction force, and the corresponding tendon strains were extracted and assigned to five standardised time points (10%, 25%, 50%, 75%, 100%) of stance phase. These strain values were matched in the FEA (see below).

7.2.3 Ultrasound Measurement of Raw Tendon Displacements

The ultrasound probe was attached using an elastic bandage and a custom-made probe holder, made from a cut-through circular plastic container (approximately 10 cm in diameter and 4 cm in depth) which hosts the probe, on the musculotendinous junction of each muscle (gastrocnemii, on the straight line between the calcaneus and medial/lateral knee epicondyle, or soleus, on the straight line between calcaneus and posterior knee) with a randomised sequence. Two additional reflective markers were placed at the superior and inferior border of the probe and any relative sagittal plane movement between the probe markers and lower leg markers were offline corrected to reduce artefacts. The instantaneous tendon length is calculated by combining the length between the calcaneus marker and the inferior probe marker and the pixel distance between the border and the tendon junction measured from the 2-D ultrasound image, assuming a straight line (Figure 7-1, *left, orange bar*).

All the kinematic data and ultrasound images were analysed using an in-house MATLAB (R2019a, MathWorks, US) code utilising the computer-vision

toolbox to semi-automatically track musculotendinous junction movements (as in Section 6.2.4).

7.2.4 Passive Tendon Length Correction

After completion of the walking trials, participants were asked to lie prone on an examination bed for passive tendon length corrections. The ultrasound probe was first fixed on the gastrocnemii musculotendinous junctions with the knee fully extended and the ankle at 90°. To obtain the relationship between tendon length and joint angle, the knee was passively flexed to 45°, measured by a goniometer, and at the same time, tendon length change was recorded from the ultrasound. Then, passive ankle movements (from 0° to 25° plantar flexion and from 0° to 10° dorsiflexion) were performed and tendon length change was recorded under two different (0° and 45° of flexion) knee angles. These values were interpolated to estimate the pure tendon length and joint angle relationship without the influence of muscle contraction. This passive tendon length was subtracted from the active tendon length (walking trials with muscular involvements) and normalised to the assumed resting length (prone, knee extended and ankle 90°, measured by a tape ruler under ultrasound guide) to calculate sub-tendon strain induced by muscle contraction. Tendon lengths were assumed as straight lines due to the limited availability of ultrasonography apparatus, and the technical difficulties to measure skin and subcutaneous tissue thickness during walking trials.

Equation 7-1. Equation used for calculating tendon strain

$$Tendon\ strain\ = \frac{(active\ junction\ displacement, walking\ trials - passive\ junction\ displacement, correction\ trials)}{resting\ tendon\ length, correction\ trials}$$

Discrete knee angles were selected for estimation due to the relatively low knee flexion range of motion during the stance phase and the change of gastrocnemii tendon lengths was less sensitive to the knee than the ankle position. The soleus tendon length and joint angle relationship was obtained using passive ankle movements only (with the knee fully extended).

7.2.5 Finite Element Analysis

The detailed computer model construction process was as described previously (Section 6.2.1) In short, three Achilles sub-tendon models were created from the dissection of three specimens. A commercially available FEA software (ANSYS v19.0, Ansys Inc, US) was used for generating mesh and performing static stress analysis. Sub-tendons were modelled as hyperelastic, neo-Hookean materials (Handsfield et al., 2017, Hansen et al., 2017) with material properties obtained from curve-fitting *in vitro* mechanical testing results. Sub-tendons were meshed into quadratic 10-node tetrahedral solid elements. Mesh convergence tests were conducted for all three models. The contact faces between sub-tendon pairs were manually selected and assigned frictionless or frictional (coefficient = 1.0) contacts. Sets of translational joints were also applied for preventing transverse plane separation of sub-tendons during simulation.

7.2.6 Boundary Conditions

Fixed displacement (mimicking fixed calcaneus insertion) was applied to the three distal faces. Proximal force (mimicking muscular contraction) exerted on each sub-tendon was approximated by 5 N increments until the strain was achieved within 5% of the measured sub-tendon strain (Equation 7-1) under frictionless interface (Figure 7-1, *right*, *white boxes*). The approximated forces for the sub-tendons were then re-applied on the models but with frictional interfaces (Figure 7-1, *right*, *black boxes*) to compare the response with the results derived from assigning a frictionless interface.

7.3 Results

7.3.1 *In Vivo* Gait Analysis and Tendon Strains

During the stance phase, the knee joint moved through a range of 6° to 33° of flexion and the ankle joint from 11° dorsiflexion to 24° plantar flexion. The range of motion increased at the faster walking speed for both knee (averaged increase: 23%) and ankle (averaged increase: 30%) joints and ranges were similar for both participants. Peak ground reaction force increased on average 6% at the fast speed (Figure 7-2).

Passive measurement of the musculotendinous junction displacements during correction trials is summarised in Table 7-1. For both participants, changing knee flexion angle from 0° to 45° has minimal influence on the displacement of gastrocnemii tendons when the ankle is dorsiflexed (plantar flexion -10°). Ankle dorsiflexion produced distal displacements of all the three

measured musculotendinous junctions while ankle plantar flexion produced proximal and higher displacement values. The relative displacement to the tendon resting length of three tendons is summarised in Table 7-2. For both participants, soleus demonstrated the highest relative displacements during passive correction trials.

Based on the corrected musculotendinous junction displacements, walking at a faster speed showed an overall increment in strain compared to slower walking for both participants (Figure 7-3). Participant 1 showed greater tendon strains at both speeds compared to Participant 2 despite having similar joint kinematics. The soleus sub-tendon reached the greatest strain in both slow and fast speed although the strain of the soleus sub-tendon was not always the highest in every phase of stance. In Participant 1, the extra push-off force required for fast walking was predominately achieved by increasing both gastrocnemii strains, while Participant 2 responded to faster speed by increasing both soleus and medial gastrocnemius sub-tendon strains. The lateral gastrocnemius was usually the least strained sub-tendon (Figure 7-3, *black lines*). The strain data was selected from 5 normalised time points (10%, 25%, 50%, 75%, and 100%) to represent different gait features (foot-flat, contralateral toe-off, midstance, heel-off, toe-off) to reduce the FEA computational cost while, at the same time, preserving sufficient information to describe different features during the stance phase.

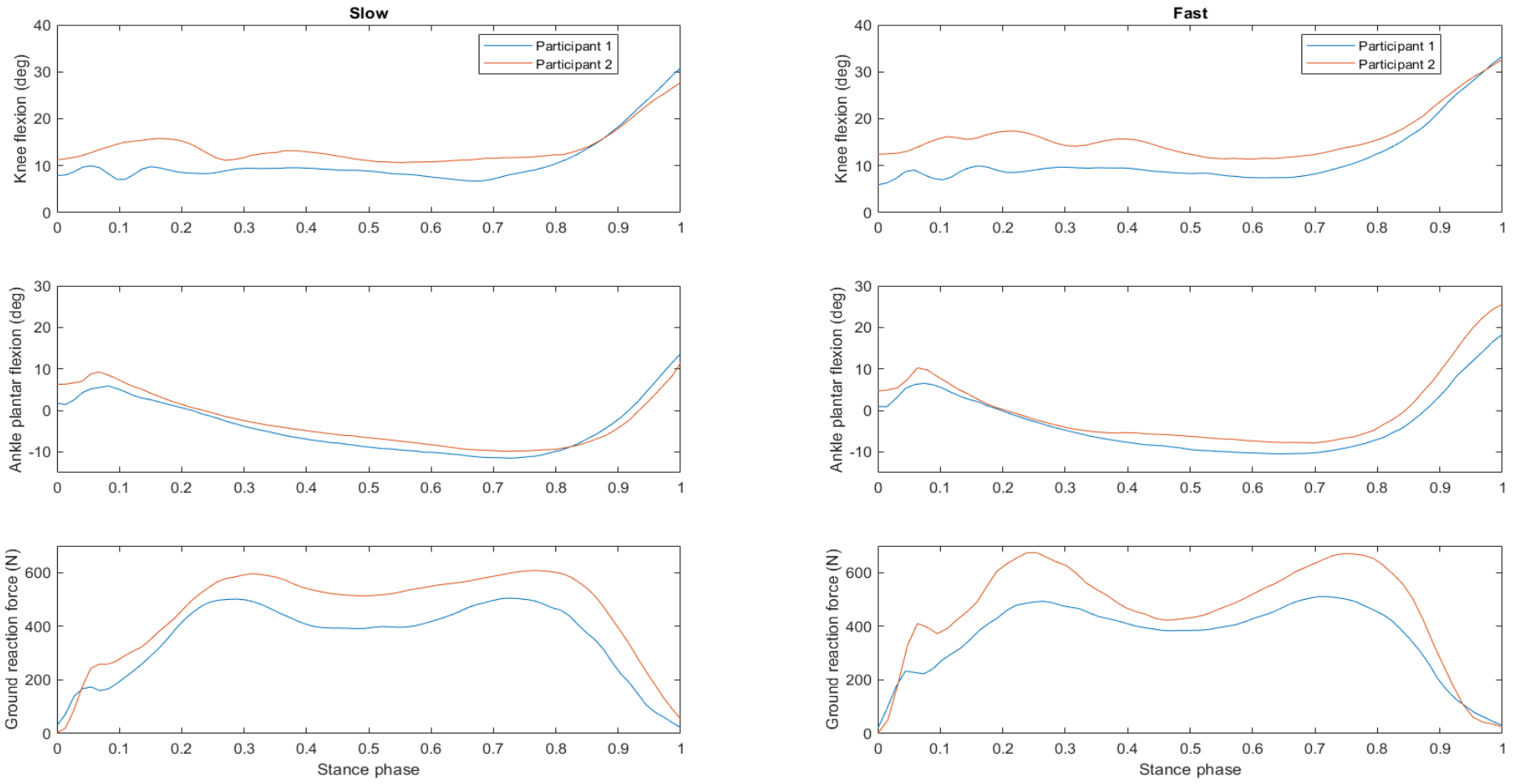

Figure 7-2. Sagittal plane knee (upper row) and ankle (middle row) joint kinematics and the ground reaction force (lower row) of both participants and different walking speeds

Table 7-1. Passive musculotendinous junction displacement (in mm) in relation to different knee and ankle range of motion. Positive values represent proximal displacements.

		Lateral G.		Medial G.		Soleus
		Knee flexion		Knee flexion		
		0°	45°	0°	45°	
Participant 1						
Ankle	-10°	-2.8	-5.0	-1.5	-2.0	-7.0
plantar flexion	25°	4.1	6.9	7.0	16.8	15.5
Participant 2						
Ankle	-10°	-2.1	-3.3	-5.4	-5.0	-4.4
plantar flexion	25°	13.8	9.2	8.2	14.6	7.2

Displacements were normalised to the length at knee flexion 0° and ankle plantar flexion 0°.

Table 7-2. Minimal and maximal relative displacements (to the resting length) of three musculotendinous junctions during passive correction trials

	Lateral G.		Medial G.		Soleus	
	Min	Max	Min	Max	Min	Max
Participant 1	1.8%	4.5%	0.9%	10.3%	4.9%	10.8%
Participant 2	0.9%	5.9%	2.3%	6.6%	3.9%	13.0%

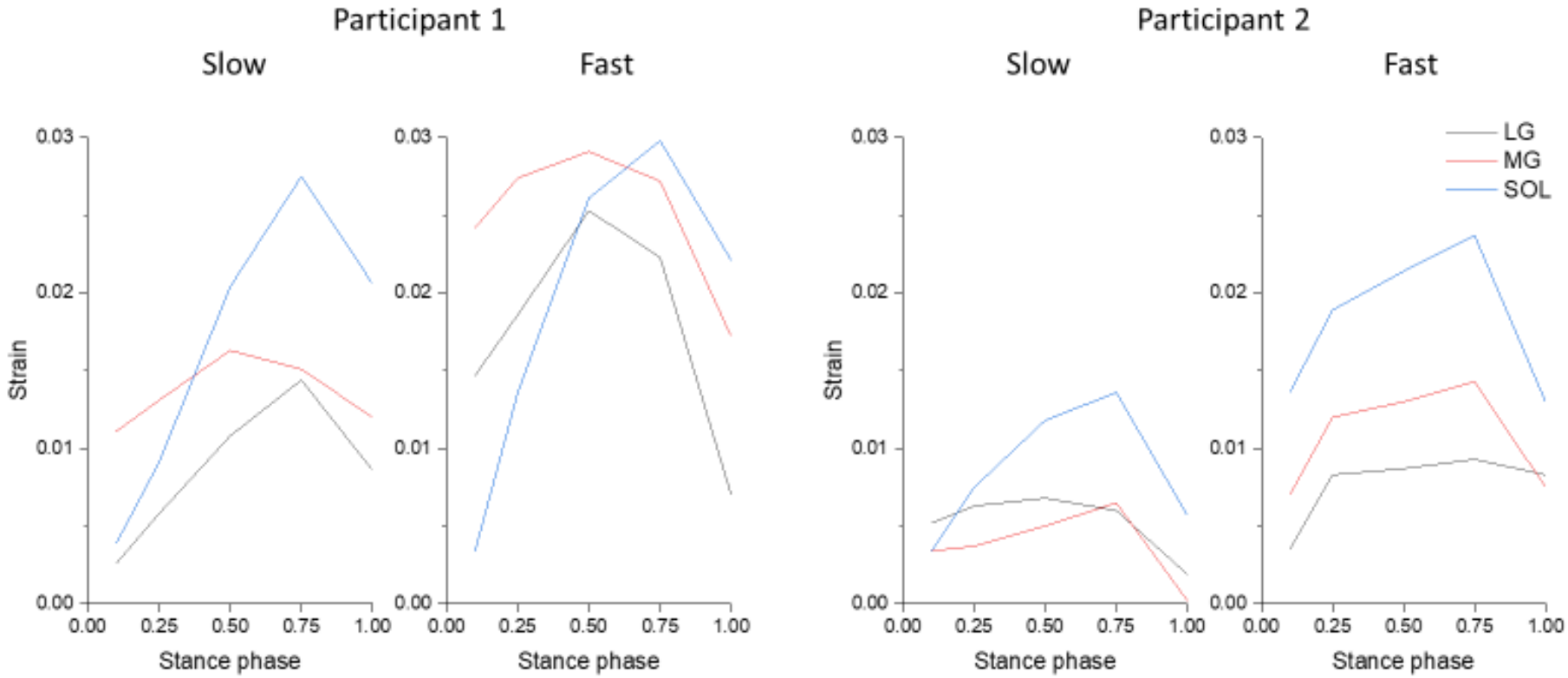

Figure 7-3. Measured musculotendinous junction strains of each muscle at different walking speeds of both participants. LG: lateral gastrocnemius, MG: medial gastrocnemius, SOL: soleus.

7.3.2 Modelling Sub-tendon Behaviour Using Experimental Strains

The maximal approximated force for each sub-tendon under different models and gaits is summarised in Table 7-3. Walking at a faster speed required a higher force to match the increased tendon strains than walking at a slower speed. A large variation in simulated forces was observed between three different tendon models, likely resulting from the different CSA of each model (Model 1: 89.1 mm^2, Model 2: 90.4 mm^2, Model 3: 42.3 mm^2). The strains obtained from simulations under the frictionless contact condition closely matched the experimental strain for all three models (Figure 7-4).

Table 7-3. Maximal simulated sub-tendon force (N) for approximation

	Model 1			Model 2			Model 3		
	LG	MG	Sol	LG	MG	Sol	LG	MG	Sol
Participant 1									
Slow	220	70	550	200	110	640	10	100	250
Fast	480	300	480	330	350	580	60	205	240
Participant 2									
Slow	60	50	300	40	100	260	10	30	125
Fast	110	110	500	70	180	520	5	65	230

LG: lateral gastrocnemius. MG: medial gastrocnemius. Sol: soleus.

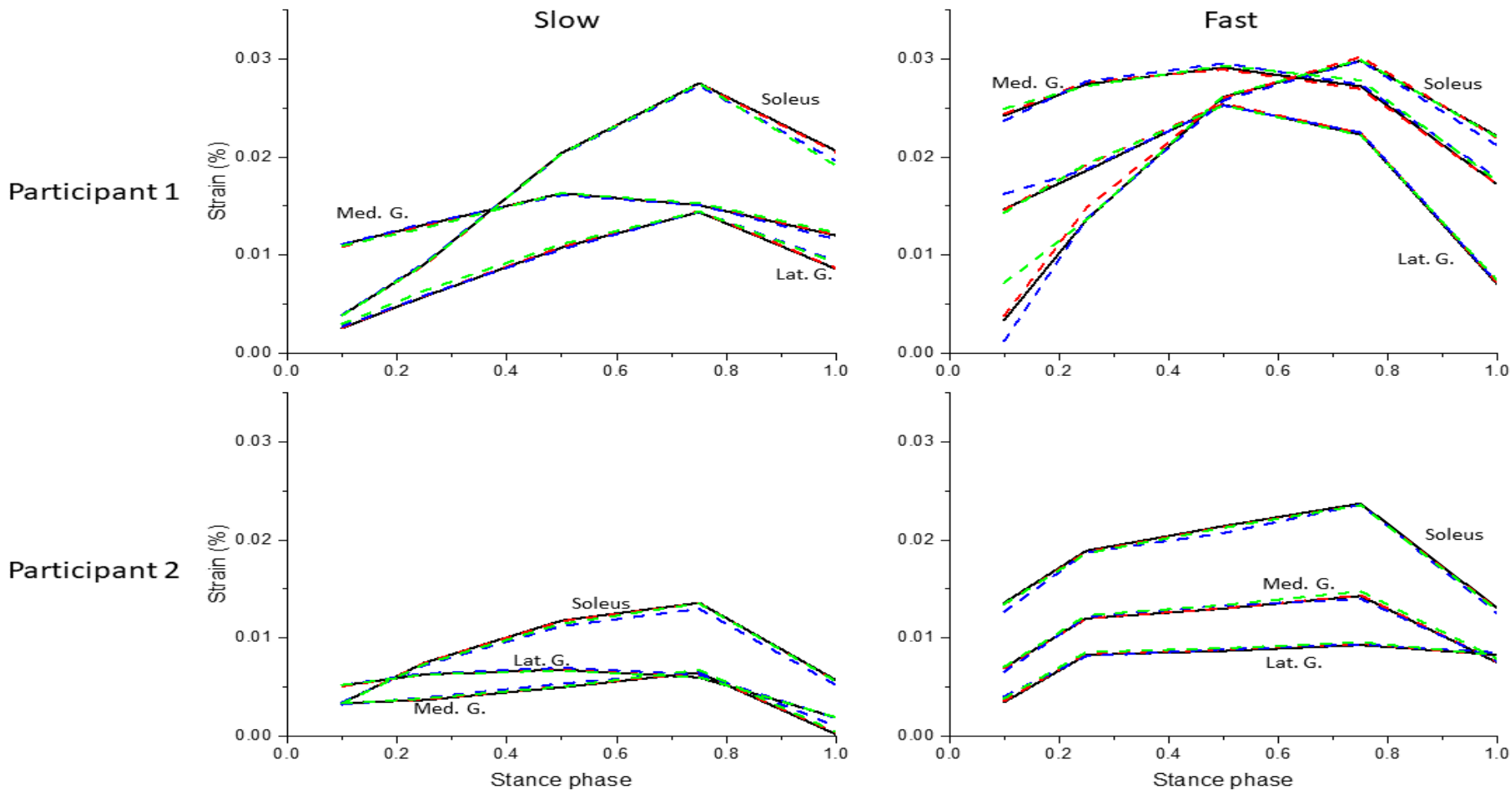

Figure 7-4. Experimental strains *(black solid lines)* and simulated strains of three different models under different gaits. Red dash lines: Model 1, blue dash lines: Model 2, green dash lines: Model 3.

Changing from frictionless to frictional contacts reduced Achilles sub-tendon displacement non-uniformity for both participants regardless of speed (Figures 7-5 to 7-8). For both participants, strains of soleus sub-tendon decreased when changing from a frictionless to a frictional interface (averaged reduction for each model: 4.2%, 9.4%, and 7.4% respectively) while strains of lateral gastrocnemius sub-tendons increased (5.5%, 7.3%, and 7.2% respectively). The change of medial gastrocnemius strain when changing the interface property was more dependent on the relative strain level of the other two sub-tendons. In Participant 1, the medial gastrocnemius strain increased at slow speed, for its strain was low and similar to the lateral gastrocnemius (Figure 7-5); but decreased at the fast speed, for its strain was high and similar to the soleus (Figure 7-6). In Participant 2, the medial gastrocnemius strain increased at slow speed (Figure 7-7) but remained stationary at fast speed since its strain was approximately the average of lateral gastrocnemius and soleus in fast walking (Figure 7-8).

Assigning a frictional contact also reduced temporal differences in strain for all sub-tendons. In slow walking, the strain of medial gastrocnemius peaked at 50% (midstance phase) while the other two sub-tendons peaked at 75% (heel-off) of the stance phase for Participant 1 (Figure 7-5). Changing to a frictional interface caused a temporal shift in peak medial gastrocnemius strain to heel-off in Models 2 and 3 (Figure 7-5, *middle and right, red dash lines*). Similarly, in fast walking, high soleus strain developed in the earlier stance phase but slightly decreased in later stages of stance in the frictional interface (Figure 7-6, *middle and right, blue dash lines*), synchronous to the gastrocnemii peaks (at 50% of stance phase).

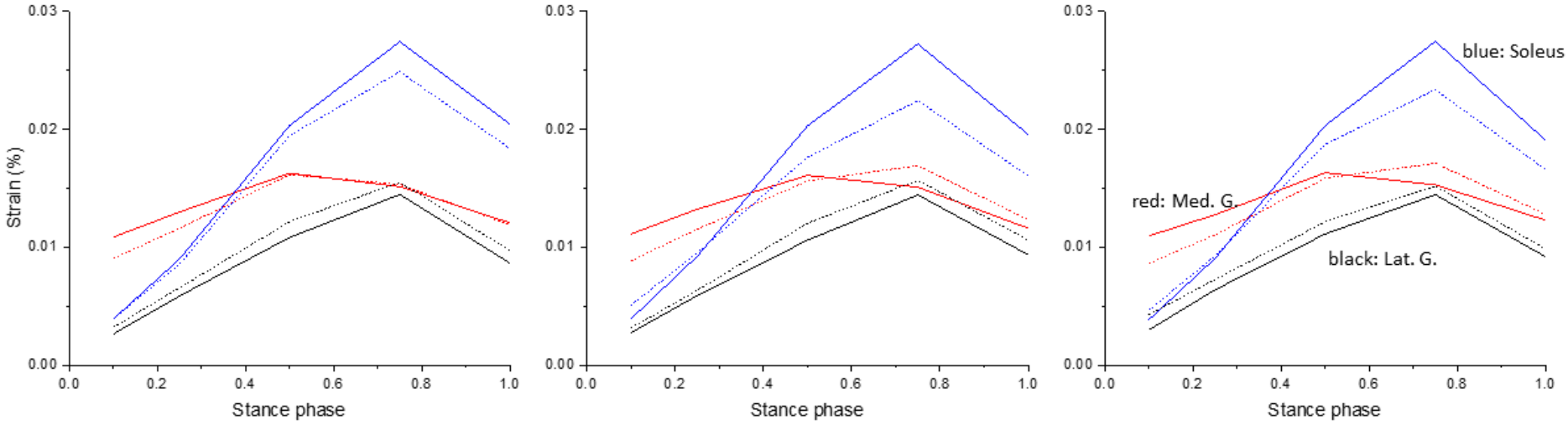

Figure 7-5. Simulated sub-tendon strains when matching the experimental strains of Participant 1 during slow walking (Figure 7-3, *left*). Reduced displacement non-uniformity is observable for all three models (Model 1: *left*, Model 2: *middle*, Model 3: *right*) when shifting from the frictionless (solid lines) to the frictional interface (dash lines).

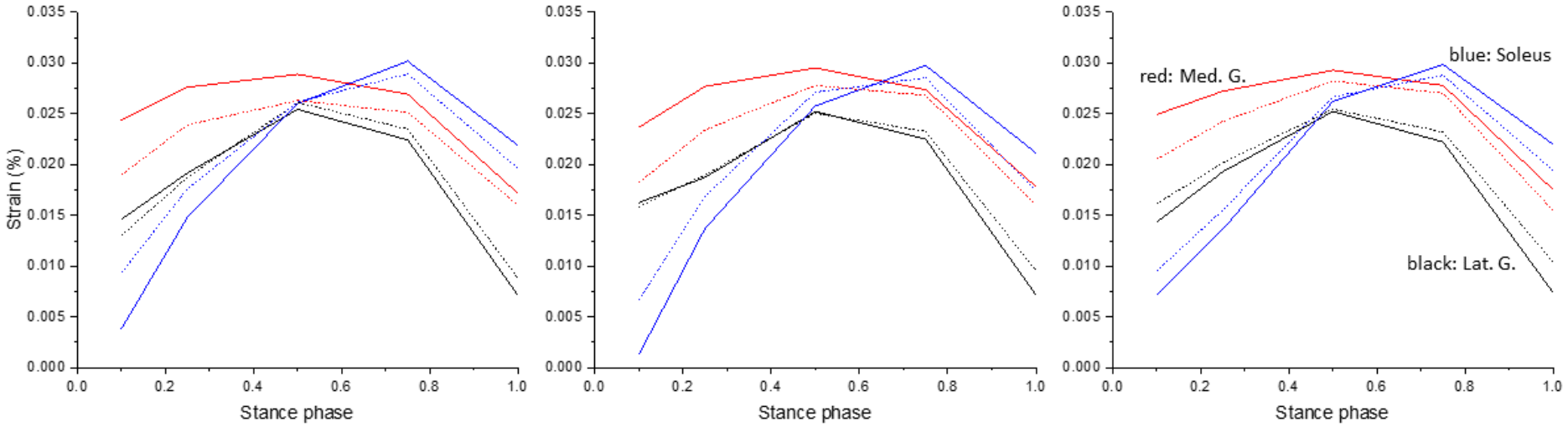

Figure 7-6. Simulated sub-tendon strains when matching the experimental strains of Participant 1 during fast walking (Figure 7-3, *left*). Reduced displacement non-uniformity is observable for all three models (Model 1: *left*, Model 2: *middle*, Model 3: *right*) when shifting from the frictionless (solid lines) to the frictional interface (dash lines).

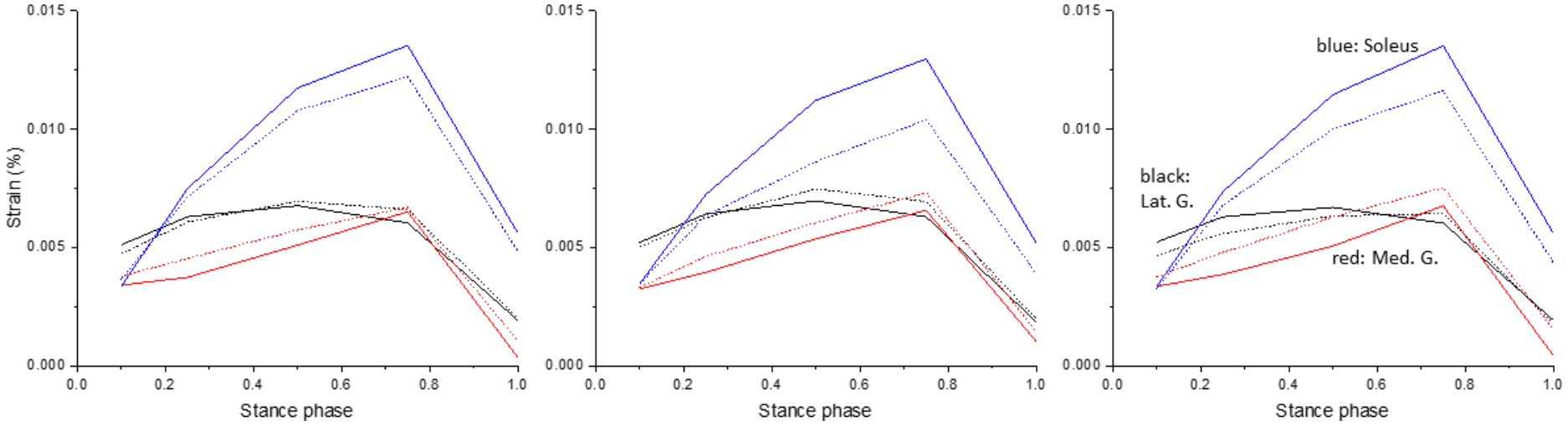

Figure 7-7. Simulated sub-tendon strains when matching the experimental strains of Participant 2 during slow walking (Figure 7-3, *right*). Reduced displacement non-uniformity is observable for all three models (Model 1: *left*, Model 2: *middle*, Model 3: *right*) when shifting from the frictionless (solid lines) to the frictional interface (dash lines).

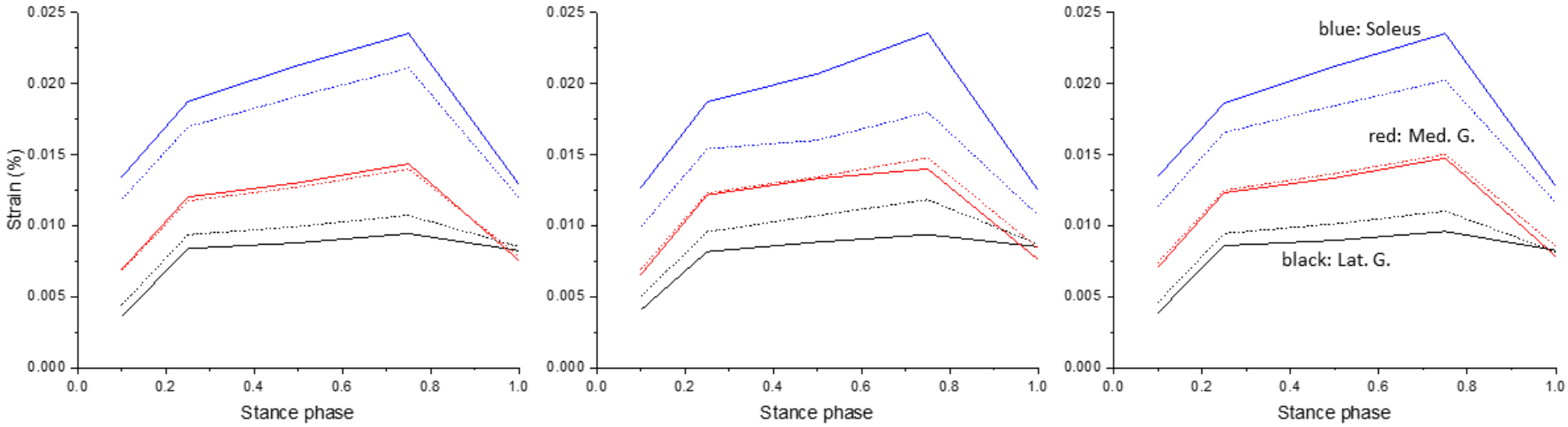

Figure 7-8. Simulated sub-tendon strains when matching the experimental strains of Participant 2 during fast walking (Figure 7-3, *right*). Reduced displacement non-uniformity is observable for all three models (Model 1: *left*, Model 2: *middle*, Model 3: *right*) when shifting from the frictionless (solid lines) to the frictional interface (dash lines).

Stress during heel-off, the time when peak stress develops, showed influences from both gait pattern and tendon model geometry. Compared to slow walking, a faster pace imposed higher stress on the tendon (Table 7-4). However, peak stress varied greatly under different simulation conditions. Increasing friction in Models 2 and 3, generally showed a decrease in peak stress while in Model 1, a slight increase in peak stress, regardless of gait.

Table 7-4. Peak von Mises stress (MPa) of different simulated conditions

		Participant 1		Participant 2	
		Slow	Fast	Slow	Fast
Model 1	Frictionless	23.4	31.2	12.0	20.8
	Frictional	24.6	32.4	12.0	22.5
Model 2	Frictionless	38.3	48.6	18.3	32.1
	Frictional	27.5	42.2	15.9	27.4
Model 3	Frictionless	21.0	26.6	11.1	19.5
	Frictional	20.8	24.6	10.9	19.2

The region where peak stress develops also showed a large variation between different gaits, speed, interface properties, and model geometry (Figure 7-9). Of all the constructed models, Model 2 was the most stable in terms of peak stress location (Figure 7-9) when changing gait pattern and interface property. The high-stress region of Model 1 was generally in the proximal one-third of the tendon, but the exact location varied from the intra-tendinous region to the periphery and from the soleus to the lateral gastrocnemius sub-tendon depending on the simulated condition.

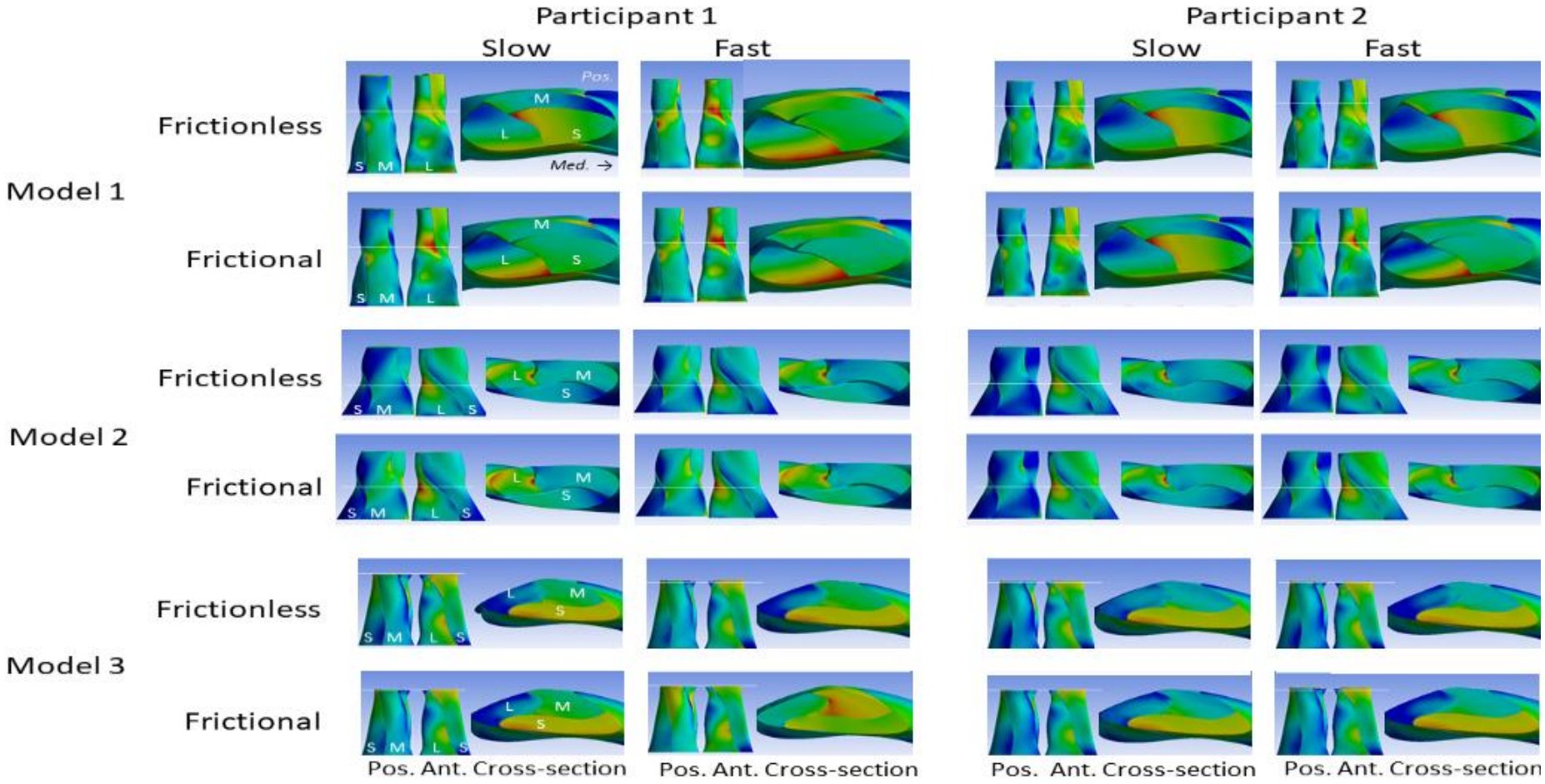

Figure 7-9. Peak von Mises stress location during heel-off under different simulated conditions for three Models. Cross-sections represent the superior view at the level of the white line. M: medial gastrocnemius. L: lateral gastrocnemius. S: soleus sub-tendon

7.4 Discussion

The results show that increasing inter-sub-tendon friction alters the displacement and stress responses of the Achilles tendon. Assigning frictional interfaces resulted in a more uniformed sub-tendon displacement compared to frictionless interfaces under all simulated conditions. Interestingly, the stress response was far more complex and varied greatly between different gaits and geometries. The peak stress, a relevant indicator for tissue integrity and the potential site to develop injury in the future, increased in a certain combination of gait and tendon geometry. This phenomenon suggests that the complex force interaction within the Achilles tendon could be different among individuals with different tendon shapes and sub-tendon sliding ability, resulting in different mechanical behaviour.

Using the strain measurements obtained *in vivo*, the modelled sub-tendon displacements are comparable to previous reports on Achilles tendon non-uniformity during walking. Franz and colleagues (Franz et al., 2015, Franz and Thelen, 2015) demonstrated that the deep region of the Achilles tendon (most likely soleus) displaced more than the superficial region during the stance phase, and this regional difference was reduced in aged tendons (mean 69.9 years). The non-uniformity was more evident when walking at a faster speed than at the slow speed, and was negatively correlated with muscular performance, which commonly decreases as age advances. Later studies using modelling techniques have demonstrated that reduced sliding between sub-tendons resulted in displacement uniformity of the Achilles tendon (Franz and Thelen, 2016, Handsfield et al., 2017). As it is demonstrated here and in the previous chapter by incorporating frictional

interfaces, without modifying force or mechanical properties of sub-tendons, both the tendon and sub-tendon level mechanics exhibit great differences between friction and frictionless interface conditions, suggesting a potential age-related change in the Achilles tendon mechanical behaviour. While a more homogenous displacement may at first appear beneficial, this potentially disrupts the temporal difference (as seen in Participant 1, Figures 7-5 and 7-6) between gastrocnemii and soleus muscle activation. Soleus activation was reported more biased toward vertical weight and gastrocnemii more related to horizontal speed (Miyoshi et al., 2006). Handsfield and colleagues (2020) demonstrated that the simulated (frictionless interface) gastrocnemii and soleus sub-tendon displacement non-uniformity differs in movements with different knee and ankle range of motion. Having a stiff, non-sliding interface between sub-tendons could inhibit this fine-tuning between gastrocnemii and soleus activation timing (Konig et al., 2018) and potentially lead to an inferior tendon function, commonly seen in aged and injured populations.

Although sub-tendon displacements showed a predictable response as sliding decreased, the stress developed in the Achilles tendon varies between different gaits and geometry models. Mean stress level across the Achilles tendon decreases when shifting from frictionless to the frictional interface, as demonstrated previously (Section 6.3.3), suggesting the improved force transmitting capacity through the interface can result in decreased tendon stress as proposed (Maas and Finni, 2018). Interestingly, shifting from frictionless to frictional contacts does not result in a uniform decrease in the peak stress, and the region where peak stress develops also

varied between different models and different gait patterns. In the tested three models, the peak stress intensity in Model 2 was consistently lower when shifting from frictionless to the frictional interface, across different gaits and speeds. It can be hypothesised that people having similar tendon geometry as Model 2 may have a lower age-related, but potentially less movement-specific, risk of developing tendon injuries in the future. The intensity and region where peak stress occurred are more variable in the other two models, and due to the large variation in geometry between all three models, it is not able to draw a firm conclusion from these results. However, the actual geometry and morphology variation between individual Achilles tendon is likely even greater than these three models (Edama et al., 2015a, Edama et al., 2016, Pękala et al., 2017). These results suggest that the Achilles tendon would be best studied in a personalised, individual-based approach which includes delineating detailed internal sub-tendon geometry, measuring the sliding ability between sub-tendons, and monitoring task- or exercise-specific movement patterns to fully characterise the mechanical behaviour of the Achilles tendon.

Combining motion analysis and ultrasonography is one of the most common approaches for studying *in vivo* tendon mechanical behaviour during activities, and can be easily combined with other advanced methods, such as speckle tracking or shear-wave elastography, to obtain more detailed information on internal tendon strains or mechanical properties. This simplified setup, which only measured the sagittal plane joint kinematics, is non-ideal due to the non-negligible rotational moment at both knee and ankle joints during walking. It is worth noting that the ultrasound probe could also

rotate during walking and can induce error since the measurement of tendon length requires the combination of the inter-marker distance (between the probe and calcaneus), assuming a straight line, and the musculotendinous junction displacement under ultrasound images. Future studies should ideally apply a full set of motion analysis markers that completely captures the lower limb joint kinematics and perform trials quantifying the probe movements and calibrating accordingly.

Due to the limited viewing window of the ultrasound images, it is possible that the measured proximal gastrocnemii junction strains were not proportional to the more distal gastrocnemii sub-tendon strains (Magnusson et al., 2003). It has been reported that gastrocnemii tendons and the soleus aponeurosis, despite lying abreast, exhibit a small degree of relative movement when changing joint angles (Bojsen-Moller et al., 2004, Bojsen-Moller et al., 2010, Tian et al., 2012). The soleus aponeurosis itself also demonstrated a unique and non-uniform mechanical response during muscle contractions (Finni et al., 2003a, Finni et al., 2003b). The passive tendon length correction used in this study for different joint angles reduced the measured raw strain values, and the corrected strains were similar to previous reports on tendon strains during walking (Ishikawa et al., 2005, Lichtwark et al., 2007, Kharazi et al., 2021). However, it is well-known that a small degree of joint rotation, induced by transverse plane movement due to the ankle inversion or eversion by the individual intermalleolar and subtalar joint axis, can result in a large error when measuring *in vivo* tendon lengths (Magnusson et al., 2001, Muramatsu et al., 2001, Maganaris and Paul, 2002, Maas et al., 2020). Performing the correction trials in prone position could

also change the overall muscle-tendon unit tension and, since the slack length could be different between gastrocnemii and soleus muscle-tendon unit at different ankle degrees (Hug et al., 2013), the correction trail could induce additional measurement error. Future studies incorporating a detailed *in vivo* ankle range of motion and sub-tendon length relationship (as in (Wang et al., 2021)) during active movements may reduce the potential measurement error and derive more accurate tendon strain values. More importantly, the exact Achilles tendon length should be quantified under imaging to minimise the error induced by the skin and the sub-cutaneous tissues. One method to reduce this measurement error is by attaching reflective markers on the skin between the ultrasound probe and calcaneus, to represent the curvature of the tendon (Kharazi et al., 2021).

As a proof-of-concept study, the sub-tendon strain was used as the input for the FEA models to inform force input since tendon length is one of the most easily measurable variables. Using force, either obtained from inverse dynamics or estimated from electromyography (EMG) requires more assumptions and more comprehensive measurement of the muscle-tendon related properties of the participant, such as muscle physiological cross-sectional areas and ankle joint moment arm. These measurements are usually made under static conditions, which could be inaccurate when the movement of interest combines both rapid concentric and eccentric muscular contractions and occurs across large joint motion ranges (Konrad, 2005). However, using muscular force as direct input reduces the need to approximate forces from sub-tendon strains and may reduce the aforementioned measurement errors. In complex geometry, assigning

displacement constraints on FEA could result in simulation errors and approximating force to match the experimental strain or displacement is a commonly accepted approach (as in (Handsfield et al., 2017)). Static stress analysis at discrete time points was conducted for simplification and reduction of computational cost. Future research however could further improve this model by obtaining *in vivo* mechanical properties of each sub-tendon and conducting time-dependent simulations for a detailed characterisation of the Achilles tendon mechanical response in each individual under specific movements.

Understanding the properties of the inter-sub-tendon matrix between Achilles sub-tendons is important for translating anatomical knowledge to clinical applications. Future research combining experimental and modelling approaches would allow feedback calculation of the interface properties (by varying the friction coefficient) to match the measured sub-tendon displacements, or feed-forward of interface properties (approximated by static muscle stimulations (Section 6.3.4) or passive ankle movements (Slane and Thelen, 2015)) to estimate tendon displacement. Conducting FEA using measured individual-specific variables allows quantification and visualisation of the Achilles tendon stress response under different loading conditions and could enable clinicians and researchers to accurately investigate sport-specific (Handsfield et al., 2020) or age-related tendon mechanical behaviour, which is currently challenging to study. Improvement of the resolution of common clinical imaging modalities, such as ultrasonography or MRI (Szaro et al., 2020), to delineate internal sub-tendon borders would allow the construction of sub-tendon geometry models accordingly. With the

help of FEA and the advancement of real-time monitoring, clinicians may be able to predict or even prevent debilitating tendon injuries from developing in the near future (as concepted in (Pizzolato et al., 2020)).

7.5 Conclusion and Chapter Summary

This study demonstrates that the Achilles tendon mechanical behaviour can be affected by a combination of factors including the properties of the interface between sub-tendons, individual tendon morphology, and different gait patterns. Decreased Achilles tendon displacement non-uniformity, as in aged or injured tendons, could result in different tendon stress levels depending on the individual gait pattern and the inherent tendon morphology. Combining gait analysis and FEA on Achilles sub-tendon models provides a possible clinical application that enables the detection of high-stress regions within the tendon.

Chapter 8 General Discussion

In this thesis, several experimental techniques were applied to investigate the complex Achilles sub-tendon mechanical behaviour, and the results identified several factors that can affect both sub-tendon and tendon level mechanical behaviour. Further investigation of these factors in detail is crucial to fully understand Achilles tendon behaviour and could potentially improve our current management of tendinopathies.

8.1 Mechanisms Governing Sub-tendon Mechanical Behaviour

8.1.1 Influence of Tendon Morphology

One of the most important findings from these studies is that tendon morphology and geometry features can have a great influence on the tendon mechanical behaviour under load. This was demonstrated first by macroscopic mechanical testing on an equine tendon model of combined sub-tendons and then further evidence came from simulations on reconstructed human Achilles tendon models.

In Chapter 6, the FEA results demonstrated that the tendon morphology alone can result in variable strains between different configurations of sub-tendons when identical sub-tendon material properties are assigned and the same forces applied, suggesting the influence of individual morphology on the tendon mechanical behaviour under load. Changing the interface (inter-sub-tendon matrix) properties and applied force levels (to simulate the human gait pattern, Chapter 7) further identified that certain morphology

could exhibit age-related (reducing sub-tendon sliding) or movement-related (changing gait) stress fluctuation that may be related to future injury development. These results could also suggest that age-related changes in tendon mechanics may have a greater impact on some individuals than others. However, the modelling approach used in this thesis overlooked the fundamental neuromuscular control between individuals. It is currently unknown whether different neuromuscular properties exist between individuals with different tendon morphologies or sub-tendon arrangements.

In the equine tendon study (Chapter 2), two possible mechanisms were proposed to explain the relationship between tendon shape and the corresponding mechanical behaviour. Due to Poisson's effect, a flat, C-shape sub-tendon (the AL) could exhibit some compressive force under tensile load; while the other sub-tendon (the DDFT), surrounded by this C-shape sub-tendon, is more likely to reduce its CSA when tensile loaded and 'escape' this compression. This phenomenon may also result in a change in the force transmission ability between different sub-tendons. It could be possible that Achilles sub-tendons (C-shape gastrocnemii surrounding the soleus sub-tendon (Szaro et al., 2009, Edama et al., 2015a, Edama et al., 2016)) exhibit similar mechanical behaviour as the equine tendon model. My hypothesis is that force transmission from the gastrocnemii to the soleus sub-tendon is more likely to occur than vice versa. Relatively few studies have focused on the influence of inherent Achilles tendon shape on its mechanical behaviour or the association with injury and this fundamental aspect of the tendon is often overlooked. Using modelling approaches, studies have identified that individual tendon shapes and different twist arrangements can influence the

tendon material strength (Shim et al., 2014, Shim et al., 2018). Interestingly, Shim and colleagues (2014) reported that the simulated rupture load was more related to the inherent tendon geometry than the assigned tendon material property. One prospective study screened 18 elite football players at baseline and after one-year follow-up reported that tendons later developed tendinopathy symptoms were statistically thicker at the baseline than those that remain asymptomatic (Jhingan et al., 2011). One recent comparative cross-sectional study reported that, besides being thicker, pathological tendons were statistically longer than the control tendons under MRI scans (Szaro and Ghali Gataa, 2021). The authors also reported a considerable degree of variation of the Achilles tendon length (distance between soleus musculotendinous junction and calcaneus), with 12.5% of all scans demonstrating short (less than 2.54 cm) tendons and the shortest tendon identified was just 8.5 mm in length. The tendon thickness in 96 asymptomatic military recruits was found positively correlated with body height and foot size (r = 0.74). However, the correlation was not statistically significant in the control group comprised of 10 young female, and the individual variation between tendon dimensions and body measurement were high (Koivunen-Niemela and Parkkola, 1995). These results suggested that the highly variable tendon dimensions could be related to the mechanical behaviour under load and is likely different between individuals.

One profound limitation for understanding (and directly inferring from the equine tendon results) this structure-function relationship in the human Achilles tendon is its highly individualised dimensions and the twisted sub-tendon morphology. Straightening of the twisted sub-tendon structure will

induce transverse plane movements (Knaus and Blemker, 2021) and affect neighbouring sub-tendons, but quantifying the effect of untwisting *in vivo* is currently technically challenging. One potential method to identify this untwisting is to measure the whole tendon level rotation during calf contractions by utilising free-hand 3-D ultrasound (Obst et al., 2014). It would also be interesting to correlate the degree of rotation with the tendon dimensions (e.g., length, width, or cross-sectional area) to identify potential factors affecting tendon mechanical behaviour.

Other technical limitations include the limited availability of healthy tendon samples for *in vitro* testing and the inability to discern sub-tendons using current imaging modalities. At this stage, combining experimental data with computational simulation appears to be an acceptable surrogate to investigate sub-tendon mechanical behaviour. Fully characterising sub-tendon mechanical behaviours with regard to the different morphologies and sub-tendon arrangements will be a breakthrough in the field.

8.1.2 Differences in Sub-tendon Mechanical Properties

Different sub-tendon mechanical properties can affect the overall tendon mechanical behaviour. Based on the results (Chapter 3) and one recent addition to the literature (Ekiert et al., 2021), the soleus sub-tendon is more compliant than the gastrocnemii sub-tendons. This is in accordance with the *in vivo* studies (Section 1.4.4.1) demonstrating that the deep tendon region, assuming this represents the soleus sub-tendon, displaced more than the superficial region during both active and passive ankle movements, although

the deep region (anterior side) locates closer to the joint rotation axis and has a shorter moment arm.

Soleus sub-tendon had the highest CSA and demonstrated the highest failure force and stiffness value (Section 3.3.1). Therefore, it is possible that being a materially more compliant sub-tendon, the ECM of the soleus sub-tendon adapts to increase its CSA to match the external demand. The muscle mass of the soleus is larger than the sum of both gastrocnemii and can generate more than half of the ankle plantarflexion torque during walking (Dayton, 2017). This high force produced by the soleus muscle may induce selective hypertrophy of the soleus sub-tendon, similar to previous reports on patellar tendons after a unilateral side training regime (Seynnes et al., 2009) and in dominant legs among athletes participating in sports with different limb loading patterns (Couppe et al., 2008). Having a higher CSA could also reduce the soleus sub-tendon displacement and potentially lower the displacement discrepancy between soleus and gastrocnemii sub-tendons, preventing traumatic longitudinal tear (Chan et al., 2017) and the separation of sub-tendons. Most of the reported *in vivo* results of the peak Achilles tendon displacement non-uniformity is approximately 1 to 2 mm between superficial and deep regions, and as previously (Section 2.4) discussed, excessively high shear could be detrimental and is considered a risk factor for developing tendinopathy. These findings imply that an optimal degree of sub-tendon displacement non-uniformity exists and tendon matrices, either between or within sub-tendons, may actively adapt to achieve this optimal non-uniformity.

Mechanical property differences can result from different matrix compositions between sub-tendons. Compositional adaptation is likely to present in the equine AL-DDFT where the joined region demonstrated significantly different water, GAG, and DNA content than the more proximal and distal regions (Section 2.3.1). Similarly, the findings from Chapter 3 demonstrated that cellularity and proteoglycan levels could be different between human Achilles sub-tendons, despite having limited specimens for testing. Future studies investigating the detailed Achilles sub-tendon composition with larger sample size and a wide range of ages are warranted. It is interesting that although Raman spectroscopy demonstrated largely similar spectral features between sub-tendons (as for conventional biochemical assays), Raman spectroscopy can differentiate between isolated sub-tendons within an individual. The major spectral differences implied variation may exist in the total protein content or the collagen secondary structure (Section 5.4.3). Future studies characterising the biochemical composition and the corresponding Raman spectra between sub-tendons may be a potential way to allow quantification of sub-tendon level composition clinically in the future.

Our findings of the fascicle level mechanical properties may affect the sub-tendon and tendon level mechanical behaviour. In the equine tendons, the fascicle level mechanics were different between the AL and the DDFT (Section 2.3.3). Despite the small sample size, the inter-sub-tendon matrix appeared to be more compliant than the AL and the DDFT IFM. It was not possible to accrue enough human samples to conduct fascicle level mechanical testing, but pilot data from one specimen (Figure 8-1) were

collected using an identical method as the equine fascicle testing, suggesting the feasibility of conducting macroscopic fascicle level mechanical testing on Achilles sub-tendons.

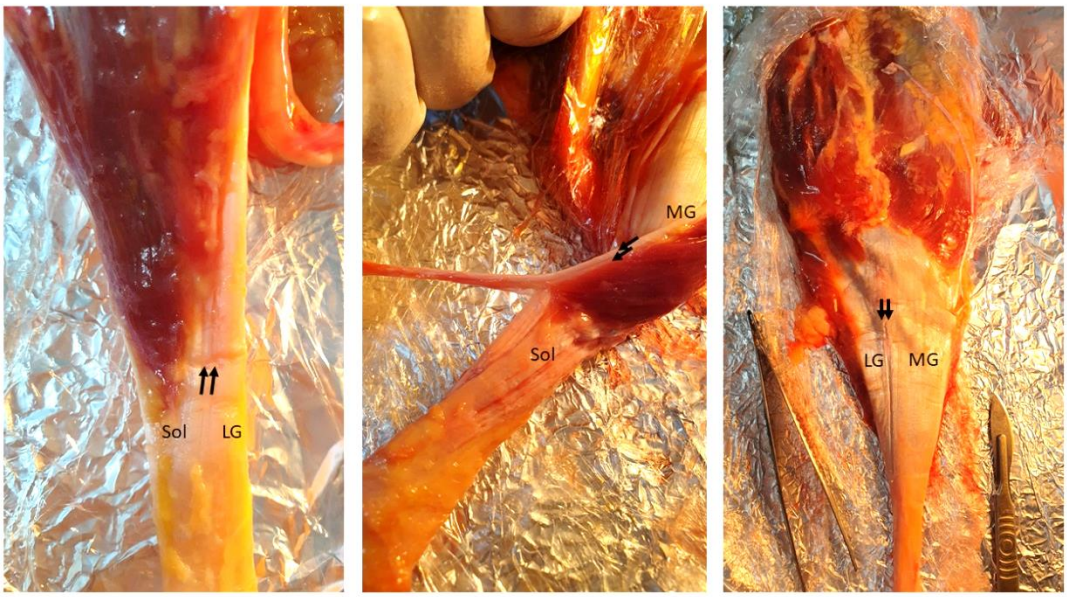

Figure 8-1. Isolation of inter-sub-tendon matrix in one specimen by identifying adjacent fascicles from different sub-tendons. LG: lateral gastrocnemius. MG: medial gastrocnemius.

Due to the twisted sub-tendon structure, the fascicles at the sub-tendon border may contact more than one fascicle from the other sub-tendon and may rotate and slide through multiple fascicles when loaded. This twisted structure is more complicated than our proposed equine AL and DDFT model, which is composed of relatively parallel fascicles, and thus greatly increases the complexity of studying *in vivo* fascicle mechanics. However full characterisation of the fascicle level mechanical behaviour will greatly improve our understanding of the Achilles tendon.

8.1.3 Age-related Reduction in Sub-tendon Sliding

The modelling and *in vivo* data suggest that the age-related reduction in displacement non-uniformity can affect the overall tendon mechanical behaviour and this can be detected *in vivo* by applying selective muscle stimulation and ultrasonography. Reduced sub-tendon sliding was successfully simulated *in silico* by assigning frictional interface properties between sub-tendons, and the data suggest that a stiffer inter-sub-tendon matrix increases the force sharing capacity between sub-tendons. Dissipation of force to a greater effective CSA results in a consequent reduction in tendon stress. Surprisingly, this reduction in mean stress did not always result in a concomitant decrease in the peak stress. Future studies are warranted to investigate how the stress response within tendons changes with age, as the result of reduced sub-tendon sliding.

A stiff inter-sub-tendon matrix effectively increases the CSA of the sub-tendon when loaded in isolation and, therefore, reduces the Achilles tendon displacement under the same load (Handsfield et al., 2017). Combining the finding often reported in the literature that *in vivo* sub-tendon material properties can decline with age (Stenroth et al., 2012), these two factors together could result in an increasing trend of tendon axial displacement but a decreasing trend in intra-tendinous non-uniformity, a widely reported phenomenon measured by ultrasonography in aged Achilles tendons (reviewed in Section 1.4.4 and 1.5.3). However, from the FEA results, it is demonstrated that the reduced displacement non-uniformity does not create a uniform peak stress response, which is more sensitive to the inherent tendon morphology, similar to the conclusion of Shim et al (2014). Although it

is technically challenging to measure and monitor tendon stress *in vivo*, understanding the complex force interactions, especially in the transverse direction (as in Figure 6-4), between sub-tendons may provide better insights into identifying high-stress tendon regions.

It is currently unknown whether different inter-sub-tendon matrices (between each pair of sub-tendons) demonstrate identical mechanical properties or exhibit a similar age-related decline in sliding. Another challenge is to successfully sample sufficient quantities of the inter-sub-tendon matrix from different locations for biochemical analysis. Immuno-histochemistry approaches are commonly used for investigating the inter-sub-tendon matrix (in rats (Gains et al., 2020)) and IFM protein distributions (Thorpe et al., 2016a, Godinho et al., 2017), but tissue sectioning protocols may require modifications to fully represent the twisted structure of human Achilles sub-tendons. Characterising the composition of these matrices could reveal the mechanisms behind the age-related decline in sub-tendon sliding.

8.2 Clinical Application Possibilities

8.2.1 Non-invasive Measurement of Matrix Composition

The studies have utilised and demonstrated that Raman spectroscopy can differentiate tendon samples of different ages and the spectral features are highly correlated with glycation crosslinks levels in human tendons. Raman spectroscopy has the potential to rapidly and non-invasively measure the ‘tendon age’ instead of chronological age. In humans, diseases, physical

activity levels, and diet preferences could all affect the tissue glycation crosslinks levels. Having a non-invasive measurement of tendon glycation level is a valuable clinical tool for screening injury-prone, high-risk tendons. Glycation crosslinks greatly affect the tendon mechanical behaviour at various hierarchical levels (Section 1.2.3.2.2 and 1.3.6); therefore, incorporating this ‘tendon age’ measurement in our proposed FEA protocol is likely to improve the accuracy of modelling results, for example by informing the age-related changes in material properties and correlating with sub-tendon sliding capacities in our sub-tendon models.

The experiments were conducted using tendon tissues with no apparent degenerative changes. Despite being purely speculative, Raman spectroscopy may be able to differentiate injured or healthy tendons based on spectral differences. It is well-documented that widespread matrix changes in tendinopathy are prevalent and include both altered molecular composition and the disruption of the collagenous matrix (Section 1.5). These pathological changes are more prominent than the subtle, slowly accumulating ageing changes. Studying pathological tendons using Raman spectroscopy may allow early detection of tendon molecular level changes that current medical imaging modality has yet to achieve. Spectral data collected from Raman spectroscopy can be further investigated using various mathematical or computational techniques, such as multivariate regression, to correlate with chronological age; curve fitting and spectral deconvolution, to reveal structural alternation at the molecule level; or machine learning algorisms, to discern and categorise healthy and injured tendons.

Raman spectroscopy is a promising tool for improving our current diagnostic and management of tendinopathy. The immediate next step is to compare the spectra obtained from the 'wet' tissues with our reported dried homogenised samples. It is expected to demonstrate differences since the hydration level of collagenous tissue affects the intensity and frequency of several dominant Raman peaks (Masic et al., 2015). Whole tissue measurement also requires clear labelling of the spectra collected from different tendon compartments, such as between fascicles or IFM, due to the reported compositional differences.

With the application of Spatially Offset Raman Spectroscopy (SORS), the clinical translation could start by measuring isolated tendon spectra directly, to obtain a baseline value for validation. Later, conducting *ex vivo* measurement, from the cadaver or amputated limbs, through the skin and then gradually removing the covered tissue and re-measuring, to validate the tendon Raman spectrum acquired. Modification of laser intensity is required to ensure safety and signal quality before *in vivo* application. Future steps could include patient cohorts from different stages of tendinopathy and compare with health, asymptomatic tendons.

8.2.2 Optimised Training Informed by FEA

Using FEA approaches has improved our understanding of the complex interaction between Achilles sub-tendons. This modelling approach may improve the current practice of tendinopathy rehabilitation by informing

optimal loading conditions based on an individual's tendon morphology, mechanical properties, and sub-tendon sliding (related to 'tendon age').

By carefully positioning ankle and knee joint angle, emphasised loading on one particular sub-tendon could be achieved (as in (Edama et al., 2015b)) and used to facilitate the targeted muscle-tendon unit, or conversely, limit certain joint angles by taping or applying braces could inhibit activation of the target muscle and reduce its sub-tendon load. One meta-analysis which synthesised 16 studies identified that limited evidence of reduced medial gastrocnemius firing and a shift in plantar pressure among Achilles tendinopathic patients during running or hopping, suggesting a potential therapeutic target for specialised, targeted training (Sancho et al., 2019). Applying FEA to individual tendon morphologies allows the exploration of different loading conditions that could lower the peak tendon stress to prevent injury. Similarly, changing the interface properties (as in Chapter 6) can predict the tendon mechanical behaviour change as individuals age, allowing early prevention possibilities. Combining the FEA and motion analysis could further inform clinicians how the tendon responds under certain movements and may act as a guide for rehabilitation progression.

The successful application of FEA in clinics is limited by the inability to delineate sub-tendon boundaries using current medical imaging modalities (Szaro et al., 2020). Besides, it is not yet possible to accurately measure *in vivo* sub-tendon mechanical properties, which is crucial for simulations. One direction for future research could be combining computer modelling, imaging, and isolated muscle-tendon unit loading to construct a pseudo-model of the Achilles tendon that correlates well with the experimental kinetic

and kinematic data. Both MRI and 3-D ultrasound can depict the ‘whole’ Achilles tendon shape which can then be easily generated into a computerised model (Devaprakash et al., 2019). Next, by measuring both forces exerting from different muscle bellies and the concomitant change in the tendon shape under imaging, combinations of force-shape relationships during different movements can be collected and incorporated into the tendon model to generate results of possible sub-tendon distributions that fit with the experimental data. This may be more likely to achieve in younger than aged people due to the more independent sub-tendon movements.

Chapter 9 Conclusions and Perspectives

This thesis has improved our understanding of the Achilles tendon mechanical behaviour by considering the influence of different sub-tendons. These findings emphasise the importance of considering the individual and combined effects from the sub-tendons when studying Achilles tendon mechanics and advise against comparing tendons without considering individual morphological features and the inter-sub-tendon sliding abilities.

Each sub-tendon demonstrates different mechanical properties which correlate with the external mechanical demands. Different shapes of sub-tendons exhibit unique local mechanical responses and contribute to the tendon level mechanics. Ageing, by affecting the inter-sub-tendon matrix properties; and movements, by changing force levels applied, can both affect the sub-tendon and tendon level displacements, resulting in a complex and difficult to predict mechanical behaviour of the Achilles tendon. These interactions can be systematically studied and manipulated using finite element analysis. Incorporating computational simulation on an individual basis may improve our current ‘one-size-fits-all’ tendinopathy prevention and training regime.

Matrix compositions are different between tendons of different ages and between Achilles sub-tendons, detectable by both biochemical assays and Raman spectroscopy. Successfully applying Raman spectroscopy to tendons could greatly enhance the ability to detect premature tendon ageing or early tendinopathy at the fibril and the molecular level, complementing current

diagnostic imaging techniques that mainly focus on structural changes at the fascicle or whole tendon level.

In summary, this thesis has identified three factors that could affect the sub-tendon level mechanical behaviour – morphological features, inherent composition and mechanical properties, and the sliding ability between sub-tendons; and two approaches with clinical application potential – Raman spectroscopy and finite element analysis. Specifically, Raman spectroscopy could provide a rapid and non-invasive way to probe tendon compositions and detect tendon age or pathology, while finite element analysis, combined with individual movement assessment and muscle-tendon properties measurement, could map the internal tendon stress distributions and provide feedback to clinicians. These influencing factors should be systematically studied to provide a better understanding of Achilles tendon mechanical function, and two clinical approaches could be further investigated and refined to translate these findings into future clinical practice.

Appendices

Journal papers published from the work in this thesis:

- YIN, N.-H., PARKER, A. W., MATOUSEK, P., & BIRCH, H. L. 2020. Detection of Age-Related Changes in Tendon Molecular Composition by Raman Spectroscopy—Potential for Rapid, Non-Invasive Assessment of Susceptibility to Injury. *Int J Mol Sci*, 21, 2150.
- YIN, N.-H., FROMME, P., MCCARTHY, I. & BIRCH H. L. 2021. Individual Variation in Achilles Tendon Morphology and Geometry Changes Susceptibility to Injury. *eLife*, 10, e63204.
- YIN, N.-H. MCCARTHY, I. & BIRCH, H. L. 2021. An Equine Tendon Model for Studying Intra-Tendinous Shear in Tendons That Have More than One Muscle Contribution. *Acta Biomater,* 127: 205–12.

Conference abstracts and posters from the work in this thesis:

- YIN, N.-H. & BIRCH, H. L. Is an Equine Tendon Model Suitable for Studying Shear Mechanics within Human Achilles Tendon? 5th International Scientific Tendinopathy Symposium, 2018 Groningen, the Netherlands.
- YIN, N.-H., PARKER, A. W., MATOUSEK, P., & BIRCH, H. L. Can Raman Spectroscopy Detect Age-related Changes in Tendon Matrix? British Society of Matrix Biology Spring Meeting "Stroma, Niche and Repair", 2019 Liverpool, UK.
- YIN, N.-H., PARKER, A. W., MATOUSEK, P., & BIRCH, H. L. Detection of Age-related Tendon Molecular Changes by Raman Spectroscopy. Orthopaedic Research Society 2020 Annual Meeting, 2020 Phoenix, Arizona.
- YIN, N.-H., PARKER, A. W., MATOUSEK, P., & BIRCH, H. L. Human Tendons with Different Levels of Age Accumulated Molecular Modifications Can Be Differentiated by Raman Spectroscopy. British Society of Matrix Biology Spring Meeting "Inflammation, Fibrosis, Resolution and the Matrix", 2021 Oxford, UK.

Bibliography

ACKERMANN, P. W. 2013. Neuronal regulation of tendon homoeostasis. *Int J Exp Pathol,* 94**,** 271-86.

ACKERMANN, P. W., SALO, P. & HART, D. A. 2016. Tendon Innervation. *In:* ACKERMANN, P. W. & HART, D. A. (eds.) *Metabolic Influences on Risk for Tendon Disorders.* Cham: Springer International Publishing.

AHMED, T., NASH, A., CLARK, K. E., GHIBAUDO, M., DE LEEUW, N. H., POTTER, A., STRATTON, R., BIRCH, H. L., ENEA CASSE, R. & BOZEC, L. 2017. Combining nano-physical and computational investigations to understand the nature of "aging" in dermal collagen. *Int J Nanomedicine,* 12**,** 3303-3314.

AKALAN, N. E. & ANGIN, S. 2020. Kinesiology of the human gait. *Comparative Kinesiology of the Human Body.*

ALIMOVA, A., CHAKRAVERTY, R., MUTHUKATTIL, R., ELDER, S., KATZ, A., SRIRAMOJU, V., LIPPER, S. & ALFANO, R. R. 2009. In vivo molecular evaluation of guinea pig skin incisions healing after surgical suture and laser tissue welding using Raman spectroscopy. *J Photochem Photobiol B,* 96**,** 178-83.

ALSAMAD, F., BRUNEL, B., VUIBLET, V., GILLERY, P., JAISSON, S. & PIOT, O. 2021. In depth investigation of collagen non-enzymatic glycation by Raman spectroscopy. *Spectrochim Acta A Mol Biomol Spectrosc,* 251**,** 119382.

AMIEL, D., FRANK, C., HARWOOD, F., FRONEK, J. & AKESON, W. 1984. Tendons and ligaments: a morphological and biochemical comparison. *J Orthop Res,* 1**,** 257-65.

ANDARAWIS-PURI, N., PHILIP, A., LAUDIER, D., SCHAFFLER, M. B. & FLATOW, E. L. 2014. Temporal effect of in vivo tendon fatigue loading on the apoptotic response explained in the context of number of fatigue loading cycles and initial damage parameters. *J Orthop Res,* 32**,** 1097-103.

ANGIN, S. & DEMIRB*Comparative Kinesiology of the Human Body.*

ANTONIOS, T. & ADDS, P. J. 2008. The medial and lateral bellies of gastrocnemius: A cadaveric and ultrasound investigation. *Clinical Anatomy,* 21**,** 66-74.

ARNDT, A., BENGTSSON, A. S., PEOLSSON, M., THORSTENSSON, A. & MOVIN, T. 2012. Non-uniform displacement within the Achilles tendon during passive ankle joint motion. *Knee Surg Sports Traumatol Arthrosc,* 20**,** 1868-74.

ARNDT, A., BRUGGEMANN, G. P., KOEBKE, J. & SEGESSER, B. 1999a. Asymmetrical loading of the human triceps surae: I. Mediolateral force differences in the Achilles tendon. *Foot Ankle Int,* 20**,** 444-9.

ARNDT, A., BRUGGEMANN, G. P., KOEBKE, J. & SEGESSER, B. 1999b. Asymmetrical loading of the human triceps surae: II. Differences in calcaneal moments. *Foot Ankle Int,* 20**,** 450-5.

ARNDT, A. N., KOMI, P. V., BRUGGEMANN, G. P. & LUKKARINIEMI, J. 1998. Individual muscle contributions to the in vivo achilles tendon force. *Clin Biomech (Bristol, Avon),* 13**,** 532-541.

ARNOCZKY, S. P., LAVAGNINO, M. & EGERBACHER, M. 2007. The mechanobiological aetiopathogenesis of tendinopathy: is it the over-stimulation or the under-stimulation of tendon cells? *Int J Exp Pathol,* 88**,** 217-26.

AVERY, N. C. & BAILEY, A. J. 2008. Restraining Cross-Links Responsible for the Mechanical Properties of Collagen Fibers: Natural and Artificial. *In:* FRATZL, P. (ed.) *Collagen: Structure and Mechanics.* Boston, MA: Springer US.

BANNISTER, D. W. & BURNS, A. B. 1970. Adaptation of the Bergman and Loxley technique for hydroxyproline determination to the AutoAnalyzer and its use in determining plasma hydroxyproline in the domestic fowl. *Analyst,* 95**,** 596-600.

BATSON, E. L., PARAMOUR, R. J., SMITH, T. J., BIRCH, H. L., PATTERSON-KANE, J. C. & GOODSHIP, A. E. 2003. Are the material properties and matrix composition of equine flexor and extensor tendons determined by their functions. *Equine Veterinary Journal,* 35**,** 314-8.

BECKER, C. K., SAVELBERG, H. H. & BARNEVELD, A. 1994. In vitro mechanical properties of the accessory ligament of the deep digital flexor tendon in horses in relation to age. *Equine Vet J,* 26**,** 454-9.

BENJAMIN, M. & RALPHS, J. R. 1998. Fibrocartilage in tendons and ligaments—an adaptation to compressive load. *J Anat,* 193**,** 481-94.

BERGHOLT, M. S., SERIO, A. & ALBRO, M. B. 2019. Raman Spectroscopy: Guiding Light for the Extracellular Matrix. *Front Bioeng Biotechnol,* 7**,** 303.

BEYER, R., AGERGAARD, A. S., MAGNUSSON, S. P. & SVENSSON, R. B. 2018. Speckle tracking in healthy and surgically repaired human Achilles tendons at different knee angles-A validation using implanted tantalum beads. *Translational Sports Medicine,* 1**,** 79-88.

BEYER, R., KONGSGAARD, M., HOUGS KJAER, B., OHLENSCHLAEGER, T., KJAER, M. & MAGNUSSON, S. P. 2015. Heavy Slow Resistance Versus Eccentric Training as Treatment for Achilles Tendinopathy: A Randomized Controlled Trial. *Am J Sports Med,* 43**,** 1704-11.

BIRCH, H., SMITH, T., TASKER, T. & GOODSHIP, A. E. Age Related Changes to Mechanical and Matrix Properties in Human Achilles Tendon. 47th Annual Meeting, Orthopaedic Research Society, 2001 San Francisco, California.

BIRCH, H. L. 2007. Tendon matrix composition and turnover in relation to functional requirements. *Int J Exp Pathol,* 88**,** 241-8.

BIRCH, H. L., BAILEY, A. J. & GOODSHIP, A. E. 1998. Macroscopic 'degeneration' of equine superficial digital flexor tendon is accompanied by a change in extracellular matrix composition. *Equine Vet J*.

BIRCH, H. L., BAILEY, J. V., BAILEY, A. J. & GOODSHIP, A. E. 1999. Age-related changes to the molecular and cellular components of equine flexor tendons. *Equine Vet J,* 31**,** 391-6.

BIRCH, H. L., PEFFERS, M. J. & CLEGG, P. D. 2016. Influence of Ageing on Tendon Homeostasis. *In:* P., A. & D., H. (eds.) *Metabolic Influences on Risk for Tendon Disorders.* 2016/08/19 ed.

BIRCH, H. L., THORPE, C. T. & RUMIAN, A. P. 2013. Specialisation of extracellular matrix for function in tendons and ligaments. *Muscles Ligaments Tendons J,* 3**,** 12-22.
BIRCH, H. L., WILSON, A. M. & GOODSHIP, A. E. 2008a. Physical activity: does long-term, high-intensity exercise in horses result in tendon degeneration? *J Appl Physiol (1985),* 105**,** 1927-33.
BIRCH, H. L., WORBOYS, S., EISSA, S., JACKSON, B., STRASSBURG, S. & CLEGG, P. D. 2008b. Matrix metabolism rate differs in functionally distinct tendons. *Matrix Biol,* 27**,** 182-9.
BLEY, B. & ABID, W. 2015. Imaging of Tendinopathy: A Physician's Perspective. *J Orthop Sports Phys Ther,* 45**,** 826-8.
BLITZ, N. M. & ELIOT, D. J. 2007. Anatomical Aspects of the Gastrocnemius Aponeurosis and Its Insertion: A Cadaveric Study. *The Journal of Foot and Ankle Surgery,* 46**,** 101-108.
BODE-LESNIEWSKA, B., DOURS-ZIMMERMANN, M. T., ODERMATT, B. F., BRINER, J., HEITZ, P. U. & ZIMMERMANN, D. R. 1996. Distribution of the large aggregating proteoglycan versican in adult human tissues. *J Histochem Cytochem,* 44**,** 303-12.
BOGAERTS, S., DE BRITO CARVALHO, C., SCHEYS, L., DESLOOVERE, K., D'HOOGE, J., MAES, F., SUETENS, P. & PEERS, K. 2017. Evaluation of tissue displacement and regional strain in the Achilles tendon using quantitative high-frequency ultrasound. *PLoS One,* 12**,** e0181364.
BOJSEN-MOLLER, J., HANSEN, P., AAGAARD, P., SVANTESSON, U., KJAER, M. & MAGNUSSON, S. P. 2004. Differential displacement of the human soleus and medial gastrocnemius aponeuroses during isometric plantar flexor contractions in vivo. *J Appl Physiol (1985),* 97**,** 1908-14.
BOJSEN-MOLLER, J., SCHWARTZ, S., KALLIOKOSKI, K. K., FINNI, T. & MAGNUSSON, S. P. 2010. Intermuscular force transmission between human plantarflexor muscles in vivo. *J Appl Physiol (1985),* 109**,** 1608-18.
BOLBOACĂ, S. D. & JôNTSCHI, L. 2007. Amino Acids Sequence Analysis on Collagen. *ulletin of University of Agricultural Sciences and Veterinary Medicine Cluj-Napoca. Animal Science and Biotechnologies,* 64**,** 311-16.
BONIFACIO, A. & SERGO, V. 2010. Effects of sample orientation in Raman microspectroscopy of collagen fibers and their impact on the interpretation of the amide III band. *Vibrational Spectroscopy,* 53**,** 314-317.
BONNIER, F. & BYRNE, H. J. 2012. Understanding the molecular information contained in principal component analysis of vibrational spectra of biological systems. *Analyst,* 137**,** 322-32.
BOTTER, A., OPRANDI, G., LANFRANCO, F., ALLASIA, S., MAFFIULETTI, N. A. & MINETTO, M. A. 2011. Atlas of the muscle motor points for the lower limb: implications for electrical stimulation procedures and electrode positioning. *Eur J Appl Physiol,* 111**,** 2461-71.
BURGESS, K. E., PEARSON, S. J., BREEN, L. & ONAMBELE, G. N. 2009. Tendon structural and mechanical properties do not differ between

genders in a healthy community-dwelling elderly population. *J Orthop Res,* 27**,** 820-5.
CARROLL, C. C., DICKINSON, J. M., HAUS, J. M., LEE, G. A., HOLLON, C. J., AAGAARD, P., MAGNUSSON, S. P. & TRAPPE, T. A. 2008. Influence of aging on the in vivo properties of human patellar tendon. *J Appl Physiol (1985),* 105**,** 1907-15.
CHAN, O., MORTON, S., PRITCHARD, M., PARKES, T., MALLIARAS, P., CRISP, T., PADHIAR, N., MAFFULLI, N., KING, J. & MORRISSEY, D. 2017. Intratendinous tears of the Achilles tendon - a new pathology? Analysis of a large 4-year cohort. *Muscles Ligaments Tendons J,* 7**,** 53-61.
CHIMENTI, R. L., FLEMISTER, A. S., KETZ, J., BUCKLIN, M., BUCKLEY, M. R. & RICHARDS, M. S. 2016. Ultrasound strain mapping of Achilles tendon compressive strain patterns during dorsiflexion. *J Biomech,* 49**,** 39-44.
CHOI, H., SIMPSON, D., WANG, D., PRESCOTT, M., PITSILLIDES, A. A., DUDHIA, J., CLEGG, P. D., PING, P. & THORPE, C. T. 2020. Heterogeneity of proteome dynamics between connective tissue phases of adult tendon. *Elife,* 9**,** 1-22.
CLARK, W. H. & FRANZ, J. R. 2020. Triceps surae muscle-subtendon interaction differs between young and older adults. *Connect Tissue Res,* 61**,** 104-113.
COLLIER, T. A., NASH, A., BIRCH, H. L. & DE LEEUW, N. H. 2018. Effect on the mechanical properties of type I collagen of intra-molecular lysine-arginine derived advanced glycation end-product cross-linking. *J Biomech,* 67**,** 55-61.
CONNIZZO, B. K. & GRODZINSKY, A. J. 2018. Release of pro-inflammatory cytokines from muscle and bone causes tenocyte death in a novel rotator cuff in vitro explant culture model. *Connect Tissue Res,* 59**,** 423-436.
COOK, J. L. & PURDAM, C. 2012. Is compressive load a factor in the development of tendinopathy? *Br J Sports Med,* 46**,** 163-8.
COOK, J. L. & SCREEN, H. R. C. 2018. Tendon Pathology: Have we missed the first step in the development of pathology? *Journal of Applied Physiology.*
CORPS, A. N., ROBINSON, A. H., MOVIN, T., COSTA, M. L., HAZLEMAN, B. L. & RILEY, G. P. 2006. Increased expression of aggrecan and biglycan mRNA in Achilles tendinopathy. *Rheumatology (Oxford),* 45**,** 291-4.
COSTA-ALMEIDA, R., GON÷ALVES, A. I., GERSHOVICH, P., RODRIGUES, M. T., REIS, R. L. & GOMES, M. E. 2015. Tendon Stem Cell Niche. *Tissue-Specific Stem Cell Niche.*
COUPPE, C., HANSEN, P., KONGSGAARD, M., KOVANEN, V., SUETTA, C., AAGAARD, P., KJAER, M. & MAGNUSSON, S. P. 2009. Mechanical properties and collagen cross-linking of the patellar tendon in old and young men. *J Appl Physiol (1985),* 107**,** 880-6.
COUPPE, C., KONGSGAARD, M., AAGAARD, P., HANSEN, P., BOJSEN-MOLLER, J., KJAER, M. & MAGNUSSON, S. P. 2008. Habitual loading results in tendon hypertrophy and increased stiffness of the human patellar tendon. *J Appl Physiol (1985),* 105**,** 805-10.

COUPPE, C., SVENSSON, R. B., GROSSET, J. F., KOVANEN, V., NIELSEN, R. H., OLSEN, M. R., LARSEN, J. O., PRAET, S. F., SKOVGAARD, D., HANSEN, M., AAGAARD, P., KJAER, M. & MAGNUSSON, S. P. 2014. Life-long endurance running is associated with reduced glycation and mechanical stress in connective tissue. *Age (Dordr),* 36**,** 9665.

COUPPE, C., SVENSSON, R. B., JOSEFSEN, C. O., KJELDGAARD, E. & MAGNUSSON, S. P. 2020. Ultrasound speckle tracking of Achilles tendon in individuals with unilateral tendinopathy: a pilot study. *Eur J Appl Physiol,* 120**,** 579-589.

CROUZIER, M., LACOURPAILLE, L., NORDEZ, A., TUCKER, K. & HUG, F. 2018. Neuromechanical coupling within the human triceps surae and its consequence on individual force-sharing strategies. *J Exp Biol,* 221.

CSAPO, R., MALIS, V., HODGSON, J. & SINHA, S. 2014. Age-related greater Achilles tendon compliance is not associated with larger plantar flexor muscle fascicle strains in senior women. *J Appl Physiol (1985),* 116**,** 961-9.

DALTON, S., CAWSTON, T. E., RILEY, G. P., BAYLEY, I. J. & HAZLEMAN, B. L. 1995. Human shoulder tendon biopsy samples in organ culture produce procollagenase and tissue inhibitor of metalloproteinases. *Ann Rheum Dis,* 54**,** 571-7.

DAYTON, P. 2017. Anatomic, Vascular, and Mechanical Overview of the Achilles Tendon. *Clin Podiatr Med Surg,* 34**,** 107-113.

DE CARVALHO, P. K., SILVEIRA, L., JR., BARBOSA, D., MUNIN, E., SALGADO, M. A. & VILLAVERDE, A. B. 2016. Analysis of experimental tendinitis in rats treated with laser and platelet-rich plasma therapies by Raman spectroscopy and histometry. *Lasers Med Sci,* 31**,** 19-26.

DEAN, B. J., GWILYM, S. E. & CARR, A. J. 2013. Why does my shoulder hurt? A review of the neuroanatomical and biochemical basis of shoulder pain. *Br J Sports Med,* 47**,** 1095-104.

DEAN, B. J. F., DAKIN, S. G., MILLAR, N. L. & CARR, A. J. 2017. Review: Emerging concepts in the pathogenesis of tendinopathy. *Surgeon,* 15**,** 349-354.

DEBELLE, L., ALIX, A. J., JACOB, M. P., HUVENNE, J. P., BERJOT, M., SOMBRET, B. & LEGRAND, P. 1995. Bovine elastin and kappa-elastin secondary structure determination by optical spectroscopies. *J Biol Chem,* 270**,** 26099-103.

DEBELLE, L., ALIX, A. J., WEI, S. M., JACOB, M. P., HUVENNE, J. P., BERJOT, M. & LEGRAND, P. 1998. The secondary structure and architecture of human elastin. *Eur J Biochem,* 258**,** 533-9.

DEHRING, K. A., SMUKLER, A. R., ROESSLER, B. J. & MORRIS, M. D. 2006. Correlating changes in collagen secondary structure with aging and defective type II collagen by Raman spectroscopy. *Appl Spectrosc,* 60**,** 366-72.

DEL BUONO, A., OLIVA, F., LONGO, U. G., RODEO, S. A., ORCHARD, J., DENARO, V. & MAFFULLI, N. 2012. Metalloproteases and rotator cuff disease. *J Shoulder Elbow Surg,* 21**,** 200-8.

DENG, S., SUN, Z., ZHANG, C., CHEN, G. & LI, J. 2017. Surgical Treatment Versus Conservative Management for Acute Achilles Tendon Rupture: A Systematic Review and Meta-Analysis of Randomized Controlled Trials. *J Foot Ankle Surg,* 56**,** 1236-1243.

DENOIX, J.-M. 1994. Functional Anatomy of Tendons and Ligaments in the Distal Limbs (Manus and Pes). *Veterinary Clinics of North America: Equine Practice,* 10**,** 273-322.

DEVAPRAKASH, D., LLOYD, D. G., BARRETT, R. S., OBST, S. J., KENNEDY, B., ADAMS, K. L., HUNTER, A., VLAHOVICH, N., PEASE, D. L. & PIZZOLATO, C. 2019. Magnetic Resonance Imaging and Freehand 3-D Ultrasound Provide Similar Estimates of Free Achilles Tendon Shape and 3-D Geometry. *Ultrasound Med Biol,* 45**,** 2898-2905.

DOURTE, L. M., PATHMANATHAN, L., JAWAD, A. F., IOZZO, R. V., MIENALTOWSKI, M. J., BIRK, D. E. & SOSLOWSKY, L. J. 2012. Influence of decorin on the mechanical, compositional, and structural properties of the mouse patellar tendon. *J Biomech Eng,* 134**,** 031005.

DOURTE, L. M., PATHMANATHAN, L., MIENALTOWSKI, M. J., JAWAD, A. F., BIRK, D. E. & SOSLOWSKY, L. J. 2013. Mechanical, compositional, and structural properties of the mouse patellar tendon with changes in biglycan gene expression. *J Orthop Res,* 31**,** 1430-7.

DUKOR, R. K. 2006. Vibrational Spectroscopy in the Detection of Cancer. *In:* CHALMERS, J. M. & GRIFFITHS, P. R. (eds.) *Handbook of Vibrational Spectroscopy.*

DUNKMAN, A. A., BUCKLEY, M. R., MIENALTOWSKI, M. J., ADAMS, S. M., THOMAS, S. J., SATCHELL, L., KUMAR, A., PATHMANATHAN, L., BEASON, D. P., IOZZO, R. V., BIRK, D. E. & SOSLOWSKY, L. J. 2014. The tendon injury response is influenced by decorin and biglycan. *Ann Biomed Eng,* 42**,** 619-30.

DYSON, S. J. 1991. Desmitis of the accessory ligament of the deep digital flexor tendon: 27 cases (1986-1990). *Equine Vet J,* 23**,** 438-44.

EDAMA, M., KUBO, M., ONISHI, H., TAKABAYASHI, T., INAI, T., YOKOYAMA, E., HIROSHI, W., SATOSHI, N. & KAGEYAMA, I. 2015a. The twisted structure of the human Achilles tendon. *Scandinavian Journal of Medicine & Science in Sports,* 25**,** e497-e503.

EDAMA, M., KUBO, M., ONISHI, H., TAKABAYASHI, T., YOKOYAMA, E., INAI, T., WATANABE, H., NASHIMOTO, S. & KAGEYAMA, I. 2016. Structure of the Achilles tendon at the insertion on the calcaneal tuberosity. *J Anat,* 229**,** 610-614.

EDAMA, M., ONISHI, H., KUMAKI, K., KAGEYAMA, I., WATANABE, H. & NASHIMOTO, S. 2015b. Effective and selective stretching of the medial head of the gastrocnemius. *Scand J Med Sci Sports,* 25**,** 242-50.

EEKHOFF, J. D., FANG, F. & LAKE, S. P. 2018. Multiscale mechanical effects of native collagen cross-linking in tendon. *Connect Tissue Res,* 59**,** 410-422.

EGERBACHER, M., ARNOCZKY, S. P., CABALLERO, O., LAVAGNINO, M. & GARDNER, K. L. 2008. Loss of homeostatic tension induces apoptosis in tendon cells: an in vitro study. *Clin Orthop Relat Res,* 466**,** 1562-8.

EKIERT, M., TOMASZEWSKI, K. A. & MLYNIEC, A. 2021. The differences in viscoelastic properties of subtendons result from the anatomical tripartite structure of human Achilles tendon - ex vivo experimental study and modeling. *Acta Biomater,* 125**,** 138-153.
ELLIOTT, D. H. 1965. Structure and Function of Mammalian Tendon. *Biol Rev,* 40**,** 392-421.
ELLIOTT, D. M., ROBINSON, P. S., GIMBEL, J. A., SARVER, J. J., ABBOUD, J. A., IOZZO, R. V. & SOSLOWSKY, L. J. 2003. Effect of Altered Matrix Proteins on Quasilinear Viscoelastic Properties in Transgenic Mouse Tail Tendons. *Annals of Biomedical Engineering,* 31**,** 599-605.
ESMONDE-WHITE, K. 2014. Raman spectroscopy of soft musculoskeletal tissues. *Appl Spectrosc,* 68**,** 1203-18.
FANG, F. & LAKE, S. P. 2015. Multiscale strain analysis of tendon subjected to shear and compression demonstrates strain attenuation, fiber sliding, and reorganization. *J Orthop Res,* 33**,** 1704-12.
FANG, F. & LAKE, S. P. 2016. Multiscale mechanical integrity of human supraspinatus tendon in shear after elastin depletion. *J Mech Behav Biomed Mater,* 63**,** 443-455.
FARNDALE, R. W., BUTTLE, D. J. & BARRETT, A. J. 1986. Improved quantitation and discrimination of sulphated glycosaminoglycans by use of dimethylmethylene blue. *Biochemica et Biophysica Acta***,** 173-7.
FARRIS, D. J., TREWARTHA, G., MCGUIGAN, M. P. & LICHTWARK, G. A. 2013. Differential strain patterns of the human Achilles tendon determined in vivo with freehand three-dimensional ultrasound imaging. *J Exp Biol,* 216**,** 594-600.
FESSEL, G., LI, Y., DIEDERICH, V., GUIZAR-SICAIROS, M., SCHNEIDER, P., SELL, D. R., MONNIER, V. M. & SNEDEKER, J. G. 2014. Advanced glycation end-products reduce collagen molecular sliding to affect collagen fibril damage mechanisms but not stiffness. *PLoS One,* 9**,** e110948.
FICHARD, A., KLEMAN, J.-P. & RUGGIERO, F. 1995. Another look at collagen V and XI molecules. *Matrix Biology,* 14**,** 515-531.
FIELDS, M., SPENCER, N., DUDHIA, J. & MCMILLAN, P. F. 2017. Structural changes in cartilage and collagen studied by high temperature Raman spectroscopy. *Biopolymers,* 107.
FINNI, T., BERNABEI, M., BAAN, G. C., NOORT, W., TIJS, C. & MAAS, H. 2018. Non-uniform displacement and strain between the soleus and gastrocnemius subtendons of rat Achilles tendon. *Scand J Med Sci Sports,* 28**,** 1009-1017.
FINNI, T., CRONIN, N. J., MAYFIELD, D., LICHTWARK, G. A. & CRESSWELL, A. G. 2017. Effects of muscle activation on shear between human soleus and gastrocnemius muscles. *Scand J Med Sci Sports,* 27**,** 26-34.
FINNI, T., HODGSON, J. A., LAI, A. M., EDGERTON, V. R. & SINHA, S. 2003a. Mapping of movement in the isometrically contracting human soleus muscle reveals details of its structural and functional complexity. *J Appl Physiol (1985),* 95**,** 2128-33.
FINNI, T., HODGSON, J. A., LAI, A. M., EDGERTON, V. R. & SINHA, S. 2003b. Nonuniform strain of human soleus aponeurosis-tendon

complex during submaximal voluntary contractions in vivo. *J Appl Physiol (1985),* 95**,** 829-37.
FINNI, T., KOMI, P. V. & LUKKARINIEMI, J. 1998. Achilles tendon loading during walking: application of a novel optic fiber technique. *Eur J Appl Physiol Occup Physiol,* 77**,** 289-91.
FRANZ, J. R., SLANE, L. C., RASSKE, K. & THELEN, D. G. 2015. Non-uniform in vivo deformations of the human Achilles tendon during walking. *Gait Posture,* 41**,** 192-7.
FRANZ, J. R. & THELEN, D. G. 2015. Depth-dependent variations in Achilles tendon deformations with age are associated with reduced plantarflexor performance during walking. *J Appl Physiol (1985),* 119**,** 242-9.
FRANZ, J. R. & THELEN, D. G. 2016. Imaging and simulation of Achilles tendon dynamics: Implications for walking performance in the elderly. *J Biomech,* 49**,** 1403-1410.
FROBERG, A., CISSE, A. S., LARSSON, M., MARTENSSON, M., PEOLSSON, M., MOVIN, T. & ARNDT, A. 2017. Altered patterns of displacement within the Achilles tendon following surgical repair. *Knee Surg Sports Traumatol Arthrosc,* 25**,** 1857-1865.
FRUSHOUR, B. G. & KOENIG, J. L. 1975. Raman scattering of collagen, gelatin, and elastin. *Biopolymers,* 14**,** 379-91.
FUKASHIRO, S., KOMI, P. V., J**?**RVINEN, M. & MIYASHITA, M. 1995. In vivo achilles tendon loading' during jumping in humans. *European Journal of Applied Physiology and Occupational Physiology,* 71**,** 453-458.
FUNAKOSHI, T., SCHMID, T., HSU, H. P. & SPECTOR, M. 2008. Lubricin distribution in the goat infraspinatus tendon: a basis for interfascicular lubrication. *J Bone Joint Surg Am,* 90**,** 803-14.
GAINS, C. C., CORREIA, J. C., BAAN, G. C., NOORT, W., SCREEN, H. R. C. & MAAS, H. 2020. Force Transmission Between the Gastrocnemius and Soleus Sub-Tendons of the Achilles Tendon in Rat. *Frontiers in Bioengineering and Biotechnology.*
GALVIS, L., DUNLOP, J. W., DUDA, G., FRATZL, P. & MASIC, A. 2013. Polarized Raman anisotropic response of collagen in tendon: towards 3D orientation mapping of collagen in tissues. *PLoS One,* 8**,** e63518.
GAUTIERI, A., PASSINI, F. S., SILVAN, U., GUIZAR-SICAIROS, M., CARIMATI, G., VOLPI, P., MORETTI, M., SCHOENHUBER, H., REDAELLI, A., BERLI, M. & SNEDEKER, J. G. 2017. Advanced glycation end-products: Mechanics of aged collagen from molecule to tissue. *Matrix Biol,* 59**,** 95-108.
GENIN, G. M., KENT, A., BIRMAN, V., WOPENKA, B., PASTERIS, J. D., MARQUEZ, P. J. & THOMOPOULOS, S. 2009. Functional grading of mineral and collagen in the attachment of tendon to bone. *Biophys J,* 97**,** 976-85.
GEREMIA, J. M., BOBBERT, M. F., CASA NOVA, M., OTT, R. D., LEMOS FDE, A., LUPION RDE, O., FRASSON, V. B. & VAZ, M. A. 2015. The structural and mechanical properties of the Achilles tendon 2 years after surgical repair. *Clin Biomech (Bristol, Avon),* 30**,** 485-92.
GLENN, J. V., BEATTIE, J. R., BARRETT, L., FRIZZELL, N., THORPE, S. R., BOULTON, M. E., MCGARVEY, J. J. & STITT, A. W. 2007.

Confocal Raman microscopy can quantify advanced glycation end product (AGE) modifications in Bruch's membrane leading to accurate, nondestructive prediction of ocular aging. *FASEB J,* 21**,** 3542-52.
GNIADECKA, M., NIELSEN, O. F., WESSEL, S., HEIDENHEIM, M., CHRISTENSEN, D. H. & WULF, H. C. 1998. Water and protein structure in photoaged and chronically aged skin. *J Invest Dermatol,* 111**,** 1129-33.
GODINHO, M. S., THORPE, C. T., GREENWALD, S. E. & SCREEN, H. R. C. 2021. Elastase treatment of tendon specifically impacts the mechanical properties of the interfascicular matrix. *Acta Biomaterialia,* 123**,** 187-196.
GODINHO, M. S. C., THORPE, C. T., GREENWALD, S. E. & SCREEN, H. R. C. 2017. Elastin is Localised to the Interfascicular Matrix of Energy Storing Tendons and Becomes Increasingly Disorganised With Ageing. *Sci Rep,* 7**,** 9713.
GOODSHIP, A. E. & BIRCH, H. L. 2005. Cross sectional area measurement of tendon and ligament in vitro: a simple, rapid, non-destructive technique. *J Biomech,* 38**,** 605-8.
GRAD, S., LEE, C. R., GORNA, K., GOGOLEWSKI, S., WIMMER, M. A. & ALINI, M. 2005. Surface motion upregulates superficial zone protein and hyaluronan production in chondrocyte-seeded three-dimensional scaffolds. *Tissue Eng,* 11**,** 249-56.
GRANT, T. M., THOMPSON, M. S., URBAN, J. & YU, J. 2013. Elastic fibres are broadly distributed in tendon and highly localized around tenocytes. *J Anat,* 222**,** 573-9.
GUILBERT, M., SAID, G., HAPPILLON, T., UNTEREINER, V., GARNOTEL, R., JEANNESSON, P. & SOCKALINGUM, G. D. 2013. Probing non-enzymatic glycation of type I collagen: a novel approach using Raman and infrared biophotonic methods. *Biochim Biophys Acta,* 1830**,** 3525-31.
GUNJA-SMITH, Z. 1985. An enzyme-linked immunosorbent assay to quantitate the elastin crosslink desmosine in tissue and urine samples. *Anal Biochem,* 147**,** 258-64.
HANDSFIELD, G. G., GREINER, J., MADL, J., ROG-ZIELINSKA, E. A., HOLLVILLE, E., VANWANSEELE, B. & SHIM, V. 2020. Achilles Subtendon Structure and Behavior as Evidenced From Tendon Imaging and Computational Modeling. *Front Sports Act Living,* 2**,** 70.
HANDSFIELD, G. G., INOUYE, J. M., SLANE, L. C., THELEN, D. G., MILLER, G. W. & BLEMKER, S. S. 2017. A 3D model of the Achilles tendon to determine the mechanisms underlying nonuniform tendon displacements. *J Biomech,* 51**,** 17-25.
HANDSFIELD, G. G., SLANE, L. C. & SCREEN, H. R. C. 2016. Nomenclature of the tendon hierarchy: An overview of inconsistent terminology and a proposed size-based naming scheme with terminology for multi-muscle tendons. *J Biomech,* 49**,** 3122-3124.
HANSEN, W., SHIM, V. B., OBST, S., LLOYD, D. G., NEWSHAM-WEST, R. & BARRETT, R. S. 2017. Achilles tendon stress is more sensitive to subject-specific geometry than subject-specific material properties: A finite element analysis. *J Biomech,* 56**,** 26-31.

HARALDSSON, B. T., AAGAARD, P., QVORTRUP, K., BOJSEN-MOLLER, J., KROGSGAARD, M., KOSKINEN, S., KJAER, M. & MAGNUSSON, S. P. 2008. Lateral force transmission between human tendon fascicles. *Matrix Biol,* 27**,** 86-95.

HEINEMEIER, K. M., SCHJERLING, P., HEINEMEIER, J., MAGNUSSON, S. P. & KJAER, M. 2013. Lack of tissue renewal in human adult Achilles tendon is revealed by nuclear bomb (14)C. *FASEB J,* 27**,** 2074-9.

HENNINGER, H. B., UNDERWOOD, C. J., ATESHIAN, G. A. & WEISS, J. A. 2010. Effect of sulfated glycosaminoglycan digestion on the transverse permeability of medial collateral ligament. *J Biomech,* 43**,** 2567-73.

HENNINGER, H. B., VALDEZ, W. R., SCOTT, S. A. & WEISS, J. A. 2015. Elastin governs the mechanical response of medial collateral ligament under shear and transverse tensile loading. *Acta Biomater,* 25**,** 304-12.

HIJAZI, K. M., SINGFIELD, K. L. & VERES, S. P. 2019. Ultrastructural response of tendon to excessive level or duration of tensile load supports that collagen fibrils are mechanically continuous. *J Mech Behav Biomed Mater,* 97**,** 30-40.

HOLZER, D., EPRO, G., MCCRUM, C., DOERNER, J., LUETKENS, J. A., SCHEEF, L., KUKUK, G. M., BOECKER, H., MIERAU, A., BRUGGEMANN, G. P., MAGANARIS, C. N. & KARAMANIDIS, K. 2018. The role of muscle strength on tendon adaptability in old age. *Eur J Appl Physiol,* 118**,** 2269-2279.

HOPKINS, C., FU, S. C., CHUA, E., HU, X., ROLF, C., MATTILA, V. M., QIN, L., YUNG, P. S. & CHAN, K. M. 2016. Critical review on the socio-economic impact of tendinopathy. *Asia Pac J Sports Med Arthrosc Rehabil Technol,* 4**,** 9-20.

HUG, F., LACOURPAILLE, L., MAISETTI, O. & NORDEZ, A. 2013. Slack length of gastrocnemius medialis and Achilles tendon occurs at different ankle angles. *Journal of Biomechanics,* 46**,** 2534-2538.

HUISMAN, E., LU, A., JAMIL, S., MOUSAVIZADEH, R., MCCORMACK, R., ROBERTS, C. & SCOTT, A. 2016. Influence of repetitive mechanical loading on MMP2 activity in tendon fibroblasts. *J Orthop Res,* 34**,** 1991-2000.

HULMES, D. J. S. 2008. Collagen Diversity, Synthesis and Assembly. *In:* FRATZL, P. (ed.) *Collagen: Structure and Mechanics.* Boston, MA: Springer US.

ISHIKAWA, M., KOMI, P. V., GREY, M. J., LEPOLA, V. & BRUGGEMANN, G. P. 2005. Muscle-tendon interaction and elastic energy usage in human walking. *J Appl Physiol (1985),* 99**,** 603-8.

IWASAKI, S., HOSAKA, Y., IWASAKI, T., YAMAMOTO, K., NAGAYASU, A., UEDA, H., KOKAI, Y. & TAKEHANA, K. 2008. The modulation of collagen fibril assembly and its structure by decorin: an electron microscopic study. *Arch Histol Cytol,* 71**,** 37-44.

JAIN, R., CALDERON, D., KIERSKI, P. R., SCHURR, M. J., CZUPRYNSKI, C. J., MURPHY, C. J., MCANULTY, J. F. & ABBOTT, N. L. 2014. Raman spectroscopy enables noninvasive biochemical characterization and identification of the stage of healing of a wound. *Anal Chem,* 86**,** 3764-72.

JARVINEN, T. A., JARVINEN, T. L., KANNUS, P., JOZSA, L. & JARVINEN, M. 2004. Collagen fibres of the spontaneously ruptured human tendons display decreased thickness and crimp angle. *J Orthop Res,* 22**,** 1303-9.

JASTRZEBSKA, M., WRZALIK, R., KOCOT, A., ZALEWSKA-REJDAK, J. & CWALINA, B. 2003. Raman spectroscopic study of glutaraldehyde-stabilized collagen and pericardium tissue. *J Biomater Sci Polym Ed,* 14**,** 185-97.

JAY, G. D. & WALLER, K. A. 2014. The biology of lubricin: near frictionless joint motion. *Matrix Biol,* 39**,** 17-24.

JHINGAN, S., PERRY, M., O'DRISCOLL, G., LEWIN, C., TEATINO, R., MALLIARAS, P., MAFFULLI, N. & MORRISSEY, D. 2011. Thicker Achilles tendons are a risk factor to develop Achilles tendinopathy in elite professional soccer players. *Muscles Ligaments Tendons J,* 1**,** 51-6.

JOMAA, G., KWAN, C. K., FU, S. C., LING, S. K., CHAN, K. M., YUNG, P. S. & ROLF, C. 2020. A systematic review of inflammatory cells and markers in human tendinopathy. *BMC Musculoskelet Disord,* 21**,** 78.

JOZSA, L., LEHTO, M., KANNUS, P., KVIST, M., REFFY, A., VIENO, T., JARVINEN, M., DEMEL, S. & ELEK, E. 1989. Fibronectin and laminin in Achilles tendon. *Acta Orthop Scand,* 60**,** 469-71.

KADLER, K. E., BALDOCK, C., BELLA, J. & BOOT-HANDFORD, R. P. 2007. Collagens at a glance. *J Cell Sci,* 120**,** 1955-8.

KANNUS, P. & JOZSA, L. 1991. Histopathological changes preceding spontaneous rupture of a tendon. A controlled study of 891 patients. *J Bone Joint Surg Am,* 73**,** 1507-25.

KARATHANASOPOULOS, N., ARAMPATZIS, G. & GANGHOFFER, J. F. 2019. Unravelling the viscoelastic, buffer-like mechanical behavior of tendons: A numerical quantitative study at the fibril-fiber scale. *J Mech Behav Biomed Mater,* 90**,** 256-263.

KAWASHIMA, N., NAKAZAWA, K., YAMAMOTO, S. I., NOZAKI, D., AKAI, M. & YANO, H. 2004. Stretch reflex excitability of the anti-gravity ankle extensor muscle in elderly humans. *Acta Physiol Scand,* 180**,** 99-105.

KEMMLER, W., VON STENGEL, S., SCHOENE, D. & KOHL, M. 2018. Changes of Maximum Leg Strength Indices During Adulthood a Cross-Sectional Study With Non-athletic Men Aged 19-91. *Front Physiol,* 9**,** 1524.

KERNS, J. G., BUCKLEY, K., CHURCHWELL, J., PARKER, A. W., MATOUSEK, P. & GOODSHIP, A. E. 2016. Is the Collagen Primed for Mineralization in Specific Regions of the Turkey Tendon? An Investigation of the Protein-Mineral Interface Using Raman Spectroscopy. *Anal Chem,* 88**,** 1559-63.

KERNS, J. G., GIKAS, P. D., BUCKLEY, K., SHEPPERD, A., BIRCH, H. L., MCCARTHY, I., MILES, J., BRIGGS, T. W., KEEN, R., PARKER, A. W., MATOUSEK, P. & GOODSHIP, A. E. 2014. Evidence from Raman spectroscopy of a putative link between inherent bone matrix chemistry and degenerative joint disease. *Arthritis Rheumatol,* 66**,** 1237-46.

KHAN, K. M., COOK, J. L., BONAR, F., HARCOURT, P. & ASTROM, M. 1999. Histopathology of common tendinopathies. Update and implications for clinical management. *Sports Med,* 27**,** 393-408.
KHARAZI, M., BOHM, S., THEODORAKIS, C., MERSMANN, F. & ARAMPATZIS, A. 2021. Quantifying mechanical loading and elastic strain energy of the human Achilles tendon during walking and running. *Sci Rep,* 11**,** 5830.
KIM, B., YOON, J. H., ZHANG, J., ERIC MUELLER, P. O. & HALPER, J. 2010. Glycan profiling of a defect in decorin glycosylation in equine systemic proteoglycan accumulation, a potential model of progeroid form of Ehlers-Danlos syndrome. *Archives of Biochemistry and Biophysics,* 501**,** 221-231.
KIM, M.-W., KIM, J.-H., YANG, Y.-J. & KO, Y.-J. 2005. Anatomic Localization of Motor Points in Gastrocnemius and Soleus Muscles. *American Journal of Physical Medicine & Rehabilitation,* 84**,** 680-683.
KIM, Y.-J., SAH, R. L. Y., DOONG, J.-Y. H. & GRODZINSKY, A. J. 1988. Fluorometric assay of DNA in cartilage explants using Hoechst 33258. *Analytical Biochemistry,* 174**,** 168-76.
KINUGASA, R., SHIN, D., YAMAUCHI, J., MISHRA, C., HODGSON, J. A., EDGERTON, V. R. & SINHA, S. 2008. Phase-contrast MRI reveals mechanical behavior of superficial and deep aponeuroses in human medial gastrocnemius during isometric contraction. *J Appl Physiol (1985),* 105**,** 1312-20.
KNAUS, K. R. & BLEMKER, S. S. 2021. 3D Models Reveal the Influence of Achilles Subtendon Twist on Strain and Energy Storage. *Frontiers in Bioengineering and Biotechnology,* 9.
KOIVUNEN-NIEMELA, T. & PARKKOLA, K. 1995. Anatomy of the Achilles tendon (tendo calcaneus) with respect to tendon thickness measurements. *Surg Radiol Anat,* 17**,** 263-8.
KOMI, P. V., SALONEN, M., JARVINEN, M. & KOKKO, O. 1987. In vivo registration of Achilles tendon forces in man. I. Methodological development. *Int J Sports Med,* 8 Suppl 1**,** 3-8.
KOMOLAFE, O. A. & DOEHRING, T. C. 2010. Fascicle-scale loading and failure behavior of the Achilles tendon. *J Biomech Eng,* 132**,** 021004.
KONDRATKO-MITTNACHT, J., DUENWALD-KUEHL, S., LAKES, R. & VANDERBY, R., JR. 2015. Shear load transfer in high and low stress tendons. *J Mech Behav Biomed Mater,* 45**,** 109-20.
KONGSGAARD, M., NIELSEN, C. H., HEGNSVAD, S., AAGAARD, P. & MAGNUSSON, S. P. 2011. Mechanical properties of the human Achilles tendon, in vivo. *Clin Biomech (Bristol, Avon),* 26**,** 772-7.
KONIG, M., HEMMERS, S., EPRO, G., MCCRUM, C., ACKERMANS, T. M. A., HARTMANN, U. & KARAMANIDIS, K. 2018. Matching Participants for Triceps Surae Muscle Strength and Tendon Stiffness Does Not Eliminate Age-Related Differences in Mechanical Power Output During Jumping. *Front Physiol,* 9**,** 1345.
KONRAD, P. 2005. *The ABC of EMG,* Scottsdale, AZ, Noraxon U.S.A., Inc.
KOOB, T. J., CLARK, P. E., HERNANDEZ, D. J., THURMOND, F. A. & VOGEL, K. G. 1992. Compression loading in vitro regulates proteoglycan synthesis by tendon fibrocartilage. *Arch Biochem Biophys,* 298**,** 303-12.

KOSTROMINOVA, T. Y. & BROOKS, S. V. 2013. Age-related changes in structure and extracellular matrix protein expression levels in rat tendons. *AGE,* 35**,** 2203-2214.
KRAGSTRUP, T. W., KJAER, M. & MACKEY, A. L. 2011. Structural, biochemical, cellular, and functional changes in skeletal muscle extracellular matrix with aging. *Scand J Med Sci Sports,* 21**,** 749-57.
KRISTENSEN, J. H. & KARSDAL, M. A. 2016. Elastin. *Biochemistry of Collagens, Laminins and Elastin.*
KUBO, K., KANEHISA, H., AZUMA, K., ISHIZU, M., KUNO, S. Y., OKADA, M. & FUKUNAGA, T. 2003. Muscle architectural characteristics in young and elderly men and women. *Int J Sports Med,* 24**,** 125-30.
KUMAMOTO, Y., HARADA, Y., TAKAMATSU, T. & TANAKA, H. 2018. Label-free Molecular Imaging and Analysis by Raman Spectroscopy. *Acta Histochem Cytochem,* 51**,** 101-110.
LANGBERG, H., SKOVGAARD, D., PETERSEN, L. J., BULOW, J. & KJAER, M. 1999. Type I collagen synthesis and degradation in peritendinous tissue after exercise determined by microdialysis in humans. *J Physiol,* 521 Pt 1**,** 299-306.
LANTTO, I., HEIKKINEN, J., FLINKKILA, T., OHTONEN, P. & LEPPILAHTI, J. 2015. Epidemiology of Achilles tendon ruptures: increasing incidence over a 33-year period. *Scand J Med Sci Sports,* 25**,** e133-8.
LARKIN, P. 2011a. Basic Principles. *Infrared and Raman Spectroscopy.*
LARKIN, P. 2011b. General Outline and Strategies for IR and Raman Spectral Interpretation. *Infrared and Raman Spectroscopy.*
LARKIN, P. 2011c. Introduction. *Infrared and Raman Spectroscopy.*
LARKIN, P. 2011d. IR and Raman Spectra-Structure Correlations. *Infrared and Raman Spectroscopy.*
LARKIN, P. 2011e. Origin of Group Frequencies. *Infrared and Raman Spectroscopy.*
LEE, A. H., SZCZESNY, S. E., SANTARE, M. H. & ELLIOTT, D. M. 2017. Investigating mechanisms of tendon damage by measuring multi-scale recovery following tensile loading. *Acta Biomater,* 57**,** 363-372.
LERSCH, C., GROTSCH, A., SEGESSER, B., KOEBKE, J., BRUGGEMANN, G. P. & POTTHAST, W. 2012. Influence of calcaneus angle and muscle forces on strain distribution in the human Achilles tendon. *Clin Biomech (Bristol, Avon),* 27**,** 955-61.
LIAN, O., SCOTT, A., ENGEBRETSEN, L., BAHR, R., DURONIO, V. & KHAN, K. 2007. Excessive apoptosis in patellar tendinopathy in athletes. *Am J Sports Med,* 35**,** 605-11.
LICHTWARK, G. A., BOUGOULIAS, K. & WILSON, A. M. 2007. Muscle fascicle and series elastic element length changes along the length of the human gastrocnemius during walking and running. *J Biomech,* 40**,** 157-64.
LICHTWARK, G. A. & WILSON, A. M. 2005. In vivo mechanical properties of the human Achilles tendon during one-legged hopping. *J Exp Biol,* 208**,** 4715-25.
LINGELBACH, L. B., MITCHELL, A. E., RUCKER, R. B. & MCDONALD, R. B. 2000. Accumulation of advanced glycation endproducts in aging male Fischer 344 rats during long-term feeding of various dietary carbohydrates. *J Nutr,* 130**,** 1247-55.

LORENZO, A. C. & CAFFARENA, E. R. 2005. Elastic properties, Young's modulus determination and structural stability of the tropocollagen molecule: a computational study by steered molecular dynamics. *J Biomech,* 38**,** 1527-33.
LUNDBORG, G., RANK, F. & HEINAU, B. 1985. Intrinsic Tendon Healing: A new Experimental Model. *Scandinavian Journal of Plastic and Reconstructive Surgery.* Taylor & Francis.
MAAS, H., ARNDT, T. & FRANZ, J. R. 2021. Editorial: Tendon Structure-Function Relationship in Health, Ageing, and Injury. *Front Sports Act Living,* 3**,** 701815.
MAAS, H. & FINNI, T. 2018. Mechanical Coupling Between Muscle-Tendon Units Reduces Peak Stresses. *Exerc Sport Sci Rev,* 46**,** 26-33.
MAAS, H., NOORT, W., BAAN, G. C. & FINNI, T. 2020. Non-uniformity of displacement and strain within the Achilles tendon is affected by joint angle configuration and differential muscle loading. *J Biomech,* 101**,** 109634.
MADEMLI, L. & ARAMPATZIS, A. 2008. Mechanical and morphological properties of the triceps surae muscle-tendon unit in old and young adults and their interaction with a submaximal fatiguing contraction. *J Electromyogr Kinesiol,* 18**,** 89-98.
MADENCI, E. & GUVEN, I. 2015. *The Finite Element Method and Applications in Engineering Using ANSYS®*.
MAFFULLI, N., EWEN, S. W., WATERSTON, S. W., REAPER, J. & BARRASS, V. 2000. Tenocytes from ruptured and tendinopathic achilles tendons produce greater quantities of type III collagen than tenocytes from normal achilles tendons. An in vitro model of human tendon healing. *Am J Sports Med,* 28**,** 499-505.
MAFFULLI, N., MOLLER, H. D. & EVANS, C. H. 2002. Tendon healing: can it be optimised? *British Journal of Sports Medicine,* 36**,** 315-316.
MAGANARIS, C. N. & PAUL, J. P. 2002. Tensile properties of the in vivo human gastrocnemius tendon. *J Biomech,* 35**,** 1639-46.
MAGNAN, B., BONDI, M., PIERANTONI, S. & SAMAILA, E. 2014. The pathogenesis of Achilles tendinopathy: a systematic review. *Foot Ankle Surg,* 20**,** 154-9.
MAGNUSSON, S. P., AAGAARD, P., DYHRE-POULSEN, P. & KJAER, M. 2001. Load-displacement properties of the human triceps surae aponeurosis in vivo. *J Physiol,* 531**,** 277-88.
MAGNUSSON, S. P., HANSEN, P., AAGAARD, P., BROND, J., DYHRE-POULSEN, P., BOJSEN-MOLLER, J. & KJAER, M. 2003. Differential strain patterns of the human gastrocnemius aponeurosis and free tendon, in vivo. *Acta Physiol Scand,* 177**,** 185-95.
MARTIN, R. L., CHIMENTI, R., CUDDEFORD, T., HOUCK, J., MATHESON, J. W., MCDONOUGH, C. M., PAULSETH, S., WUKICH, D. K. & CARCIA, C. R. 2018. Achilles Pain, Stiffness, and Muscle Power Deficits: Midportion Achilles Tendinopathy Revision 2018. *J Orthop Sports Phys Ther,* 48**,** A1-A38.
MARTINEZ, M. G., BULLOCK, A. J., MACNEIL, S. & REHMAN, I. U. 2019. Characterisation of structural changes in collagen with Raman spectroscopy. *Applied Spectroscopy Reviews,* 54**,** 509-542.

MASIC, A., BERTINETTI, L., SCHUETZ, R., CHANG, S. W., METZGER, T. H., BUEHLER, M. J. & FRATZL, P. 2015. Osmotic pressure induced tensile forces in tendon collagen. *Nat Commun,* 6**,** 5942.
MASIC, A., BERTINETTI, L., SCHUETZ, R., GALVIS, L., TIMOFEEVA, N., DUNLOP, J. W., SETO, J., HARTMANN, M. A. & FRATZL, P. 2011. Observations of multiscale, stress-induced changes of collagen orientation in tendon by polarized Raman spectroscopy. *Biomacromolecules,* 12**,** 3989-96.
MATOUSEK, P., DRAPER, E. R., GOODSHIP, A. E., CLARK, I. P., RONAYNE, K. L. & PARKER, A. W. 2006. Noninvasive Raman spectroscopy of human tissue in vivo. *Appl Spectrosc,* 60**,** 758-63.
MATUSZEWSKI, P. E., CHEN, Y. L., SZCZESNY, S. E., LAKE, S. P., ELLIOTT, D. M., SOSLOWSKY, L. J. & DODGE, G. R. 2012. Regional variation in human supraspinatus tendon proteoglycans: decorin, biglycan, and aggrecan. *Connect Tissue Res,* 53**,** 343-8.
MCCRUM, C., LEOW, P., EPRO, G., KONIG, M., MEIJER, K. & KARAMANIDIS, K. 2018a. Alterations in Leg Extensor Muscle-Tendon Unit Biomechanical Properties With Ageing and Mechanical Loading. *Front Physiol,* 9**,** 150.
MCCRUM, C., OBERLANDER, K. D., EPRO, G., KRAUSS, P., JAMES, D. C., REEVES, N. D. & KARAMANIDIS, K. 2018b. Loading rate and contraction duration effects on in vivo human Achilles tendon mechanical properties. *Clin Physiol Funct Imaging,* 38**,** 517-523.
MCGOWAN, C. P., NEPTUNE, R. R. & KRAM, R. 2008. Independent effects of weight and mass on plantar flexor activity during walking: implications for their contributions to body support and forward propulsion. *J Appl Physiol (1985),* 105**,** 486-94.
MILLAR, N. L., WEI, A. Q., MOLLOY, T. J., BONAR, F. & MURRELL, G. A. 2009. Cytokines and apoptosis in supraspinatus tendinopathy. *J Bone Joint Surg Br,* 91**,** 417-24.
MITCHELL, W. K., WILLIAMS, J., ATHERTON, P., LARVIN, M., LUND, J. & NARICI, M. 2012. Sarcopenia, dynapenia, and the impact of advancing age on human skeletal muscle size and strength; a quantitative review. *Front Physiol,* 3**,** 260.
MIYOSHI, T., NAKAZAWA, K., TANIZAKI, M., SATO, T. & AKAI, M. 2006. Altered activation pattern in synergistic ankle plantarflexor muscles in a reduced-gravity environment. *Gait Posture,* 24**,** 94-9.
MOURA JUNIOR MDE, J., ARISAWA, E. A., MARTIN, A. A., DE CARVALHO, J. P., DA SILVA, J. M., SILVA, J. F. & SILVEIRA, L., JR. 2014. Effects of low-power LED and therapeutic ultrasound in the tissue healing and inflammation in a tendinitis experimental model in rats. *Lasers Med Sci,* 29**,** 301-11.
MOURA JUNIOR MDE, J., MAIA FILHO, A. L., PESSOA, D. R., ALVES, M. D., JUSTINO JDE, S., ANDRADE MDOS, S., REBELO, A. M., DE LIMA, C. J., PINHEIRO, A. L. & SILVEIRA, L., JR. 2015. Assessing the biochemical changes of tendons of rats in an experimental model of tenotomy under therapeutic ultrasound and LEDs (625 and 945 nm) by near-infrared Raman spectroscopy. *Lasers Med Sci,* 30**,** 1729-38.
MURAMATSU, T., MURAOKA, T., TAKESHITA, D., KAWAKAMI, Y., HIRANO, Y. & FUKUNAGA, T. 2001. Mechanical properties of tendon

and aponeurosis of human gastrocnemius muscle in vivo. *J Appl Physiol (1985),* 90**,** 1671-8.
MURPHY, G. 2016. Matrix Metalloproteinases. *Encyclopedia of Cell Biology.* Elsevier.
NASH, A., NOTOU, M., LOPEZ-CLAVIJO, A. F., BOZEC, L., DE LEEUW, N. H. & BIRCH, H. L. 2019. Glucosepane is associated with changes to structural and physical properties of collagen fibrils. *Matrix Biology Plus,* 4.
NASH, A., SAïMANNSHAUSEN, J., BOZEC, L., BIRCH, H. L. & DE LEEUW, N. H. 2017. Computational study of glucosepane-water and hydrogen bond formation: an electron topology and orbital analysis. *J Biomol Struct Dyn,* 35**,** 1127-1137.
NICOL, C. & KOMI, P. V. 1998. Significance of passively induced stretch reflexes on achilles tendon force enhancement. *Muscle & Nerve,* 21**,** 1546-1548.
NURI, L., OBST, S. J., NEWSHAM-WEST, R. & BARRETT, R. S. 2017. Regional three-dimensional deformation of human Achilles tendon during conditioning. *Scand J Med Sci Sports,* 27**,** 1263-1272.
OBST, S. J., BARRETT, R. S. & NEWSHAM-WEST, R. 2013. Immediate effect of exercise on achilles tendon properties: systematic review. *Med Sci Sports Exerc,* 45**,** 1534-44.
OBST, S. J., HEALES, L. J., SCHRADER, B. L., DAVIS, S. A., DODD, K. A., HOLZBERGER, C. J., BEAVIS, L. B. & BARRETT, R. S. 2018. Are the Mechanical or Material Properties of the Achilles and Patellar Tendons Altered in Tendinopathy? A Systematic Review with Meta-analysis. *Sports Med,* 48**,** 2179-2198.
OBST, S. J., RENAULT, J. B., NEWSHAM-WEST, R. & BARRETT, R. S. 2014. Three-dimensional deformation and transverse rotation of the human free Achilles tendon in vivo during isometric plantarflexion contraction. *J Appl Physiol (1985),* 116**,** 376-84.
PANG, X., WU, J. P., ALLISON, G. T., XU, J., RUBENSON, J., ZHENG, M. H., LLOYD, D. G., GARDINER, B., WANG, A. & KIRK, T. B. 2017. Three dimensional microstructural network of elastin, collagen, and cells in Achilles tendons. *J Orthop Res,* 35**,** 1203-1214.
PARKINSON, J., SAMIRIC, T., ILIC, M. Z., COOK, J., FELLER, J. A. & HANDLEY, C. J. 2010. Change in proteoglycan metabolism is a characteristic of human patellar tendinopathy. *Arthritis Rheum,* 62**,** 3028-35.
PARKINSON, J., SAMIRIC, T., ILIC, M. Z., COOK, J. & HANDLEY, C. J. 2011. Involvement of proteoglycans in tendinopathy. *J Musculoskelet Neuronal Interact,* 11**,** 86-93.
PASCHALIS, E. P., VERDELIS, K., DOTY, S. B., BOSKEY, A. L., MENDELSOHN, R. & YAMAUCHI, M. 2001. Spectroscopic characterization of collagen cross-links in bone. *J Bone Miner Res,* 16**,** 1821-8.
PATEL, D., SPIESZ, E., THORPE, C. T., BIRCH, H., RILEY, G., CLEGG, P. & SCREEN, H. Energy storing and positional human tendons: mechanics and changes with ageing. The Grey Area – Age and the Extracellular Matrix, 2016.

PATEL, D., ZAMBOULIS, D. E., SPIESZ, E. M., BIRCH, H. L., CLEGG, P. D., THORPE, C. T. & SCREEN, H. R. C. 2021. Structure-function specialisation of the interfascicular matrix in the human achilles tendon. *Acta Biomater,* 131**,** 381-390.

PATTERSON-KANE, J. C., BECKER, D. L. & RICH, T. 2012. The pathogenesis of tendon microdamage in athletes: the horse as a natural model for basic cellular research. *J Comp Pathol,* 147**,** 227-47.

PEARCE, C. J., ISMAIL, M. & CALDER, J. D. 2009. Is apoptosis the cause of noninsertional achilles tendinopathy? *Am J Sports Med,* 37**,** 2440-4.

PĘKALA, P. A., HENRY, B. M., OCHAŁA, A., KOPACZ, P., TATOŃ, G., MŁYNIEC, A., WALOCHA, J. A. & TOMASZEWSKI, K. A. 2017. The twisted structure of the Achilles tendon unraveled: A detailed quantitative and qualitative anatomical investigation. *Scandinavian Journal of Medicine & Science in Sports,* 27**,** 1705-1715.

PENTEADO, S. C., FOGAZZA, B. P., CARVALHO CDA, S., ARISAWA, E. A., MARTINS, M. A., MARTIN, A. A. & MARTINHO HDA, S. 2008. Diagnosis of degenerative lesions of supraspinatus rotator cuff tendons by Fourier transform-Raman spectroscopy. *J Biomed Opt,* 13**,** 014018.

PEREIRA, L., T¢LLEZ SOTO, C. A., DOS SANTOS, L., FAVERO, P. P. & MARTIN, A. A. 2015. Confocal Raman Spectroscopy as an Optical Sensor to Detect Advanced Glycation End Products of the Skin Dermis. *Sensor Letters,* 13**,** 791-801.

PEREZ-CASTRO, A. V. & VOGEL, K. G. 1999. In situ expression of collagen and proteoglycan genes during development of fibrocartilage in bovine deep flexor tendon. *J Orthop Res,* 17**,** 139-48.

PICHLER, W., TESCH, N. P., GRECHENIG, W., LEITHGOEB, O. & WINDISCH, G. 2007. Anatomic variations of the musculotendinous junction of the soleus muscle and its clinical implications. *Clinical Anatomy,* 20**,** 444-447.

PINGEL, J., LU, Y., STARBORG, T., FREDBERG, U., LANGBERG, H., NEDERGAARD, A., WEIS, M., EYRE, D., KJAER, M. & KADLER, K. E. 2014. 3-D ultrastructure and collagen composition of healthy and overloaded human tendon: evidence of tenocyte and matrix buckling. *J Anat,* 224**,** 548-55.

PIZZOLATO, C., SHIM, V. B., LLOYD, D. G., DEVAPRAKASH, D., OBST, S. J., NEWSHAM-WEST, R., GRAHAM, D. F., BESIER, T. F., ZHENG, M. H. & BARRETT, R. S. 2020. Targeted Achilles Tendon Training and Rehabilitation Using Personalized and Real-Time Multiscale Models of the Neuromusculoskeletal System. *Front Bioeng Biotechnol,* 8**,** 878.

PURSLOW, P. 2009. The shear modulus of connections between tendon fascicles. *TIC-STH'09: 2009 IEEE Toronto International Conference - Science and Technology for Humanity.*

RAVARY, B., POURCELOT, P., BORTOLUSSI, C., KONIECZKA, S. & CREVIER-DENOIX, N. 2004. Strain and force transducers used in human and veterinary tendon and ligament biomechanical studies. *Clin Biomech (Bristol, Avon),* 19**,** 433-47.

REES, J. D., STRIDE, M. & SCOTT, A. 2014. Tendons--time to revisit inflammation. *Br J Sports Med,* 48**,** 1553-7.

REES, S. G., FLANNERY, C. R., LITTLE, C. B., HUGHES, C. E., CATERSON, B. & DENT, C. M. 2000. Catabolism of aggrecan, decorin and biglycan in tendon. *Biochem J,* 350 Pt 1**,** 181-8.

REESE, S. P., ELLIS, B. J. & WEISS, J. A. 2013. Micromechanical model of a surrogate for collagenous soft tissues: development, validation and analysis of mesoscale size effects. *Biomech Model Mechanobiol,* 12**,** 1195-204.

REESE, S. P., MAAS, S. A. & WEISS, J. A. 2010. Micromechanical models of helical superstructures in ligament and tendon fibers predict large Poisson's ratios. *J Biomech,* 43**,** 1394-400.

RILEY, G. 2011. Tendon and ligament biochemistry and pathology. *In:* HUTSON, M. & SPEED, C. (eds.) *Sports Injuries.* Oxford University Press.

ROBINSON, K. A., SUN, M., BARNUM, C. E., WEISS, S. N., HUEGEL, J., SHETYE, S. S., LIN, L., SAEZ, D., ADAMS, S. M., IOZZO, R. V., SOSLOWSKY, L. J. & BIRK, D. E. 2017. Decorin and biglycan are necessary for maintaining collagen fibril structure, fiber realignment, and mechanical properties of mature tendons. *Matrix Biol,* 64**,** 81-93.

RUMIAN, A. P., WALLACE, A. L. & BIRCH, H. L. 2007. Tendons and ligaments are anatomically distinct but overlap in molecular and morphological features--a comparative study in an ovine model. *J Orthop Res,* 25**,** 458-64.

RYAN, C. N., SORUSHANOVA, A., LOMAS, A. J., MULLEN, A. M., PANDIT, A. & ZEUGOLIS, D. I. 2015. Glycosaminoglycans in Tendon Physiology, Pathophysiology, and Therapy. *Bioconjug Chem,* 26**,** 1237-51.

RYGULA, A., MAJZNER, K., MARZEC, K. M., KACZOR, A., PILARCZYK, M. & BARANSKA, M. 2013. Raman spectroscopy of proteins: a review. *Journal of Raman Spectroscopy,* 44**,** 1061-1076.

SAMIRIC, T., ILIC, M. Z. & HANDLEY, C. J. 2004. Characterisation of proteoglycans and their catabolic products in tendon and explant cultures of tendon. *Matrix Biol,* 23**,** 127-40.

SANCHO, I., MALLIARAS, P., BARTON, C., WILLY, R. W. & MORRISSEY, D. 2019. Biomechanical alterations in individuals with Achilles tendinopathy during running and hopping: A systematic review with meta-analysis. *Gait Posture,* 73**,** 189-201.

SATO, N., TANIGUCHI, T., GODA, Y., KOSAKA, H., HIGASHINO, K., SAKAI, T., KATOH, S., YASUI, N., SAIRYO, K. & TANIGUCHI, H. 2016. Proteomic Analysis of Human Tendon and Ligament: Solubilization and Analysis of Insoluble Extracellular Matrix in Connective Tissues. *J Proteome Res,* 15**,** 4709-4721.

SCAGLIONI, G., NARICI, M. V., MAFFIULETTI, N. A., PENSINI, M. & MARTIN, A. 2003. Effect of ageing on the electrical and mechanical properties of human soleus motor units activated by the H reflex and M wave. *J Physiol,* 548**,** 649-61.

SCOTT, A., KHAN, K. M., HEER, J., COOK, J. L., LIAN, O. & DURONIO, V. 2005. High strain mechanical loading rapidly induces tendon apoptosis: an ex vivo rat tibialis anterior model. *Br J Sports Med,* 39**,** e25.

SCOTT, A., LIAN, O., ROBERTS, C. R., COOK, J. L., HANDLEY, C. J., BAHR, R., SAMIRIC, T., ILIC, M. Z., PARKINSON, J., HART, D. A., DURONIO, V. & KHAN, K. M. 2008. Increased versican content is associated with tendinosis pathology in the patellar tendon of athletes with jumper's knee. *Scand J Med Sci Sports,* 18**,** 427-35.

SCREEN, H. R., LEE, D. A., BADER, D. L. & SHELTON, J. C. 2004. An investigation into the effects of the hierarchical structure of tendon fascicles on micromechanical properties. *Proc Inst Mech Eng H,* 218**,** 109-19.

SEYNNES, O. R., ERSKINE, R. M., MAGANARIS, C. N., LONGO, S., SIMONEAU, E. M., GROSSET, J. F. & NARICI, M. V. 2009. Training-induced changes in structural and mechanical properties of the patellar tendon are related to muscle hypertrophy but not to strength gains. *Journal of Applied Physiology,* 107**,** 523-530.

SEYNNES, O. R., MAGANARIS, C. N., DE BOER, M. D., DI PRAMPERO, P. E. & NARICI, M. V. 2008. Early structural adaptations to unloading in the human calf muscles. *Acta Physiol (Oxf),* 193**,** 265-74.

SHEARER, T., THORPE, C. T. & SCREEN, H. R. C. 2017. The relative compliance of energy-storing tendons may be due to the helical fibril arrangement of their fascicles. *J R Soc Interface,* 14.

SHERMAN, V. R., YANG, W. & MEYERS, M. A. 2015. The materials science of collagen. *J Mech Behav Biomed Mater,* 52**,** 22-50.

SHIM, V. B., FERNANDEZ, J. W., GAMAGE, P. B., REGNERY, C., SMITH, D. W., GARDINER, B. S., LLOYD, D. G. & BESIER, T. F. 2014. Subject-specific finite element analysis to characterize the influence of geometry and material properties in Achilles tendon rupture. *J Biomech,* 47**,** 3598-604.

SHIM, V. B., HANDSFIELD, G. G., FERNANDEZ, J. W., LLOYD, D. G. & BESIER, T. F. 2018. Combining in silico and in vitro experiments to characterize the role of fascicle twist in the Achilles tendon. *Sci Rep,* 8**,** 13856.

SHOULDERS, M. D. & RAINES, R. T. 2009. Collagen structure and stability. *Annu Rev Biochem,* 78**,** 929-58.

SILVER, F. H., FREEMAN, J. W. & SEEHRA, G. P. 2003. Collagen self-assembly and the development of tendon mechanical properties. *J Biomech,* 36**,** 1529-53.

SIMPSON, C. L., KIM, B. D. H., BOURCET, M. R., JONES, G. R. & JAKOBI, J. M. 2017. Stretch training induces unequal adaptation in muscle fascicles and thickness in medial and lateral gastrocnemii. *Scand J Med Sci Sports,* 27**,** 1597-1604.

SLANE, L. C., DEWALL, R., MARTIN, J., LEE, K. & THELEN, D. G. 2015. Middle-aged adults exhibit altered spatial variations in Achilles tendon wave speed. *Physiol Meas,* 36**,** 1485-96.

SLANE, L. C. & THELEN, D. G. 2014. Non-uniform displacements within the Achilles tendon observed during passive and eccentric loading. *J Biomech,* 47**,** 2831-5.

SLANE, L. C. & THELEN, D. G. 2015. Achilles tendon displacement patterns during passive stretch and eccentric loading are altered in middle-aged adults. *Med Eng Phys,* 37**,** 712-6.

SNEDEKER, J. G. & FOOLEN, J. 2017. Tendon injury and repair - A perspective on the basic mechanisms of tendon disease and future clinical therapy. *Acta Biomater,* 63**,** 18-36.
SNEDEKER, J. G. & GAUTIERI, A. 2014. The role of collagen crosslinks in ageing and diabetes - the good, the bad, and the ugly. *Muscles Ligaments Tendons J,* 4**,** 303-8.
SPIESZ, E. M., THORPE, C. T., THURNER, P. J. & SCREEN, H. R. C. 2018. Structure and collagen crimp patterns of functionally distinct equine tendons, revealed by quantitative polarised light microscopy (qPLM). *Acta Biomater,* 70**,** 281-292.
STENROTH, L., PELTONEN, J., CRONIN, N. J., SIPILA, S. & FINNI, T. 2012. Age-related differences in Achilles tendon properties and triceps surae muscle architecture in vivo. *J Appl Physiol (1985),* 113**,** 1537-44.
STENROTH, L., THELEN, D. & FRANZ, J. 2019. Biplanar ultrasound investigation of in vivo Achilles tendon displacement non-uniformity. *Transl Sports Med,* 2**,** 73-81.
STEPHENS, P. R., NUNAMAKER, D. M. & BUTTERWECK, D. M. 1989. Application of a Hall-effect transducer for measurement of tendon strains in horses. *Am J Vet Res,* 50**,** 1089-95.
SUN, Y., BERGER, E. J., ZHAO, C., JAY, G. D., AN, K. N. & AMADIO, P. C. 2006. Expression and mapping of lubricin in canine flexor tendon. *J Orthop Res,* 24**,** 1861-8.
SUN, Y. L., WEI, Z., ZHAO, C., JAY, G. D., SCHMID, T. M., AMADIO, P. C. & AN, K. N. 2015. Lubricin in human achilles tendon: The evidence of intratendinous sliding motion and shear force in achilles tendon. *J Orthop Res,* 33**,** 932-7.
SUN, Y. L., ZHAO, C., JAY, G. D., SCHMID, T. M., AN, K. N. & AMADIO, P. C. 2013. Effects of stress deprivation on lubricin synthesis and gliding of flexor tendons in a canine model in vivo. *J Bone Joint Surg Am,* 95**,** 273-8.
SUYDAM, S. M., SOULAS, E. M., ELLIOTT, D. M., SILBERNAGEL, K. G., BUCHANAN, T. S. & CORTES, D. H. 2015. Viscoelastic properties of healthy achilles tendon are independent of isometric plantar flexion strength and cross-sectional area. *J Orthop Res,* 33**,** 926-31.
SVENSSON, R. B., HEINEMEIER, K. M., COUPPE, C., KJAER, M. & MAGNUSSON, S. P. 2016. Effect of aging and exercise on the tendon. *J Appl Physiol (1985),* 121**,** 1237-1246.
SVENSSON, R. B., HERCHENHAN, A., STARBORG, T., LARSEN, M., KADLER, K. E., QVORTRUP, K. & MAGNUSSON, S. P. 2017. Evidence of structurally continuous collagen fibrils in tendons. *Acta Biomater,* 50**,** 293-301.
SVENSSON, R. B., SMITH, S. T., MOYER, P. J. & MAGNUSSON, S. P. 2018. Effects of maturation and advanced glycation on tensile mechanics of collagen fibrils from rat tail and Achilles tendons. *Acta Biomater,* 70**,** 270-280.
SWANSTROM, M. D., STOVER, S. M., HUBBARD, M. & HAWKINS, D. A. 2004. Determination of passive mechanical properties of the superficial and deep digital flexor muscle-ligament-tendon complexes in the forelimbs of horses. *American Journal of Veterinary Research.*

SZARO, P., CIFUENTES RAMIREZ, W., BORKMANN, S., BENGTSSON, A., POLACZEK, M. & CISZEK, B. 2020. Distribution of the subtendons in the midportion of the Achilles tendon revealed in vivo on MRI. *Sci Rep,* 10**,** 16348.

SZARO, P. & GHALI GATAA, K. 2021. The correlations between dimensions of the normal tendon and tendinopathy changed Achilles tendon in routine magnetic resonance imaging. *Sci Rep,* 11**,** 6131.

SZARO, P., WITKOWSKI, G., SMIGIELSKI, R., KRAJEWSKI, P. & CISZEK, B. 2009. Fascicles of the adult human Achilles tendon - an anatomical study. *Ann Anat,* 191**,** 586-93.

SZCZESNY, S. E. & ELLIOTT, D. M. 2014a. Incorporating plasticity of the interfibrillar matrix in shear lag models is necessary to replicate the multiscale mechanics of tendon fascicles. *J Mech Behav Biomed Mater,* 40**,** 325-338.

SZCZESNY, S. E. & ELLIOTT, D. M. 2014b. Interfibrillar shear stress is the loading mechanism of collagen fibrils in tendon. *Acta Biomater,* 10**,** 2582-90.

SZCZESNY, S. E., FETCHKO, K. L., DODGE, G. R. & ELLIOTT, D. M. 2017. Evidence that interfibrillar load transfer in tendon is supported by small diameter fibrils and not extrafibrillar tissue components. *J Orthop Res,* 35**,** 2127-2134.

TALARI, A. C. S., MOVASAGHI, Z., REHMAN, S. & REHMAN, I. U. 2014. Raman Spectroscopy of Biological Tissues. *Applied Spectroscopy Reviews,* 50**,** 46-111.

THORNTON, G. M., LEMMEX, D. B., ONO, Y., BEACH, C. J., RENO, C. R., HART, D. A. & LO, I. K. Y. 2015. Aging affects mechanical properties and lubricin/PRG4 gene expression in normal ligaments. *Journal of Biomechanics,* 48**,** 3306-3311.

THORPE, C. T. 2010. *Extracellular Matrix Synthesis and Degradation in Functionally Distinct Tendons.* PhD, Univeristy College London.

THORPE, C. T., BIRCH, H. L., CLEGG, P. D. & SCREEN, H. R. 2013a. The role of the non-collagenous matrix in tendon function. *Int J Exp Pathol,* 94**,** 248-59.

THORPE, C. T., CHAUDHRY, S., LEI, II, VARONE, A., RILEY, G. P., BIRCH, H. L., CLEGG, P. D. & SCREEN, H. R. 2015a. Tendon overload results in alterations in cell shape and increased markers of inflammation and matrix degradation. *Scand J Med Sci Sports,* 25**,** e381-91.

THORPE, C. T., CLEGG, P. D. & BIRCH, H. L. 2010a. A review of tendon injury: why is the equine superficial digital flexor tendon most at risk? *Equine Vet J,* 42**,** 174-80.

THORPE, C. T., GODINHO, M. S. C., RILEY, G. P., BIRCH, H. L., CLEGG, P. D. & SCREEN, H. R. C. 2015b. The interfascicular matrix enables fascicle sliding and recovery in tendon, and behaves more elastically in energy storing tendons. *J Mech Behav Biomed Mater,* 52**,** 85-94.

THORPE, C. T., KARUNASEELAN, K. J., NG CHIENG HIN, J., RILEY, G. P., BIRCH, H. L., CLEGG, P. D. & SCREEN, H. R. 2016a. Distribution of proteins within different compartments of tendon varies according to tendon type. *J Anat,* 229**,** 450-8.

THORPE, C. T., KLEMT, C., RILEY, G. P., BIRCH, H. L., CLEGG, P. D. & SCREEN, H. R. 2013b. Helical sub-structures in energy-storing tendons provide a possible mechanism for efficient energy storage and return. *Acta Biomater,* 9**,** 7948-56.

THORPE, C. T., MCDERMOTT, B. T., GOODSHIP, A. E., CLEGG, P. D. & BIRCH, H. L. 2016b. Ageing does not result in a decline in cell synthetic activity in an injury prone tendon. *Scand J Med Sci Sports,* 26**,** 684-93.

THORPE, C. T., PEFFERS, M. J., SIMPSON, D., HALLIWELL, E., SCREEN, H. R. & CLEGG, P. D. 2016c. Anatomical heterogeneity of tendon: Fascicular and interfascicular tendon compartments have distinct proteomic composition. *Sci Rep,* 6**,** 20455.

THORPE, C. T., RILEY, G. P., BIRCH, H. L., CLEGG, P. D. & SCREEN, H. R. 2014. Effect of fatigue loading on structure and functional behaviour of fascicles from energy-storing tendons. *Acta Biomater,* 10**,** 3217-24.

THORPE, C. T., RILEY, G. P., BIRCH, H. L., CLEGG, P. D. & SCREEN, H. R. C. 2016d. Fascicles and the interfascicular matrix show adaptation for fatigue resistance in energy storing tendons. *Acta Biomater,* 42**,** 308-315.

THORPE, C. T., RILEY, G. P., BIRCH, H. L., CLEGG, P. D. & SCREEN, H. R. C. 2017. Fascicles and the interfascicular matrix show decreased fatigue life with ageing in energy storing tendons. *Acta Biomater,* 56**,** 58-64.

THORPE, C. T. & SCREEN, H. R. C. 2016. Tendon Structure and Composition. *In:* ACKERMANN, P. W. & HART, D. A. (eds.) *Metabolic Influences on Risk for Tendon Disorders.* Cham: Springer International Publishing.

THORPE, C. T., STARK, R. J., GOODSHIP, A. E. & BIRCH, H. L. 2010b. Mechanical properties of the equine superficial digital flexor tendon relate to specific collagen cross-link levels. *Equine Vet J Suppl***,** 538-43.

THORPE, C. T., STREETER, I., PINCHBECK, G. L., GOODSHIP, A. E., CLEGG, P. D. & BIRCH, H. L. 2010c. Aspartic acid racemization and collagen degradation markers reveal an accumulation of damage in tendon collagen that is enhanced with aging. *J Biol Chem,* 285**,** 15674-81.

THORPE, C. T., UDEZE, C. P., BIRCH, H. L., CLEGG, P. D. & SCREEN, H. R. 2012. Specialization of tendon mechanical properties results from interfascicular differences. *J R Soc Interface,* 9**,** 3108-17.

THORPE, C. T., UDEZE, C. P., BIRCH, H. L., CLEGG, P. D. & SCREEN, H. R. 2013c. Capacity for sliding between tendon fascicles decreases with ageing in injury prone equine tendons: a possible mechanism for age-related tendinopathy? *Eur Cell Mater,* 25**,** 48-60.

TIAN, M., HERBERT, R. D., HOANG, P., GANDEVIA, S. C. & BILSTON, L. E. 2012. Myofascial force transmission between the human soleus and gastrocnemius muscles during passive knee motion. *J Appl Physiol (1985),* 113**,** 517-23.

TIELAND, M., TROUWBORST, I. & CLARK, B. C. 2018. Skeletal muscle performance and ageing. *J Cachexia Sarcopenia Muscle,* 9**,** 3-19.

VAN GILS, C. C., STEED, R. H. & PAGE, J. C. 1996. Torsion of the human achilles tendon. *The Journal of Foot and Ankle Surgery,* 35**,** 41-48.
VAN GULICK, L., SABY, C., MORJANI, H. & BELJEBBAR, A. 2019. Age-related changes in molecular organization of type I collagen in tendon as probed by polarized SHG and Raman microspectroscopy. *Sci Rep,* 9**,** 7280.
VESENTINI, S., REDAELLI, A. & MONTEVECCHI, F. M. 2005. Estimation of the binding force of the collagen molecule-decorin core protein complex in collagen fibril. *Journal of Biomechanics,* 38**,** 433-443.
VOGEL, K. G. 2004. What happens when tendons bend and twist? Proteoglycans. *J Musculoskelet Neuronal Interact,* 4**,** 202-3.
VOGEL, K. G., ORDOG, A., POGANY, G. & OLAH, J. 1993. Proteoglycans in the compressed region of human tibialis posterior tendon and in ligaments. *J Orthop Res,* 11**,** 68-77.
WAGGETT, A. D., RALPHS, J. R., KWAN, A. P., WOODNUTT, D. & BENJAMIN, M. 1998. Characterization of collagens and proteoglycans at the insertion of the human Achilles tendon. *Matrix Biol,* 16**,** 457-70.
WANG, H. K., CHIANG, H., CHEN, W. S., SHIH, T. T., HUANG, Y. C. & JIANG, C. C. 2013a. Early neuromechanical outcomes of the triceps surae muscle-tendon after an Achilles' tendon repair. *Arch Phys Med Rehabil,* 94**,** 1590-8.
WANG, R., YAN, S., SCHLIPPE, M., TARASSOVA, O., PENNATI, G. V., LINDBERG, F., KORTING, C., DESTRO, A., YANG, L., SHI, B. & ARNDT, A. 2021. Passive Mechanical Properties of Human Medial Gastrocnemius and Soleus Musculotendinous Unit. *Biomed Res Int,* 2021**,** 8899699.
WANG, T., LIN, Z., DAY, R. E., GARDINER, B., LANDAO-BASSONGA, E., RUBENSON, J., KIRK, T. B., SMITH, D. W., LLOYD, D. G., HARDISTY, G., WANG, A., ZHENG, Q. & ZHENG, M. H. 2013b. Programmable mechanical stimulation influences tendon homeostasis in a bioreactor system. *Biotechnol Bioeng,* 110**,** 1495-507.
WEI, D., CHEN, S. & LIU, Q. 2015. Review of Fluorescence Suppression Techniques in Raman Spectroscopy. *Applied Spectroscopy Reviews,* 50**,** 387-406.
WEISS, J. A., MAKER, B. N. & GOVINDJEE, S. 1996. Finite element implementation of incompressible, transversely isotropic hyperelasticity. *Computer Methods in Applied Mechanics and Engineering,* 135**,** 107-128.
WILLIAMS, K. E. & OLSEN, D. R. 2009. Matrix metalloproteinase-1 cleavage site recognition and binding in full-length human type III collagen. *Matrix Biol,* 28**,** 373-9.
WINTER, E., WEISE, K., WELLER, S. & AMBACHER, T. 1998. Surgical repair of Achilles tendon rupture. Comparison of surgical with conservative treatment. *Arch Orthop Trauma Surg,* 117**,** 364-7.
WOPENKA, B., KENT, A., PASTERIS, J. D., YOON, Y. & THOMOPOULOS, S. 2008. The tendon-to-bone transition of the rotator cuff: a preliminary Raman spectroscopic study documenting the gradual mineralization across the insertion in rat tissue samples. *Appl Spectrosc,* 62**,** 1285-94.

WREN, T. A., YERBY, S. A., BEAUPRE, G. S. & CARTER, D. R. 2001. Mechanical properties of the human achilles tendon. *Clin Biomech (Bristol, Avon),* 16**,** 245-51.

WU, W., BILLINGHURST, R. C., PIDOUX, I., ANTONIOU, J., ZUKOR, D., TANZER, M. & POOLE, A. R. 2002. Sites of collagenase cleavage and denaturation of type II collagen in aging and osteoarthritic articular cartilage and their relationship to the distribution of matrix metalloproteinase 1 and matrix metalloproteinase 13. *Arthritis Rheum,* 46**,** 2087-94.

XU, S. Y., HE, Y. B., DENG, S. Y., LIU, S. Y., XU, L. & NI, G. X. 2018. Intensity-dependent effect of treadmill running on rat Achilles tendon. *Exp Ther Med,* 15**,** 5377-5383.

YEUNG, C.-Y. C. & KADLER, K. E. 2019. Importance of the circadian clock in tendon development. *Vertebrate Skeletal Development.* Elsevier.

YIN, N. H., CHEN, W. S., WU, Y. T., SHIH, T. T., ROLF, C. & WANG, H. K. 2014. Increased patellar tendon microcirculation and reduction of tendon stiffness following knee extension eccentric exercises. *J Orthop Sports Phys Ther,* 44**,** 304-12.

YOON, J. H. & HALPER, J. 2005. Tendon proteoglycans: biochemistry and function. *J Musculoskelet Neuronal Interact,* 5**,** 22-34.

ZHANG, G., YOUNG, B. B., EZURA, Y., FAVATA, M., SOSLOWSKY, L. J., CHAKRAVARTI, S. & BIRK, D. E. 2005. Development of tendon structure and function: regulation of collagen fibrillogenesis. *J Musculoskelet Neuronal Interact,* 5**,** 5-21.